N-Heterocyclic Silylenes as Tools in Coordination Chemistry and Catalysis

vorgelegt von

M. Sc. Chemie

Yu-Peng Zhou

aus Yunnan (V. R. China)

Von der Fakultät II – Mathematik und Naturwissenschaften

der Technischen Universität Berlin

Institut für Chemie

zur Erlangung des akademischen Grades

Doktor der Naturwissenschaften

- Dr. rer. nat. -

genehmigte Dissertation

Promotionsausschuss:

Vorsitzender: Prof. Dr. Reinhard Schomäcker (Technische Universität Berlin)

1. Gutachter: Prof. Dr. Matthias Driess (Technische Universität Berlin)

2. Gutachter: Prof. Dr. Christian Müller (Freie Universität Berlin)

Tag der wissenschaftlichen Aussprache: 13.06.2018

Berlin 2018

DISSERTATION

by

M. Sc. Chemistry

Yu-Peng Zhou

from Yunnan (P. R. China)

Von Herzen kommend gilt mein Dank meinem verehrten Lehrer

Herrn Professor Dr. Matthias Driess

für die Aufnahme in seinen Arbeitskreis, für seine engagierte Unterstützung, und für die Forschungsfreiheit.

Acknowledgment

Publications during doctoral study

1. **Y. P. Zhou**, S. Raoufmoghaddam, T. Szilvási, M. Driess*, *Angew. Chem. Int. Ed.* **2016**, *55*, 12868-12872.

   A Bis(silylene) Substituted *ortho*-Carborane as a Superior Ligand in the Nickel-Catalyzed Amination of Arenes

2. **Y. P. Zhou**, M. Karni, S. Yao, Y. Apeloig*, M. Driess*, *Angew. Chem. Int. Ed.* **2016**, *55*, 15096-15099. (**Hot Paper**)

   A Bis(silylenyl)pyridine Zero-Valent Germanium Complex and Its Remarkable Reactivity

3. **Y. P. Zhou**, Z. Mo, M. P. Luecke, M. Driess*, *Chem. Eur. J.* **2017**, DOI: 10.1002/chem.201705745. (**Hot Paper & Front Cover**)

   Stereoselective Transfer Semi-Hydrogenation of Alkynes to *E*-Olefins with *N*-Heterocyclic Silylene–Manganese Catalysts

4. S. Raoufmoghaddam, **Y. P. Zhou**, Y. Wang, M. Driess*, *J. Organomet. Chem.* **2017**, *829*, 2-10.

   N-heterocyclic silylenes as powerful steering ligands in catalysis

5. Z. Mo, T. Szilvási, **Y. P. Zhou**, S. Yao, M. Driess*, *Angew. Chem. Int. Ed.* **2017**, *56*, 3699 –3702. (**Hot Paper**)

   An Intramolecular Silylene Borane Capable of Facile Activation of Small Molecules, Including Metal-Free Dehydrogenation of Water

6. H. Ren, **Y. P. Zhou**, Y. Bai, C. Cui*, M. Driess, *Chem. Eur. J.* **2017**, *23*, 5663–5667.

   Cobalt-Catalyzed Regioselective Borylation of Arenes: N-Heterocyclic Silylene as Electron Donors in Metal-Mediated Activation of C-H Bonds

7. M. P. Luecke, D. Porwal, A. Kostenko, **Y. P. Zhou**, S. Yao, M. Keck, C. Limberg, M. Oestreich, M. Driess*, *Dalton Trans.*, **2017**, *46*, 16412–16418.

Bis(silylenyl)-substituted Ferrocene-stabilized η^6-arene Iron(0) Complexes: Synthesis, Structure and Catalytic Application

ABSTRACT

Low-valent main-group chemistry, especially the chemistry of *N*-heterocyclic silylenes (NHSis), is one of the most attractive research topics in contemporary organometallic chemistry. In this dissertation, a series of NHSis and their derivatives were developed and used as ligands to stabilize low-valent germanium compounds as well as in transition metal-mediated homogenous catalysis.

The synthesis, reactivity, and electronic structure of the first Ge^0 iron carbonyl complex is described in chapter 3.1. The compound was obtained from the reaction of a pyridine-based bis-NHSi ligand stabilized chlorogermyliumylidene chloride precursor with Collman's reagent, $K_2Fe(CO)_4$. Remarkably, the reaction of the Ge^0 iron carbonyl complex with one equivalent of $GeCl_2\cdot(dioxane)$ furnished the first push–pull germylone–germylene donor–acceptor complex, through the insertion of $GeCl_2$ into the dative $Ge^0 \rightarrow Fe^0$ bond.

The synthesis and structures of the first bis-NHSi-substituted *ortho*-carborane $[(LSi:)C]_2B_{10}H_{10}$ (L=PhC(N*t*Bu)$_2$) and its nickel complexes are discussed in chapter 3.2. The CO stretching vibration modes of the corresponding $Ni(CO)_2$ complex indicate that the Si^{II} atoms in the ligand are even stronger σ donors than the P^{III} atoms in phosphines and C^{II} atoms in N-heterocyclic carbene (NHC) ligands. Moreover, the strong donor character of the ligand enables Ni^{II} complex to act as an outstanding precatalyst (0.5 mol % loading) in the catalytic aminations of arenes.

In chapter 3.3, the synthesis and structures of the Si^{II}-donor supported Mn^{II} complexes, bearing a pyridine-based bis-NHSi ligand, bidentate ferrocene-based bis-NHSi ligand, and two monodentate NHSi ligands are described, respectively. They act as active and stereoselective manganese-based precatalysts (1 mol % loading) in transfer semi-hydrogenations of alkynes to give the corresponding (*E*)-olefins using ammonia–borane as a convenient hydrogen source under mild reaction conditions.

Finally, the synthesis and structure of cobalt silyl, silylene, and η^2-(Si−H) complexes derived from *N*-heterocyclicsilylcarbene $L^1Si(H)(CH_2)NHC$ (L^1 = $CH\{C=CH_2\}(CMe)(NAr)_2$, Ar = 2,6-*i*Pr$_2$C$_6$H$_3$, NHC = 3,4,5-trimethylimidazol-2-ylidene) is discussed in chapter 3.4. The complex $[L^1Si(CH_2)NHC]CoH(PMe_3)_2$ is found to be a very active (pre)catalyst for the hydrosilylation of olefins.

ZUSAMMENFASSUNG

Die Chemie der niedervalenten Hauptgruppen und besonders die Chemie der *N*-heterocyclischen Silylene (NHSis) ist einer der attraktivsten Forschungsbereiche der modernen metallorganischen Chemie. In dieser Arbeit wurden eine Reihe von NHSis sowie ihre Derivate entwickelt und als Liganden eingesetzt, um niedervalente Spezies der Gruppe 14 zu stabilisieren und, Übergangsmetalle zu Koordinieren. Des Weiteren wurden neue katalytische Anwendungen von Übergangsmetallkomplexen in Aminierungs-, Semi-Transferhydrierungs- und Hydrosilylierungsreaktionen entwickelt.

Die Synthese, Reaktionsfähigkeit und Elektronenstruktur eines Ge^0-Eisen-Carbonyl-Komplexes wird in Kapitel 3.1 beschrieben. Die Verbindung entstand aus der Reaktion des auf Pyridin basierenden bis-NHSi-Liganden-stabilisierten Chlorogermyliumyliden-Chlorid-Precursors mit dem Collmans Reagenz, $K_2Fe(CO)_4$. Bemerkenswert war, dass die Reaktion des Ge^0-Eisencarbonylkomplexes mit einem Äquivalent des $GeCl_2\cdot$(Dioxan) durch die Einschiebung des $GeCl_2$ in die koordinative $Ge^0\rightarrow Fe^0$-Bindung den ersten Push-Pull Germylon-Germylen Donor-Akzeptor-Komplex ergab.

Die Synthese und Strukturen des ersten bis-NHSi-substituierten *ortho*-Carborans $[(LSi:)C]_2B_{10}H_{10}$ (L=PhC(N*t*Bu)$_2$) und seines Nickel-Komplexes sind in Kapitel 3.2 dargelegt. Die CO-Streckschwingungsarten des korrespondierenden $Ni(CO)_2$-Komplexes weisen darauf hin, dass die Si^{II}-Atome im Liganden noch stärkere σ-Donoren sind als die P^{III}-Atome in Phosphanen und die C^{II}-Atome in N-heterocyclischen Carben (NHC)-Liganden. Außerdem kann der Ni^{II}-Komplex durch die starken Donor-Eigenschaften des Liganden als hervorragender Präkatalysator (0,5 mol % Beladung) in der katalytischen Aminierung von Arenen fungieren.

In Kapitel 3.3 werden die Synthese und Strukturen der ersten Si^{II}-Donor-unterstützten Mn^{II}-Komplexe beschrieben, die einen Pyridin-basierten bis-NHSi-Liganden, einen zweizähnigen Ferrocen-basierten bis-NHSi-Liganden und zwei einzähnige NHSi-Liganden tragen. Sie fungieren als aktive und stereoselektive Mangan-basierte Präkatalysten (1 mol % Beladung) in Semi-Transferhydrierungen

von Alkinen mit Amminboran als geeigneter Wasserstoffquelle unter milden Reaktionsbedingungen wobei die korrespondierenden (E)-Olefine entstehen.

Schließlich beschreibt meine Dissertationschrift in Kapital 3.4 die Synthese und Strukturen von Cobalt-Silyl, Silylen und η^2-(Si−H) Komplexen aus dem N-heterocyclischem Silylcarben $L^1Si(H)(CH_2)NHC$ (L1 = CH{C=CH$_2$}(CMe)(NAr)$_2$, Ar = 2,6-iPr$_2$C$_6$H$_3$, NHC = 3,4,5-trimethylimidazol-2-ylidene). Der Komplex $[L^1Si(CH_2)NHC]CoH(PMe_3)_2$ erwies sich als sehr aktiver (Prä-)Katalysator für die Hydrosilylierung von Olefinen.

CONTENTS

ABBREVIATIONS

APCI	atmospheric-pressure chemical ionization	MHz	Megahertz
Ar	aryl	min	minute(s)
B3LYP	Becke's three-parameter hybrid functional using the Lee, Yang, and Parr correlation "functional."	mmol	millimole
		MS	mass spectrometry
		MW	molecular weight
br	broad	*m/z*	mass/charge
°C	Celsius degree	Naph	naphthyl
ca.	about	NBO	natural bond orbital
calcd.	calculated	NHC	*N*-Heterocyclic Carbene
cod, COD	1,5-cyclooctadiene	NHSi	*N*-Heterocyclic Silylene
Cp	cyclopentadienyl	NMR	Nuclear Magnetic Resonance
d	doublet	NPA	natural population analysis
DFT	density functional theory	Ph	phenyl
Dipp	2,6-iPr$_2$C$_6$H$_3$	ppm	parts per million
EI	electron impact ionization	iPr	isopropyl
equiv.	equivalent(s)	q	quartet
ESI	electrospray ionization	R	organic substituent
Et	ethyl	R.T.	room temperature
eV	Electronvolt	s	singlet; strong
Fc	ferrocendiyl	sept	septet
(m)g	(mili)gram(s)	t	triplet
h	hour(s)	THF	tetrahydrofuran
HOMO	highest occupied molecular orbital	Tip	2,4,6-^{i}Pr$_2$C$_6$H$_2$
Hz	Hertz	tmeda	N,N'-tetramethylethyldiamine
IR	infrared	TMS	tetramethylsilane
INT	intermediate	TS	transition state
K	Kelvin	UV-vis	ultraviolet-visible
LUMO	lowest unoccupied molecular orbital	VT	variable temperature
		w	weak
M	Metal	WBI	Wiberg Bond Index
m	multiplet; medium	δ	chemical shift

1. INTRODUCTION

1.1 Silylenes: Divalent silicon compounds

Silylenes are divalent silicon compounds in which the silicon atoms prefer a single ground state (Figure 1-1, left). Similar to their lighter analogues carbenes, silylenes are both Lewis acids, due to empty 3p orbitals, and Lewis bases because of the presence of a lone pair of electrons.[1] Silylenes are highly reactive species that, before 1980's, could only be observed spectroscopically at low temperatures, or when they were isolated as silylene metal complexes. The scenario changed with the isolation of the first stable Si^{II} compound, decamethylsiliocene, by Jutzi and co-workers in 1986,[2] followed by the isolation of several other stable silylenes (e.g. *N*-heterocyclic silylenes (NHSis), cyclic dialkyl silylenes, cyclic alkyl(amino) silylenes, and acyclic silylenes), which employ thermodynamic or kinetic stabilization (Figure 1-1, middle and right). These silylenes can be employed in the metal-free activation of unreactive bonds in small molecules, and as stabilization ligands for the low-valent main-group compounds, or as steering ligands in metal-mediated catalysis. In this chapter, the progress in the chemistry of stable silylenes (1.1), the existence of silylene stabilized low-valent main-group compounds (1.2), and their applications in catalysis (1.3) will be discussed.
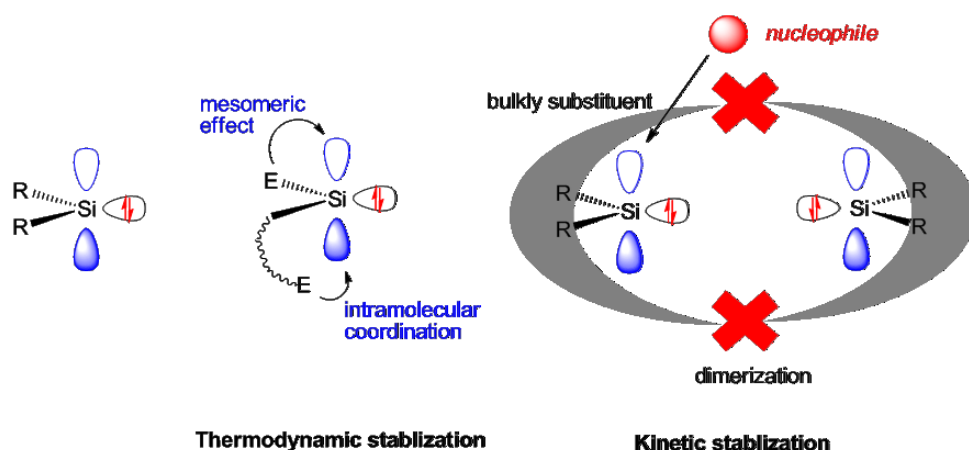
Figure 1-1. The electronic configuration of singlet silylene (left); thermodynamic using Lewis base (middle); and kinetic (right) stabilization using bulky substituents.

1.1.1 Cyclic silylenes

1.1.1.1 *N*-Heterocyclic silylenes (NHSis)

N-Heterocyclic carbenes (NHCs), first isolated by Arduengo and co-workers,[2] are isolable compounds stabilized by two adjacent nitrogen atoms bearing bulky substituent groups. A heavier analogue *N*-heterocyclic silylene (NHSi) was first synthesized in 1994 by West and Denk by reduction of the *N*-heterocyclic dichlorosilane precursor **I-1** with elemental potassium in THF solutions (Scheme 1-1).[3] The NHSi **I-2** is thermally stable, both in aprotic organic solvents and in the solid state.
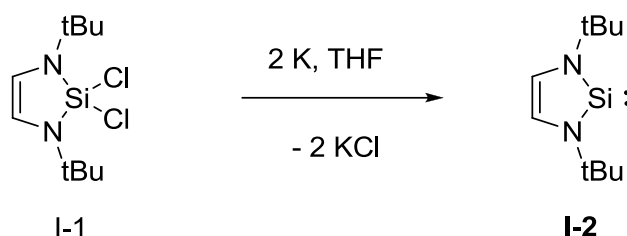
Scheme 1-1. Synthesis of the *N*-heterocyclic silylene **I-2**.

In the following years, analogues of the silylene **I-2** bearing different substituents at nitrogen (e.g., **I-3**, **I-4**, and **I-5**) have been reported by different groups.[4] Moreover, *N*-heterocyclic silylenes with saturated backbones (**I-6** to **I-10**)[5] have also been synthesized by similar methods through reduction reactions of the corresponding dibromosilane precursors with KC_8 (Scheme 1-2).
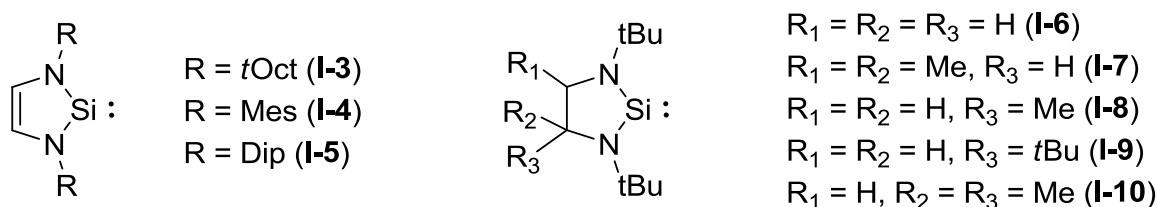
Scheme 1-2. Selected examples of the isolable *N*-heterocyclic silylenes **I-3 – I-10**.

N-heterocyclic silylenes stabilized by benzo- or pyrido-fused backbones (e.g., **I-11**, **I-12,** and **I-13**) have also been reported.[6] Similarly, the bis-silylene-based biphenyl scaffold **I-14** was synthesized by Lappert et al. in 2005 (Scheme 1-3).[7]

R = H, X = CH (**I-11**)
R = Me, X = CH (**I-12**)
R = H, X = N (**I-13**)

I-14
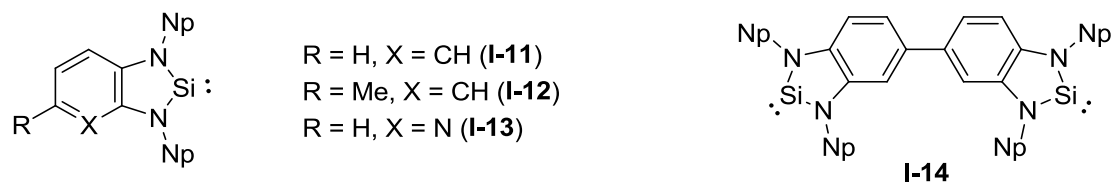
Scheme 1-3. Selected examples of the *N*-heterocyclic silylene.

In 2006, our group obtained the first NHSi stabilized by a *β*-diketiminate-like backbone (**I-16**).[8] It was synthesized by reduction of the respective dibromosilane precursor **I-15** with KC_8 in THF solutions in the form of yellow crystals. Interestingly, the resonance structure of **I-16a** indicated that silylene **I-16** contains two possible nucleophilic centers, one at the Si^{II} atom and the other at the CH_2 carbon atom of backbone (Scheme 1-4).

I-15   **I-16**   **I-16a**
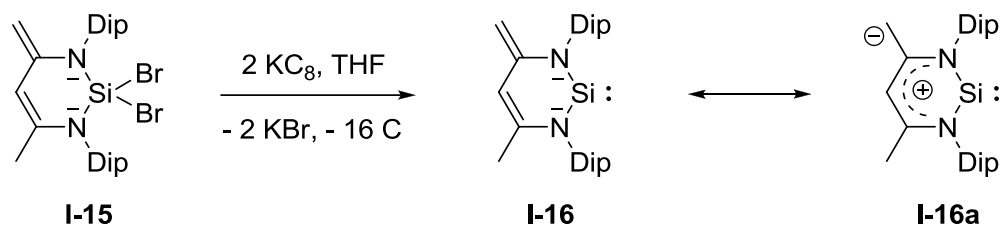
Scheme 1-4. Synthesis of the *N*-heterocyclic silylene **I-16** and its resonance structure

I-16a.

Silylene **I-16** reacts with [Ni(cod)$_2$] in the presence of arenes, giving the corresponding $Ni^0(\eta^6$-arene) complexes, which further reacted with CO to produce the silylene complex **I-17**. The reaction of **I-17** with HX (HX = H_2O, HOTf, HCl, H_2S, NH_3, and NH_2(iPr)) gave the 1,4-addition products (**I-18** to **I-23,** Scheme 1-5).[9]
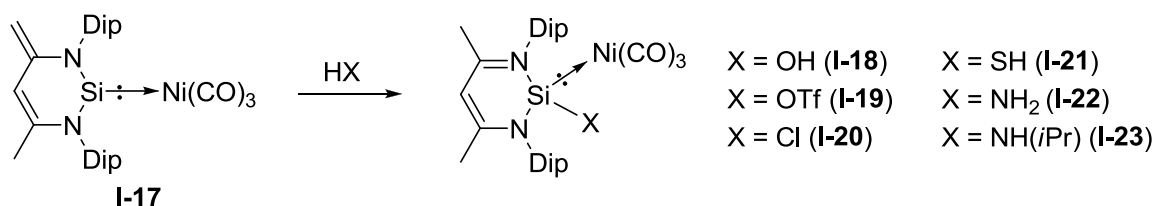
Scheme 1-5. Reactivity of the *N*-heterocyclic silylene Ni complex **I-17**

When silylene **I-16** was allowed to react with 1,3,4,5,-tetramethylimidzol-2-ylidene, an NHSi-NHC adduct was generated at low temperature. However, when the temperature was increased, an sp³ C-H activation took place at the nucleophilic Si^{II} center that yielded the 1,2-addition product *N*-heterocyclic silylcarbene **I-24**.[10] Further treatment of **I-24** with NiBr$_2$(dme) induced a proton migration from the Si center to the nucleophilic center at the *β*-diketiminate-like backbone, and consequently, the silylene–carbene Ni^{II} complex **I-25** was formed (Scheme 1-6).[11]
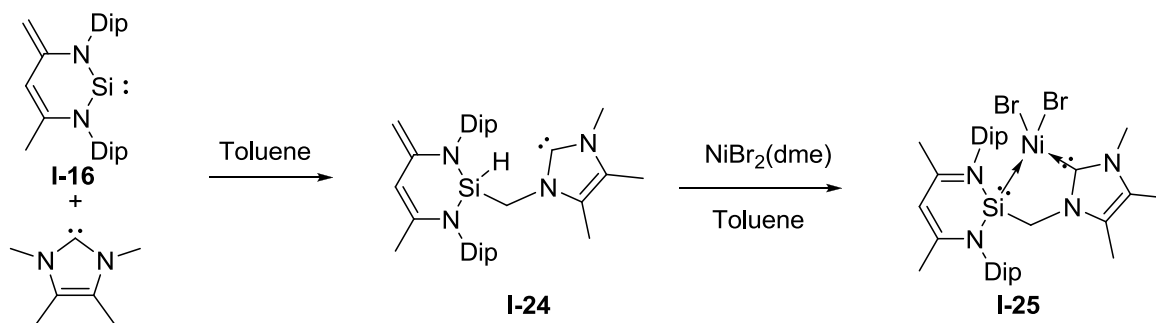
Scheme 1-6. Synthesis of the *N*-heterocyclic silylcarbene **I-24** and silylene–carbene Ni complex **I-25**

In addition to the realization of an *N*-heterocyclic silylene **I-16**, in 2006, Roesky et al. reported the synthesis of the *N,N*-di(*tert*-butyl)amidinato NHSi **I-28**. It was first synthesized by the reduction of a five-coordinate trichlorosilane **I-26** with elemental potassium in THF.[12] Owing to the low yield (10 %), the same group modified the method and employed dichlorohydridosilane **I-27** as a starting material. The dehydrochlorination of **I-27** by LiN(SiMe$_3$)$_2$ or NHCs in toluene gained considerably higher yields (90 %) in gram-scale which enabled and facilitated the further

investigation of silylene **I-28** and its derivatives as ligands in catalysis (Scheme 1-7).[13]
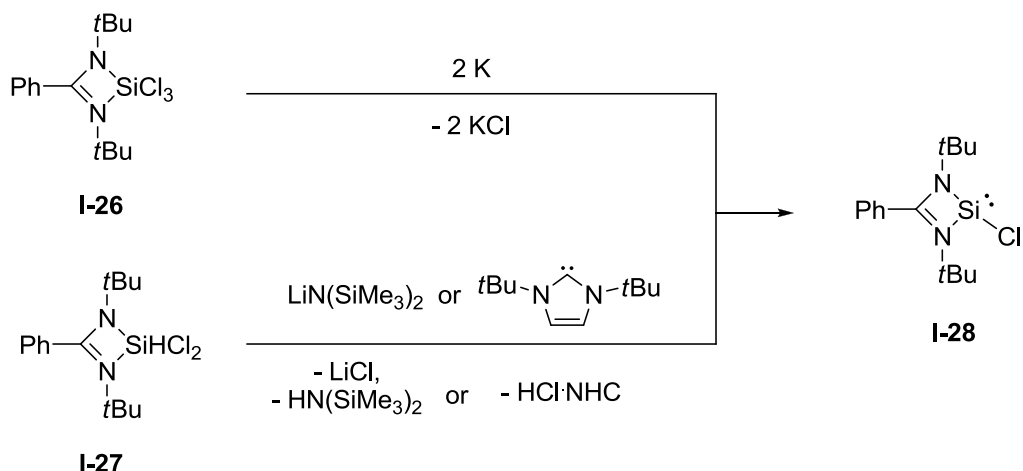
Scheme 1-7. Synthetic routes to the *N*-heterocyclic silylene **I-28** stabilized by the chelating *N,N*-di(*tert*-butyl)amidinato ligand.

When trichlorosilane **I-26** was reduced with 3 molar equivalents of KC_8 in THF, the 1,2-bis-silylene **I-29** was obtained in 5 % yields (Scheme 1-8).[14]
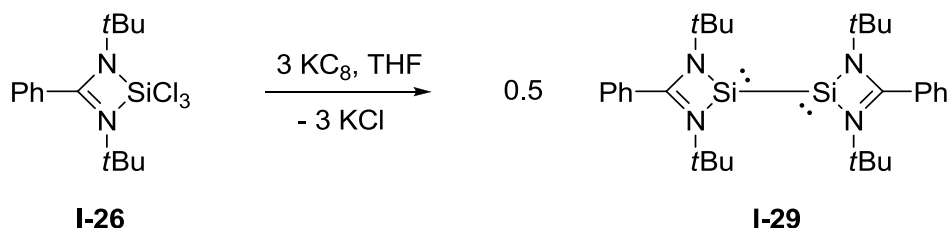
Scheme 1-8. Synthesis of bis-silylene **I-29**.

In 2012 and 2013, Tacke et al. reported the synthesis of silylenes **I-34** and **I-35** stabilized by *N,N*-di(*iso*-propyl)amidinato and guanidinato ligands. They were synthesized through the reduction of six-coordinate chlorohydridosilane precursors **I-32** and **I-33**, respectively.[15] The DFT and spectroscopic evidence pertaining to silylenes **I-34** indicate a rapid exchange of four nitrogen sites of ligands that involves a four-coordinate Si^{II} species in the solutions (Scheme 1-9).
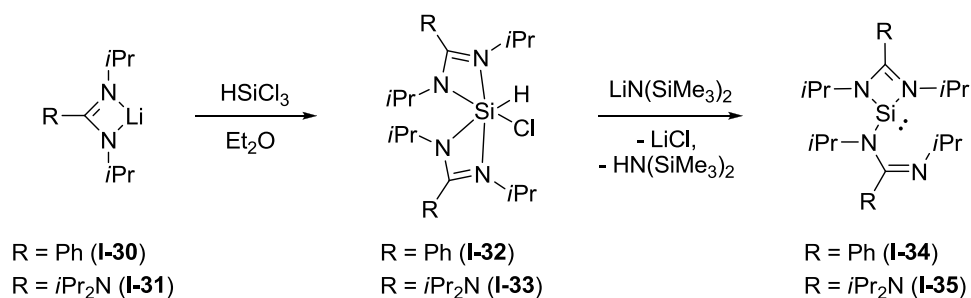
Scheme 1-9. Synthesis of the *N*-heterocyclic silylenes **I-34** and **I-35** stabilized by *N,N*-di(*iso*-propyl)amidinato and guanidinato ligands.

1.1.1.2 Cyclic dialkyl silylenes

For the first time, a silylene stabilized by bulky dialkyl substituents was reported by Kira et al. in 1999.[16] Dialkylsilylene**s I-37** was prepared through the reduction of the dibromosilane precursor at low temperature. **I-37** remains stable in the solid state at room temperature but easily undergoes intramolecular 1,2-silyl migration to generate the cyclic silylene **I-38** (Scheme 1-10).
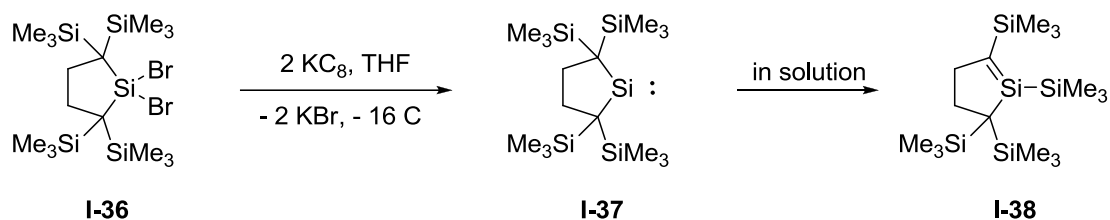
Scheme 1-10. Synthesis and thermal isomerization of dialkylsilylenes **I-37**.

The analogues of silylene **I-37** have also been synthesized by other research groups. However, instead of intramolecular 1,2-silyl migration, silylene **I-39** undergoes dimerization that produced the disilene (**I-39**)$_2$.[17] In sharp contrast to silylene **I-39**, the intramolecular 1,2-silyl migration of silylene **I-40** takes place at an extremely fast rate in solutions (the half-life time is only 20 min at 20 °C).[18] Furthermore, silylenes **I-41** and **I-42** bearing phosphorus ylide moieties were obtained through the reaction of the corresponding dibromosilane precursors with an excess of KC$_8$ in THF or DME (Scheme 1-11).[19]
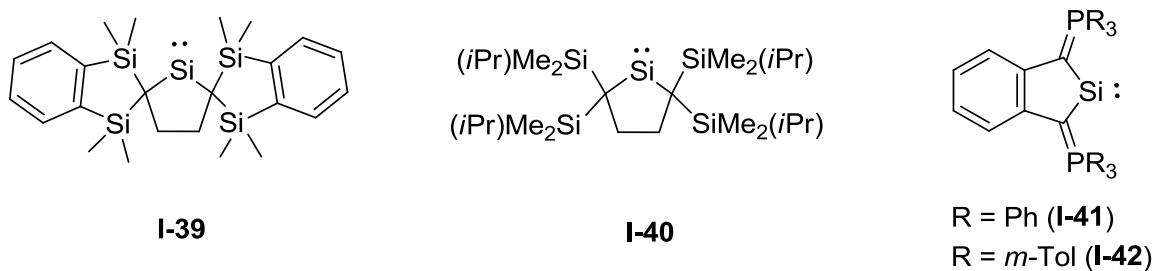
Scheme 1-11. Selected examples of dialkylsilylene**s, I-39 – I-42**.

1.1.1.3 N,P- and C,N- Stabilized silylenes

Phosphine-containing backbones have also been employed as ligands for the stabilization of silylenes. Kato and Baceiredo et al. reported the first phosphine stabilized silylene **I-43** in 2009.[20] It was synthesized by reducing the dichlorophenylsilane starting material with elemental magnesium in THF solutions. Subsequently, in 2011, the same group isolated the analogues **I-44** and **I-45** with a similar synthetic method (Scheme 1-12).[21]
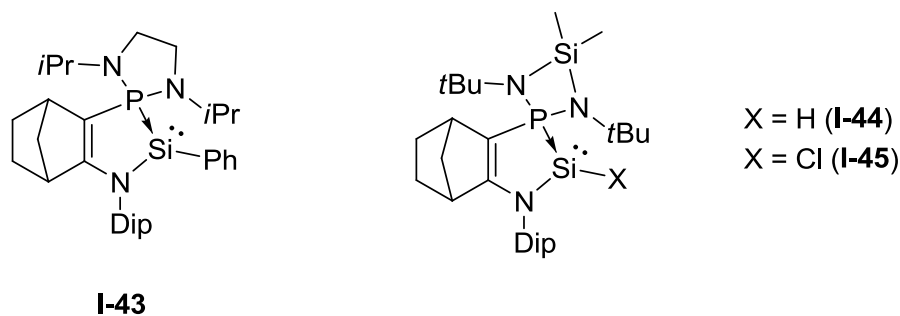
Scheme 1-12. Selected examples of phosphine-stabilized silylenes, **I-43 – I-45**.

The reduction of trichlorosilane with an excess amount of elemental lithium (3 molar equivalents) in THF solutions gave the bis-silylene **I-47** in 13 % yields (Scheme 1-13).[22]
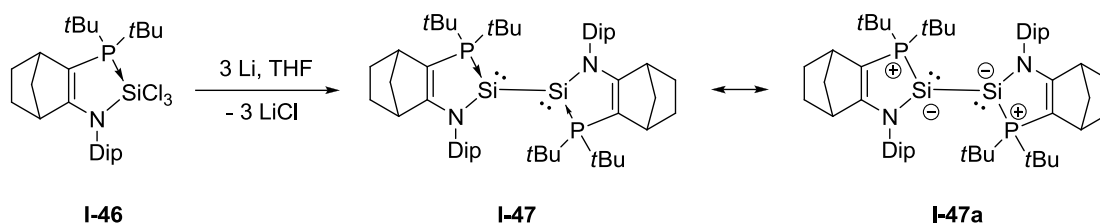
Scheme 1-13. Synthesis of phosphine-stabilized bis-silylene**s I-47**.

Quite recently, cyclic silylenes stabilized by one nitrogen and one carbon substituent were developed by different research groups. These include the cyclic amino(ylide)silylene **I-48** reported by Kato and Baceiredo et al. in 2016.[23] In the same year, Iwamoto et al. prepared the cyclic alkyl(amino) silylene **I-49** with the application of a similar reduction method.[24] Very recently, Xie et al. obtained an NHC stabilized cyclic amino(carboranyl) silylene **I-50** by dehydrochlorination of the corresponding chlorohydridosilane precursor. (Scheme 1-14).[25]
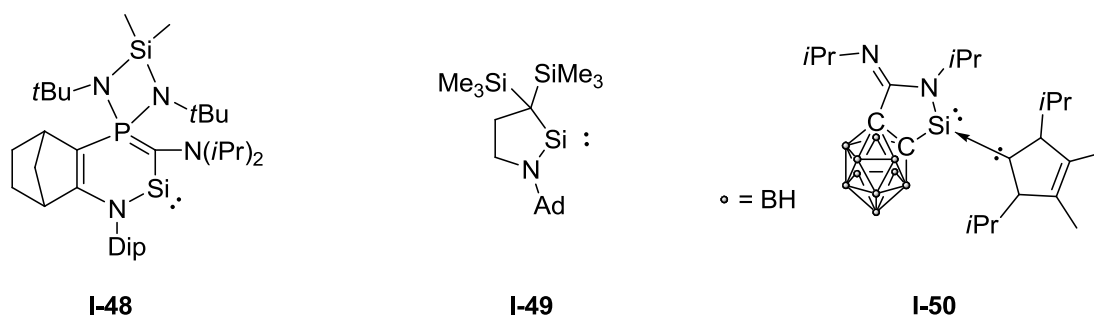
Scheme 1-14. Selected examples of cyclic *N,C*-chelating silylene**s I-48 – I-50**.

1.1.2 Acyclic silylenes

The acyclic silylene **I-51** was generated through the reduction of the corresponding dibromosilane precursor with KC$_8$.[26] However, **I-51** was persistent only for 12 hours at − 20°C and decomposed at room temperature. When bulkier substituents were introduced, the stable acyclic silylenes **I-52, I-53,** and **I-54** could be prepared.[27] Remarkably, it was observed that acyclic silylene **I-53** undergoes H$_2$ activation at room temperature owing to the smaller HOMO–LUMO gap by taking

advantages of the widened bond angle at silicon and the strong σ-donor character of the boryl ligand. Furthermore, Power et al. reported the thioaryl stabilized acyclic silylene **I-55** and **I-56** in 2012, obtained through the reduction of the corresponding dibromosilane precursors (Scheme 1-15).[28]

I-51   **I-52**   **I-53**

I-54

R = Mes (**I-55**)
R = Dip (**I-56**)
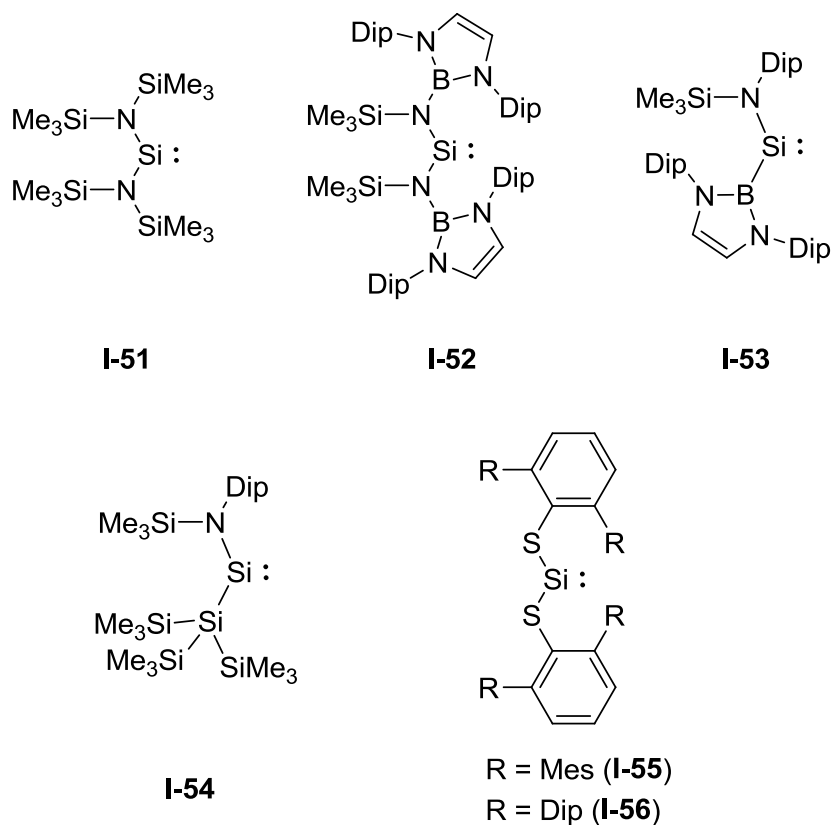
Scheme 1-15. The acyclic silylenes **I-51 – I-56**.

Interestingly, through the reaction of the disilene (*t*Bu$_2$MeSi)$_2$Si=Si(SiMe*t*Bu$_2$)$_2$ with metal naphthalenide (M = Li, Na) in the presence of crown ethers, the silylene radicals anions **I-57** and **I-58** could be synthesized in 56% yields by Sekiguchi et al. in 2007.[29] Compound **I-59** represents another ionic silylene that was prepared by exposing the corresponding cationic chromium silylidyne complex to CO in fluorobenzene solutions (Scheme 1-16).[30]
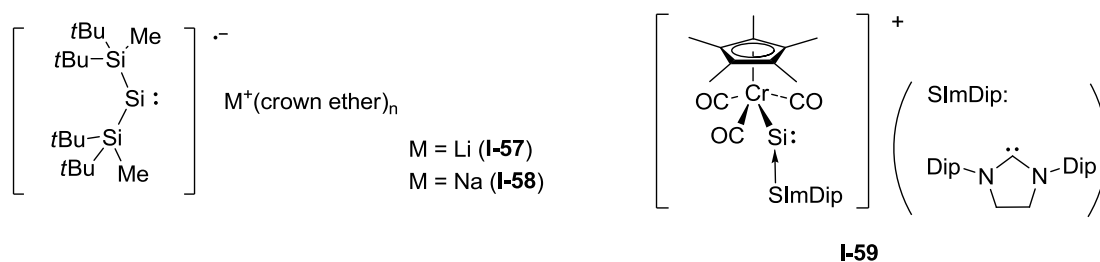
Scheme 1-16. The ionic acyclic silylenes **I-57 – I-59**.

The first isolable stable Si^{II} compound, decamethylsilicocene **I-60** ($Cp*_2Si$), was synthesized in 1986 by Juzti et al. through the reduction of dichlorosilane precursors with lithium/sodium/potassium naphthalenides (MNap, M = Li, Na, K) or decamethylsamarocenes ($Cp*_2Sm$, $Cp*_2Sm(THF)_2$).[2] The reaction of decamethylsilicocene **I-60** with protonated pentamethylcyclopentadiene yielded a $Cp*Si^+$ salt that further reacted with different kinds of metallated ligands to generate the derivatives **I-61 – I-63** (Scheme 1-17).[31]
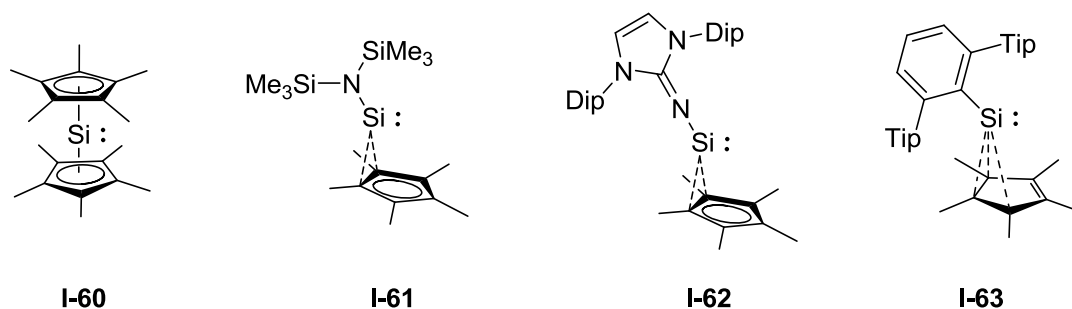
Scheme 1-17. Decamethylsiliocene **I-60** and its derivatives **I-61 – I-63**.

1.2 Silylene-supported low-valent main-group compounds

Low-valent main-group compounds (e.g., containing B^I, C^0, C^{II}, Al^I, Si^0, Si^{II}, P^I, Ga^I, Ge^0, As^I) are highly reactive species. The synthesis and isolation of these compounds attracted much research attention in recent years.[1c-1e] In addition to the widely used ligands containing C, N, P centers, Si^{II}-based ligands have recently also been developed to stabilize the low-valent main-group compounds. Here in this part, the progress of silylene stabilized low-valent main-group species will be summarized.
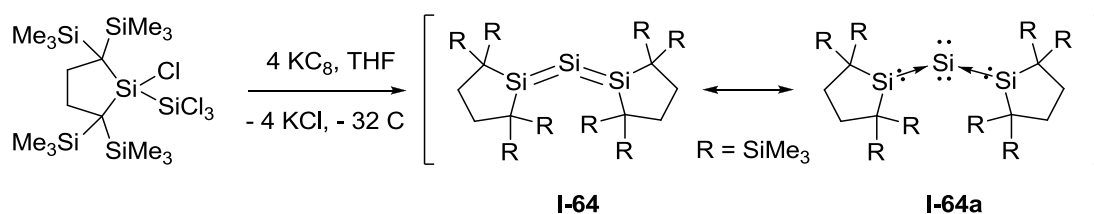
Scheme 1-18. Synthesis of silicon(0) compound **I-64**.

Recently, the isolations and X-ray characterizations of 14 group heavier analogues of allenes, (trisilaallene **I-64**, trigermaallene, 1,3-digermasilaallene, and 2-germadisilaallene **I-65**) were reported by Kira et al.[32] In sharp contrast to allenes, these heavy analogues of allenes possessed bent configuration (E-E'-E bond angels = 122 - 156°) and terminal substituents deviated from the orthogonal arrangement. These results indicated that the heavier allenes are more similar to carbodicarbene $C'(HNC)_2$, which had experimental C-C'-C bond angle of 134.8° for $C'(HNC^{Bz})_2$ (benzoannelated carbodicarbene) and theoretical calculated C-C'-C bond angle of 131.8° for $C'(HNC^{Me})_2$.[33] Later, theoretical calculation by groups of Frenking and Apeloig also suggested that these heavy allenes can be described as ylidones, $L \rightarrow :E: \leftarrow L$ (**I-64a** and **I-65a**), in which the E atom bears two lone pairs and have donor-acceptor interactions with the silylene ligands (Scheme 1-18 and 1-19).[33b, 34]
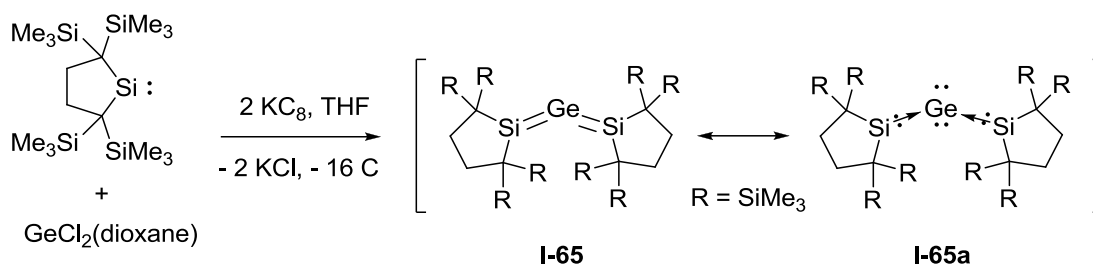
Scheme 1-19. Synthesis of germanium(0) compound **I-65**.

Very recently, Kato et al. prepared an isolable donor-stabilized silavinylidene phosphorane from the reaction of the corresponding phosphine-stabilized silylenes (**I-66 – I-68**) with P,S-bis-ylide **I-69**.[35] Compounds **I-70 – I-72** can be considered as carbon(0) complexes featuring a phosphine and a donor-stabilized silylene ligand, present central carbon atoms with remarkably high electron density (−1.82) (Scheme 1-20).

$X = (CH_2)_2, Y = CH_2$ (**I-66**)
$X = Y = CH_2$ (**I-67**)
$X = Y = (CH_2)_2$ (**I-68**)

I-69

$X = (CH_2)_2, Y = CH_2$ (**I-70**)
$X = Y = CH_2$ (**I-71**)
$X = Y = (CH_2)_2$ (**I-72**)
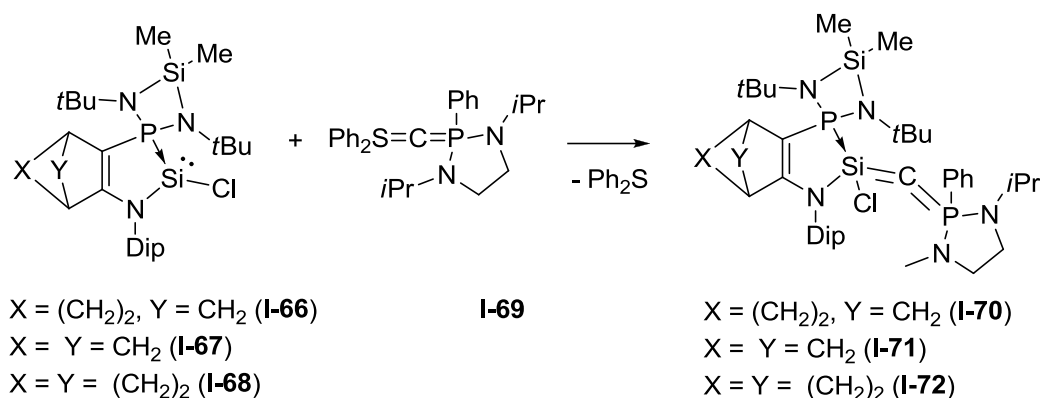
Scheme 1-20. Synthesis of carbon(0) compound **I-70 – I-72**.

The experimental electron-density study suggests the delocalization of the σ-lone pair at the carbon atom toward the silicon center, which is remarkably different from the electronic situation of other bent allene-type molecules. These observations indicate the electron-donating ability of donor-stabilized silylene ligands, as well as their excellent electron acceptor properties.

The utilization of mono-silylene **I-73** as a ligand for low-valent group 14 species was developed by So et al. The reaction of the amidinato silylene **I-73** with

GeCl$_2$(dioxane), SnCl$_2$ and PbBr$_2$ in toluene afforded the corresponding mono-silylene adducts (**I-74 – I-76**, Scheme 1-21).[36]
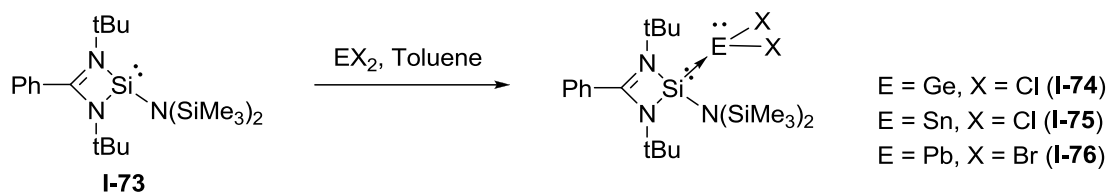
Scheme 1-21. Synthesis of metallylenes **I-74 – I-76** stabilized by silylene **I-73**.

Further reduction of **I-74** with two molar equivalents of KC$_8$ in toluene at room temperature gave the silylene-stabilized digermanium(0) complex **I-77**.[36b] X-Ray crystallography and theoretical studies showed that the silylene ligands stabilize the singlet digermanium(0) moiety by a weak synergetic donor-acceptor interaction (Scheme 1-22).
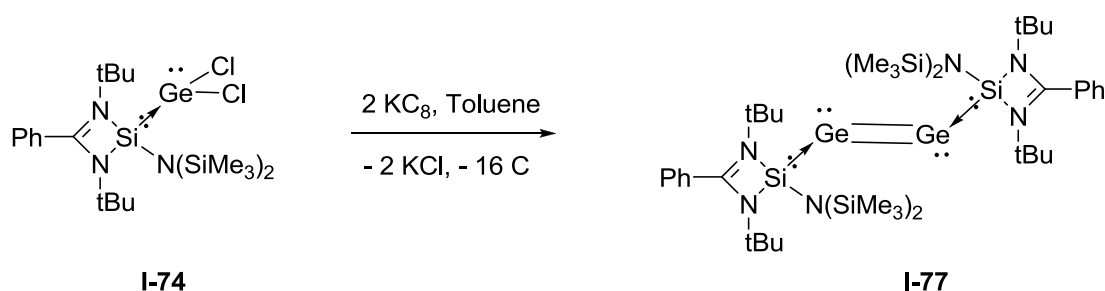
Scheme 1-22. Synthesis of digermanium(0) complex **I-77** stabilized by silylene **I-73**.

Very recently, a bis-silylene ligand has been used to stabilize boron(I) compounds. Xie et al. prepared the bromoborylene **I-78** by reducing the bis-silylene stabilized boron tribromide.[37] A borylene cation stabilized by bis-silylene and CO (**I-79**) was generated via the reaction of **I-78** with W(CO)$_6$. The borylene cation **I-79** was found to cleave dihydrogen in THF at 80 °C and afforded the corresponding borane cation **I-80** (Scheme 1-23).
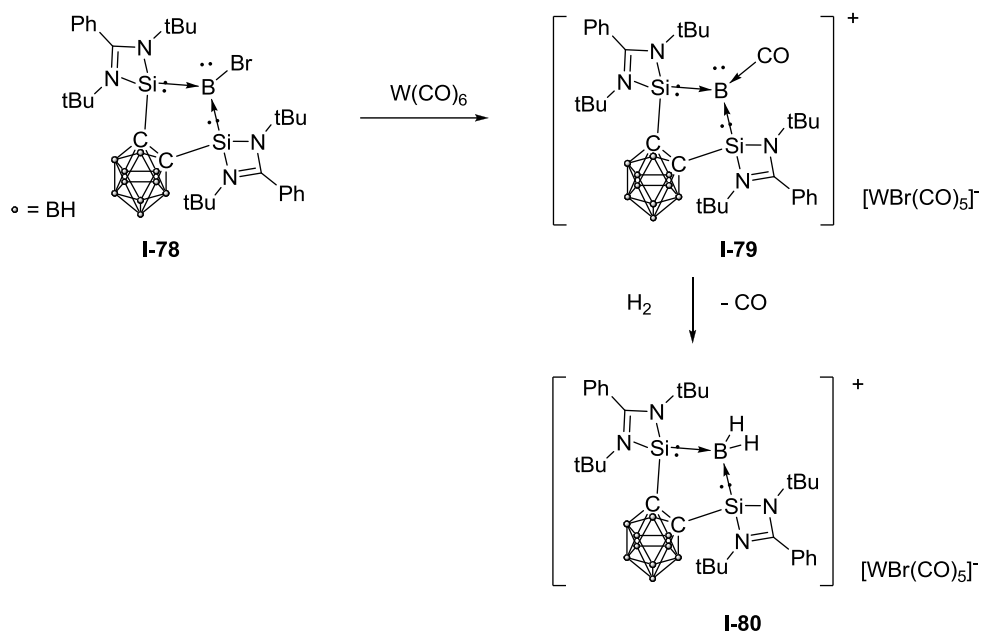
Scheme 1-23. Reactivity of boron(I) complex **I-78** stabilized by bis-silylene.

1.3 Silylene ligands in catalysis

NHCs and their metal complexes have been employed as versatile (pre)catalysts for various types of organic catalytic transformations since 1990's.[38] Subsequently, silylenes, the silicon analogues of carbenes, are no longer laboratory curiosities but valuable building blocks for the synthesis of new functional silicon compounds with high potential exceeding the Lewis donor properties of NHCs and phosphines. Since the first report on Suzuki cross-coupling using the monodentate silylene-Pd^0 complex as (pre)catalyst, substantial progress has been made in this field.
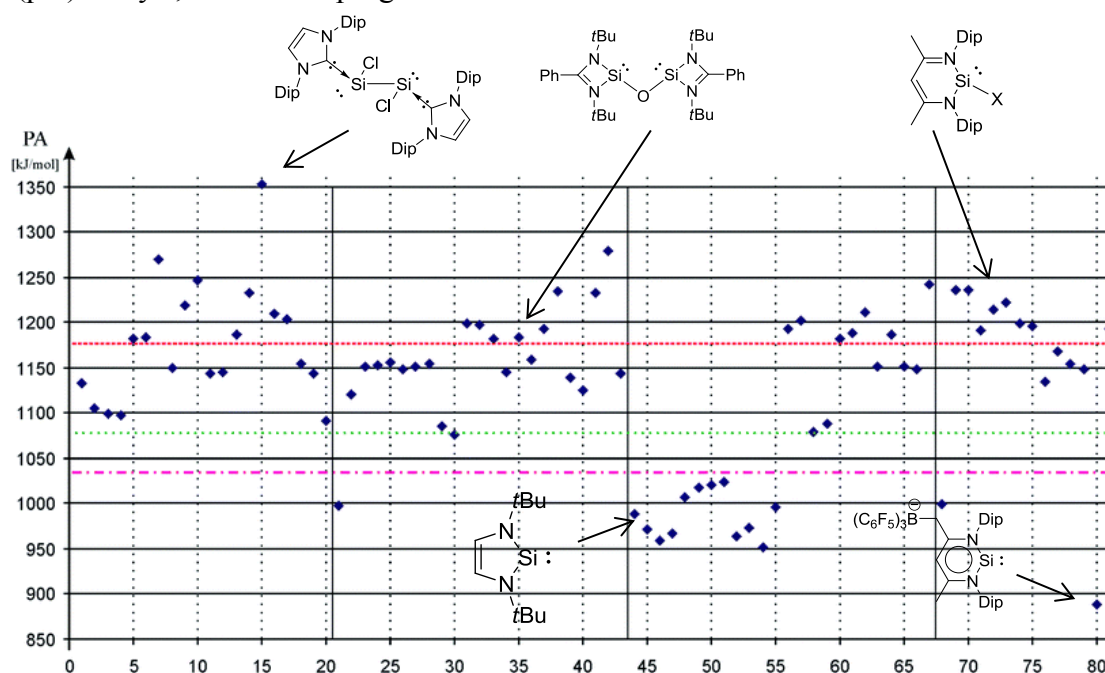
Figure 1-2, DFT calculated proton affinity (PA) of Si^{II} compounds in kJ·mol^{-1}. Horizontal red, green, and pink lines show proton affinity of NHC^{Dip} (1176 kJ·mol^{-1}), PPh$_3$ (1031 kJ·mol^{-1}), and PCy$_3$ (1072 kJ·mol^{-1}), respectively.[38d]

Moreover, the σ-donor and π-acceptor ability, ligand-to-metal charge transfer, and steric parameters of several low-valent silicon compounds have been calculated at B97-D/6-31G* level, with Def2-TZVP basis on heavier atoms by Szilvási et al.[38d] Proton affinity (PA) is a widely used theoretical parameter to quantify the σ-donor strength. According to DFT calculation, silylenes bearing two-coordinate Si centers show relatively low proton affinities. However, the proton affinities of most silylenes

bearing three-coordinate Si centers are higher than those of phosphines (1031 and 1072 kJ·mol^{-1}), and NHC (1176 kJ·mol^{-1}) (Figure 1-2), which indicate that corresponding Si^{II} ligands could compete the widely used phosphine and NHC ligands due to their stronger σ-donor strengths.

Silylene ligands have demonstrated their excellence in various catalytic transformations including carbon-carbon bond formation reactions, carbon-heteroatom bond formation reactions, and reduction reactions. Silylene ligands are not a simply isoelectronic replacement for phosphine and carbene ligands, but facilitate catalytic efficiencies by taking advantage of the strong σ donating ability along with cooperative effects. Excellent chemo-, region-, and stereo-selective have also been achieved by versatile silylene containing catalyst systems. In this part, the progress of silylenes in catalysis research will be summarized.

1.3.1 Classification of silylene ligands

Monodentate silylenes are the simplest silylene ligands. The first example of silylene applied in catalysis was NHSi **I-2** bearing a two-coordinate Si^{II} center.[39] Then, *β*-diketiminate NHSi **I-20**[40] and *N,N*-di(*tert*-butyl)amidinato NHSi **I-28** and **I-82**[41] bearing three-coordinate Si^{II} centers were also introduced as ligands. Very recently, the base-stabilized silacyclopropylidene **I-85** (Kato and Beceiredo et al. in 2016),[42] dialkylsilylene **I-37** (Iwamoto et al. in 2016),[43] and cyclic alkyl(amino) silylene **I-49** (Iwamoto et al. in 2017)[44] have also been used as ligands in hydrosilylation reactions (Scheme1-23).

I-2   I-20   R = Cl (**I-28**)   R = NMe$_2$ (**I-83**)
                          R = H (**I-82a**)   R = Ph (**I-84**)
                          R = Me (**I-82b**)

I-85   I-37   I-49
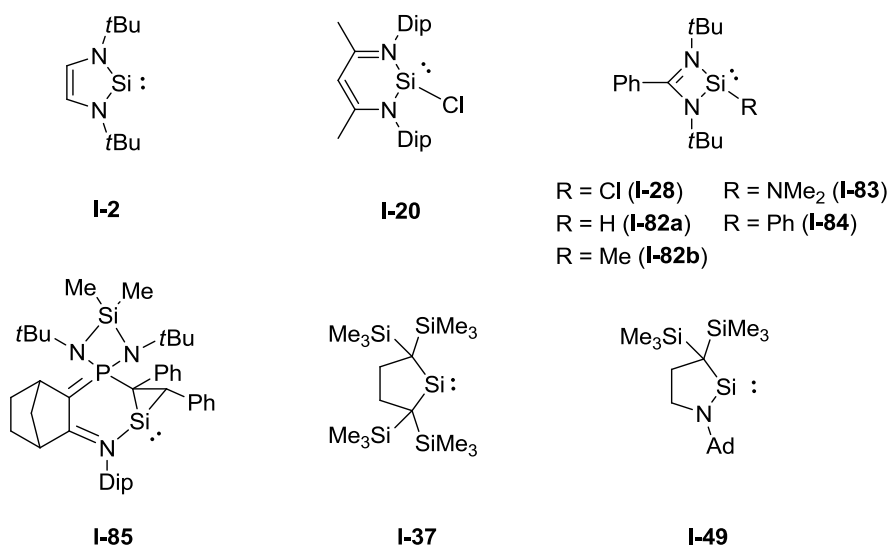
Scheme 1-23. Chemical structures of monodentate silylene ligands used in metal-mediated catalysis.

Apart from the monodentate silylenes, multidentate chelating silylenes constitute another important family of ligands. The largest number of bidentate silylene ligands is constituted by the derivatives of *N,N*-di(*tert*-butyl)amidinato NHSi, which were mainly (except **I-87**) synthesized by the salt metathesis reactions of *N,N*-di(*tert*-butyl)amidinato chloro-silylene **I-28** with the corresponding metallated spacing groups. Among these ligands, **I-86**, **I-87**, **I-88**, and **I-89** represent known bis-silylenes ligands. In addition, **I-90** and **I-91** represent silylene-mesitylenyl and silylene-silyl mixed ligands. Moreover, **I-92** constitutes a mixed NHC-NHSi chelate ligand tautomerized through proton migration from the silicon center of silane **I-24** to the *β*-diketiminate backbone owing to the pronounced Brønsted basicity of the exocyclic methylene carbon (Scheme1-24).
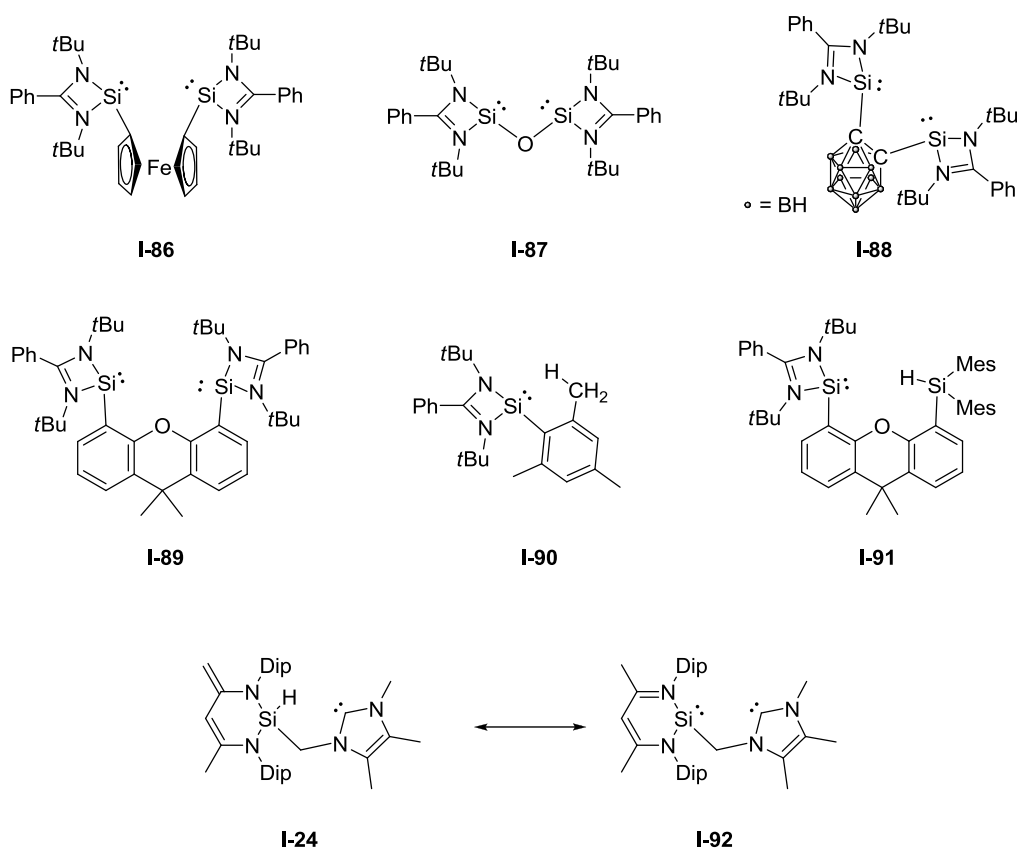
Scheme 1-24. Chemical structures of bidentate silylene ligands.

Pincer-type ligands signify multidentate scaffolds. Due to their versatile nature and the facile entry of different functional groups into their backbone, their application has been instrumental in the development of organometallic chemistry, and in particular, in studying homogeneous catalysis. The pincer-type silylene ligands **I-93** (SiCSi), and **I-94** (SiNSi) were prepared through salt metathesis reactions of chloro-silylene **I-28** with metallated pincer-like arene backbone and pyridine backbone, respectively (Scheme1-25).
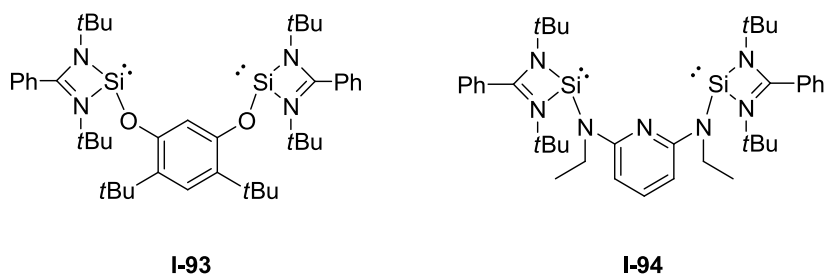
Scheme 1-25. Chemical structures of tridentate silylene (pincer) ligands.

Multidentate silylenes with different spacers possess specific structural and electronic features. For instance, the flexibility of bis-silylene can be controlled by the desired spacing groups. The ferrocene-based bis-silylene is flexible due to the possible rotation of the C_5H_4SiL ring along the axis crossing the C_5H_4SiL rings and Fe atom. However, if the xanthene backbone is employed, the corresponding bis-silylene becomes semi-flexible. Two phenyl rings can twist toward each other along the axis crossing the O and C(9). For example, the dihedral angle of two phenyl rings in Ni^0 coordinated bis-silylene ligand is 38.22°, signifying a high degree of folding, compared to that observed in the free ligand (the dihedral angle of 7.61°).[45] In sharp contrast to these flexible backbones, when the rigid *ortho*-carborane is introduced, corresponding bis-silylene become a fixed ligand (Scheme1-26).

Flexible backbone   Semi-flexible backbone   Fixed backbone
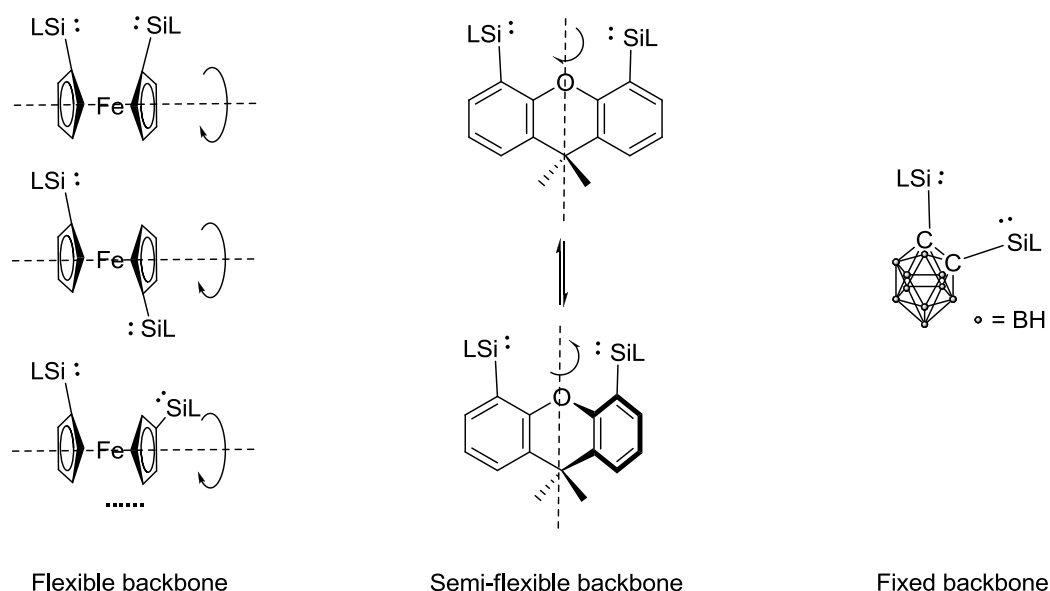
Scheme 1-26. The flexibility of multidentate silylene ligands.

1.3.2 Electronic features of silylene ligands

The electronic features of silylene ligands vary according to the different backbones. Dialkylsilylene ligand **I-37** bears the most electronically deficient two-coordinate Si^{II} center with ^{29}Si NMR shift of 576.4 ppm.[16] Cyclic alkyl(amino)

silylene ligand **I-49** has a more shielded Si^{II} nucleus (^{29}Si NMR around 280 ppm) because of the π-donor bonding interaction with the nitrogen atom.[42] In stark contrast, two-coordinate NHSi ligands **I-2** hold relatively electron-rich Si^{II} centers with ^{29}Si NMR chemical shifts around 120 ppm.[3] Through additional donor stabilization, three-coordinate silylenes have more electron-rich Si^{II} centers. For instance, the ^{29}Si NMR shift of -87.5 ppm in base-stabilized silacyclopropylidene ligand **I-85** indicates a quite electron-rich Si^{II} center.[46] Remarkably, among three-coordinate silylenes bearing *β*-diketiminate and *N,N*-di(*tert*-butyl)amidinato backbones enable tuning of the σ donor strengths by taking advantage of easily modified X substitutions (Scheme1-27).
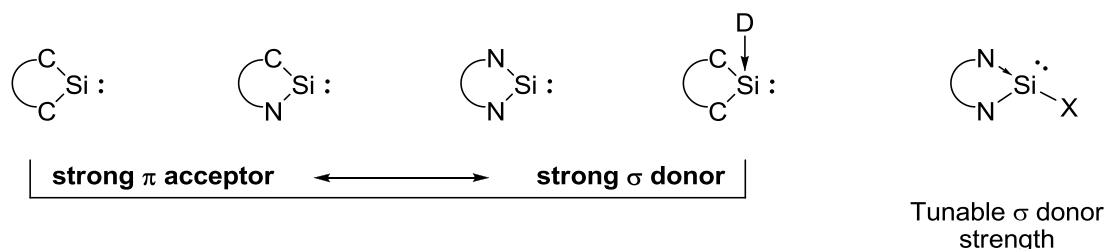
Scheme 1-27. Tuning the σ-donor abilities of different cyclic silylene ligands.

The tunable σ donor strengths of *β*-diketiminate silylene ligands were investigated by monitoring the IR spectra of the carbonyl stretching frequencies ($v(CO)$) of corresponding $Ni(CO)_3$ complexes.[9a] The reactions of silylene Ni^0 complex **I-17** ($v(CO) = 2076$ cm^{-1}) with NH_3, $NH_2(iPr)$, H_2O, H_2S, and HOTf gave corresponding 1,4-adducts **I-22** ($v(CO) = 2046$ cm^{-1}), **I-23** ($v(CO) = 2048$ cm^{-1}), **I-18** ($v(CO) = 2050$ cm^{-1}), **I-21** ($v(CO) = 2054$ cm^{-1}), and **I-19** ($v(CO) = 2066$ cm^{-1}). Among these, the $v(CO)$ value of complex **I-17** is comparable to that of the $Ni(CO)_3$ complex **I-98** with the weak σ-donor and strong π-acceptor PF_3 ligand (2111 cm^{-1}). In contrast, 1,4-adducts **I-22**, **I-23**, and **I-18** show lower $v(CO)$ values akin to that of $Ni(CO)_3$ complex **I-95** with an NHC ligand (2054 cm^{-1}) (Scheme1-28).
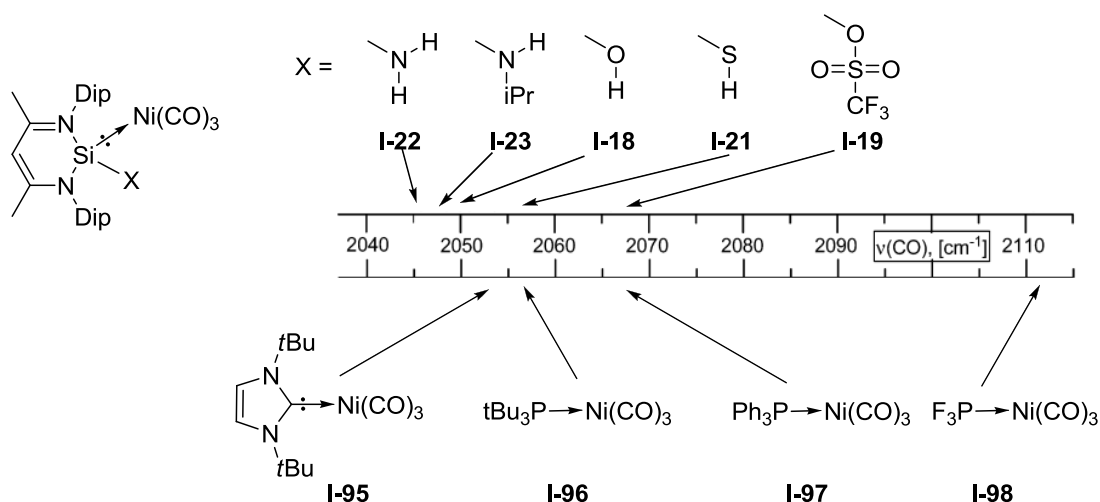
Scheme 1-28. Comparison of the carbonyl stretching modes (A$_1$) of silylene-Ni(CO)$_3$ complexes with related phosphine and NHC analogous.

Compared to these of *β*-diketiminate silylene ligands, the modifications of *N,N*-di(*tert*-butyl)amidinato-based silylene ligands are considerably straightforward. The reaction of the chlorosilylene precursor **I-28** with the corresponding metallated compounds allow the exchanges carried out between chloro-substitution and other more sophisticated spacing groups (e.g., multidentate spacing groups). Since the first report of bis- (amidinato silylene) ligand bridged with an oxygen atom in 2010, Driess et al. have developed a series of bis-(amidinato silylene) ligands that can be classified as 1) strong σ donating electron-rich ligands bearing nitrogen and oxygen substitutions with ^{29}Si NMR chemical shift from –24.0 ppm to –14.9 ppm; 2) moderate strength σ donating ligands bearing carbon substitutions with ^{29}Si NMR from 17.3 ppm to 18.9 ppm; 3) weak σ donating electron-deficient ligand bearing ferrocene substitution with a ^{29}Si NMR chemical shift of 43.3 ppm (Scheme1-29).
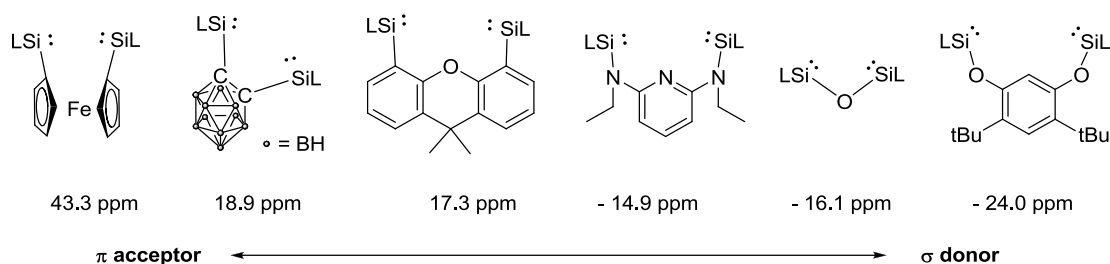
Scheme 1-29. Tunable donor-acceptor abilities of multidentate silylene ligands based on N,N-di(*tert*-butyl)amidinato backbones. (L = PhC(N*t*Bu)$_2$).

1.3.3 Applications in catalysis

1.3.3.1 Carbon-carbon bond formation reactions

In 2001, silylene ligand **I-2** was first time introduced into catalysis by Fürstner et al.[39] The dinuclear Pd^0 complex **I-99** bearing bridged silylene ligand was synthesized by directly reacting Pd(PPh$_3$)$_4$ with silylene ligand **I-2**. Catalytic tests indicated silylene complex **I-99** is a very active catalyst in the Suzuki coupling reaction of aryl boronic acids with bromoarenes (Scheme 1-30).
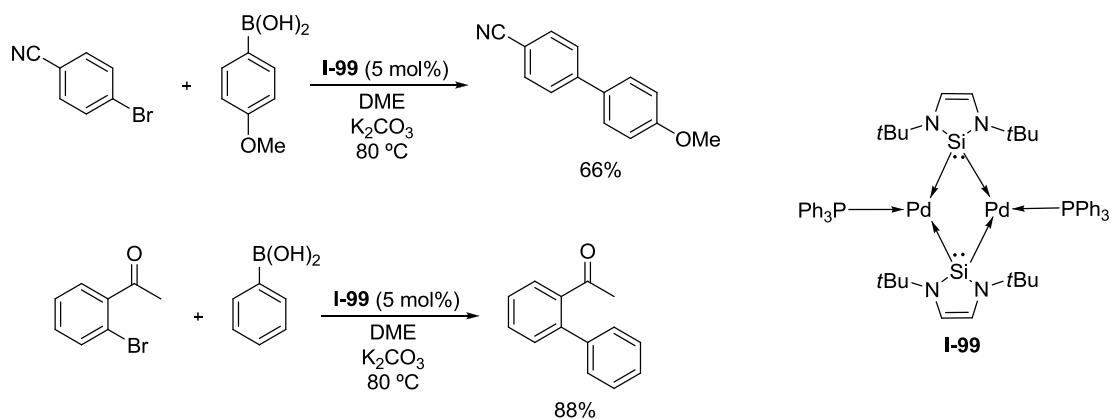
Scheme 1-30. Suzuki cross-coupling using the monodentate silylene-Pd^0 complex **I-99**.

In 2008, Roesky et al. prepared another catalytically active Pd^{II} complex **I-100** bearing same silylene ligand (**I-2**) in a similar method.[47] Complex **I-100** was

subsequently employed in the Heck coupling of bromoacetophenone and styrene at 140 °C (full conversion after 24h, Scheme1-31).
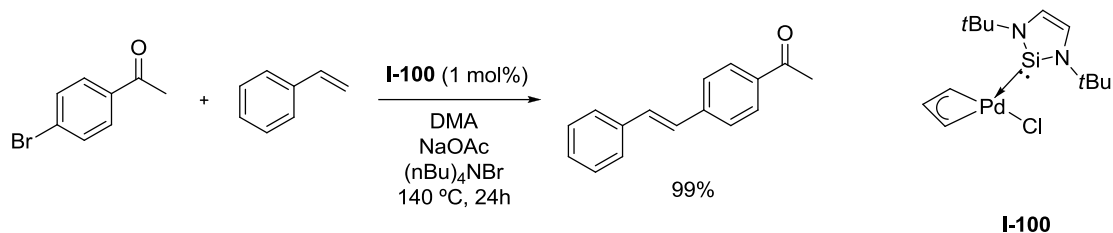
Scheme 1-31. Heck coupling of bromoacetophenone and styrene using silylene-Pd^{II} complex **I-100**.

In 2010, the first chelating bis-silylene ligand **I-87** was developed by dehydrochlorination of the amidinate disiloxane [LSiH(Cl)-O-SiH(Cl)L] (L = PhC(N*t*Bu)$_2$) precursor with [(CH$_3$)$_3$Si]$_2$NLi.[48] Further reaction of **I-87** with Ni(cod)$_2$ in toluene gave the corresponding Ni^0 complex **I-101** (Scheme 1-32).
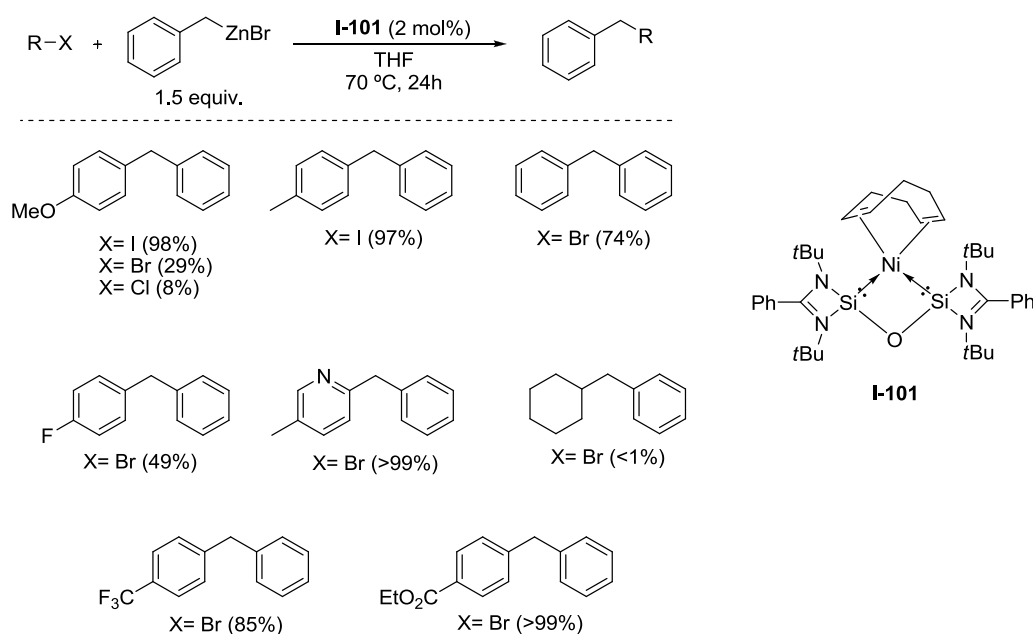
Scheme 1-32. Nickel-catalyzed C–C bond formation of benzylzinc bromide with various aryl halides using **I-101** as precatalyst.

Three years later, Inoue and Enthaler et al. employed the complex **I-101** as precatalyst for C-C bond coupling reactions.[49] It was shown that the **I-101** efficiently catalyzes the C-C cross-coupling reaction of aryl halides with Grignard and organometallic zinc reagents with good yields (Schemes 1-32 and 1-33).
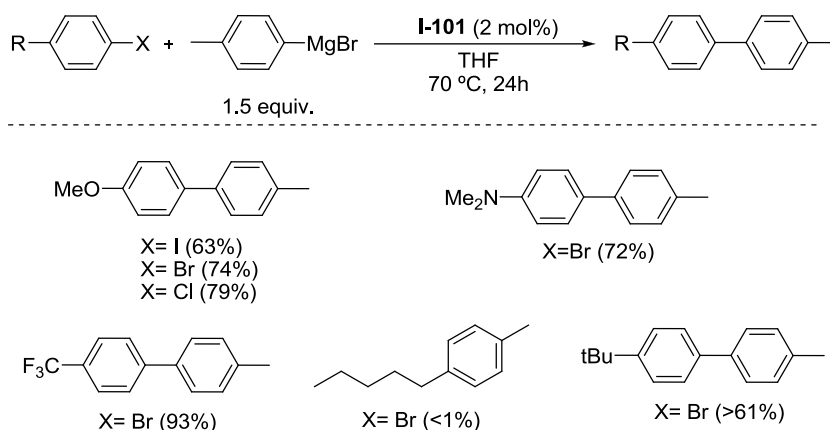
Scheme 1-33. C–C bond formation of Grignard reagents with different aryl halide derivatives using the **I-101** precatalyst.

In 2015, mixed chelating NHC-NHSi ligand coordinated Ni^{II} complex **I-102** was synthesized through the reaction of NiBr$_2$(dme) with *N*-heterocyclic silylcarbene **I-24**.[11] **I-102** was then exploited in Kumada–Corriu-type cross-coupling reactions and found to give very promising catalytic performances with the highest yield of 99 % (Scheme 1-34).
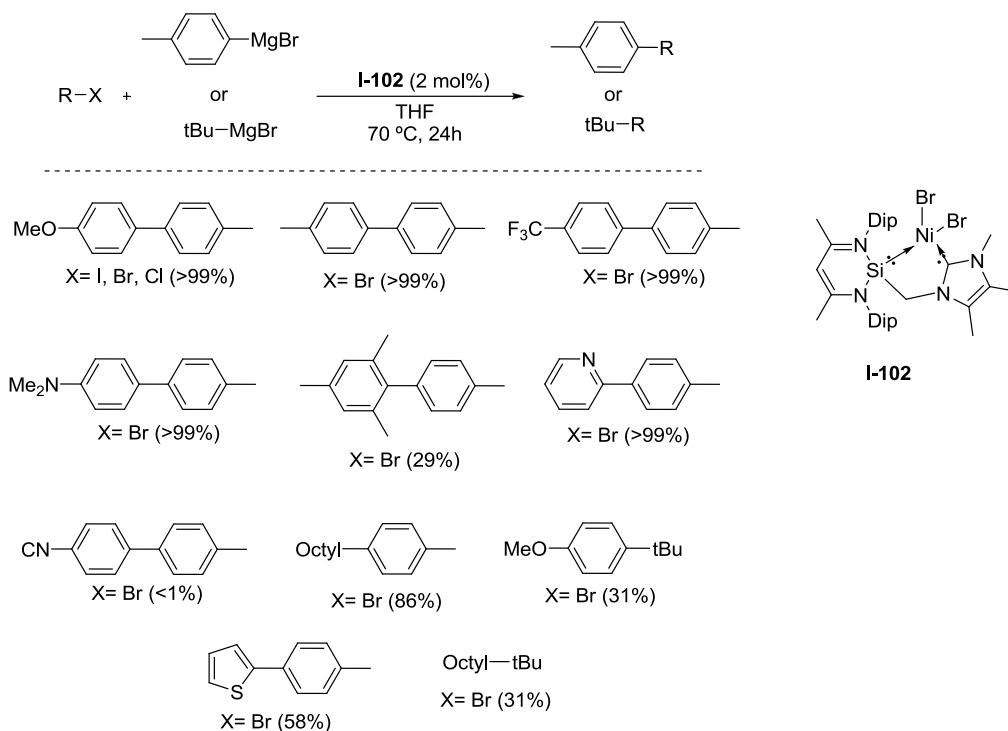
Scheme 1-34. Kumada–Corriu-type cross-coupling reactions catalyzed by silylene-Ni complex **I-102**.

The corresponding pincer-type nickel complex **I-103** was prepared through the reaction of silylene ligand **I-93** with NiBr$_2$(dme) in the presence of excess NEt$_3$.[50] **I-103** was found to be a superior candidate for C-H activations and applied successfully for the Sonogashira cross-coupling reaction of phenylacetylene with 1-octenyl iodide (Scheme 1-35).
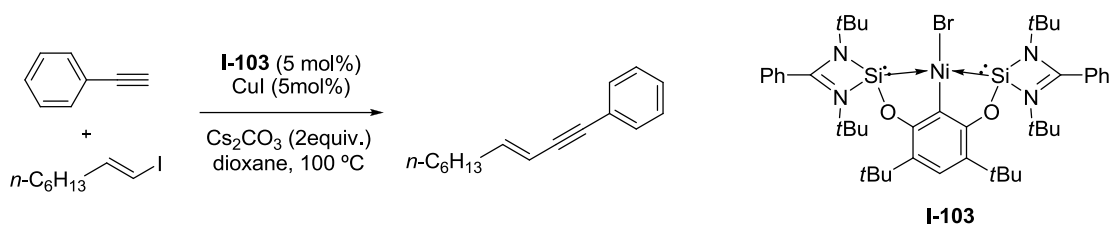
Scheme 1-35. Sonogashira cross-coupling reaction catalyzed by silylene-Ni complex **I-103**.

In addition to C-C cross-coupling reactions, silylene ligands have also been applied in cyclotrimerization and hydroformylation reactions for C-C bond formations. In 2012, the catalytically active Co^I complex **I-104** bearing the ferrocene bridged bis-silylene ligand **I-86** was synthesized by reducing the $CoBr_2$ coordinated silylene with KC_8 in the presence of NaCp.[51] Complex **I-104** was investigated as (pre)catalyst for the [2 + 2 + 2] cyclotrimerization reaction of phenylacetylene, forming two isomeric species of triphenylbenzene, and phenylacetylene/acetonitrile, which resulted in the formation of substituted pyridines (Scheme 1-36).
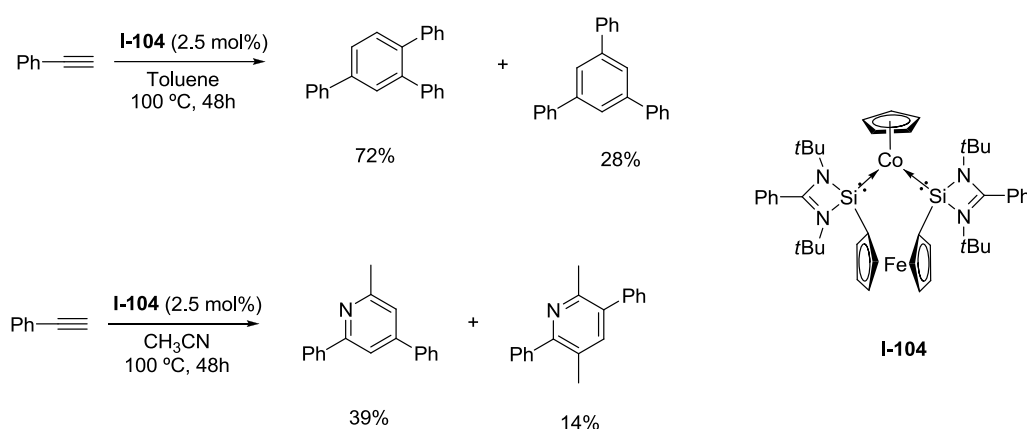
Scheme 1-36. Catalytic cyclotrimerization using silylene- Co^I complex **I-104** as a (pre)catalyst.

Very recently, rhodium-catalyzed hydroformylation of styrene by using silylene ligands was reported by Schomäcker and Driess et al. The hydroformylation of styrene at 30 bar CO/H_2 pressure in the presence of $[HRh(CO)(PPh_3)_3]$ with an excess of the bis-silylene ligand **I-86** resulted in superior catalytic activity.[52] In contrast, the reactions with an excess of the monodentate silylene ligands **I-2** and **I-83** under same reaction conditions revealed considerably slower conversion to the aldehyde products than $[HRh(CO)(PPh_3)_3]$, with or without an excess of PPh_3, showing catalyst deactivation (Scheme 1-37).
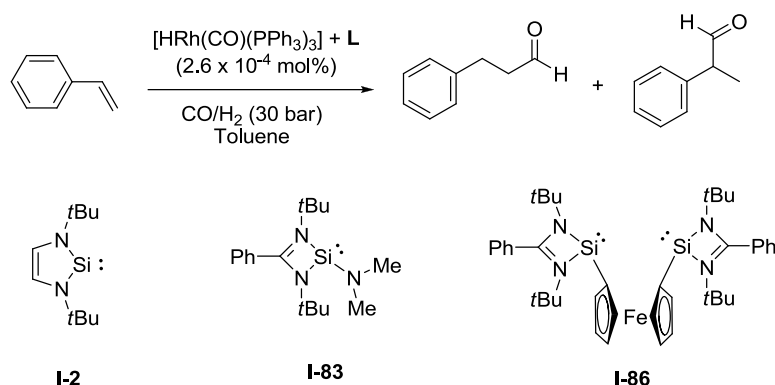
Scheme 1-37. Hydroformylation of styrene using Rh^I catalyst with silylene ligands.

1.3.3.2 Carbon-heteroatom bond formation

In 2012, Hartwig and Driess et al. reported the first SiCSi pincer-type silylene ligand **I-93**.[53] The corresponding iridium complex [SiCSi]IrHCl(COE) **I-105** was synthesized through the reaction of **I-93** with 0.5 equiv. of [IrCl(COE)$_2$]. Complex **I-105** was found to be a precatalyst for the C-H borylation of arenes using pinacolborane (HBPin). Comparative studies on the catalytic performances of the silylenes against related phosphine-based pincer analogues suggested that the silylene ligand has stronger donor capacity enabling an increased catalytic efficiency (Scheme 1-38).
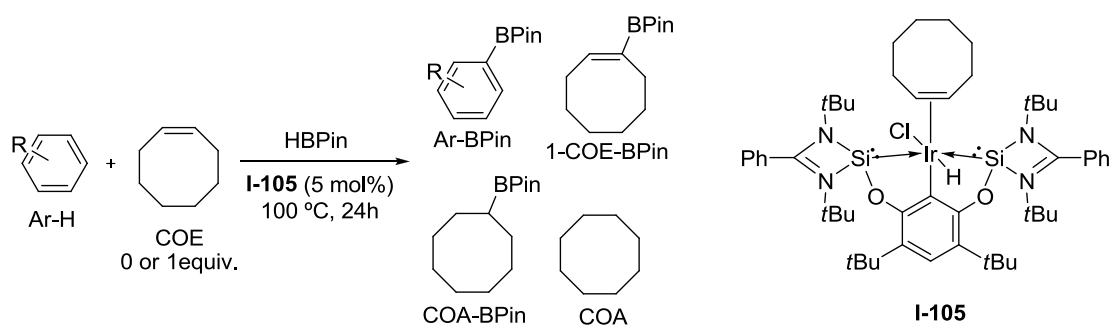
Scheme 1-38. Catalytic borylation of arenes, employing the pincer type silylene Ir^{II} complex **I-105** as precatalyst.

In 2017, Cabeza and García-Álvarez et al. reported a new type of mesitylenyl-silylene mixed ligand **I-90**.[54] Reactions of silylene **I-90** with corresponding iridium precursors at room temperature led to C-H activation and the oxidative addition of C-H to Ir centers which gave iridium(III) complexes (**I-106a** and **I-106b**) featuring cyclometallated silylene ligands. The deuteriation reactions of styrene and 1,3,5-trimethoxybenzene were carried out using **I-106a** as a (pre)catalyst and CD_3OD as a deuterium donor (Scheme 1-39).
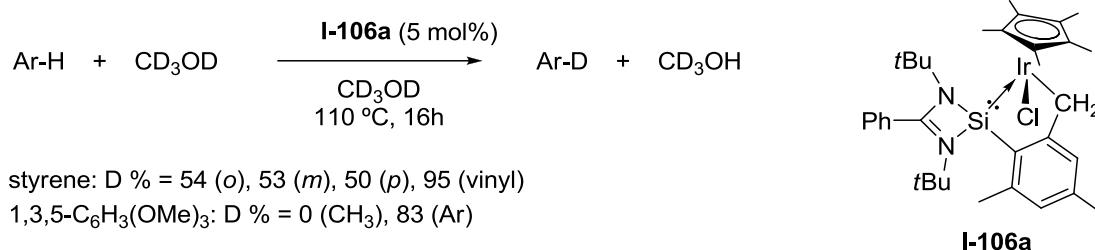
Scheme 1-39. Catalytic H/D exchange reaction catalyzed by silylene Ir^{III} complex **I-106a**.

Dehydrogenative borylation of benzene and toluene was tested using complex **I-106b** as (pre)catalysts (Scheme 1-40). The reactions went fast in the presence of COE (71 % yield for benzene in 3 hours and 31 % yield for toluene in 5 hours) and slowed down without COE (56 % yield for benzene in 24 hours and 52 % yield for toluene in 48 hours).
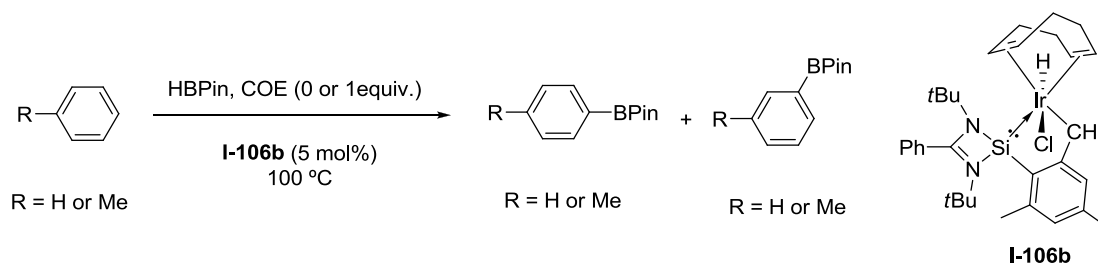
Scheme 1-40. Catalytic dehydrogenative borylation of arens catalyzed by silylene Ir^{III} complex **I-106b**.

In 2017, Co^{II} complex **I-107** bearing pincer type silylene ligand **I-94** was reported by Cui and Driess et al. through the reaction of ligand **I-94** with CoBr$_2$ in THF.[55] **I-107** enabled the regioselective catalytic C−H borylation of different heterocycles and fluorinated arenes. The borylation of 2,6-lutidine gave the 4-position substituted product with high yields. However, the reaction of 2-methoxy-6-methyl pyridine was much slower and yielded only 71 % of the desired product. The borylation of 2,3-lutidine selectively borylated the 5-position of the ring, whereas borylation of 2-benzylpyridine furnished a mixture containing almost the same amounts of 4- and 5-borylated isomers (Scheme 1-41).
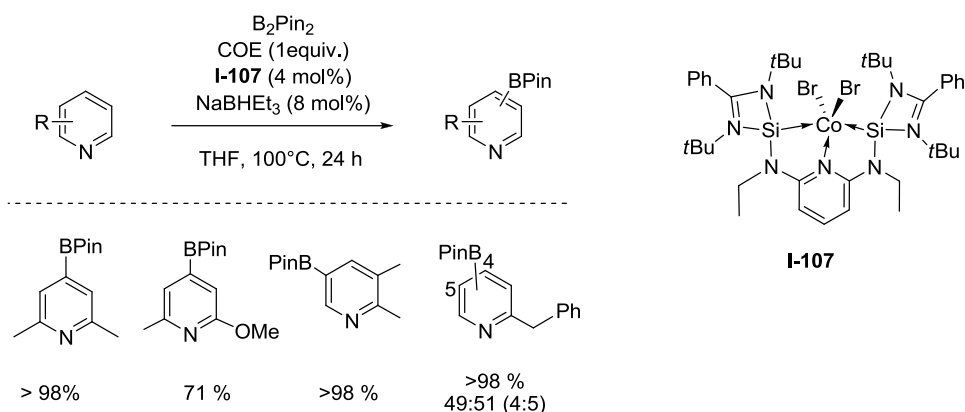
Scheme 1-41. Borylation of pyridine derivatives catalyzed by pincer type silylene Co^{II} complex **I-107**.

In contrast to pyridine derivatives, the borylation of furan analogues was carried out without cyclohexene. The borylation of furan gave 2,5-diborylation products (Scheme 1-42), whereas 2-methylfuran was selectively borylated at the 5-position with 0.5 molar equivalent of B$_2$Pin$_2$ (Scheme 1-42).
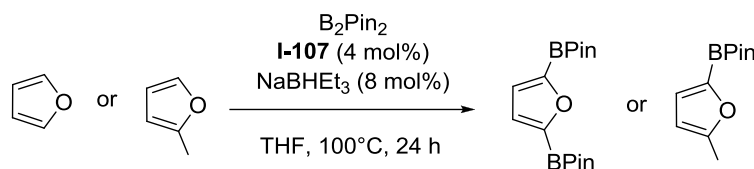
Scheme 1-42. Borylation of furan and its derivatives using pincer type silylene Co^{II} complex **I-107** as precatalyst.

Catalytic borylations of fluoro- and trifluoromethylarenes employing Co^{II} complex **I-107** were also tested. Disubstituted trifluoromethylbenzene derivatives underwent selective borylation at the least hindered position (Scheme 1-43), suggesting the selectivity is controlled by steric effects. Borylation of 1,2-difluorobenzene yielded the 4-borylated product as a major regioisomer (24:76). 1,3-difluorobenzene predominantly gave the 5-borylated product in 97 % yield. Borylation of 2-substituted 1,3-difluorobenzenes proceeded at the 5-position in good yields, whereas 1,2,3-trifluorobezene led to 78 % selectivity at the 5-position. Fluorobenzene yielded the 3-borylated regioisomer as the major product. Borylation of 2-methylfluorobenzene occurred at the 4-position with 72 % selectivity. The bis-borylation of naphthalene yielded the 6- and 7-borylated products in a molar ratio of 1:3, whereas borylation of pyrene selectively gave the 2,7-borylated product (Scheme 1-43).
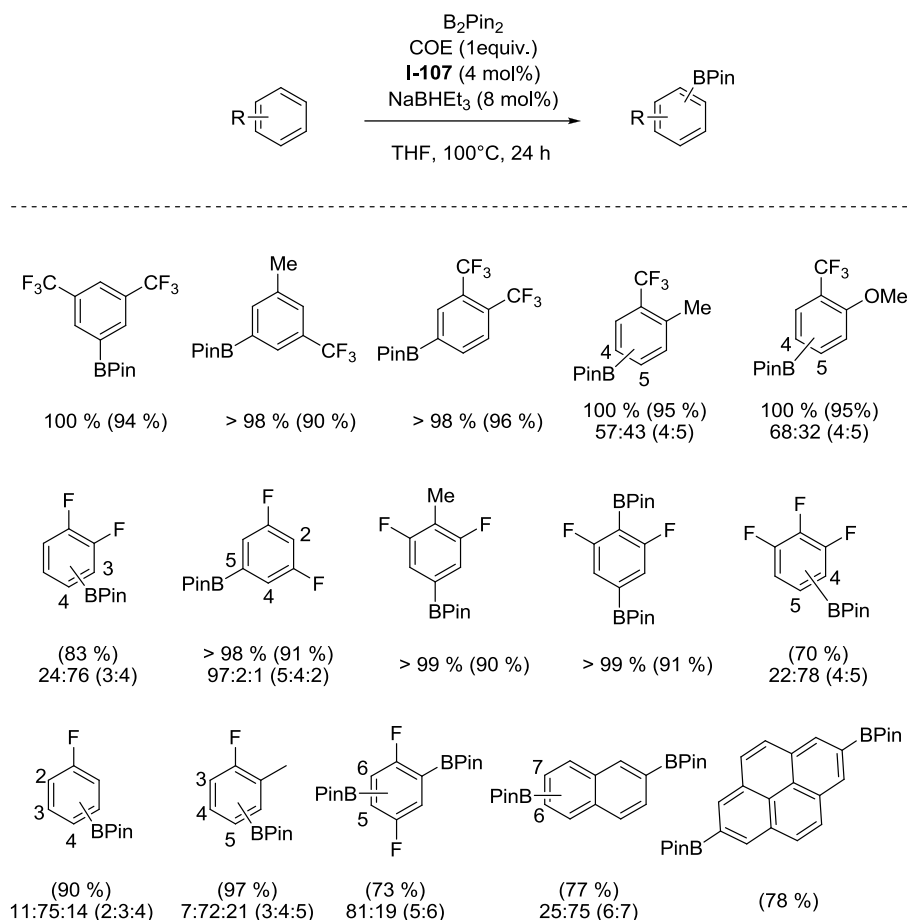
Scheme 1-43. Borylation of fluoro-arenes and fluoro-polyarenes catalyzed by pincer type silylene Co^{II} complex **I-107**.

In 2016, Baceiredo and Kato et al. first time applied the base-stabilized silacyclopropylidene ligand **I-85** in catalysis.[42] The reaction of **I-85** at room temperature with 0.5 equiv of Karstedt complex [Pt$_2$(dvtms)$_3$] (dvtms = Divinyltetramethyldisiloxane) afforded air-stable Pt^0 complex **I-108**. Hydrosilylation of 1-octene catalyzed by complex **I-108** (30 ppm) is as fast as that with the Karstedt catalyst (>95% conversion = 20 vs. 15 min) and proceeds in a more selective manner (isolated yield = 91% vs. 78%) (Scheme 1-44).
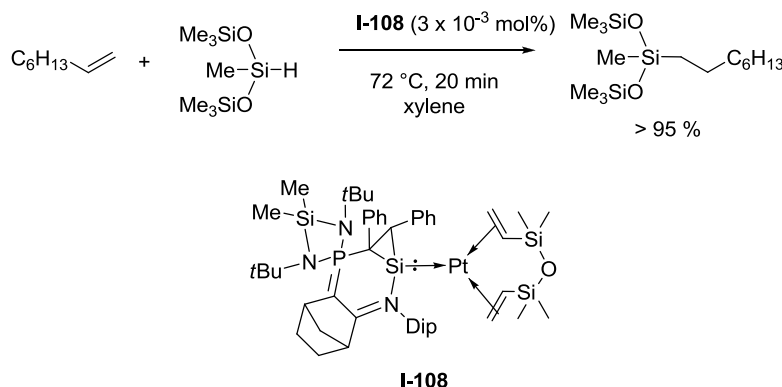
Scheme 1-44. Hydrosilylation of olefins catalyzed by silylene Pt^0 complex **I-108**.

In the same year, Iwamoto et al. reported the olefin hydrosilylation catalyzed by Pt^0 complex **I-109** bearing a dialkylsilylene **I-37** as a ligand.[43] The catalytic activity of **I-109** was assessed for the hydrosilylation of (Me$_3$SiO)$_2$SiMeH and 1-hexene in the presence of 30 ppm (w/w) of **I-109** at 50 °C for 5 h. Additionally, **I-109** also catalyzes the hydrosilylation of terminal alkenes bearing different functional groups with very high conversion rates (Scheme 1-45).
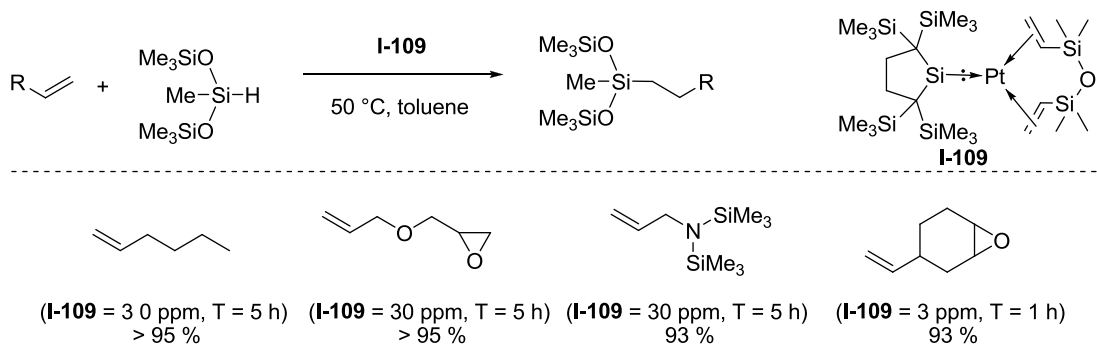
Scheme 1-45. Hydrosilylation of olefins catalyzed by silylene Pt^0 complex **I-109**.

One year later, cyclic alkyl(amino) silylene **I-49** was employed as a ligand in Pt-catalyzed olefin hydrosilylation by Iwamoto et al.[44] The Pt^0 complex **I-110** bearing silylene **I-49** was synthesized by the same group. The performance of **I-110** in the catalytic hydrosilylation of $(Me_3SiO)_2MeSiH$ with various terminal alkenes that contain functional groups was comparable to Pt^0 complex **I-109** bearing a dialkylsilylene (Scheme 1-46).
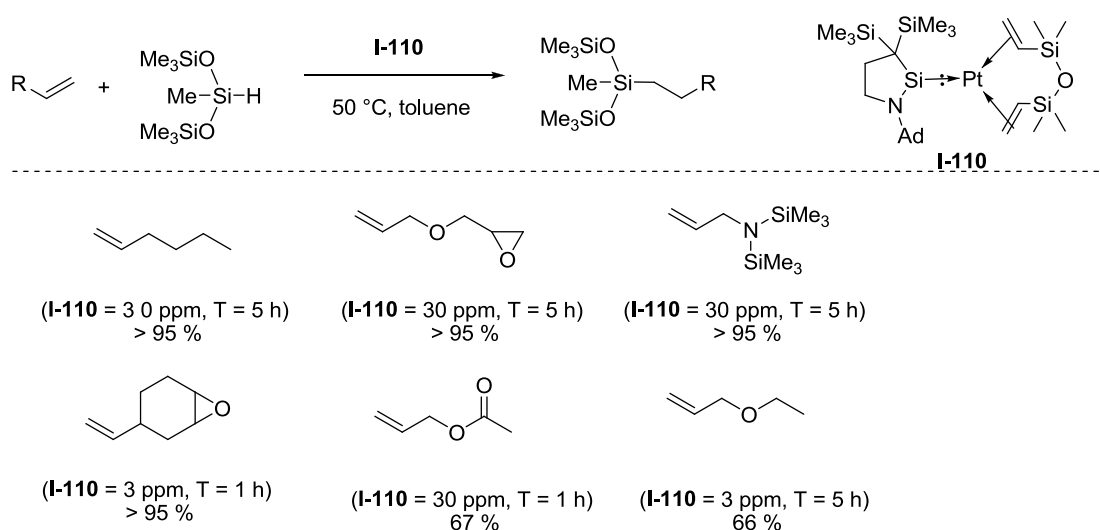
Scheme 1-46. Hydrosilylation of olefins catalyzed by silylene Pt^0 complex **I-110**.

1.3.3.3 Reduction reactions

In 2012, our group reported the first example of NHSi-Fe^0 complexes, **I-111a**, **I-111b**, and **I-111c**, bearing the *N,N*-di(*tert*-butyl)amidinato silylene ligands **I-28**, **I-82a**, and **I-82b**, respectively.[41] The catalytic performance of **I-111b** was further tested in hydrosilylation of ketones with different steric and electronic properties and resulted in the formation of the corresponding alcohols after workup process with yields up to > 99 % (Scheme 1-47). Further experimental and theoretical results reveal a ketone-mediated 1,2-H migration from Si^{II} to Fe^0 mechanism, which indicate the NHSi ligand play a key role in the catalytic cycle.

Scheme 1-47. Hydrosilylation of ketones using silylene Fe^0 complex **I-111** as precatalyst.

In 2014, our group reported the Fe complexes based on the tridentate SiNSi ligand **I-94**.[56] The Fe^0 complex **I-112** was prepared through the reaction of ligand **I-94** with Fe(PMe$_3$)$_4$. Alternatively, **I-112** can also be obtained by reduction of silylene FeCl$_2$ complex bearing ligand **I-94** with KC$_8$ in the presence of excess PMe$_3$. Catalytic carbonyl hydrosilylation reactions were checked using complex **I-112**.[57] It was found that besides the Et$_2$N group, the catalyst showed excellent functional group tolerance for both electron-donating and electron-withdrawing substituents at the aryl group. However, the steric hindrance, especially at the *ortho* positions, lowers the catalytic performance (Scheme 1-48).

The mechanism of hydrosilylation catalyzed by complex **I-112** has been investigated by Driess and Oestreich et al. in 2015.[57] The catalytically active species **I-112a** was isolated through the stoichiometric reaction of precatalyst complex **I-112** and (Et$_3$O)$_3$SiH. Interestingly, the further experimental and theoretical analysis suggests that the iron center of complex **I-112a** is not directly involved in the catalytic cycle due to the steric effects. The C=O activation occurs at the Si^{IV} Lewis acid center of complex **I-112a** and intermediate **I-112b** is generated. A (Et$_3$O)$_3$SiH then coordinates to **I-112b** gives the intermediate **I-112c**, which further releases the hydrosilylation product (Scheme 1-49).
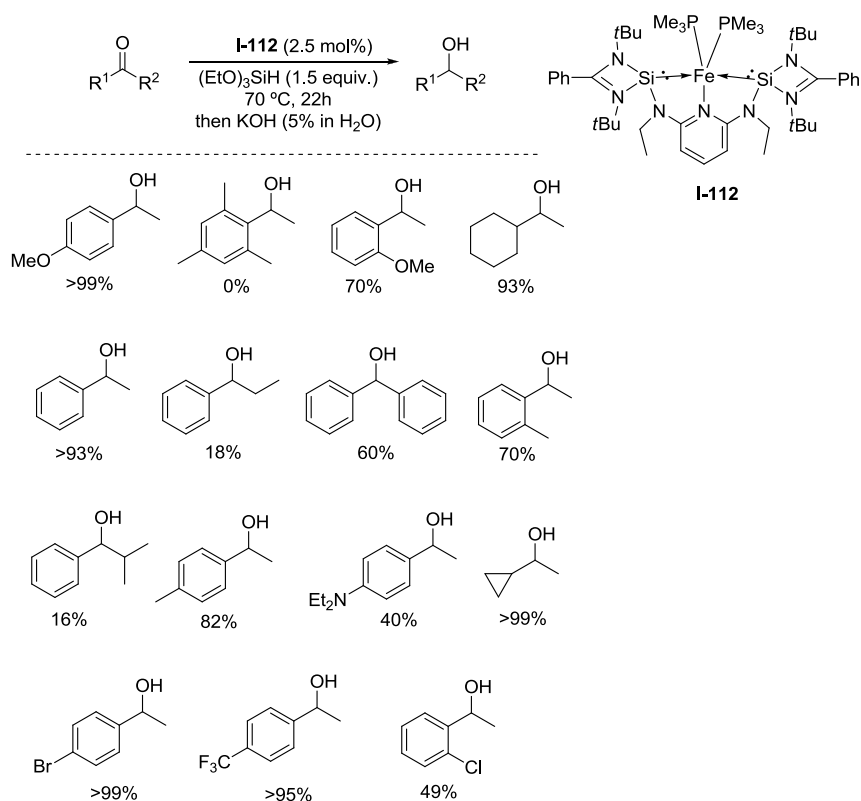
Scheme 1-48. Hydrosilylation of ketones using silylene Fe^0 complex **I-112** as precatalyst.
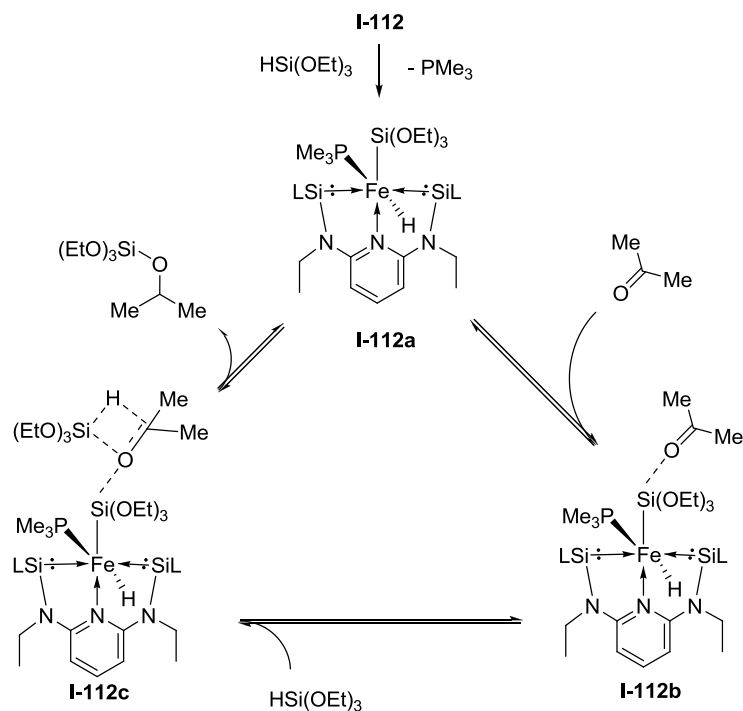
Scheme 1-49. Peripheral mechanism for hydrosilylation of ketones using silylene Fe^0 complex **I-112** as precatalyst.

Cu^I complex **I-113** bearing base-stabilized silacyclopropylidene ligand **I-85** has also been used as a catalyst for the hydrosilylation of bulky ketones such as 1-adamantyl methyl ketone.[42] Complex **I-113** is considerably more active than the corresponding Ph$_3$P-CuI complex and is as efficient as those with an extremely bulky bowl-shaped phosphine ligand developed by Tsuji et al. (Scheme 1-50).
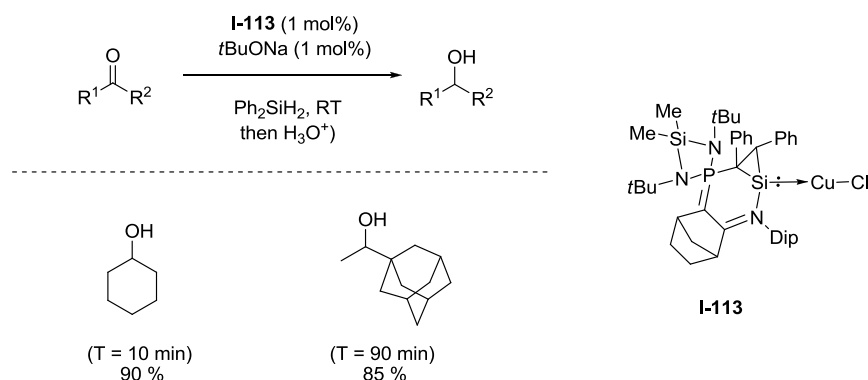
Scheme 1-50. Hydrosilylation of ketones catalyzed by silylene Cu^I complex **I-113**.

Very recently, our group prepared the new bis-silylene ligand **I-89** with the xanthene backbone.[45] The reaction of **I-89** with Ni(cod)$_2$ gave the corresponding Ni^0 complex **I-144**, which was found to be a very active catalyst in the hydrogenation of olefins under mild condition (1 bar H$_2$ at room temperature). Screening experiments revealed that terminal alkenes were readily reduced to the corresponding alkanes in quantitative yields. Longer reaction times were required for hydrogenation of internal alkenes, especially more sterically hindered ones. Functional groups such as -OMe, -CF$_3$, -CN, and pyridine ring, carbonyl were well tolerated. Nonconjugated and conjugated dienes yielded the corresponding alkanes quantitatively. Turnover number (TON) and turnover frequency (TOF) of 1-dodecene and styrene could reach up to 1000 and 250 h^{-1}, respectively (Scheme 1-51). Moreover, a unique Si^{II} assistant-H$_2$ activation mode, in which the low-valent silicon centers are involved in the key step of dihydrogen cleavage and transfer, are suggested by DFT calculations.
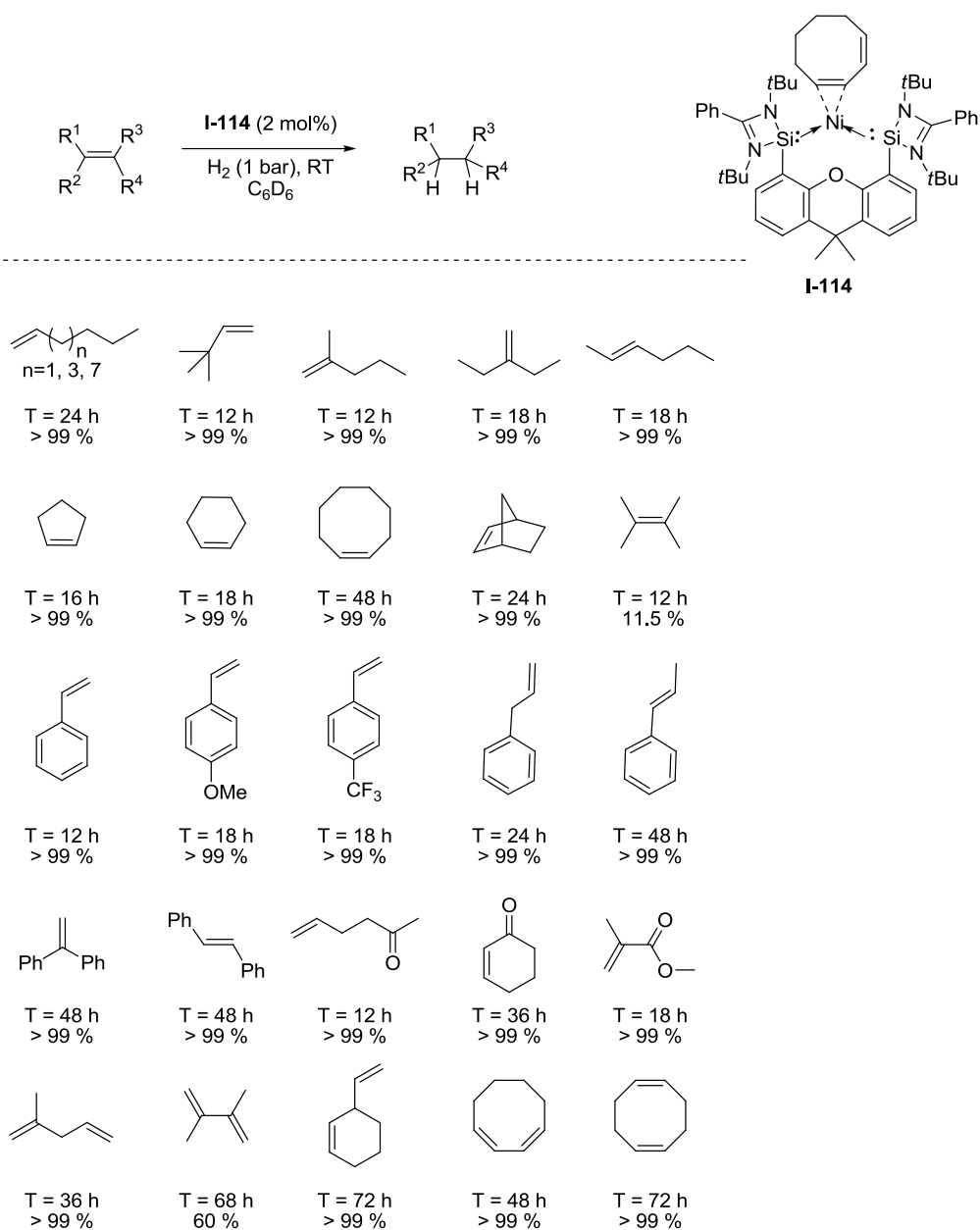
Scheme 1-51. Hydrogenation of olefins catalyzed by silylene Ni^0 complex **I-114**.

Very recently, bis(silylene) **I-86** stabilized η^6-arene Fe^0 complex **I-115** was also prepared by Driess et al. through reduction of the Fe^{II} di-halide precursors bearing bis(silylene) **I-86** in the presence of benzene.[58] The catalytic hydrogenation of various ketones and an aldehyde were carried out using complex **I-115**. The scope experiment suggested the hydrogenation of aldehyde and ketone derivatives gave moderate to good yields of corresponding alcohols. Remarkably, the high

chemoselectivity of C=O over C=C reduction was achieved by using allylacetone and chalcone as substrates (Scheme 1-52).

> 99 % (90 %) > 99 % (92 %) > 99 % (90 %) > 60 % (44 %)

99 % (87 %) 70 % (61 %) 80 % (64 %) 94 % (84 %)

60 % (42 %) 63 % (50 %) 39 % (28 %) 70 % (58 %)

96 % (83 %) 65 % (51 %) 72 % (56 %) > 99 % (90 %)

> 99 % (79 %) 51 % (30 %)
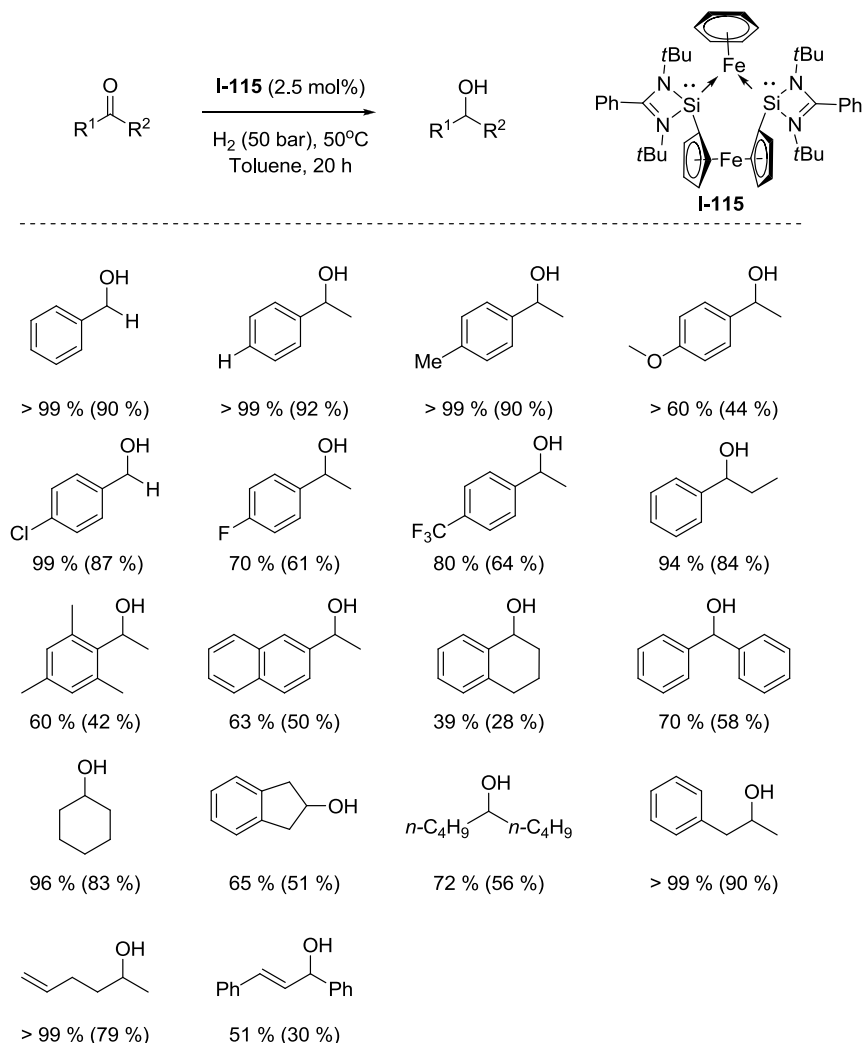
Scheme 1-52. Hydrogenation of carbonyl compounds catalyzed by silylene Fe^0 complex **I-115**.

The silylene-Rh^I and –Ir^I complexes **I-116a** and **I-116b** bearing β-diketiminate silylene ligand **I-20** were applied in the reduction of amide substrates.[40] A selective C-O bond cleavage was observed (up to 61%) when the precatalyst **I-116a** was used. However, employing the precatalyst **I-116b** led to a mixture of C-O and C-N cleavage products under the same conditions (Scheme 1-53).
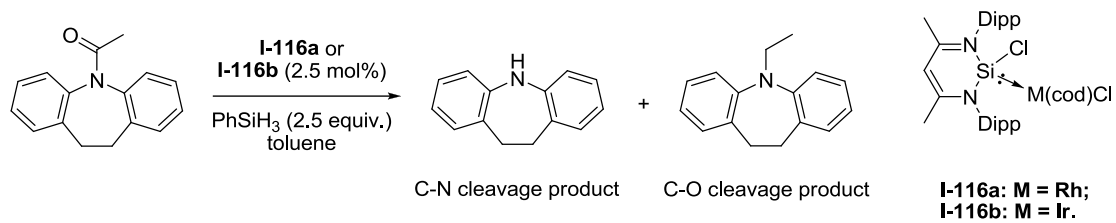
Scheme 1-53. Reduction of the dibenzoazepine using the **I-116** precatalyst.

2. MOTIVATION

Considering the unique electronic properties of NHSis, the purpose of this research is to study the application of NHSi ligands in stabilizing low-valent germanium compounds and to explore the application of new NHSi ligands in metal-mediated catalysis.
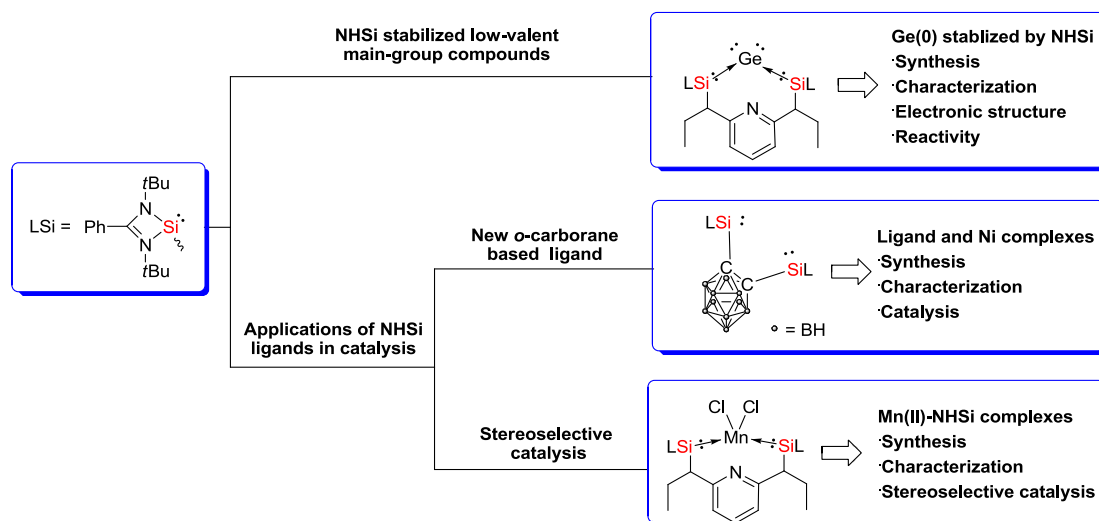
Chart 2-1. The N,N-di(tert-butyl)amidinato NHSi derivatives and their germanium, nickel, and manganese complexes.

The objectives of this work are as follows:

1) synthesizing the pyridine-based bis-NHSi stabilized low-valent germanium compounds (Chart 2-1);

2) synthesizing new *ortho*-dicarbadodecaborane ($C_2B_{10}H_{12}$)-based bis-NHSi ligand and investigating its catalytic performance (Chart 2-1);

3) achieving the stereoselective reduction of alkynes by using bis-NHSi metal complexes (Chart 2-1);
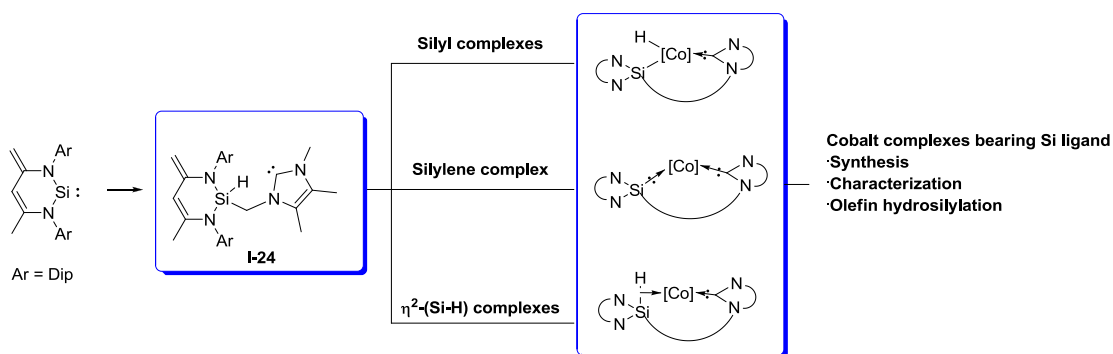
Chart 2-2. The NHSi derivatives based on *β*-diketiminate-like backbone and their cobalt complexes.

4) studying the different coordination modes of ligand **I-24** in coordination chemistry and investigating the catalytic performances of corresponding cobalt complexes (Chart 2-2).

3. RESULTS AND DISCUSSION

3.1 Synthesis and reactivity of NHSi-stabilized low-valent germanium complexes

Ylidones are zero-valent group 14 compounds E^0 (E = C, Si, Ge) bearing two lone pairs of electrons. NHCs,[59] heavier metallylenes, or imino donors have been introduced as supporting σ donor ligands to stabilize ylidones.[60] For instance, the silylone and germylone **A,** bearing a singlet ground state and relatively short C-E distances (E = Si, 1.841(2) Å; E = Ge, 1.9386(16) -1.9417(15) Å), stabilized by cyclic alkyl(amino) carbenes (cAAC) (Scheme 3-1).[59a, 59d] At the same year, our group reported the the silylone and germylone **B** stabilized by a relatively strong σ donor bis-NHC ligand, which resulted in longer C-E distances (E = Si, 1.864(1) - 1.874(1) Å; E = Ge, 1.965(3) - 1.961(3) Å).[59b, 59c] Compounds **C,** E=E'=E, (E, E' = Si, Ge, and Sn: trisilaallenes, trigermaallenes, 1,3-digermasilaallenes, 2-germadisilaallene, and tristannaallene respectively) were described as heavier allenes by Kira and coworkers [32, 61] and Wiberg et al. [62], respectively. However, DFT calculation indicated that **C** could also be described as ylidones **D**, in which the central atoms E' are zero-valent, bearing two lone pairs of electrons and are stabilized by two cyclic dialkylmetallylene ligands.[16]

As discussed in chapter 1.2 and 1.3, electronically rich donor ligands NHSis[63] have been successfully used as supporting ligands in coordination chemistry since the first NHSi metal complex reported in 1977.[38c, 64] Very recently, NHSi have also been employed the ligands which stabilize the low-valent main-group compounds. For instance, the first digermanium(0) complex NHSi→:Ge=Ge:←NHSi stabilized by amidinate-based silylene {[PhC(N*t*Bu)$_2$]SiN(SiMe$_3$)$_2$} which was reported by So and co-workers in 2014.[36b] However, mononuclear E^0 complexes (ylidones) of type E, NHE→:E:←NHE, are currently unknown but were predicted as isolable species by DFT calculations.[34d, 34e] Encouraged by the theoretical prediction, it is interesting to test whether or not the strong σ donor bis-NHSi ligand **I-94**, which was reported by our group in 2014,[56-57] is suitable to stabilize the germylone species (type **E**, Scheme 3-1).
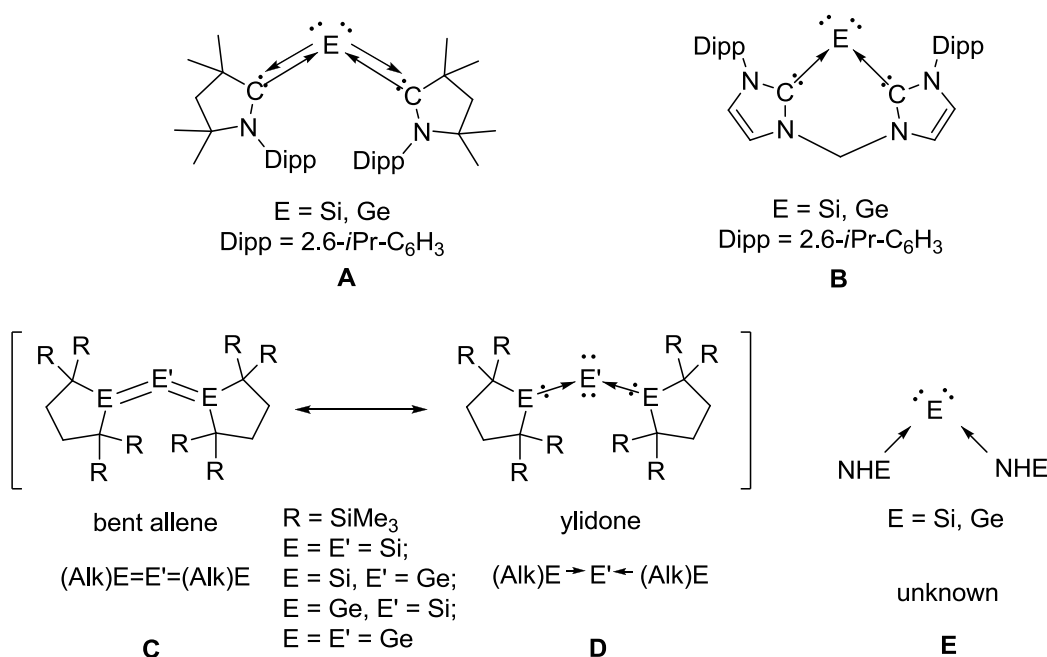
Scheme 3-1. Ylidones stabilized by carbenes and their heavier analogues.

3.2.1 Synthesis of germanium complexes supported by NHSi ligands

The reaction of GeCl$_2$·dioxane with the bis-NHSi pyridine pincer ligand **I-94** in THF at room temperature afforded the bis-NHSi stabilized chlorogermyliumylidene **3-1** as a yellow powder in 62% yield (Scheme 3-2). Because the ionic nature of **3-1,** it is almost insoluble in toluene and THF but only soluble in dichloromethane. The ^{29}Si NMR singlet resonance at δ = 3.60 ppm is downfield shifted compared to the free bis-NHSi ligand **I-94** (δ = −14.9 ppm) due to the donor coordination of the Si^{II} atoms.
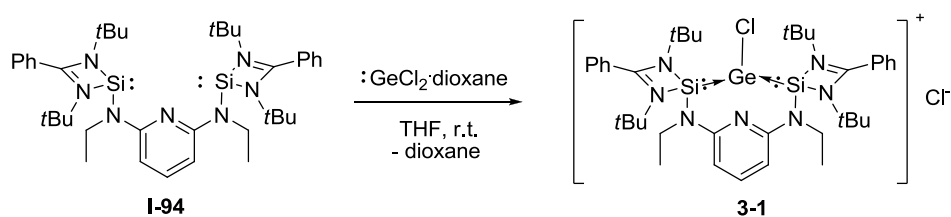
Scheme 3-2. Synthesis of the chlorogermyliumylidene chloride **3-1** stabilized by the bis-NHSi pyridine pincer SiNSi ligand **I-94**.
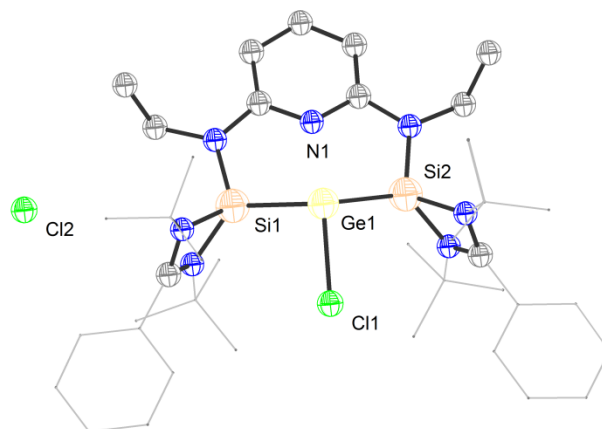
Figure 3-1. Molecular structure of chlorogermyliumylidene chloride **3-1**. Thermal ellipsoids are set at 50 % probability level. Hydrogen atoms and solvent molecules are omitted for clarity. Selected distances [Å] and angles [°]: Ge(1)-Si(1) 2.3503(6), Ge(1)-Si(2) 2.3513(6), Ge(1)-Cl(1) 2.3757(6), Si(1)-N(2) 1.723(2), Si(1)-N(5) 1.8000(19), Si(1)-N(4) 1.8141(19), Si(2)-N(3) 1.7293(19), Si(2)-N(6) 1.8040(19), Si(2)-N(7) 1.8194(17), Si(1)-Ge(1)-Si(2) 119.31(2), Si(1)-Ge(1)-Cl(1) 96.35(2), Si(2)-Ge(1)-Cl(1) 97.30(2).

Single-crystals of **3-1**, suitable for X-ray diffraction analysis, could be obtained by crystallization in a THF/toluene (1:1) mixed solutions. The crystals belong to the space group $P2_1$/c (Figure 3-1).The Ge(1)-Cl(1) bond distance of 2.3757(6) Å is longer than those observed in a germyliumylidene cation stabilized by a bis(tributylphosphazenyl)naphthalene (2.278(1) Å),[65] bis-NHC (2.310(1) Å),[59b] and diiminopyridine ligand (2.2433(9) Å).[66] The Ge(1)-Si(2) and Ge(1)-Si(1) distances of 2.3513(6) Å and 2.3503(6) Å, respectively, are drastically shorter than that in a GeCl$_2$ mono-NHSi adduct (2.5259(13) Å) reported by So et al.,[36b] presumably due to the stronger donor coordination of the bis-NHSi ligand **I-94**. However, the Ge(1)-N(1) distance of 2.594 Å in **3-1** is longer than that of the three-coordinate germyliumylidene stabilized by a diiminopyridine ligand (2.071(2) Å),[66] suggesting that the pyridine N atom is only weakly coordinated to the Ge^{II} center. The eight-membered GeSi$_2$N$_3$C$_2$ ring in **3-1** adopts an envelope conformation with a nearly co-planar Si$_2$N$_3$C$_2$ moiety and a displaced Ge atom. The Ge center adopts a trigonal pyramidal geometry with the sum of angles around the Ge atom of 312.96°.
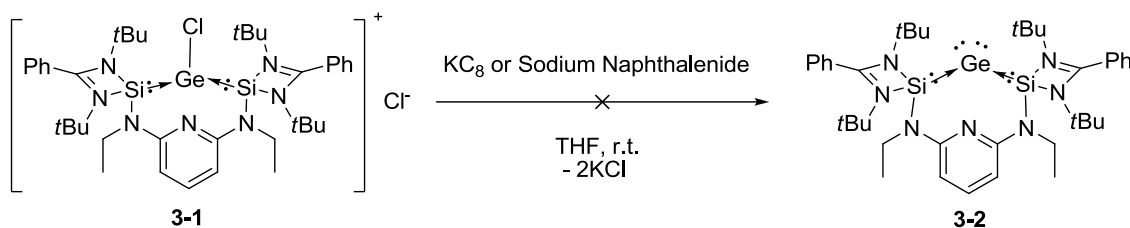
Scheme 3-3. Attempts to synthesize the germylone **3-2** stabilized by the bis-NHSi pyridine pincer SiNSi ligand.

Attempts to synthesize the corresponding Ge^0 compound, **3-2**, through reduction of **3-1** by sodium naphthalenide or KC_8 were not successful (Scheme 3-3). DFT calculations (calculated using the Gaussian 09 Rev. D01 program suit at the B3LYP-D3(BJ)/6-311G(d,p) level) suggest that **3-2** is too labile due to the strong σ donor strength of the bis-NHSi ligand **I-94** which oversaturates the Ge^0 center. An s-type orbital lone pair on the Ge^0 center of **3-2**, which is occupied by 1.9 electrons, was observed by DFT calculations. The relatively short Ge1-Si2 bond (2.311 Å, Figure 3-2) and Wiberg bond indices of 1.45 suggest a significant Si-Ge double bond character (Figure 3-3). The electronic situation of the Ge^0 center in **3-2** suggested that the highly electron-rich Ge^0 atom could be stabilized through coordinating to a strong electron-acceptor.
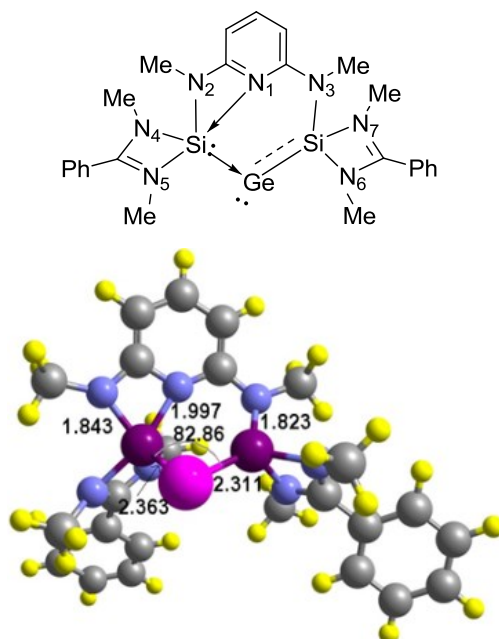
Figure 3-2. Calculated (B3LYP/6-311G(d,p) important structural parameters of model complex **3-2.** The bond length in Å, the bond angle in degrees.
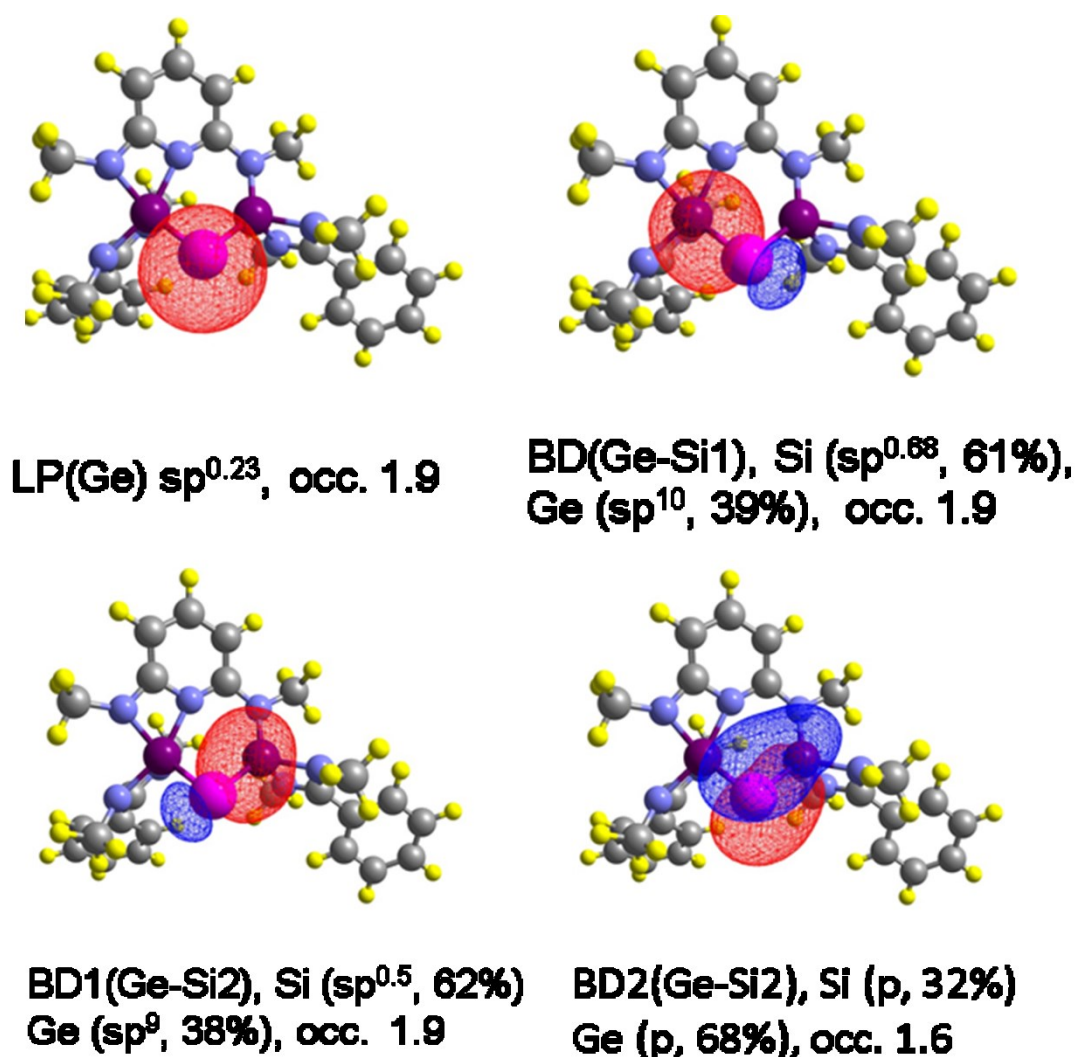
Figure 3-3. Selected NBO orbitals of **3-2**. LP: lone-pair, BD: bonding orbital; in parenthesis for each element (Ge, Si) is its hybridization and the polarization of the electron density; occ is the occupancy of the orbital in electrons.

Then the Lewis-acidic metal complex fragment (e.g., $Fe(CO)_4$) was introduced as an electron acceptor coordinated to the Ge^0 center. The coordination of $Fe(CO)_4$ fragment might increase the stability of the germylone compound. In fact, this was achieved by the one-step reaction of **3-1** with Collman's reagent, $K_2Fe(CO)_4$, affording the desired germylone-iron carbonyl complex **3-3** in 49% yield (Scheme 3-4). The ^{29}Si NMR of **3-3** THF-d_8 gave a singlet at $\delta = -5.92$ ppm which is up-field shifted compared to the chlorogermyliumylidene **3-1**.
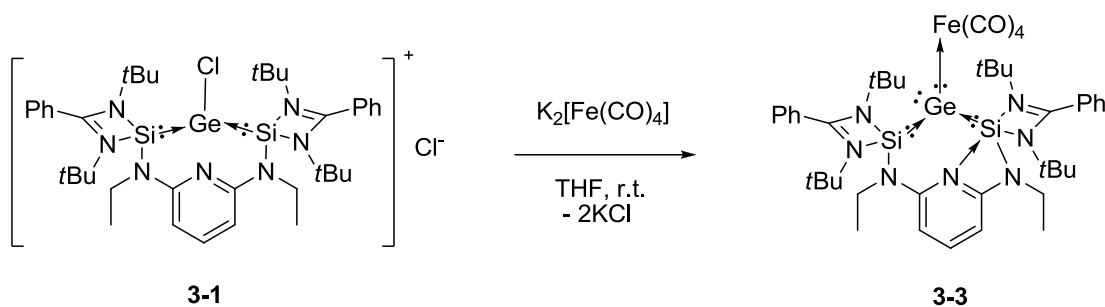
Scheme 3-4. Synthesis of the germylone iron carbonyl complex [SiNSi]GeFe **3-3** stabilized by the bis-NHSi pyridine pincer SiNSi ligand.

Single-crystals of **3-3** could be produced in an Et$_2$O/THF mixture in the monoclinic space group $P2_1$/c (Figure 3-4). The Ge(1)-Si(2) and Ge(1)-Si(1) distances of 2.3729(6) Å and 2.3875(6) Å, respectively, are significantly longer than those in 2-germadisilaallene (2.2366(7) Å and 2.2373(7) Å) reported by Kira et al.[32a] and in **3-1** (2.3513(6) Å and 2.3503(6) Å), but shorter than the Ge-Si distances in a digermanium(0) complex (2.406(2) Å) reported by So et al.[36b] Surprisingly, but predicted by DFT-calculation, the pyridine N atom in complex **3-3** is coordinated to one of the Si^{II} atoms instead of Ge^{0} center, resulting in a five-coordinate Si^{II} atom. A similar five-coordinate Si^{II} was also observed in bis[N,N′‑diisopropylbenzamidinato(−)]silicon(II) species reported by Tacke et al.[67] The Si(1)-N(1) distance of 2.1038(19) Å is longer than those of Si(1)-N(4) and Si(1)-N(5) as well as the Si-N distance in NHSi which was stabilized by p-dimethylaminopyridine (DMAP).[68] The Si(2)-Ge(1)-Si(1) angle of 95.66(2)° is smaller than those of germylones **A** which were stabilized by cAAC ligands (114.71(6)° − 117.24(8)°)[59d] and germadisilaallene **C** (132.38(2)°),[32a] but larger than the C-Ge-C angle of the germylone **B** stabilized by a bis-NHC ligand (86.6(1)°).[59b] Similar to those in germylone-GaCl$_3$ complexes which were stabilized by a bis-NHC ligand,[69] the Ge^{0} center of **3-3** also adopts a trigonal pyramidal geometry.[70]
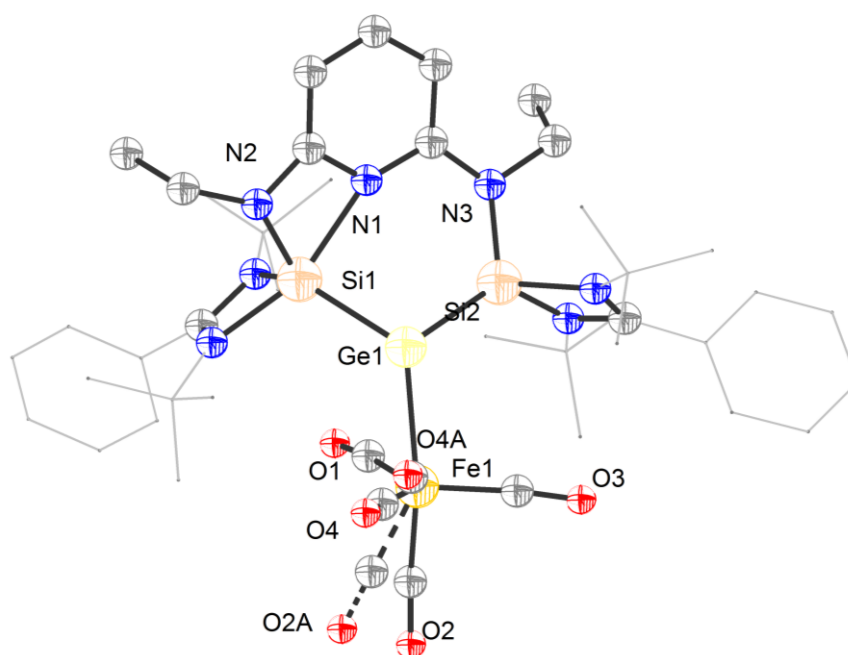
Figure 3-4. Molecular structure of the bis-NHSi pyridine-stabilized germylone-Fe(CO)4 complex, **3-3**. Thermal ellipsoids are set at 50 % probability level. Hydrogen atoms and solvent molecules are omitted for clarity. Selected distances [Å] and angles [°]: Ge(1)-Si(2) 2.3729(6), Ge(1)-Si(1) 2.3875(6), Ge(1)-Fe(1) 2.4987(5), Si(1)-N(2) 1.7962(18), Si(1)-N(4) 1.8601(18), Si(1)-N(5) 1.8964(18), Si(1)-N(1) 2.1038(19), Si(2)-N(3) 1.762(2), Si(2)-N(6) 1.8432(18), Si(2)-N(7) 1.8550(18); Si(2)-Ge(1)-Si(1) 95.66(2), Si(2)-Ge(1)-Fe(1) 108.25(2), Si(1)-Ge(1)-Fe(1) 118.68(2).

The IR frequencies of CO in complex **3-3** were observed at 1830, 1865, 1886, and 1969 cm^{-1}, respectively. Compared to the IR stretching of an amino(imino)germylene iron carbonyl complex (1930, 1965, and 2039 cm^{-1}),[71] the red-shift of the IR frequencies indicates that the CO ligands act as electron acceptors at the Fe center.
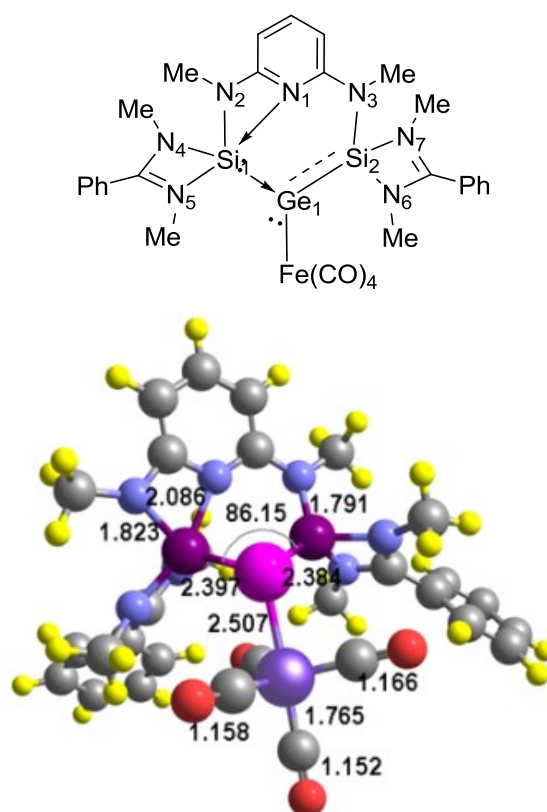
Figure 3-5. Calculated (B3LYP/6-311G(d,p) important structural parameters of the model compound of **3-3.** The bond length in **Å,** the bond angle in degrees.

To get insight into the electronic structure of complex **3-3,** DFT calculations at B3LYP/6-311G(d,p) were performed on the model compound, where the methyl groups replace the *t*Bu groups on the N(2) and N(3) atoms in the synthesized compounds. The calculated geometries of the model compounds are in good agreement with the metric data obtained from X-ray diffraction analyses of the synthesized compounds (Figure 3-5). The important structural parameters of the model compound of **3-3** are**:** The Ge-Si distances are in the range of 2.384 - 2.397 Å, the Ge1-Fe1 bond length is 2.507 Å and the Si1-Ge1-Si2 angle is 86.15°.
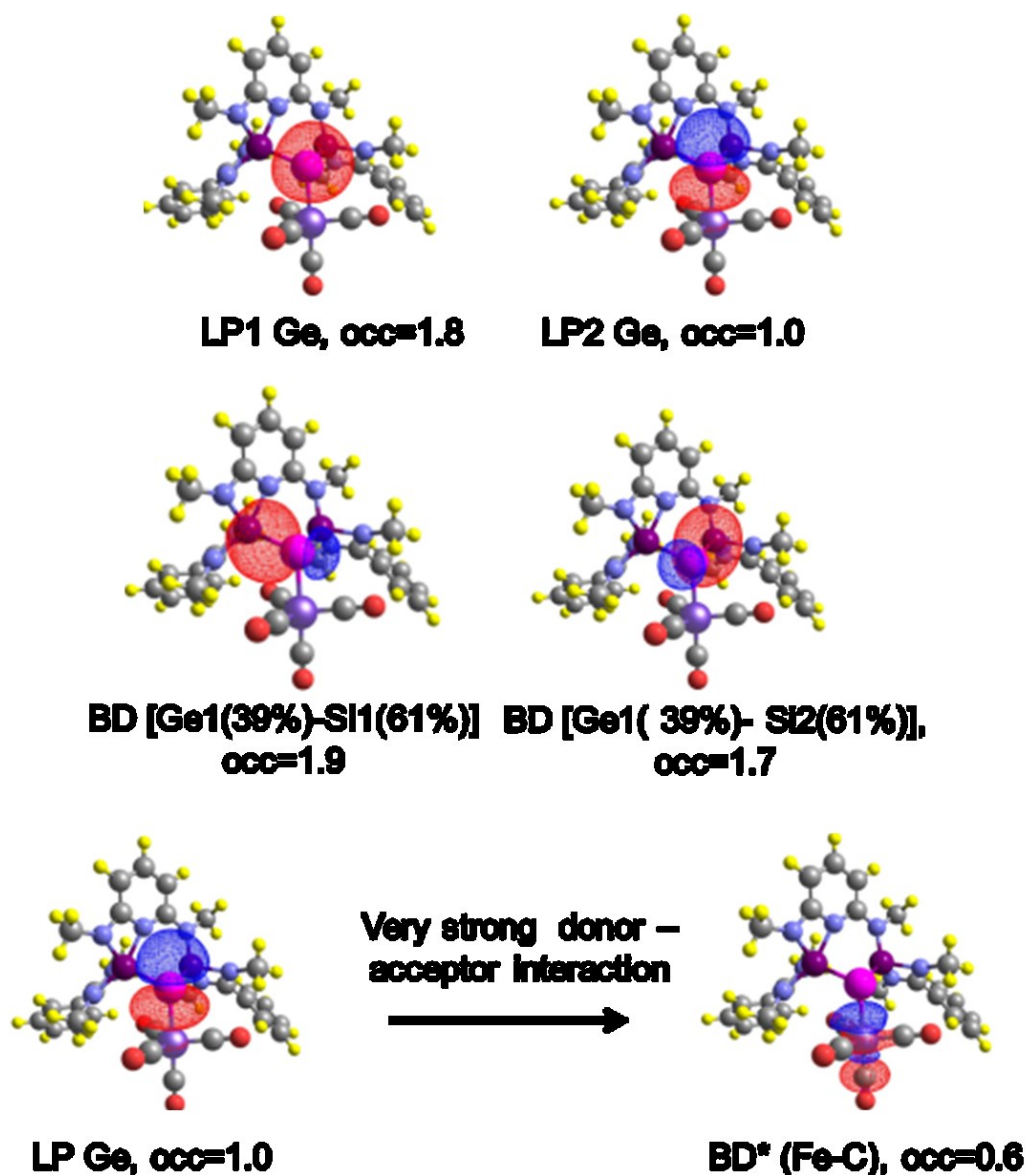
Figure 3-6. Selected NBO orbitals of the DFT-calculated model complex **3-3**. LP denotes a lone-pair orbital; BD denotes a bonding orbital and BD* denotes an antibonding orbital. The polarity of the BD orbitals is given by the percentage of the electron density on Ge and Si. occ is the occupancy of the orbital in electrons. Contour value=0.03.

According to NBO analysis, a Ge s-type (occupied by 1.77 electrons) and a Ge p-type (occupied by 1 electron) lone-pair orbitals were found in the model complex **3-3**. The single bonds Ge1-Si2 and Ge1-Si1 were occupied by ca. 2 electrons (Figure 3-6).[38a] The WBIs of Ge1-Si1 and Ge1-Si2 bonds are 0.96 and 1.08, respectively. The calculated Ge-Fe distance of 2.507 Å (exp. 2.499 Å, WBI = 0.39), is significantly

longer than the Ge-Fe distance (2.378 Å) in the Fe(CO)$_4$ complex of Tip(SiClR$_2$)Si=Ge:←NHC[72] (Tip = 2,4,6-iPr$_3$C$_6$H$_2$; NHC = N-heterocyclic carbene) and in the amino(imino) germylene-Fe(CO)$_4$ complex[71] (calc. 2.32 Å (exp. 2.30 Å), WBI = 0.56).

It is of interest to analyze first the bonding situation and electronic structure in the yet unknown "germylone" **3-2** "precursor" and of the complex **3-3**. In complex **3-2**, the Ge1-Si1 distance is 2.363Å, and that of Ge1-Si2 is 2.311Å being significantly longer than the Si-Ge distances in Kira's disilagermaallene. The respective calculated Wiberg bond indices of 1.13 and 1.45, exhibit a significant double bond character in the Ge1-Si2 bond. The Ge1-Si2 double bond character is nicely reflected in the NBO orbitals of complex **3-2** (Figure 3-6). The electronic structure of **3-2** as predicted by the NBO analysis can be interpreted as a silagermylidene stabilized by a silylene. A similar bonding motif was found in (Tip)$_2$Si=Ge:←NHC and Tip(SiClR$_2$)Si=Ge:←NHC synthesized by Scheschkewitz et al.[71] In both cases the NHC is in an allylic position. The Si=Ge bond lengths are 2.252 Å and 2.276 Å, respectively, somewhat shorter than the Si=Ge bond in model complex **3-2** (2.328Å).

3.2.2 Reactivity study of Ge^0 complex stabilized by NHSi ligand and Fe(CO)$_4$
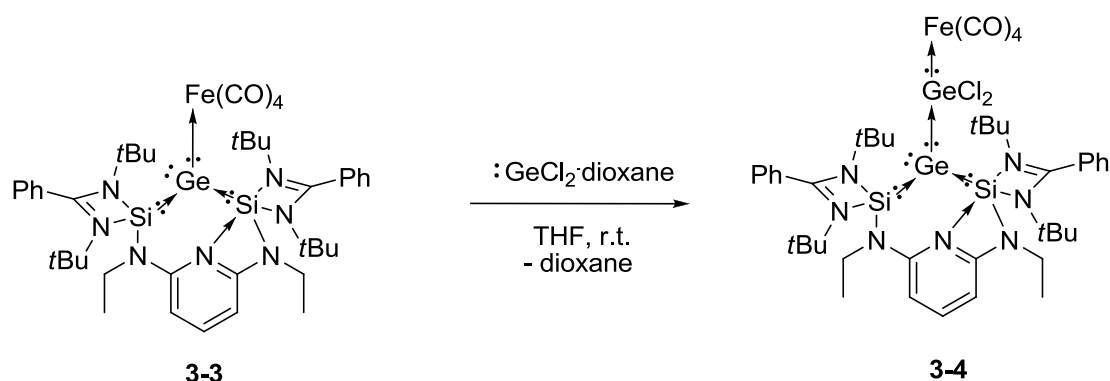
Scheme 3-5. Synthesis of the germylone iron carbonyl complex [SiNSi]GeGeFe **3-4** stabilized by the bis-NHSi pyridine pincer SiNSi ligand.

Unexpectedly, complex **3-3** undergoes further reaction with GeCl$_2$·dioxane in THF at room temperature. The complex **3-4** was generated by the insertion of GeCl$_2$ moiety into the donor-acceptor Ge^0–Fe^0 bond (Scheme 3-5). The ^{29}Si NMR shift of complex **3-4** in THF-d$_8$ reveals a singlet at δ = 2.14 ppm which is downfield shifted compared to germylone iron carbonyl complex **3-3**.

The single crystal suitable for X-ray analysis was grown from diethyl ether and THF mixed solutions of **3-4** at room temperature in the monoclinic space group $P2_1/c$ (Figure 3-7). A mixed-valent Ge$_2$Cl$_2$ moiety stabilized by the bis-NHSi ligand **I-94** and iron carbonyl Fe(CO)$_4$ was observed by single-crystal X-ray diffraction analysis. The Ge(1)-Ge(2) distance (2.4784(7) Å) is significantly longer than that in digermanium(0) NHSi:→:Ge=Ge:←:NHSi reported by So and co-workers[36b] and in the digermavinylidene ((HCDippN)$_2$B)$_2$Ge=Ge: (Dipp = 2,6 - iPr$_2$C$_6$H$_3$) reported by Aldridge et al.,[73] consistent with those Ge-Ge single bonds in dichlorogermylene oligomers.[74] The Ge^{II} center of the Ge$_2$Cl$_2$ moiety in **3-4** adopts a pyramidal geometry (sum of bond angles around Ge(2) is 288.47°) which is different from the co-planer configuration of the R$_2$E moiety in a ((HCDippN)$_2$B)$_2$Ge=Ge: reported by

Aldridge and co-workers as well as for other heavier vinylidene analogues published by the Filippou and Scheschkewitz groups. [72-73, 75]
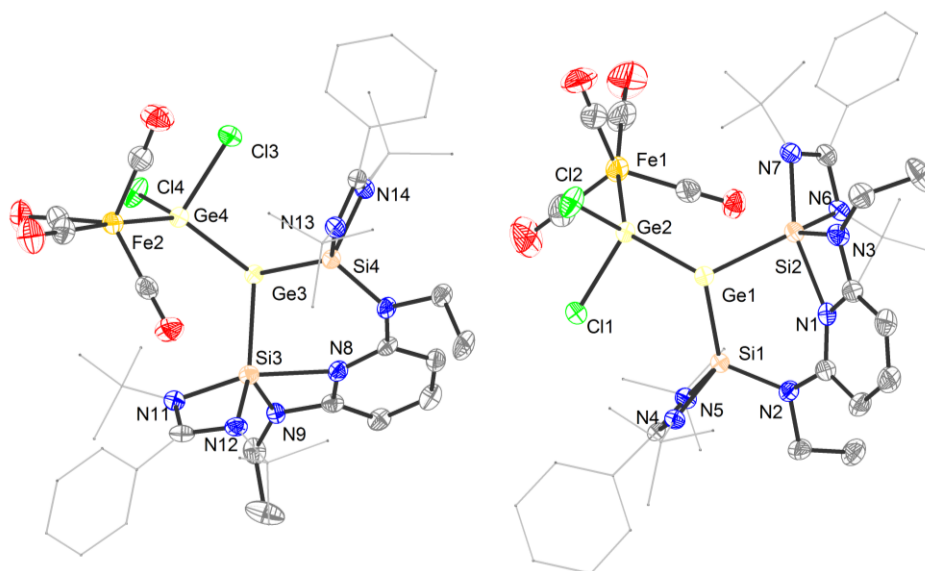
Figure 3-7. Molecular structure of the germylone iron complex **3-4**. Thermal ellipsoids are set at 50 % probability level. Hydrogen atoms and solvent molecules are omitted for clarity. Selected bond lengths [Å] and angles [°]: Ge(1)-Si(2) 2.3854(13), Ge(1)-Si(1) 2.4000(13), Ge(1)-Ge(2) 2.4784(7), Fe(1)-Ge(2) 2.3592(10), Ge(3)-Si(4) 2.3734(13), Ge(3)-Si(3) 2.3878(13), Ge(3)-Ge(4) 2.4877(7), Fe(2)-Ge(4) 2.3738(9); Si(2)-Ge(1)-Si(1) 99.83(4), Si(2)-Ge(1)-Ge(2) 114.99(4), Si(1)-Ge(1)-Ge(2) 102.96(4), Cl(1)-Ge(2)-Cl(2) 94.06(5), Cl(1)-Ge(2)-Fe(1) 113.40(5), Cl(2)-Ge(2)-Fe(1) 110.53(5), Cl(1)-Ge(2)-Ge(1) 95.49(4), Cl(2)-Ge(2)-Ge(1) 98.92(4), Fe(1)-Ge(2)-Ge(1) 136.13(3).

In order to get insight into the electronic structure of **3-4,** DFT calculations at B3LYP/6-311G(d,p) were performed on the model compound, where the methyl groups replace the *t*Bu groups on the N(2) and N(3) atoms in the synthesized compounds. The calculated geometry of the model compounds is in good agreement with the metric data obtained from X-ray diffraction analyses of the synthesized compounds. The important structural parameters of the model compound of **3-4** are**:**

The Ge-Si distances are in the range of 2.387 - 2.390 Å. Ge2-Ge1 bond length is 2.502 Å. Ge2-Fe1 bond length is 2.389 Å. Si1-Ge1-Si2 angle is 89.40° (Figure 3-8).
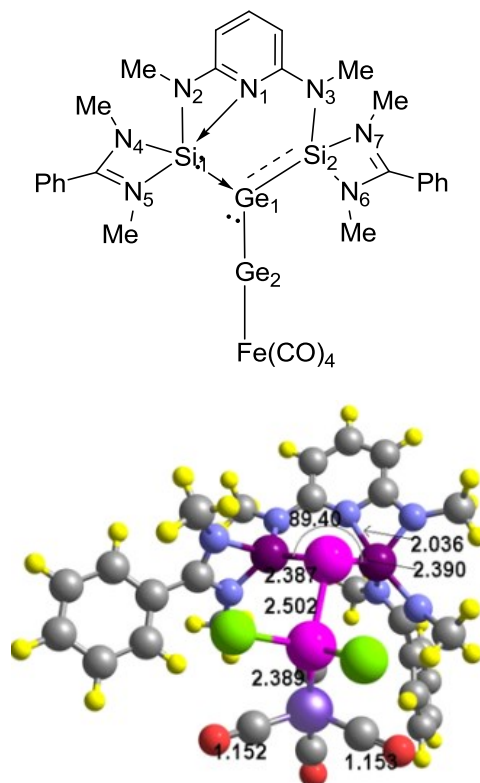
Figure 3-8. Calculated (B3LYP/6-311G(d,p) important structural parameters of model complex **3-4.** The bond length in **Å,** the bond angle in degrees.

A free s-type lone-pair on Ge1 (occupancy of 1.8 ele.) and a p-type lone pair orbital on Ge2 (occupancy of one electron) were found by NBO analysis (Figure 3-9). Ge1 and Ge2 are bound by a non-polar single bond. The DFT calculated Ge2-Fe distance of 2.389 Å (exp. 2.359 Å, WBI = 0.47) is significantly shorter than the Ge-Fe distance in model complex **3-3**, but very similar to the distances in Tip(SiClR$_2$)Si=Ge←NHC[72] (Tip = 2,4,6-triisopropylphenyl) and in the germylene iron carbonyl complex[71]. The NBO electronic structure is in line with the description of push-pull stabilization, Ge^0→Ge^{II}→Fe(CO)$_4$, of model complex **3-4**. The charges on Ge^0 center (+0.96), Ge^{II} atom (-0.45), and iron center (-0.51) are consistent with a push-pull nature of this complex (Table 3-1).

LP Ge1, occ 1.8   LP Ge2, occ 1.0.   BD [Ge1(43%)- Ge2(57%)], occ 1.9

LP Ge2, occ 1.0.   BD*[Fe-C], occ 0.50

Very strong donor – acceptor interaction
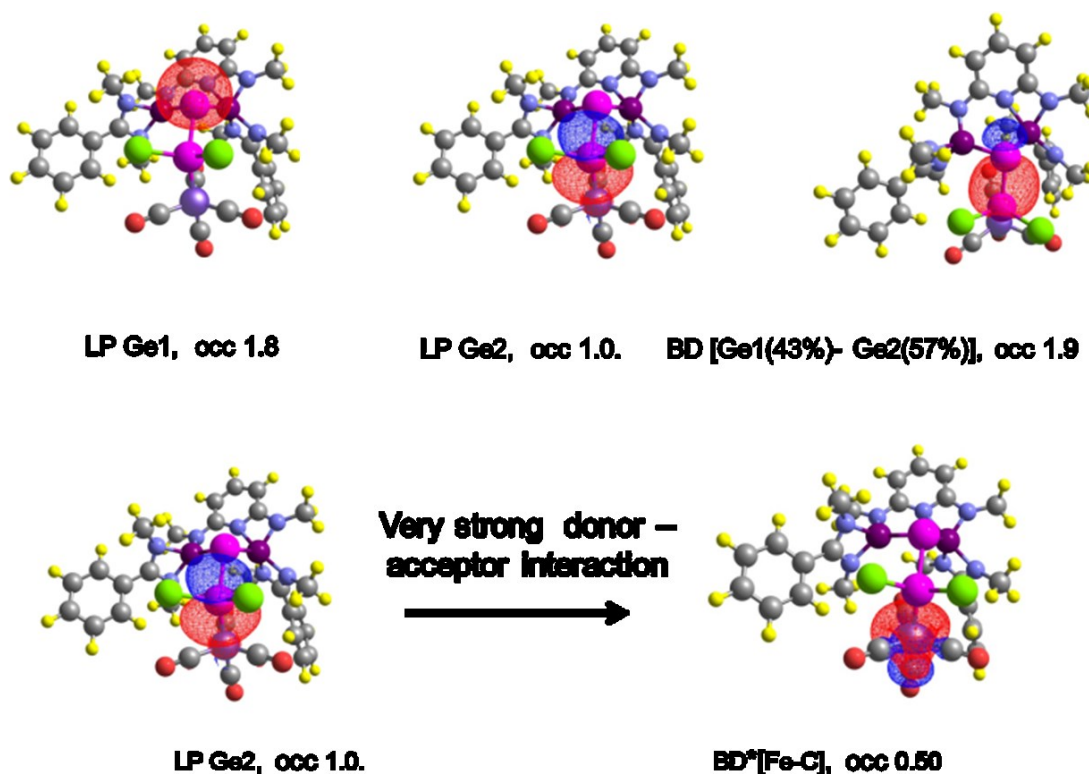
Figure 3-9. Selected NBO orbitals of the DFT-calculated model complex **3-4**. LP denotes a lone-pair orbital; BD denotes a bonding orbital and BD* denotes an antibonding orbital. The polarity of the BD orbitals is given by the percentage of the electron density on Ge and Si. occ is the occupancy of the orbital in electrons. Contour value = 0.03.

A summary of calculated structural and electronic properties of model complex **3-3, 3-4** and for comparison of reported amino(imino)germylene-Fe(CO)$_4$ is provided in Table 3-1

Table 3-1. Calculated [a] structural and electronic properties of model [b] compounds of **[SiNSi]GeFe** and **[SiNSi]GeGeFe** in comparison with a model [c] of the isolated amino(imino)germylene-Fe(CO)$_4$ complex.[d]

Adduct	**[SiNSi] GeFe**	**[SiNSi]GeGeFe**	**Amino(imino)germylene-Fe(CO)$_4$**

54

r(Si1-Ge1)[f]	2.397 (2.388)	2.390 (2.385)	-
WBI	0.96		-
r(Si2-Ge1)[f]	2.384 (2.373)	2.387 (2.400)	-
WBI	1.08	1.07	-
r(Ge1-Fe)	2.507 (2.499)	-	2.29 (2.30)
WBI	0.39	-	0.57 (0.82)[c,d]
r(Ge1-Ge2)	-	2.502 (2.478)	-
WBI	-	0.85	-
r(Ge2-Fe)	-	2.389 (2.359)	-
WBI	-	0.47	-
Natural charges (el.)			
Fe	+0.31	+0.27	+0.23
(CO)4	-1.04	-0.75	-0.63
Fe(CO)$_4$	-0.73	-0.51	-0.40
[SiNSi]Ge	+0.73	+0.96	-
Ge$_2$Cl$_2$	-	-0.45	-
Stretching vibrational frequencies (cm^{-1})			
ν1(CO)	1896 (1830)	1958	2002
ν2(CO)	1939 (1865)	2009	2016 (1930)[d]
ν3(CO)	1994 (1886)	2033	2053 (1965)[d]
ν4(CO)	2067 (1969)	2099	2117 (2039)[d]
WBI			
(CO)1	1.82	1.88	1.98
(CO)2	1.88	1.99	1.98
(CO)3	1.95	2.00	2.01
(CO)4	2.00	2.03	2.06

[a] At B3LYP-D3(BJ)/6-311G(d,p) including dispersion, bond length in Å, in parenthesis experimental values; [b] A Me replaces the *t*Bu groups; [c] A model compound where Me groups replace the Dip groups; [d] Ref [12]; [e] For the real molecule, at B3LYP/6-31G(d)/LANL2Z(Ge, Fe); [f] In **[SiNSi]Ge** r(Si1-Ge1) and r(Si2-Ge1) are 2.363Å (WBI = 1.14) and 2.311 Å (WBI = 1.44), respectively.

3.2 Synthesis of bis(silylene)-substituted ortho-carborane and the application in nickel-catalyzed amination of arenes

As discussed in chapter 1.3, as a new generation of powerful steering ligands; NHSis are no longer laboratory curiosities but valuable building blocks for the synthesis of new functional silicon compounds with high potential exceeding the Lewis donor properties of NHCs and phosphines.[76][9a, 11, 40-41, 48, 50-51, 53, 56-57, 77] However, compared to the huge numbers of phosphine and NHC ligands which are widely used in catalysis, multidentate NHSis are still less explored. Very recently, the introduction of the *ortho*-dicarbadodecaborane backbone ($C_2B_{10}H_{12}$) in ligand design have been reported by different research groups by taking advantage of its unique electronic and chemical property.[78] Here the synthesis of bis-NHSi-substituted *o*-carborane ligand and corresponding nickel complexes as well as their superior suitability to serve as (pre)catalysts in the Ni-catalyzed Buchwald-Hartwig coupling reactions were described.

3.2.1 Synthesis of *o*-carborane-based bis-NHSi ligand and its Ni complexes
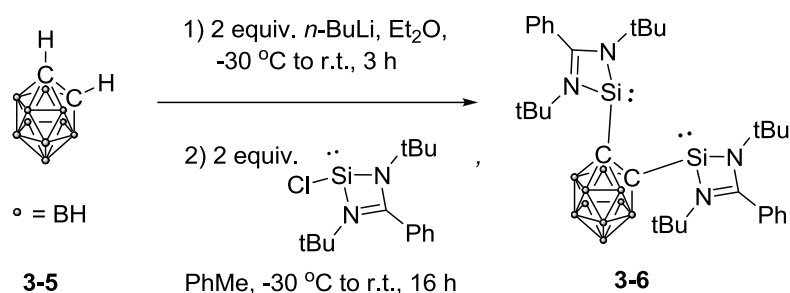
Scheme 3-6. Synthesis of bis-silylene substituted *o*-carborane **3-6**.

The reaction of *n*-BuLi with *o*-carborane ($C_2B_{10}H_{12}$) **3-5** at −30 °C generated the di-lithiated *o*-carborane ($C_2B_{10}H_{10}Li_2$) as a white suspension in diethyl ether. The slurry was then cooled to −30 °C and two molar equivalents of *N,N'*-di-*tert*-butyl(phenylamidinato)chlorosilylene in toluene were added dropwise *via* syringe. The bis-silylene substituted *o*-carborane **3-6** was obtained after the salt metathesis

reaction at low temperature as light yellow crystals in 84% yield (Scheme 3-6). In the ^{1}H NMR spectrum, the protons of the *tert*-butyl and phenyl groups result in a singlet and multiplet resonance signals at δ = 1.25 ppm and 6.87−7.30 ppm, respectively. However, the respective B-H ^{1}H NMR signals lead to broad peaks at about 3 ppm. The ^{29}Si NMR signal of **3-6** is observed at δ = 18.9 ppm, which is relatively down-field shifted compared with the bis-NHSi bridged by oxygen atoms **I-87** (δ = −16.1 ppm) and[48] **I-93** (δ = −24.0 ppm).[53] or nitrogen atoms **I-94** (δ = −14.9 ppm)[56] but high-field shifted compared with the bis(NHSi)- substituted ferrocene **I-86** (δ = 43.3 ppm) (Scheme 3-7).[51]
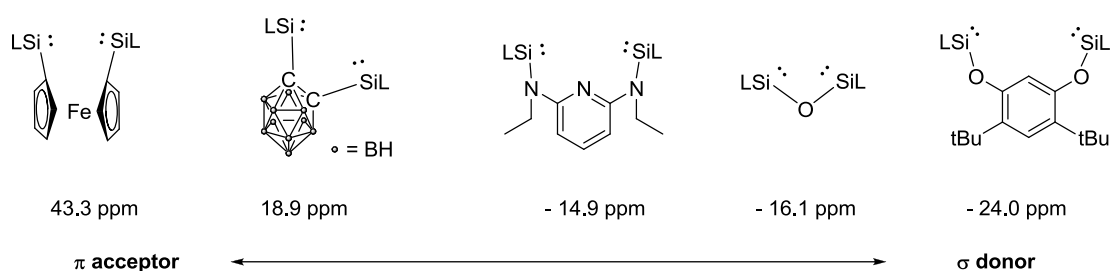
Scheme 3-7. Comparison of donor-acceptor abilities of different bis-silylene ligands based on *N,N*-di(*tert*-butyl)amidinato backbones. (L = PhC(N*t*Bu)$_2$)

Single-crystals of **3-6** suitable for an X-ray diffraction analysis could be grown in concentrated toluene solutions at 0 °C; the compound crystallizes in the monoclinic space group *P*2$_1$/c (Figure 3-10). The C1–Si2 and C2–Si1 distances are 2.001(2) and 1.991(2) Å, respectively. The NHSi motifs are pointed to each other with a Si−Si distance of 3.267 Å, indicating that SiCCSi could be a suitable chelating ligand.
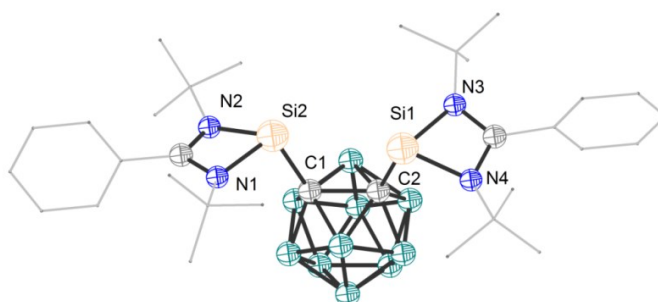

Figure 3-10. The molecular structure of **3-6**. Thermal ellipsoids are set at 50 % probability level. Hydrogen atoms and solvent molecules are omitted for clarity.

Selected bond lengths [Å] and angles [°]: Si(1)-N(4) 1.8644(15), Si(1)-N(3) 1.8689(15), Si(1)-C(2) 1.991(2), N(1)-Si(2) 1.8685(16), C(1)-Si(2) 2.001(2), Si(2)-N(2) 1.8787(16); N(4)-Si(1)-N(3) 69.82(7), N(4)-Si(1)-C(2) 99.18(7), N(3)-Si(1)-C(2) 100.86(7), N(1)-Si(2)-N(2) 69.81(7), N(1)-Si(2)-C(1) 96.79(8), N(2)-Si(2)-C(1) 99.85(8).

Treatment of bis-silylene ligand **3-6** with $NiBr_2(dme)$ (dme = 1,2-dimtheoxyethane) in toluene at room temperature afforded the Ni^{II} complex **3-7** (Scheme 3-8). The groups of tert-butyl and aromatic protons resonate at $\delta = 1.33$ ppm and 6.83−7.55 ppm, respectively, in the ^1H NMR spectrum, which are relatively downfield shifted due to metal coordination. Complex **3-7** exhibits a ^{29}Si NMR signal at $\delta = 58.7$ ppm, which is also drastically downfield shifted compared with the ligand **3-6** ($\delta = 18.9$ ppm) and other reported $NHSi-Ni^{II}$ complexes (e.g. Ni^{II} complexes with a NHC-NHSi ligand **I-92** [$LSi:(CH_2)NHCNiBr_2$] ($\delta = 8.3$ ppm; L = $CH(C=CH_2)(CMe)(NAr)_2$, Ar = $2,6-iPr_2C_6H_3$; NHC = 3,4,5-trimethylimidazol-2-yliden-6-yl)[11] and pincer-type ligand **I-93** ($\delta = 20.2$ ppm)).[50]
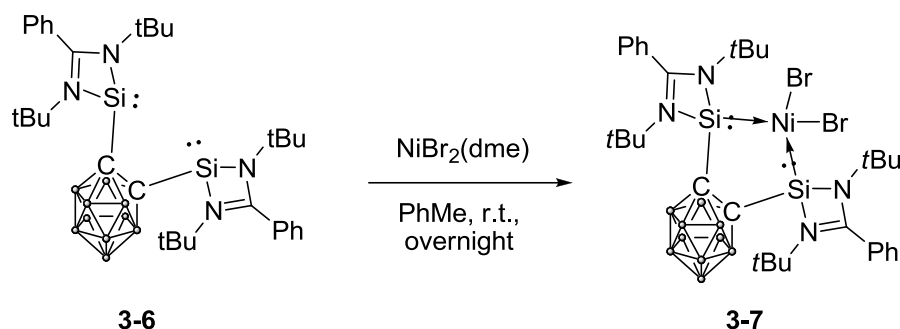
Scheme 3-8. Synthesis of bis-silylene Ni^{II} complex **3-7**.

Single-crystals of Ni^{II} complex **3-7** (monoclinic space group $P2_1/c$) were obtained in concentrated toluene solutions at 0 °C (Figure 3-11). The X-ray analysis of the latter revealed that the Ni^{II} center in complex **3-7** is in a square-planar environment with the sum of angles around the Ni atom of 360.02°. The Ni(1)–Si(1) (2.1378(5) Å)

and Ni(1)–Si(2) (2.1447(5) Å) distances are shorter than the reported NHSi- Ni^{II} complexes supported by the pincer-type ligand **I-93** (2.1737(7) Å) and a related NHC-NHSi ligand **I-92** in [LSi:(CH$_2$)NHCNiBr$_2$] (2.1553(8) Å; L = CH(C=CH2)(CMe)(NAr)2, Ar = 2,6-iPr$_2$C$_6$H$_3$; NHC = 3,4,5-trimethylimidazol-2-yliden-6-yl).[11]
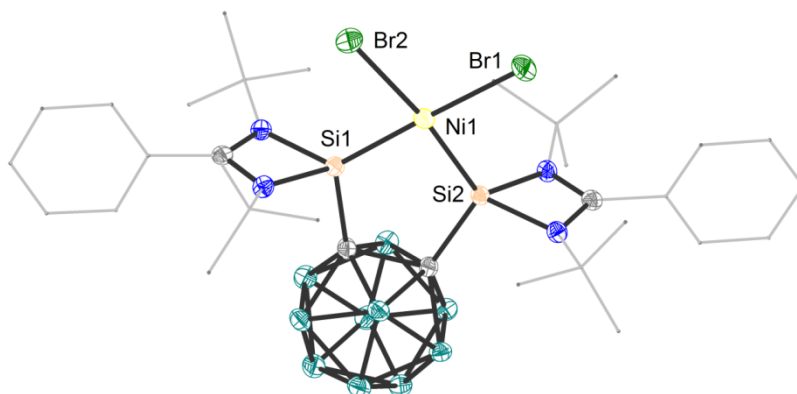

Figure 3-11. Molecular structure of **3-7**. Thermal ellipsoids are set at 50 % probability level. Hydrogen atoms and solvent molecules are omitted for clarity. Selected bond lengths [Å] and angles [°]: Br(1)–Ni(1) 2.3523(4), Ni(1)–Si(1) 2.1378(5), Ni(1)–Si(2) 2.1447(5), Ni(1)–Br(2) 2.3322(3); Si(1)–Ni(1)–Si(2) 88.42(2), Si(1)–Ni(1)–Br(2) 83.009(17), Si(2)–Ni(1)–Br(2) 171.12(2), Si(1)–Ni(1)–Br(1) 178.64(2), Si(2)–Ni(1)–Br(1) 90.364(17), Br(2)–Ni(1)–Br(1) 98.231(13).

DFT calculations (B97-D/6-31G(d)[Fe, Ni, Si, Br: def2-TZVP] and B3LYP/6-31G(d)[Fe, Ni, Si, Br: def2-TZVP]) also confirm the square-planar geometry around the d^8-Ni atom (sum of angles around Ni is 360.17°), and the Ni-Si distances (2.131(2) Å) are also in very good agreement with the respective experimental data. The LUMO is the antibonding orbital for the Si→Ni donation orbital. The HOMO is always a d orbital, and the other 4 d orbitals are also close to the HOMO in energy (LUMO: -2.11 eV, HOMO: -4.37 eV, HOMO-1: -4.39 eV, HOMO-2: -4.45 eV, HOMO-4: -4.81 eV, HOMO-5: -5.36 eV, HOMO-9: -5.90 eV, Figure 3-12).
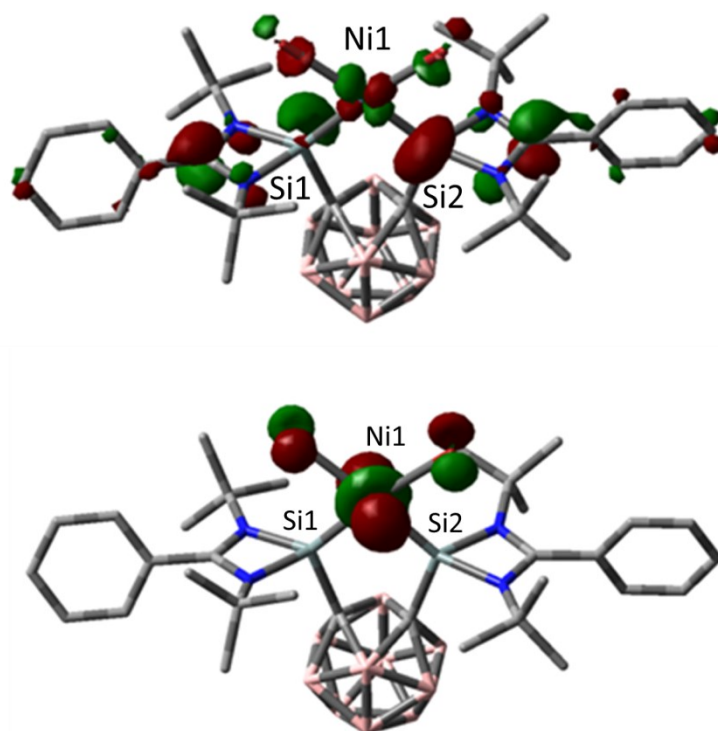
Figure 3-12. Selected molecular orbitals of Ni^{II} complex **3-7**. Electronic structure analysis was executed both at B97-D/6-31G(d)[Fe, Ni, Si, Br: def2-TZVP] and B3LYP/6-31G(d)[Fe, Ni, Si, Br: def2-TZVP].

The corresponding Ni^0 carbonyl complex **3-8** was synthesized by reduction of complex **3-7** with KC$_8$ in the presence of carbon monoxide atmosphere (Scheme 3-9). The ^{29}Si NMR signal of complex **3-8** appears at $\delta = 86.0$ ppm, which is significantly downfield shifted compared with the Ni^{II} complex **3-7** ($\delta = 58.7$ ppm), suggesting the strong π acceptor nature of carbonyl ligands. The ^{13}C NMR signal of the carbonyl ^{13}C nucleus in **3-8** appears at 207.6 ppm, which is downfield shifted compared with other carbonyl nickel complexes bearing NHC ligands [(NHC^R)$_2$Ni(CO)$_2$] ($\delta = 198.3$, and 194.3 ppm; R = cyclohexyl and 2,4,6-Me$_3$C$_6$H$_2$, respectively)[79] or NHC-NHSi mixed ligand [LSi:(CH$_2$)NHCNi(CO)$_2$] ($\delta = 198.2$ ppm; L = CH(C=CH$_2$)(CMe)(NAr)$_2$, Ar=2,6-iPr$_2$C$_6$H$_3$; NHC = 3,4,5-trimethylimidazol-2-yliden-6-yl).[11]
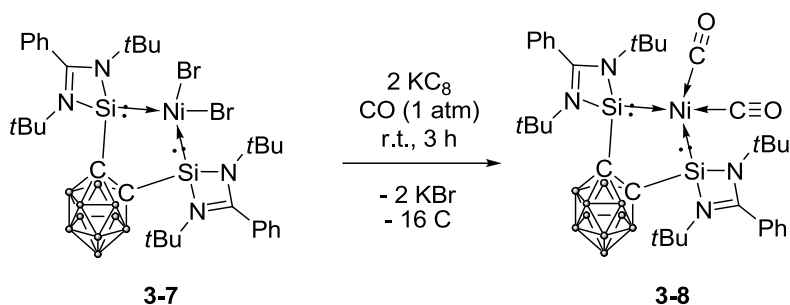
Scheme 3-9. Synthesis of the bis-silylene Ni^0 complex **3-8**.

Single crystals of Ni^0 complex **3-8** were obtained in concentrated toluene solutions. Preliminary single-crystal X-ray diffraction data of complex **3-8** and DFT calculations (B97-D/6-31G(d)[Fe, Ni, Si, Br: def2-TZVP] and B3LYP/6-31G(d)[Fe, Ni, Si, Br: def2-TZVP]) confirm a tetrahedral four-coordinate Ni^0 center (Figure 3-13 and Figure 3-14).
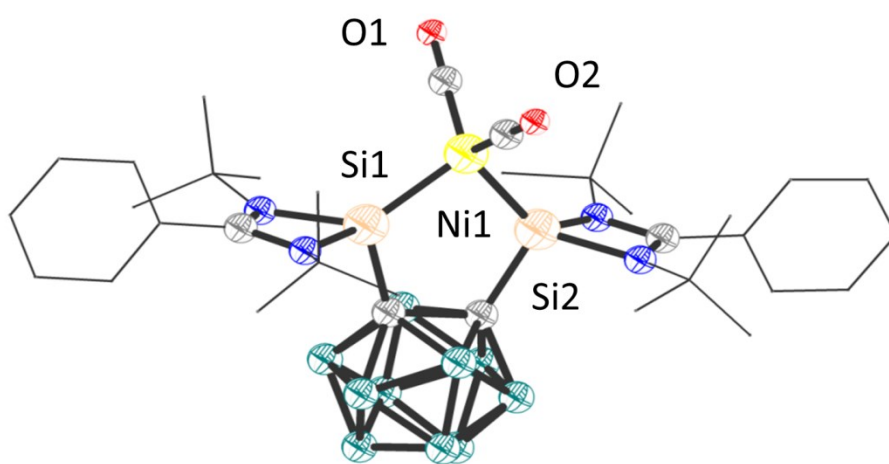
Figure 3-13. The molecular structure of **3-8** determined by a preliminary X-ray diffraction analysis Thermal ellipsoids are set at 50 % probability level. Hydrogen atoms and solvent molecules are omitted for clarity. Due to the moderate crystal quality, the metric parameters are not discussed.
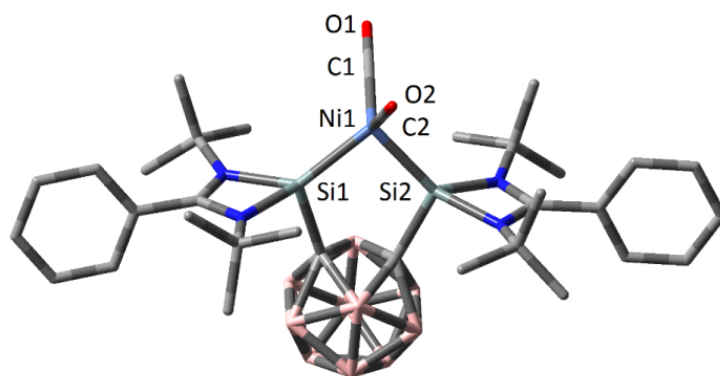
Figure 3-14. DFT-derived molecular structure of **3-8**. Hydrogen atoms are omitted for clarity. Selected distances [Å] and angles [°]: C(1)-Ni(1) 1.789, Ni(1)-Si(1) 2.195, Ni(1)-Si(2) 2.191, Ni(1)-C(2) 1.793, C(1)-O(1) 1.173, C(2)-O(2) 1.172; Si(1)-Ni(1)-Si(2) 92.25, Si(1)-Ni(1)-C(2) 113.19, Si(2)-Ni(1)-C(2) 110.16, Si(1)-Ni(1)-C(1) 109.54, Si(2)-Ni(1)-C(1) 109.73, C(2)-Ni(1)-C(1) 118.77.
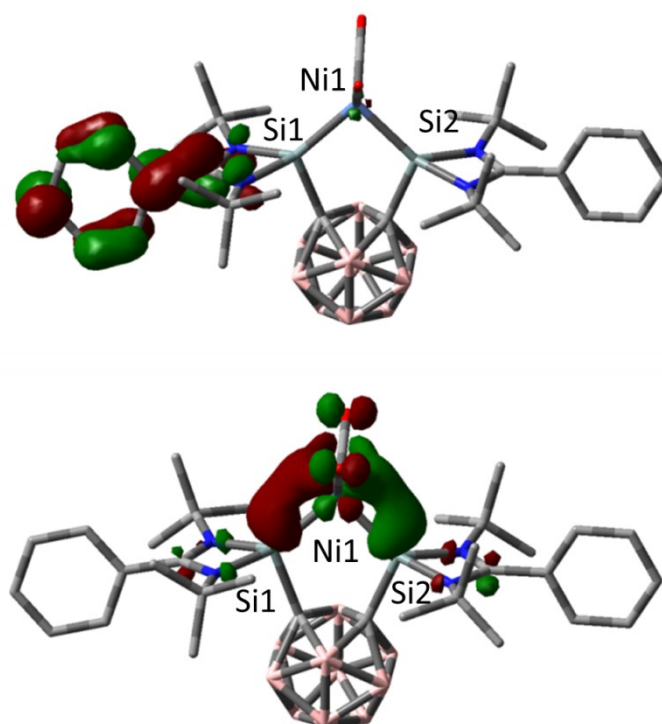
Figure 3-15. selected molecular orbitals of Ni^0 complex **3-8** (top: LUMO; bottom: HOMO). Electronic structure analysis was executed both at B97-D/6-31G(d)[Fe, Ni, Si, Br: def2-TZVP] and B3LYP/6-31G(d)[Fe, Ni, Si, Br: def2-TZVP].

The complex shows very similar orbitals compared to those of **3-7**. The LUMO is a π* phenyl orbital indicating that the Ni is an 18 electron closed-shell stable atom.

The HOMO is a d orbital (the Si lone pair also has a contribution to this), and the other 4 d orbitals are also close to the HOMO in energy. (LUMO: -1.57 eV, HOMO: -3.93 eV, HOMO-1: -4.41 eV, HOMO-2: -4.84 eV, HOMO-5: -5.50 eV, HOMO-6: -5.63 eV, HOMO-7: -6.16 eV, Figure 3-15).

The IR stretching vibration frequencies of the carbonyl groups in **3-8** were observed at ν = 1982 and 1934 cm^{-1}. They are red-shifted compared with a NHSi-NHC Ni^0 carbonyl complex reported by our group (ν = 1952, 1887 cm^{-1})[11] and NHC Ni^0 carbonyl complex [(NHC^{Cy})$_2$Ni(CO)$_2$] (ν = 1949, 1878 cm^{-1})[9] but blue-shifted compared with Ni^0 complex bearing the bis-phosphine analogous ligand in {[(Ph$_2$PC)$_2$B$_{10}$H$_{10}$]Ni(CO)$_2$} (ν = 2021 and 1966 cm^{-1}),[9b] {[(Et$_2$PC)$_2$B$_{10}$H$_{10}$]Ni(CO)$_2$} (ν = 2013 and 1955 cm^{-1}),[9] and NHC Ni^0 carbonyl complex [(NHC^{Mes})$_2$Ni(CO)$_2$] (ν = 2051, 1887 cm^{-1}),[9] which indicate that the σ-donor strength of o-carborane-based NHSi ligand is similar or even stronger than NHC or phosphine ligands.
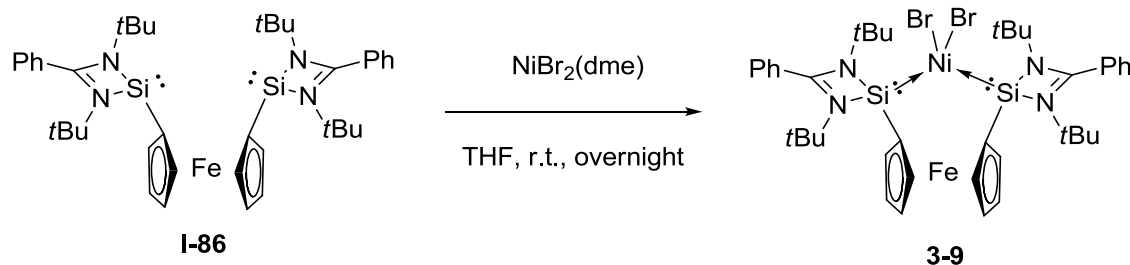
Scheme 3-10. Synthesis of the bis-silylene Ni^{II} complex **3-9**.

For comparison, the bis-silylene Ni^{II} complex **3-9** supported by a ferrocendiyl bridged ligand **I-86** was also synthesized (Scheme 3-10). Treatment of bis-silylene ligand **I-86** with NiBr$_2$(dme) (dme = 1,2-dimtheoxyethane) in THF at room temperature overnight afforded the desired Ni^{II} complex **3-9**. The groups of *tert*-butyl, ferrocene, and aromatic protons resonate at δ = 1.44, 4.28−4.50, and 6.73−8.08 ppm, respectively, in the ^{1}H NMR spectrum. Complex **3-9** exhibits a ^{29}Si NMR signal at δ = 49.31 ppm, which is also downfield shifted compared with the 'free' ligand (δ =

43.3 ppm) but upfield shifted compared with the Ni^{II} complex **3-7** bearing the *o*-carborane-based bis-silylene ligand **3-6**.
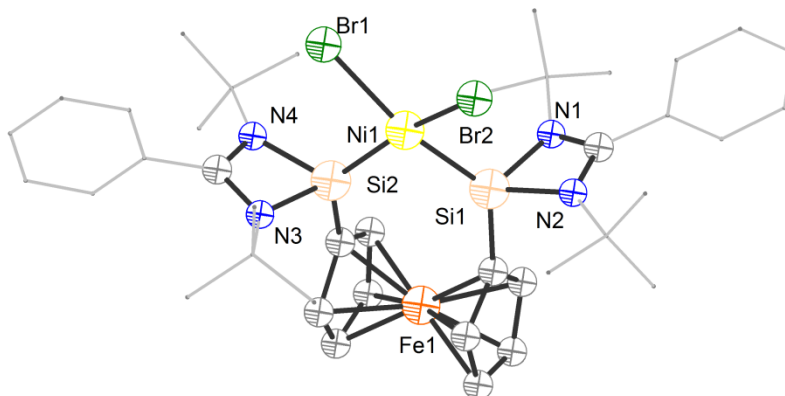
***Figure 3-16***. The molecular structure of **3-9**. Thermal ellipsoids are set at 50 % probability level. Hydrogen atoms and solvent molecules are omitted for clarity. Selected distances [Å] and angles [°]: Br(1)-Ni(1) 2.3737(6), Ni(1)-Si(1) 2.1786(10), Ni(1)-Si(2) 2.2005(10), Ni(1)-Br(2A) 2.323(10), Ni(1)-Br(2) 2.379(3), Si(1)-Ni(1)-Si(2) 92.69(3), Si(1)-Ni(1)-Br(2A) 90.4(3), Si(2)-Ni(1)-Br(2A) 173.7(13), Si(1)-Ni(1)-Br(1) 165.17(4), Si(2)-Ni(1)-Br(1) 89.83(3), Br(2A)-Ni(1)-Br(1) 88.6(6), Si(1)-Ni(1)-Br(2) 89.02(8), Si(2)-Ni(1)-Br(2) 164.41(8), Br(2A)-Ni(1)-Br(2) 10.1(15), Br(1)-Ni(1)-Br(2) 92.46(8).

The toluene solutions of **3-9** were concentrated and left in a freezer at 0°C overnight affording orange crystals of the desired complex in 60% yields. **3-9** crystallizes in the monoclinic space group $P2_1/c$ (Figure 3-16). Akin to **3-7**, its Ni^{II} center adopts a square-planar geometry but with slight distortion (with the sum of angles around Ni atom of 364.01°). However, the Ni(1)–Si(1) (2.1786(10) Å) and Ni(1)–Si(2) (2.2005(10) Å) distances are slightly longer than those in complex **3-7**.
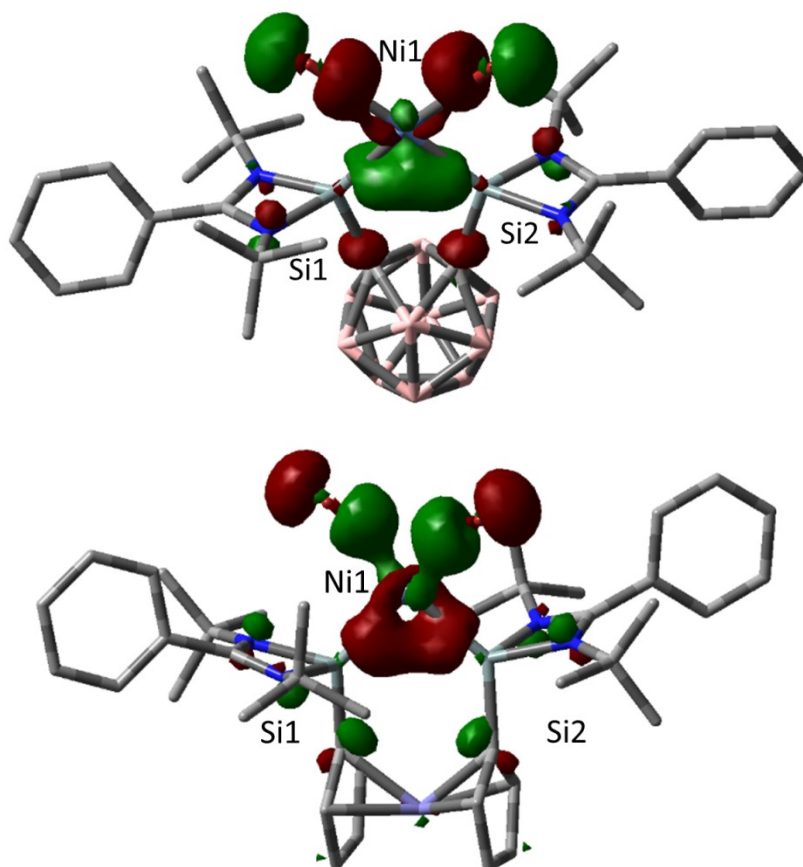
Figure 3-17. HOMO-9 (-5.90 eV) of [SiCCSi]NiBr2 and HOMO-12 (-5.49 eV) of [FcSiSi]NiBr.

DFT calculations confirm the elongation of the Ni-Si distances in complex **3-9** compared to **3-7** resulting from a weaker donor ability of the ferrocene-based ligand towards Ni. The LUMO of **3-9** is the antibonding orbital for the Si→Ni donation orbital (Figure 3-17). The HOMO is a d orbital. (LUMO: -1.87 eV, HOMO: -3.69 eV, HOMO-1: -3.97 eV, HOMO-7: -4.89 eV, HOMO-8: -5.03 eV, HOMO-12: -5.49 eV, HOMO-14: -5.81 eV). The calculated charge of the Ni center is +0.72 in **3-7** but +0.78 in **3-9**. The orbitals of **3-9** are similar to those of **3-7**. The Si→Ni donation orbital of **3-7** is always more stable than the corresponding Si→Ni orbital of **3-9** which might indicate a stronger donation to the Ni center which might be related to the catalytic activity.
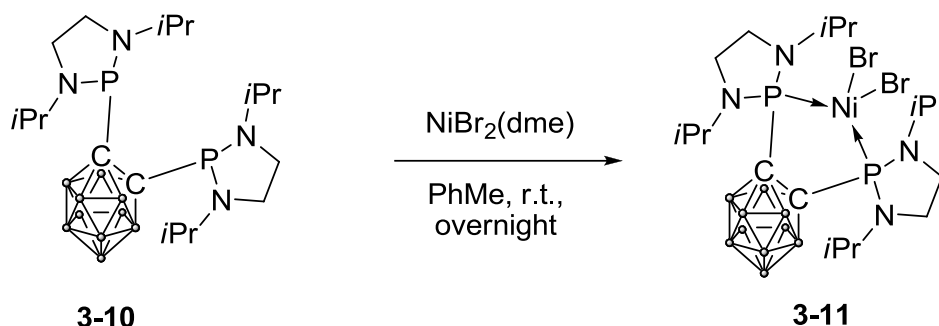
Scheme 3-11. Synthesis of the bis-phosphine Ni^{II} complex **3-11**.

For comparison, the bis-phosphine Ni^{II} complex supported by *o*-carborane-based ligands **3-10** and **3-12** were synthesized (Scheme 3-11). Electron-rich phosphine bis(cyclodiaminophosphanyl)-*o*-carborane **3-10** reported by Bourissou et al. was synthesized according to reported procedures. Treatment of ligand **3-10** with NiBr$_2$(dme) (dme = 1,2-dimtheoxyethane) in toluene at room temperature overnight afforded the bis-phosphine Ni^{II} complex **3-11**. The groups of *iso*-propyl and -CH$_2$- of phosphine backbone protons resonate at δ = 1.16−4.41 ppm in the ^{1}H NMR spectrum. However, the respective B-H proton signals lead to broad resonance signals around 3 ppm. The complex **3-11** exhibits a ^{31}P NMR signal at δ = 133.96 ppm, which is also downfield shifted compared with the 'free' ligands because of the coordination. The toluene solutions of **3-11** were concentrated and left in a freezer at 0°C overnight affording crystals of the desired complex in 46 % yields. **3-11** crystallizes in the monoclinic space group *P*2$_1$/c. Akin to **3-7**, its Ni^{II} center adopts a square-planar geometry with the Ni(1)–P(1) and Ni(1)–P(2) distances of 2.1432(12) Å and 2.1539(12) Å, respectively.
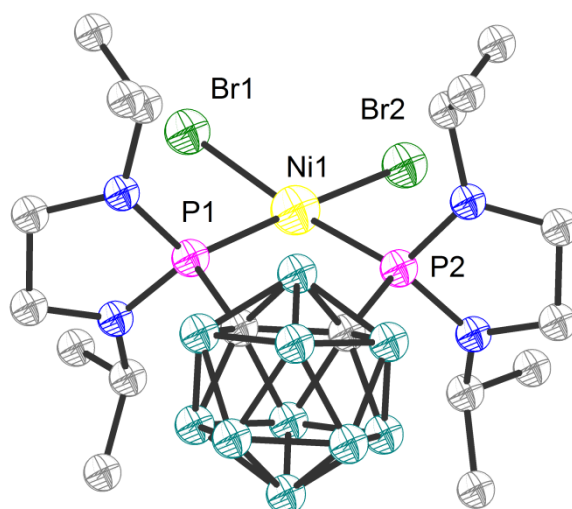
Figure 3-18. The molecular structure of **3-11**. Thermal ellipsoids are set at 50 % probability level. Hydrogen atoms and solvent molecules are omitted for clarity. Selected distances [Å] and angles [°]: Br(1)-Ni(1) 2.3375(8), Ni(1)-P(1) 2.1432(12), Ni(1)-P(2) 2.1539(12), Ni(1)-Br(2) 2.3154(8), P(1)-Ni(1)-P(2) 95.61(5), P(2)-Ni(1)-Br(2) 86.14(4), P(1)-Ni(1)-Br(1) 85.95(4), Br(2)-Ni(1)-Br(1) 92.75(3).

Treatment of bis-(diphenylphosphanyl) ligand **3-12** with $NiBr_2(dme)$ (dme = 1,2-dimtheoxyethane) in toluene at room temperature overnight afforded the bis-phosphine Ni^{II} complex **3-13** (Scheme 3-12). The spectroscopic data of Ni^{II} complex **3-13** agree with the reported ones.
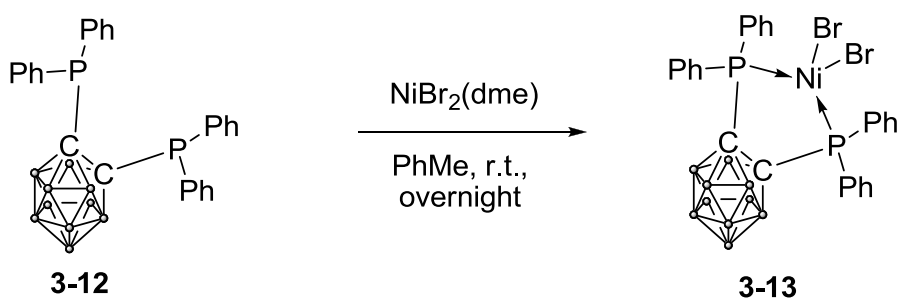
Scheme 3-12. Synthesis of the bis-phosphine Ni^{II} complex **3-13**.

3.2.2 Buchwald-Hartwig amination reactions catalyzed by o-carborane bis-NHSi Ni complexes

Buchwald-Hartwig amination, a C-N bond formation reaction catalyzed by palladium complexes, is important in organic synthesis since a large amount of medically important molecules and materials contain arylamine motifs.[80] However, in recent years, for declining the use of expensive and natural less abundance precious metal complexes in catalysis, developing the cheap and earth-abundant first-row complexes as a replacement has attracted much attention.[81] Among first-row TMs, nickel is a promoting alternative metal which could facilitate the oxidative addition of a substrate at the metal center.[81i, 81k-81n, 82] In the past few years, either structure-defined or in situ generated Ni complexes have been demonstrated to be the pre-catalysts of Buchwald-Hartwig amination. Among these cases, phosphines, NHCs, and N-based ligands have been demonstrated to promote the catalytic performance.[82-83] Considering the electron-rich properties of NHSi ligands, the combination of NHSi ligands and nickel precursor would further facilitate the oxidative addition step, thus offering massive opportunities in such reactions. Therefore, developing new NHSi ligand system for Buchwald-Hartwig amination is demanding.

Initial screening experiments revealed that already 0.5 mol% of **3-7** can catalyze the desired transformation effectively in high yield (93%) after 25 hours at 100 °C in the presence of catalytic amounts of AgBPh$_4$ and 1.2 molar equivalents of KOtBu as a base (Table 3-2). The reactions without silver salt gave lower conversion (5 – 45%). The bulky AgBPh$_4$ shows the best conversion and selectivity (71 % and 99 %) compared with AgBF$_4$ and AgOTf. Next, the influence of the different bases was tested. When K$_2$CO$_3$ and Cs$_2$CO$_3$ were used, the reactions gave very low conversion (4 % and 5 %). However, the lithium salts (LiOMe and LDA) could promote the catalytic performances (26 % and 59 %) but showed relatively poor selectivity (25 % and 96 %).

Table 3-2. The nickel-catalyzed Buchwald-Hartwig coupling using various reaction conditions[a]
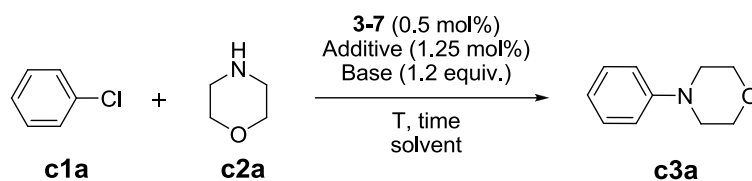
| Entry | additive | Base | Solvent | t | T | Conversion[b] | Selectivity %[b] |
		1.2eq	1.5mL	h	°C	%	c3a
1		KO*t*Bu	dioxane	16	80	5	40
2		KO*t*Bu	dioxane	16	100	45	91
3	AgOTf	KO*t*Bu	Toluene	16	100	64	96
4	AgBF$_4$	KO*t*Bu	Toluene	16	100	69	97
5	AgBPh$_4$	KO*t*Bu	Toluene	16	100	71	99
6	NaBARF	KO*t*Bu	Toluene	16	100	68	97
7	AgBPh$_4$	K$_2$CO$_3$	Toluene	16	100	4	18
8	AgBPh$_4$	Cs$_2$CO$_3$	Toluene	16	100	5	14
9	AgBPh$_4$	LiOMe	Toluene	16	100	26	25
10	AgBPh$_4$	LDA	Toluene	16	100	59	96
11	AgBPh$_4$	KO*t*Bu	dioxane	16	100	76	99
12	AgBPh$_4$	KO*t*Bu	dioxane	25	100	94	99

[a] Reaction conditions: **c1a** (0.5 mmol), **c2a** (0.75 mmol), [Ni] (0.5 mol%), additive (1.25 mol%), base (1.2 equiv), T=80-100 °C, solvent = 1.5 mL, internal standard = decane, t =16-25 h. [b] the conversions and selectivities are determined based on the substrate **c1a**.

Table 3-3. The nickel-catalyzed Buchwald-Hartwig coupling using various reaction conditions[a]
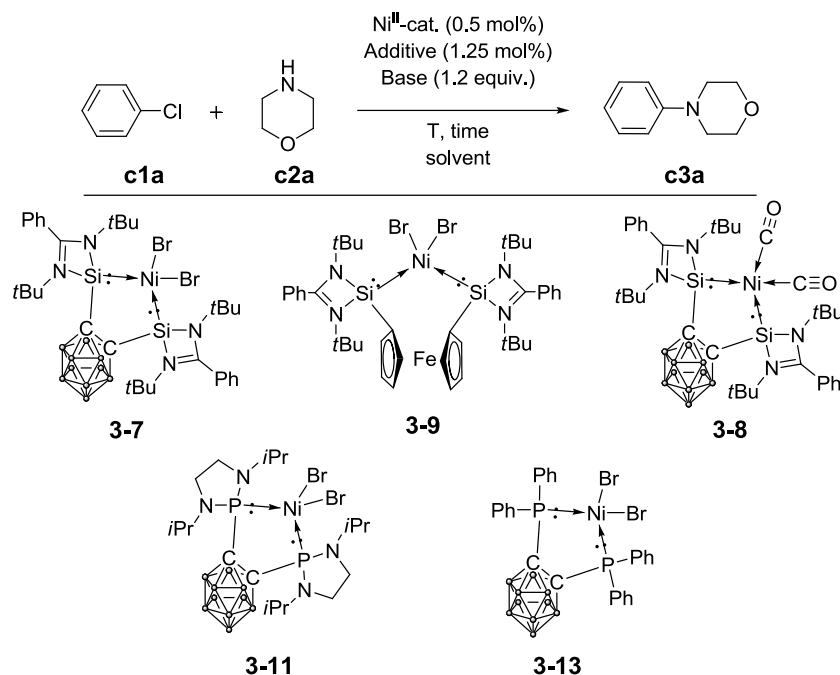
Entry	Cat 0.5 mol%	additive	t h	Conversion[b] %	Selectivity %[b] c3a
1	NiBr$_2$(dme)		16	29	84
2	**3-7**	AgBPh$_4$	25	94	99
3	**3-9**	AgBPh$_4$	25	80	98
4	**3-11**	AgBPh$_4$	25	69	96
5	**3-13**	AgBPh$_4$	25	67	94
6	**3-8**	AgBPh$_4$	25	82	96
7[c]	**3-7**	AgBPh$_4$	25	87	95
8[d]	**3-7**	AgBPh$_4$	25	88	93

[a] Reaction conditions: **c1a** (0.5 mmol), **c2a** (0.75 mmol), [Ni] (0.5 mol%), AgBPh$_4$ (1.25 mol%), KO*t*Bu (1.2 equiv), T= 100 °C, solvent = 1.5 mL, internal standard = decane, t =16-25 h. [b] the conversions and selectivities are determined based on the substrate **c1a**. [c] 1-2 equiv. of Mercury added. [d] 1-2 equiv. of tetramethylthiourea (TMTU) added.
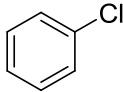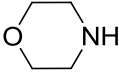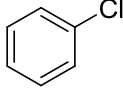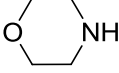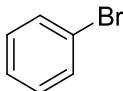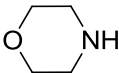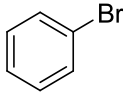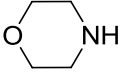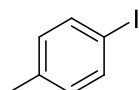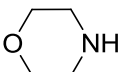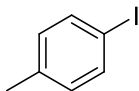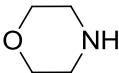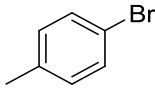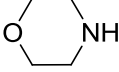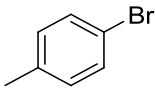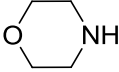
In contrast, employing NiBr$_2$(dme) as a precatalyst leads to lower yields of product (24%; see Table 3-3, Entry 1). Moreover, poisoning studies and control experiments proved that the reaction is mediated by a molecular nickel catalyst (Table 3-3, Entries 7-8). Because the complex **3-9** contains a less σ-donor strength bis-NHSi ligand, the yields of **c3a** (78%) is relatively lower. The higher activity of **3-7** can be explained with the stronger donor character of the *o*-carborane bis-NHSi ligand towards Ni^{II}, which facilitates the oxidative addition step at the nickel site. Furthermore, for comparison of the catalytic performances of the *o*-carborane bis-NHSi complex **3-7** with those of related phosphine-Ni^{II} complexes containing the bis(diphenylphosphine)- and a bis-(cyclodiaminophosphine)-substituted *o*-carborane ligand, the respective complexes **3-11** and **3-13** were also tested in the catalytic amination of **c1a** with **c2a** under identical conditions; it turned out that both catalyze the desired formation of c3a in considerably lower yields (66 and 69%, respectively; for details see Tabs 3-3).
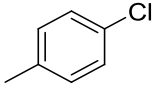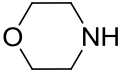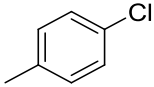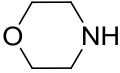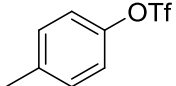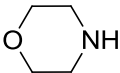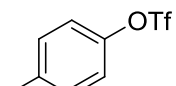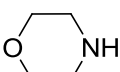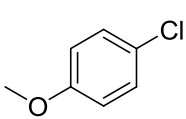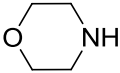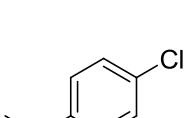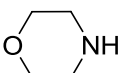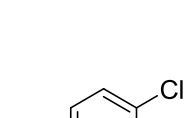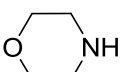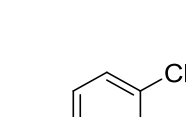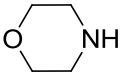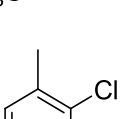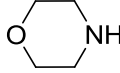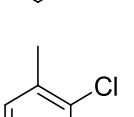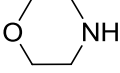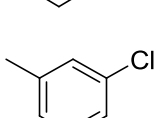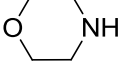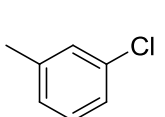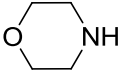
The effect of different leaving groups such as halides (I, Br, Cl) and trifluoromethylsulfonate (OTf) was also studied. It was shown that changing from I to OTf lowers the overall rate of the reaction (from 87% to 11% conversion; Table 3-4). Moreover, the reaction of the aryl halides bearing electron-donating groups gave lower conversions, while electron-withdrawing groups at the para position increase the overall reaction rate (OMe < Me < H < CF$_3$; Table 3-4). In other words, the reaction rate depends on the electronic nature of the substrates applied in the reaction. Aryl substrates with a substituent at the para position gave higher yields compared to those in meta and ortho positions (2-Me < 3-Me < 4-Me; Table 3-4), which suggests steric effects play a role as well.
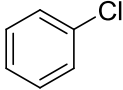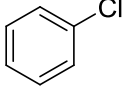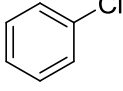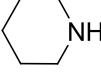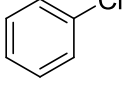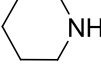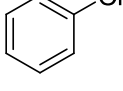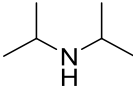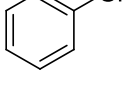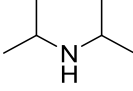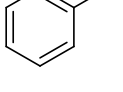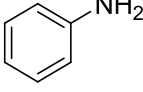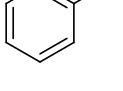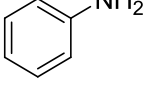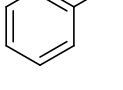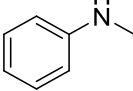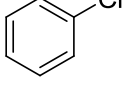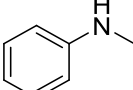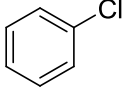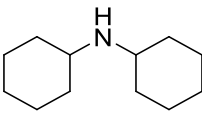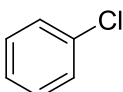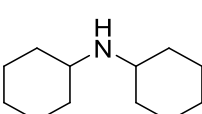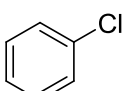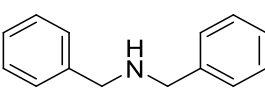
The promising catalytic performance of **3-7** was further demonstrated using various amines with different steric and electronic properties. It was found that the amination of phenyl chloride results in moderate to high yields (44 to 96%, Table 3-4) depending on the steric and electronic nature of the amine substrates. In general, bulky substituents in the amine substrates hamper the catalytic performance of the catalyst thus resulting in lower yields (i.e., diisopropylamine 3d, 69%, Table 3-4). On the other hand, the relatively low yield of diphenylamine (44%, Table 3-4) is due to the fact that diphenylamine undergoes further reaction with phenyl chloride to form
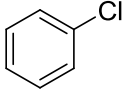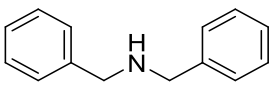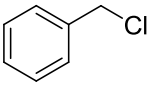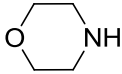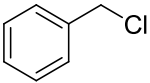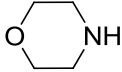
triphenylamine as a side product. It was also shown that the reaction of benzyl chloride with morpholine proceeds very efficiently, yielding the corresponding product in 83% yields.

Table 3-4. The nickel-catalyzed Buchwald-Hartwig coupling using various reaction conditions[a]

$$R-Cl \ + \ R^1{-}\overset{H}{N}{-}R^2 \xrightarrow[\substack{100\ °C,\ 25\ h \\ dioxane}]{\substack{\textbf{3-7}\ (0.5\ mol\%) \\ AgBPh_4\ (1.25\ mol\%) \\ KOtBu\ (1.2\ equiv.)}} R-N\overset{R_2}{\underset{R_1}{<}}$$

Entry	ArX	amine (1.5eq)	t h	Conversion[b] %	Selectivity %[b]
1	Cl (benzene)	O_NH (morpholine)	16	76	99
2	Cl (benzene)	O_NH (morpholine)	25	94	99
3	Br (benzene)	O_NH (morpholine)	16	78	97
4	Br (benzene)	O_NH (morpholine)	25	95	96
5	I (toluene)	O_NH (morpholine)	16	87	45
6	I (toluene)	O_NH (morpholine)	25	99	42
7	Br (toluene)	O_NH (morpholine)	16	86	97
8	Br (toluene)	O_NH (morpholine)	25	100	97

#	Aryl halide	Amine			
9	p-Cl, p-CH$_3$ phenyl	morpholine (O, NH)	16	62	99
10	m-Cl, p-CH$_3$ phenyl	morpholine (O, NH)	25	89	59
11	p-OTf, p-CH$_3$ phenyl	morpholine (O, NH)	16	11	15
12	p-OTf, p-CH$_3$ phenyl	morpholine (O, NH)	25	23	16
13	p-Cl, p-OCH$_3$ phenyl	morpholine (O, NH)	16	61	98
14	p-Cl, p-OCH$_3$ phenyl	morpholine (O, NH)	25	83	97
15	p-Cl, m-CF$_3$ phenyl	morpholine (O, NH)	16	81	98
16	p-Cl, m-CF$_3$ phenyl	morpholine (O, NH)	25	99	98
17	o-Cl, o-CH$_3$ phenyl	morpholine (O, NH)	16	33	99
18	o-Cl, o-CH$_3$ phenyl	morpholine (O, NH)	25	59	98
19	m-Cl, m-CH$_3$ phenyl	morpholine (O, NH)	16	50	96
20	m-Cl, m-CH$_3$ phenyl	morpholine (O, NH)	25	67	97

21	Cl (chlorobenzene)	pyrrolidine (NH)	16	82	98
22	Cl (chlorobenzene)	pyrrolidine (NH)	25	95	98
23	Cl (chlorobenzene)	piperidine (NH)	16	67	99
24	Cl (chlorobenzene)	piperidine (NH)	25	98	98
25	Cl (chlorobenzene)	diisopropylamine	16	42	99
26	Cl (chlorobenzene)	diisopropylamine	25	70	98
27	Cl (chlorobenzene)	aniline (NH2)	16	87	48
28	Cl (chlorobenzene)	aniline (NH2)	25	96	46
29	Cl (chlorobenzene)	N-methylaniline	16	79	98
30	Cl (chlorobenzene)	N-methylaniline	25	94	99
31	Cl (chlorobenzene)	dicyclohexylamine	16	56	99
32	Cl (chlorobenzene)	dicyclohexylamine	25	88	98
33	Cl (chlorobenzene)	dibenzylamine	16	68	98

34	[structure: chlorobenzene]	[structure: dibenzylamine]	25	92	98
35	[structure: benzyl chloride]	[structure: morpholine]	16	54	99
36	[structure: benzyl chloride]	[structure: morpholine]	25	84	99

[a] Reaction conditions: ArX (0.5 mmol), amine (0.75 mmol), [Ni] (0.5 mol%), AgBPh$_4$ (1.25 mol%), KOtBu (1.2 equiv), T=100 °C, solvent = dioxane (1.5 mL), internal standard = decane, t =16-25 h. [b] the conversions and selectivities are determined based on the ArX.

According to the previously proposed mechanism for this type of coupling reaction,[84] the catalytic cycle starts with formation of the bis-NHSi Ni^0 active intermediate **A** from the base-assisted reduction of complex **3-7** (Scheme 3-13). The intermediate **A** then undergoes oxidative addition of the aryl chloride and yields bis-NHSi Ni^{II} intermediate **B,** the later then reacts with one molar equivalent of KOtBu to give the salt metathesis product **C**, which furnishes the corresponding [Ni(Ar)NR$_2$] intermediate **D** by subsequent replacement of -OtBu by an amide group. The desired C-N coupling product is then liberated through a reductive elimination step regenerating the Ni^0 species **A**. Accordingly, the Ni^0-based complex **3-8** can also be used as a precatalyst but results in significantly lower yields of the desired C-N coupling products (e.g., 22% lower yield compared with complex **3-7**), indicating that CO decreases the activity of the catalyst due to favorable OC→Ni coordination. The higher catalytic activity of the **3-7** *vs*. **3-9** and the related bis(phosphine)Ni systems, in turn, can be attributed to the stronger donor character of the ligand **3-6** which facilitates the oxidative addition step, and its bulkiness favors the reductive elimination step, thus enabling a superior steering role of that ligand throughout the reaction.
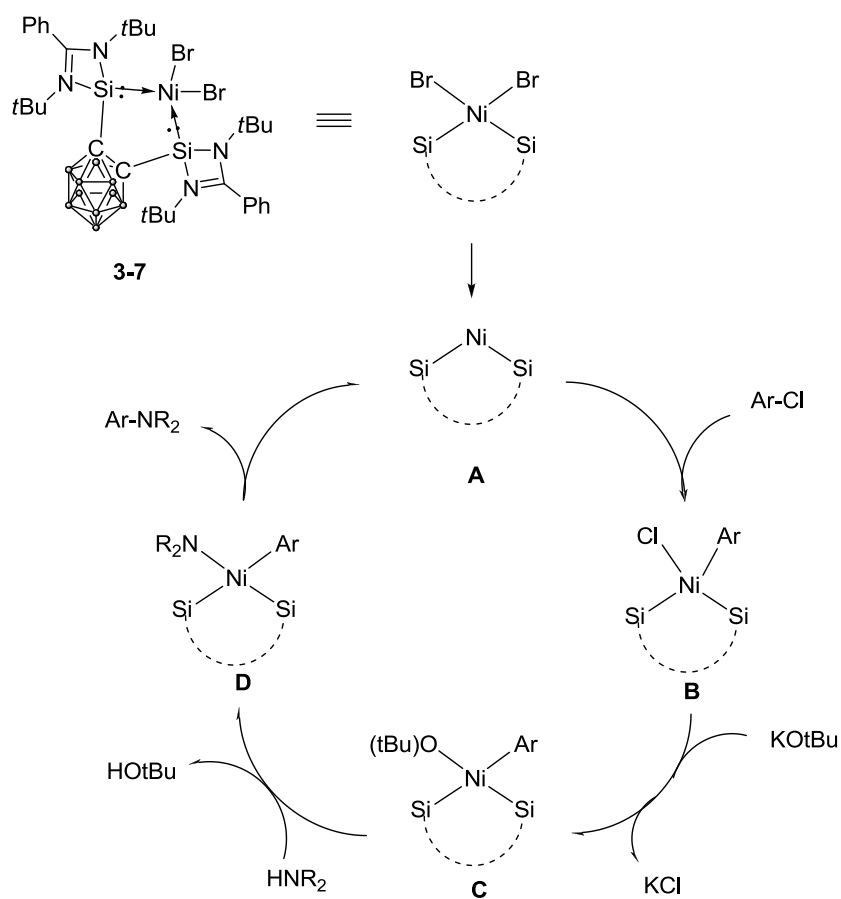
Scheme 3-13. Proposed mechanism for amination reaction catalyzed by Ni-silylene complexes.

3.3 Synthesis of N-heterocyclic silylene manganese complexes and their applications in transfer hydrogenation of alkynes

As the third most abundant transition metal which plays an important role in nature, manganese is known to serve as the oxygen-evolving complex (OEC) in photosystem II. In recent year, out of the numerous water splitting Mn catalysts inspired by the Mn_4CaO_5 cluster present in photo-system II,[89] the coordination complexes of manganese have also become rising stars in homogeneous catalysis.[90] Among numerous Mn-catalyzed reactions, manganese complexes have been applied in reduction reactions, for instance, the hydrogenations,[91] transfer hydrogenation,[92] or hydrosilylation/hydroboration/hydrosilative reduction [93] of polar C=O or C≡N bonds (Scheme 3-14). However, as far as our knowledge, manganese-catalyzed reduction of C≡C bond has not been reported in the literature. Taking these into account, the first catalytically active Mn-NHSi complexes were synthesized and tested for transfer semi-hydrogenations of alkynes using ammonia-borane (AB) as a hydrogen source.
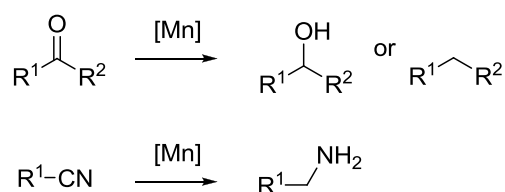
Previous: **This work:**
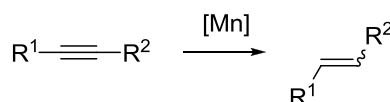
Scheme 3-14. Reported reduction of C=O, C≡N, as well as C≡C multiple bonds catalyzed by Mn-based (pre)catalysts.

3.3.1 Synthesis of Mn complexes stabilized by NHSi ligands

Treatment of pincer-type silylene ligand **I-94** with $MnCl_2$ in THF dioxane mixed solvent at room temperature afforded the Mn^{II} complex **3-14** in 74 % yields as off-white solid (Scheme 3-15). The single crystal of **3-14** was obtained from the toluene

solutions of **3-14** at 0°C overnight. **3-14** crystallizes in the monoclinic space group $P2_1/c$.
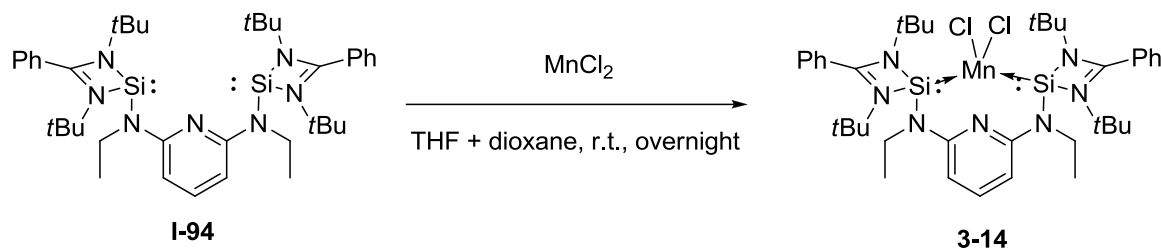
Scheme 3-15. Synthesis of bis-silylene Mn^{II} complex **3-14**.
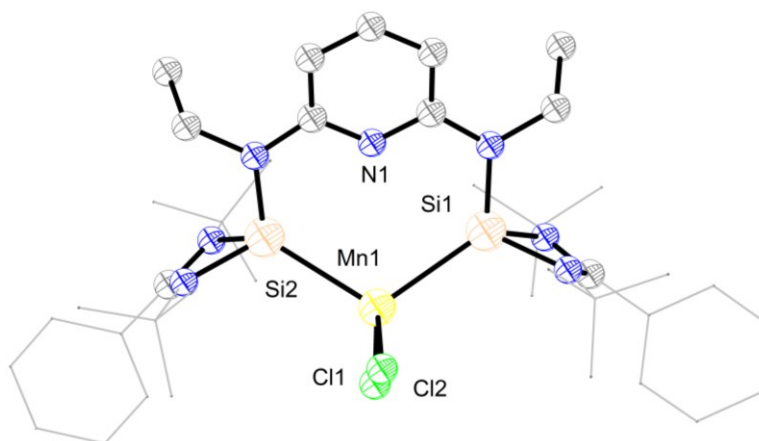
Figure 3-19. Molecular structure of compound **3-14** in solid state. Thermal ellipsoids are drawn at 50% probability level. The hydrogen atoms and solvent molecules are omitted for clarity. Selected bond lengths (Å) and angles (deg): Mn(1)-Cl(1) 2.3466(6), Mn(1)-Cl(2) 2.3478(6), Mn(1)-Si(2) 2.5923(5), Mn(1)-Si(1) 2.6038(6), Cl(1)-Mn(1)-Cl(2) 110.06(3), Cl(1)-Mn(1)-Si(2) 107.01(2), Cl(2)-Mn(1)-Si(2) 109.71(2), Cl(1)-Mn(1)-Si(1) 109.30(3), Cl(2)-Mn(1)-Si(1) 108.11(2), Si(2)-Mn(1)-Si(1) 112.646(18).

Crystal structure of **3-14** revealed the distorted tetrahedral coordinated Mn^{II} centers with the Si$_{NHSi}$-Mn-Si$_{NHSi}$ angles of 112.646(18)° (Figure 3-19). These observations are quite similar to those in Mn^{II}-NHC complexes

[MnCl$_2$(C{N(iPr)C(Me)}$_2$)$_2$][94] and [MnCl$_2$(IMes)$_2$] (IMes = 1,3-dimesitylimidazol-2-ylidene).[95] However, similar to those observations in the Fe^{II} complexes stabilized by pincer type silylene ligand **I-94**, **3-14** remained with N atom not coordinated to the manganese atom with the Mn(1)-N(1) distance of 3.259 Å. This observation contrasts to those in PNP pincer ligand stabilized Mn^{II} complexes,[56, 96] which could be rationalized as the increased electron density of Mn^{II} atom declined the N coordination induced by the coordination of strong σ-donor Si^{II} atom. The Mn^{II}-Si^{II} distances in **3-14**, ranging from 2.5923(5) Å to 2.6038(6) Å, is significantly longer than those Mn^{I}-Si^{II} bond distances in [L$_a$Mn(CO)$_4$]$^{+}$ (2.2789(8) Å and 2.2816(8) Å, L$_a$ = PhC(NtBu)$_2$SiCl) and [L$_b$Mn(CO)$_4$]$^{+}$ (2.3521(7) Å and 2.3571(7) Å, L$_b$ = PhC(NtBu)$_2$SiNPh$_2$) as well as longer than Mn^{I}-Si^{IV} distances in silyl manganese complex [(Me$_3$Si)$_3$SiMn(CO)$_5$] (2.564(6) Å) and [(Me$_3$Si)Mn(CO)$_4$PPh$_3$] (2.453(4) Å).[97]
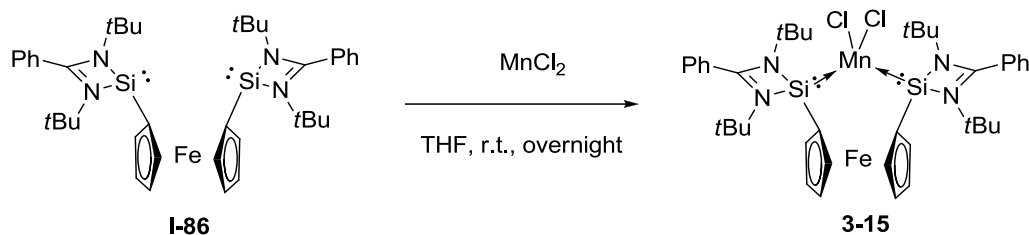
Scheme 3-16. Synthesis of bis-silylene Mn^{II} complex **3-15**.
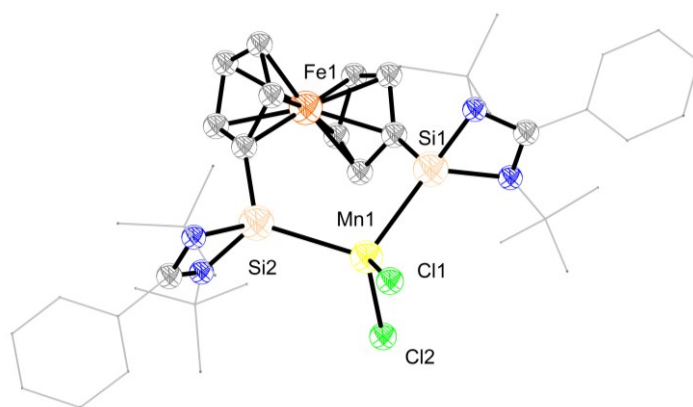
Figure 3-20. Molecular structure of compound **3-15** in solid state. Thermal ellipsoids are drawn at 50% probability level. The hydrogen atoms and solvent molecules are

omitted for clarity. Selected bond lengths (Å) and angles (deg): Mn(1)-Cl(1) 2.3213(7), Mn(1)-Cl(2) 2.3503(7), Mn(1)-Si(1) 2.6134(7), Mn(1)-Si(2) 2.6347(7), Cl(1)-Mn(1)-Cl(2) 112.88(3), Cl(1)-Mn(1)-Si(1) 112.93(3), Cl(2)-Mn(1)-Si(1) 104.75(2), Cl(1)-Mn(1)-Si(2) 118.12(3), Cl(2)-Mn(1)-Si(2) 103.77(2), Si(1)-Mn(1)-Si(2) 102.99(2).

Treatment of bis-silylene ligand **I-86** with $MnCl_2$ in THF at room temperature afforded the Mn^{II} complex **3-15** in 56 % yield as yellow solid (Scheme 3-16). The single crystal of **3-15** was obtained from the toluene THF dioxane mixed solutions of **3-15** at 0°C overnight. **3-15** crystallizes in the triclinic space group *p*-1 (Figure 3-20). Single crystal structures of **3-15** reveal the distorted tetrahedral coordinated Mn^{II} centers with the Si_{NHSi}-Mn-Si_{NHSi} angels of 102.99(2)°, which are quite similar to those in Mn^{II}-NHC complexes $[MnCl_2(C\{N(iPr)C(Me)\}_2)_2]$[94] and $[MnCl_2(IMes)_2]$ (IMes = 1,3-dimesitylimidazol-2-ylidene).[95] **3-15** shows a four-coordinate Mn^{II}. This observation contrasts to the six coordinated Mn^{II} center in the Mn^{II} dibromide analogue supported by bidentate phosphine dmpe (1,2-bis(dimethylphosphino)ethane) which could be explained as the presence of bulky and strong σ-donor ligand **I-86**. The Mn^{II}-Si^{II} distances in **3-15**, ranging from 2.6134(7) Å to 2.6347(7) Å, is significantly longer than those Mn^{I}-Si^{II} bond distances in $[L_aMn(CO)_4]^+$ (2.2789(8) Å and 2.2816(8) Å, L_a = $PhC(NtBu)_2SiCl$) and $[L_bMn(CO)_4]^+$ (2.3521(7) Å and 2.3571(7) Å, L_b = $PhC(NtBu)_2SiNPh_2$) as well as longer than Mn^{I}-Si^{IV} distances in silyl manganese complex $[(Me_3Si)_3SiMn(CO)_5]$ (2.564(6) Å)[15] and $[(Me_3Si)Mn(CO)_4PPh_3]$ (2.453(4) Å).[97]
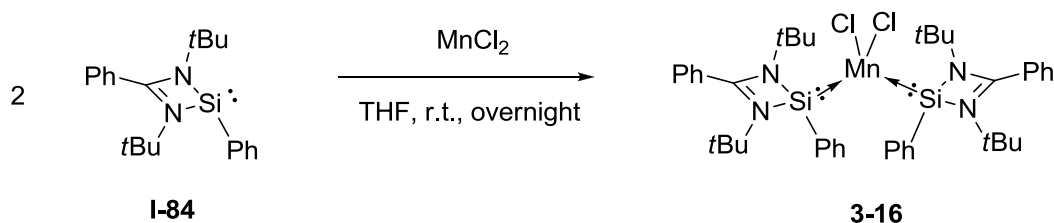
Scheme 3-17. Synthesis of bis-silylene Mn^{II} complex **3-16**.
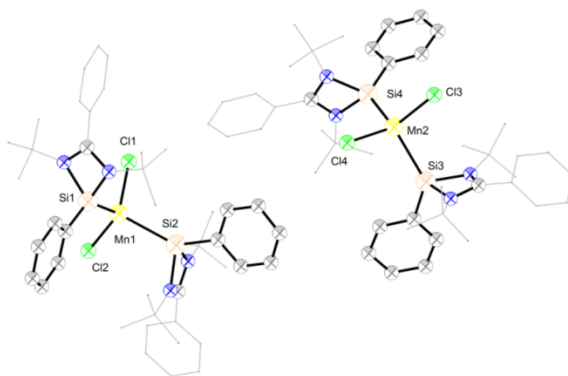
Figure 3-21. Molecular structure of compound **3-16** in solid state. Thermal ellipsoids are drawn at 50% probability level. The hydrogen atoms and solvent molecules are omitted for clarity. Selected bond lengths (Å) and angles (deg): Mn(1)-Cl(1) 2.319(3), Mn(1)-Cl(2) 2.333(2), Mn(1)-Si(1) 2.607(2), Mn(1)-Si(2) 2.616(2), Mn(2)-Cl(3) 2.339(2), Mn(2)-Cl(4) 2.333(3), Mn(2)-Si(3) 2.609(2), Mn(2)-Si(4) 2.605(2), Cl(1)-Mn(1)-Cl(2) 115.79(11), Cl(1)-Mn(1)-Si(1) 104.74(10), Cl(2)-Mn(1)-Si(1) 111.80(9), Cl(1)-Mn(1)-Si(2) 107.13(11), Cl(2)-Mn(1)-Si(2) 100.26(8), Si(1)-Mn(1)-Si(2) 117.52(8), Cl(3)-Mn(2)-Cl(4) 116.98(11), Cl(3)-Mn(2)-Si(3) 103.03(9), Cl(4)-Mn(2)-Si(3) 107.00(9), Cl(3)-Mn(2)-Si(4) 110.19(9), Cl(4)-Mn(2)-Si(4) 103.45(10), Si(3)-Mn(2)-Si(4) 116.73(8).

Treatment of two molar equivalents of mono-silylene ligand **I-84** with $MnCl_2$ in THF at room temperature afforded the Mn^{II} complex **3-15** in 50 % yield as off-white solid (Scheme 3-17). The single crystal of **3-16** was obtained from the toluene and dioxane mixed solutions of **3-16** at 0°C overnight. **3-16** crystallizes in the triclinic space group *p-1* (Figure 3-21). Single crystal structures of **3-16** reveal the distorted tetrahedral coordinated Mn^{II} centers with the Si-Mn-Si angels of 117.52(8)°, which are quite similar to those in Mn^{II}-NHC complexes $[MnCl_2(C\{N(iPr)C(Me)\}_2)_2]$[94] and $[MnCl_2(IMes)_2]$ (IMes = 1,3-dimesitylimidazol-2-ylidene).[95] The coordination geometry of **3-16** (distorted tetrahedral coordination) is similar to its phosphine analogue $(PPh_3)_2MnI_2$ and $(PEt_3)_2MnI_2$. The Mn^{II}-Si^{II} distances in **3-16**, ranging from 2.605(2) Å to 2.616(2) Å, is significantly longer than those Mn^I-Si^{II} bond distances in $[L_aMn(CO)_4]^+$ (2.2789(8) Å and 2.2816(8) Å, L_a = $PhC(NtBu)_2SiCl$) and $[L_bMn(CO)_4]^+$ (2.3521(7) Å and 2.3571(7) Å, L_b = $PhC(NtBu)_2SiNPh_2$) as well as longer than Mn^I-Si^{IV} distances in silyl manganese complex $[(Me_3Si)_3SiMn(CO)_5]$ (2.564(6) Å) and $[(Me_3Si)Mn(CO)_4PPh_3]$ (2.453(4) Å).[97]

3.3.2 Stereo-selective transfer semi-hydrogenation of alkynes catalyzed by Mn-NHSi complexes

Manganese NHSi complexes **3-14**, **3-15**, and **3-16** were applied successfully in transfer semi-hydrogenation of alkynes using NH_3BH_3 as H-source. Compared with the traditional direct hydrogenation method using H_2 gas, the reaction conditions of transfer hydrogenation are much gentler.[98] Due to the high percentage of H content (19.5 wt %) as well as the non-flammable and stable nature, ammonia-borane (AB) has been considered as a potential hydrogen storage material.[99] In addition to hydrogen storage, AB has been employed as H-source for transfer hydrogenation of various unsaturated compounds.[88g, 100] Among these, the transfer semi-hydrogenations of alkynes have been reported using nickel, cobalt, gold, and copper complexes.[88g, 100b, 100h, 100j] However, to the best of our knowledge, Mn complexes have been only demonstrated as (pre)catalysts for AB dehydrogenation[101] but not yet in transfer hydrogenation.

Firstly, the dehydrogenation of AB was tested using 5 mol% of complex **3-14** loading in THF-d_8 at 60 ˚C. The reaction was traced using ^{11}B NMR spectroscopy (Figure 3-22). The formation of dehydrogenation products were assigned as oligomers species called polyborazanes or polyaminoboranes (quartet around $\delta_B = -19$ ppm, triplet around $\delta_B = -11$ ppm, and doublet around $\delta_B = -6$ ppm), aromatic ring species borazine (doublet around $\delta_B = 29$ ppm), and cross-linked borazine called polyborazylene (broad signal around $\delta_B = 25$ ppm) according to literature ^{11}B NMR data.[99a]
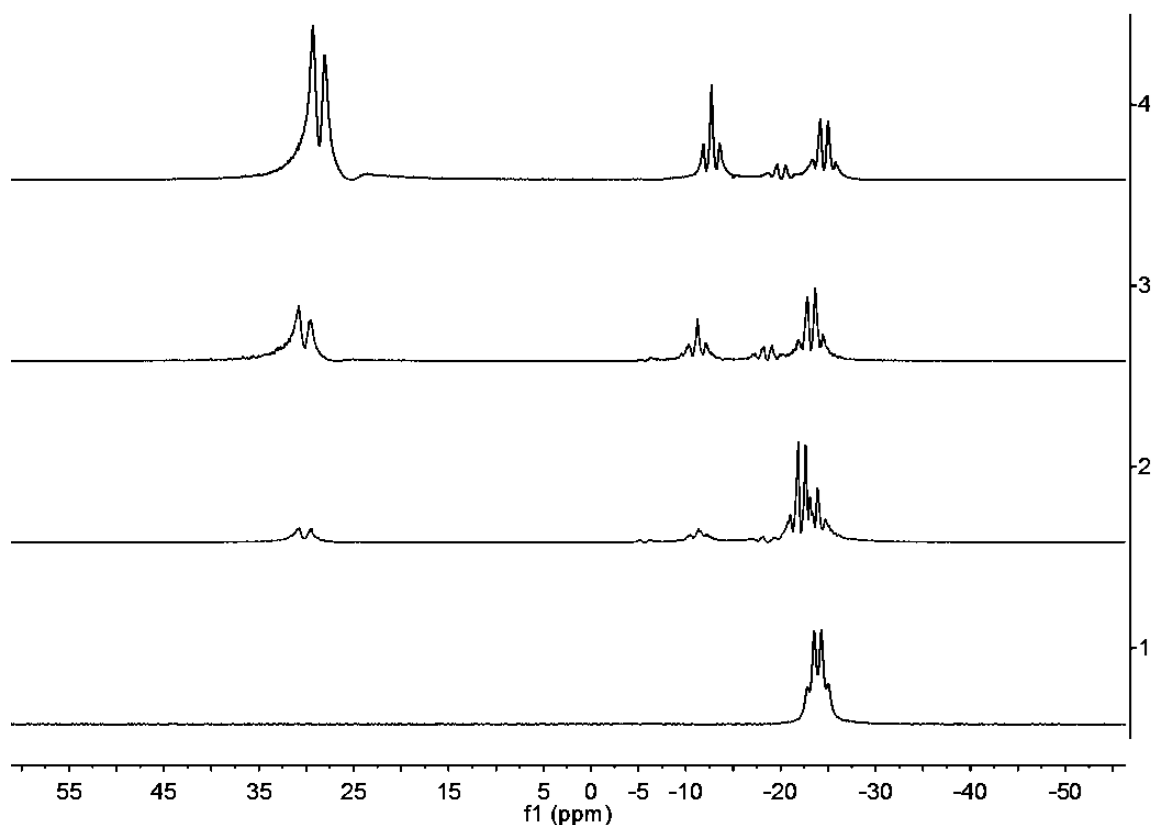
Figure 3-22. ^{11}B NMR spectra of ammonia-borane dehydrogenation reaction catalyzed by **3-14** (from bottom to top: 0 h, 4 h, 14 h, and 24 h).

The initial optimization experiments indicate 1 mol% loading of **3-14** could catalyze the transfer semi-hydrogenation between 1-phenyl-1-hexyne and AB with high conversion(> 99 %) and high stereo-selective (*E*-alkene selectivity of 90 %) at 55 °C in THF (Table 3-5, entry 1-5). This observation is different from the industrially applied Lindlar's catalysts and most homo/heterogeneous semi-(transfer)hydrogenation (pre)catalysts which yield *Z*-alkenes. Further optimization indicates that NH$_3$BH$_3$ gave the highest conversion compared to other H-sources: BH$_3$NMe$_2$H (24 %), BH$_3$NMe$_3$ (35 %), NaBH$_4$ (17 %), and H$_2$ (0 %) (Table 3-5, entry 6-9).

Table 3-5. The NHSi-Mn complexes catalyzed transfer hydrogenation of alkynes using various reaction conditions[a]
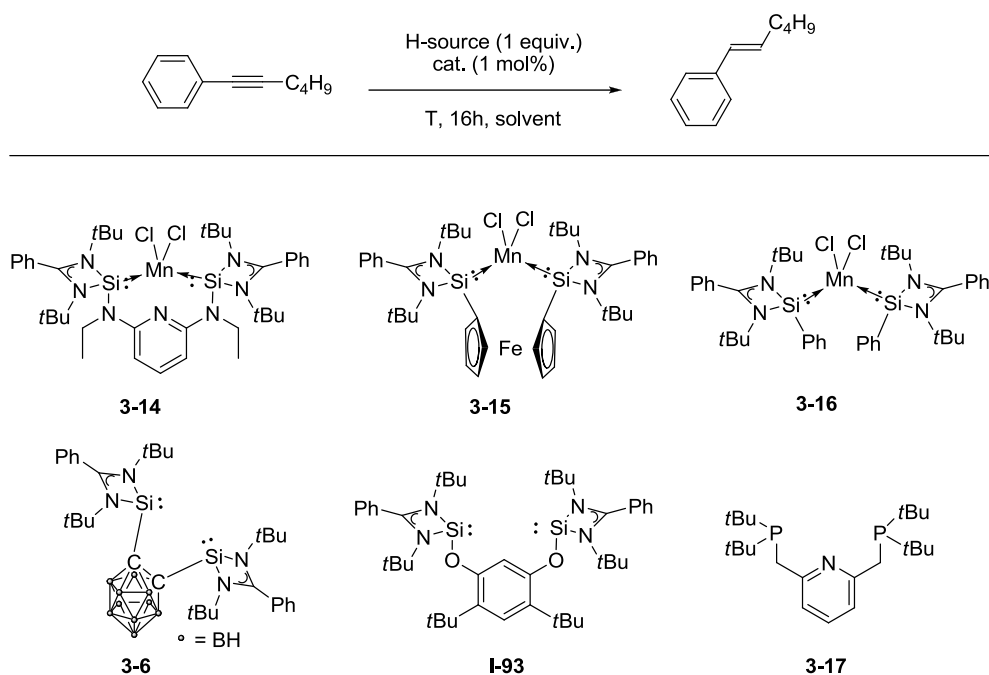
Entry	cat.	H-source	Solvent	T	Conversion[b]	E-selectivity[b]
			3 mL	°C	%	%
1	**3-14**	NH_3BH_3	THF	25	0	-
2	**3-14**	NH_3BH_3	THF	55	>99	90
3	**3-14**	NH_3BH_3	MeOH	55	<10	-
4	**3-14**	NH_3BH_3	MeCN	55	60	56
5	**3-14**	NH_3BH_3	toluene	55	51	44
6	**3-14**	$NHMe_2BH_3$	THF	55	24	73
7	**3-14**	NMe_3BH_3	THF	55	35	71
8	**3-14**	$NaBH_4$	THF	55	17	82

9	**3-14**	H$_2$	THF	55	0	-
10	**3-15**	NH$_3$BH$_3$	THF	55	99	69
11	**3-16**	NH$_3$BH$_3$	THF	55	>99	68
12	MnCl$_2$	NH$_3$BH$_3$	THF	55	35	76
13	**3-6** + MnCl$_2$	NH$_3$BH$_3$	THF	55	48	48
14	**I-93** + MnCl$_2$	NH$_3$BH$_3$	THF	55	41	66
15	**3-17** + MnCl$_2$	NH$_3$BH$_3$	THF	55	43	49
16[c]	**3-14**	NH$_3$BH$_3$	THF	55	99	85
17[d]	**3-14**	NH$_3$BH$_3$	THF	55	99	87
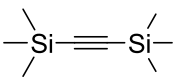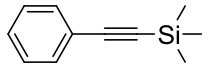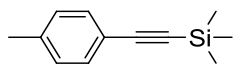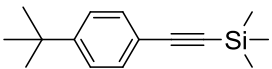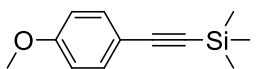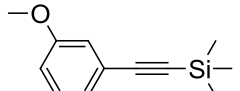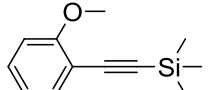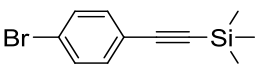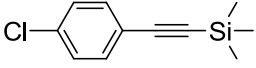
[a] Reaction conditions: alkyne (0.5 mmol), H-source (0.5 mmol), [Mn] (1 mol%), T=55 °C, solvent = 3 mL, internal standard = decane, t =16 h. [b] Conversions and selectivities were determined by GC or NMR. [c] 1 drop of Mercury added. [d] 1-2 equiv. of (2,2,6,6-Tetramethylpiperidin-1-yl)oxyl (TEMPO) added.
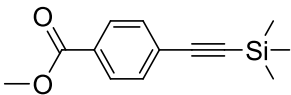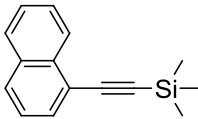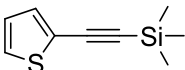
Mn^{II} complexes bearing different NHSi ligands were also tested for this reaction. Structure defined complexes **3-15** with bidentate bis-NHSi ligand **I-86** and complex **3-16** bearing monodentate NHSi ligand revealed the same high activity with almost full conversion (99 % and >99 %, respectively, Table 3-5, entry 10-11). However, **3-15** and **3-16** gave relatively lower stereo-selectivity (69 % and 68 %, respectively, Table 3-5, entry 10-11) compared to those of **3-14**. Since the isolation of structure defined complexes with multidentate NHSi ligand **3-6** and **I-93** were not successful, **3-6** or **I-93** were directly employed in catalysis in the present of MnCl$_2$ but gave poor conversion and stereoselectivity (48 % and 41 % conversion, respectively, Table 3-5, entry 13-14). Pincer-type phosphine pyridine ligand **3-17** was also tested and gave relatively lower conversion (43 %, Table 3-5, entry 15).

To gain the mechanic insights of the transfer semi-hydrogenation reaction, control experiment of substrate 1-phenyl-1-hexyne in the presence of mercury was carried out. The high conversion and stereoselectivity (99 % and 85 %, respectively, Table 3-5, entry 16), indicate the catalytic reaction undergoes molecular mechanism rather than nanoparticles (mercury is known to poison catalytically active metal nanoparticles). Furthermore, the transfer semi-hydrogenation of 1-phenyl-1-hexyne gave also high conversion and stereoselectivity (99 % and 87 %, respectively, Table 3-5, entry 17) in the presence of TEMPO (2,2,6,6-tetramethyl-l-piperidinoxyl), which ruled out the possible radical mechanism (TEMPO is known to trap the radical species). According to the previous report, metal hydride was proposed as active intermediate for the transfer semi-hydrogenation of alkyne.[99a] However, metal hydride species are also known as the active intermediate for dehydrogenation of ammonia-borane. Therefore it is necessary to check whether the reaction undergoes dehydrogenation-hydrogenation mechanism or direct transfer hydrogenation mechanism. Then, as a control experiment, the complex **3-14** was tested for the direct hydrogenation of 1-phenyl-1-hexyne (Table 3-5, entry 9) under an H_2 atmosphere which gave no conversion. These observations suggest the H was directly transferred to substrates without involving the dehydrogenation-hydrogenation process.

Table 3-6. The NHSi-Mn complexes catalyzed transfer semi-hydrogenation of different alkynes [a]

Entry	Alkynes	Conversion[b] %	E-selectivity[b] %
1		>99	90
2		97	92

3	$n\text{-}C_5H_{11}\!\!-\!\!\!\equiv\!\!\!-n\text{-}C_5H_{11}$	67	50
4	$-\!Si\!\equiv\!Si\!-$	-[c]	-[c]
5	Ph$-\!\equiv\!-Si$	98	92
6	98	93
7	90	91
8	95	92
9	97	82
10	99	79
11	99	94
12	> 99	96

13		> 99	60
14		96	98
15		81	95

[a] Reaction conditions: alkyne (0.5 mmol), H-source (0.5 mmol), **3-14** (1 mol%), T=55 °C, solvent = 3 mL, internal standard = decane, t =16 h. [b] Conversions and selectivities were determined by GC/MS and NMR respectively.
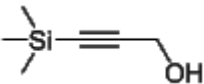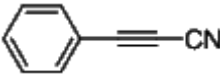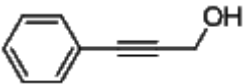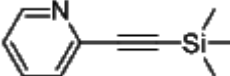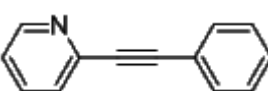
Further, the catalytic performance of **3-14** with different alkynes was investigated (Table 3-6 and 3-7). It turned out that the catalyst tolerates different functional groups and leads to the corresponding (*E*)-alkenes as main products. The reaction of the alkynes with phenyl/alkyl substitutes, diphenyl substitutes, and phenyl/silyl substituents gives both good conversion (97 to >99 %) and *E*-selectivities (90-92 %). However, the dialkyl substituted alkyne results in lower conversion (67 %) without stereoselectivity (E/Z = 1:1), and the disilyl substituted alkyne bis(trimethylsilyl)acetylene does not react at all.

The semi-hydrogenation tolerated various functional group based on the substructures of 1-phenyl-2-trimethylsilylacetylene. The reactions of the alkynes bearing 4-position substituents at the phenyl ring (Me, tBu, OMe, Br, and Cl) gave both high conversions (90 to >99 %) and high stereoselectivities (92-96 %; Table 3-6). However, a substrate with the electron-withdrawing COOMe group in the *para* position led to high conversion (> 99 %) but poor *E*-selectivity (60 %). Notably, the presence of CN, NH_2, NO_2, and OH groups at the phenyl group poisoned the anticipated catalytic transfer hydrogenation (Table 3-7). Steric effects also play a role as shown by comparison of the alkynes with a MeO substituent in *para, meta* and

ortho position, respectively (conversions: 2-OMe > 3-OMe > 4-OMe; stereoselectivities: 4-OMe > 3-OMe > 2-OMe; Table 3-6).

Table 3-7. The NHSi-Mn complexes catalyzed transfer semi-hydrogenation of different alkynes [a]

Entry	Alkynes	Conversion[b] %	E-selectivity[b] %
1		ND	-
2		ND	-
3		ND	-
4		ND	-
5		ND	-
6		ND	-

7		ND	-
8		ND	-
9		ND	-
10		ND	-
11		ND	-

[a] Reaction conditions: alkyne (0.5 mmol), H-source (0.5 mmol), **3-14** (1 mol%), T=55 °C, solvent = 3 mL, internal standard = decane, t =16 h. [b] Conversions and selectivities were determined by GC/MS and NMR respectively.

According to a previously proposed mechanism for metal-mediated transfer semi-hydrogenation,[88g] the catalytic cycle starts with the generation of bis-NHSi manganese hydride **A** from the ammonia-borane-induced reduction of complex **3-14** (Scheme 3-18). The intermediate **A** then coordinates to an alkyne molecule that gives alkyne complex intermediate **B**, which further undergoes the insertion of alkyne into Mn-H bond and generation of intermediate **C.** The subsequent cleavage of the Mn–C bond by ammonia-borane affords the desired semi-hydrogenation product (*E*)-olefin, boron-contain side-product (e.g., polyborazane/polyaminoborane, borazine, or polyborazylene), and the regenerated manganese hydride **A**.
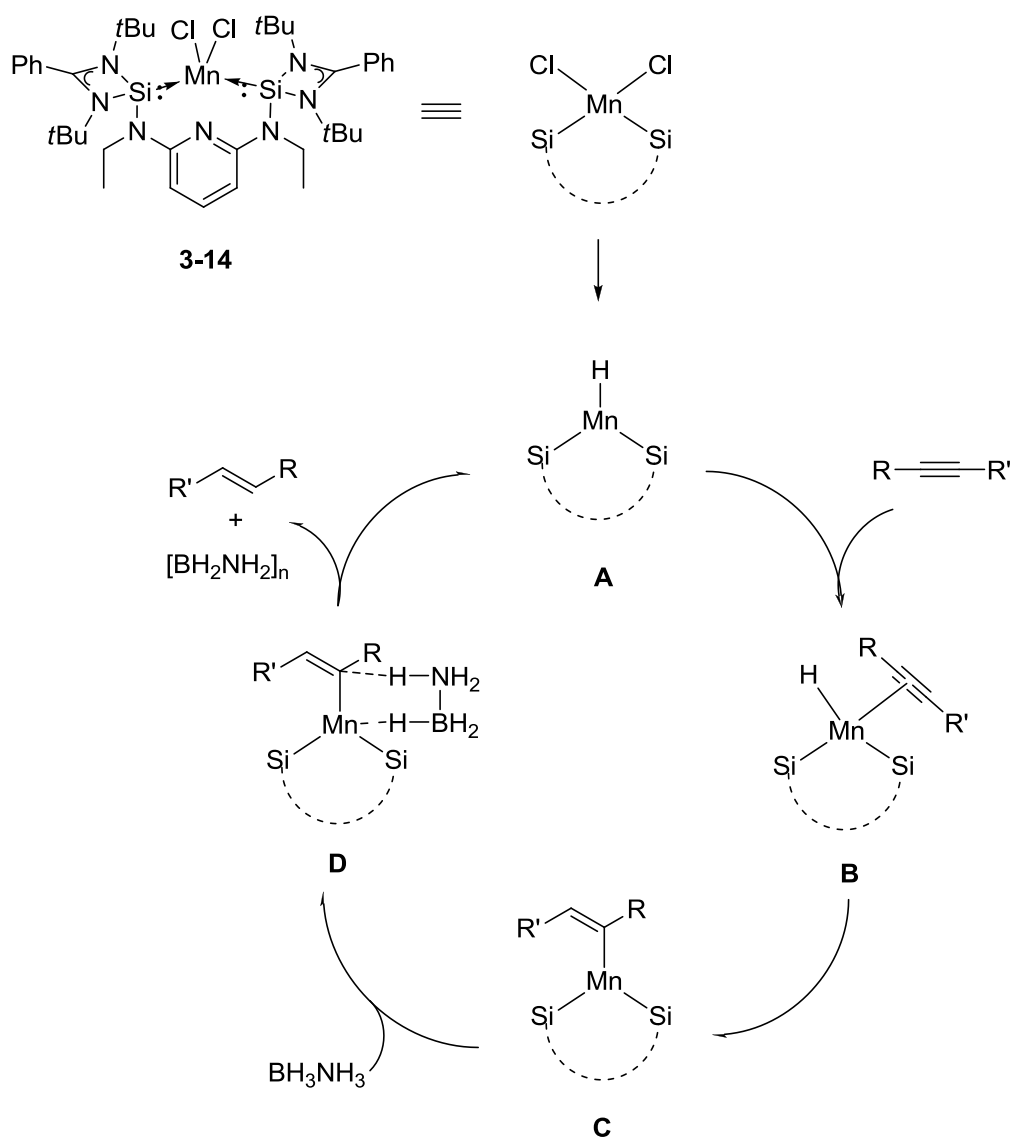
Scheme 3-18. Proposed mechanism for transfer semi-hydrogenation catalyzed by Mn-silylene complexes.

3.4 Synthesis of *N*-heterocyclic silyl, silylene, and η²-(Si-H) cobalt complexes and their applications in olefin hydrosilylations

Silicon-based ligands have attracted considerable attention in recent years due to their unique electronic and steric properties that enhance the catalytic activity and selectivity of transition metal catalysts. Silyl ligands are the most widely used Si-based ligands bearing negatively charged Si^{IV} center that favors the stabilizations of high oxidation state intermediate and produces the strong *trans* effect.[102] The oxidative addition of hydrosilanes is a common method for synthesizing silyl complexes. If the Si-H is not fully oxidatively added to metal centers, σ-complexes or agnostic bonded complexes via η²-(Si-H) coordinated 2-electron, 3-center bonds are formed.[103] Apart from Si^{IV}-based ligands, low-valent silicon spices silylenes, especially *N*-heterocyclic silylenes (NHSis) constitute another important family of Si-based ligands that feature strong σ-donor Si^{II} coordination centers and metal-Si cooperating effects which facilitate high activity and selectivity.[38a, 38c] In this part, the synthesis, coordination chemistry, and catalytic studies of a Si-based ligand, which enables three different coordination modes (e.g., silyl, silylene, and η²-(Si-H), Scheme 3-19), were described.
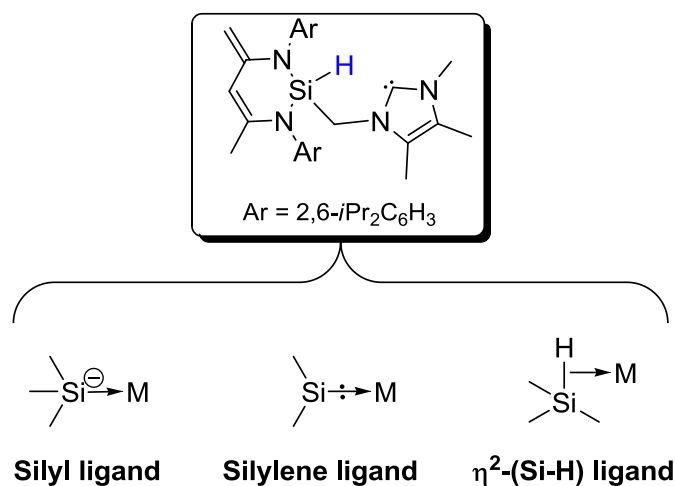
Scheme 3-19. Three possible coordination modes by ligand **I-24**.

As one of the most important homogenous reactions at the industrial scale, hydrosilylation reactions have wide applications in the synthesis of different silicon-containing molecules and materials. Pt-based complexes could efficiently catalyze the

hydrosilylation reactions and are widely applied as a catalyst in the silicon industry.[104] In recent years, to prevent the usages of high costs, low abundant and more toxic Pt catalysts, several 1st-row transition metal complexes have been developed as a new generation of catalysts for hydrosilylation reactions.[105] Cobalt complexes represent an important family of 1st-row transition metal catalysts for the process of hydrosilylation. As early as in the 1960's, $Co_2(CO)_8$ was tested as the catalyst for the hydrosilylation of olefins and the well-known Chalk-Harrod mechanism was proposed based on these investigations.[106] Subsequently, research interests became increasingly concentrated on precious metal catalysts rather than Co-based catalysts.[107] Until recently, the developments of highly efficient Co-based catalysts for olefin hydrosilylation attracted considerable attention. In 2013, silyl-NHC cobalt(II) complexes **A** were reported by Deng group.[108] In following years, cobalt(I) bis(imino)pyridine complex **B**, cobalt(I) β-diketiminato complex **C**, and cobalt(II) phosphine-iminopyrdine complexes **D** were reported as efficient pre-catalysts for olefin hydrosilylation by Chirik, Holland, Huang, and others groups respectively (Scheme 3-20).[109] In this case, the cobalt complex **3-18** was also tested and found to be a very active (pre)catalysts for olefin hydrosilylations.
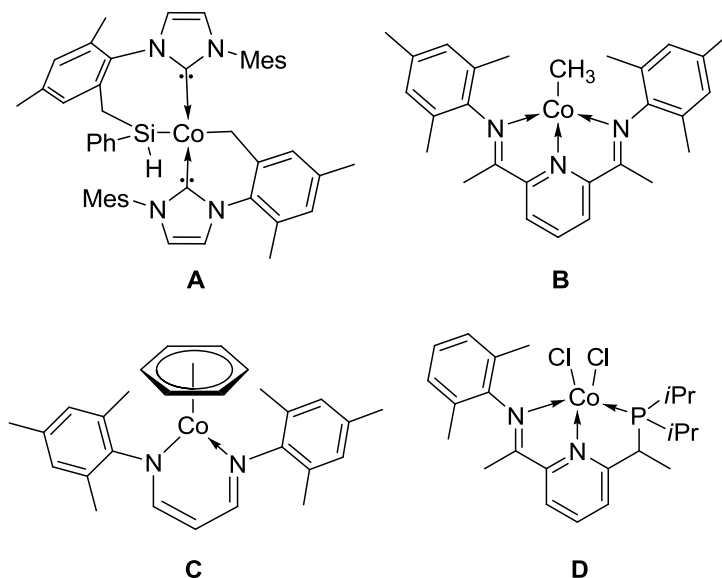
Scheme 3-20. Selected examples of structure defined cobalt (pre)catalysts of olefin hydrosilylation.

3.4.1 Synthesis of Co complexes stabilized Si-based NHC ligands

Recently, our group reported the reaction of $NiBr_2(dme)$ with N-heterocyclicsilylcarbene **I-24**, $L^1Si(H)(CH_2)(NHC)$ (L^1 = $CH(C=CH_2)$-$(CMe)(NAr)_2$, Ar = 2,6-iPr$_2$C$_6$H$_3$; NHC = 3,4,5-trimethylimidazol-2-ylidene-6-yl), which gave the N-heterocyclic silylene-NHC Ni complexes $[L^2Si:(CH_2)(NHC)NiBr_2]$ (L^2 = $CH(MeC=NAr)_2$). However, the reaction of **I-24** with $CoBr_2$ did not lead to the similar N-heterocyclic silylene-NHC Co complex. The reaction of ligand **I-24** with $CoBr_2$, KC_8 and trimethylphosphine in THF gave the silyl-cobalt(II) complex $[L^1Si(CH_2)(NHC)CoH(PMe_3)_2]$ **3-18** as main product (in 56 % yield) which might be due to the oxidative addition of Si-H bond into in situ generated Co^0 center (Scheme 3-21). Single crystals of **3-18** were crystallized from concentrated Et$_2$O solutions at 0 °C in the triclinic space group P-1 (Figure 3-23). The Co1-C36 and Co1-Si1 bond distances are 1.950(3) Å and 2.2178(9) Å, respectively, which are similar to those Co-C and Co-Si bond distances in reported Co-NHC and Co-sily complexes, respectively. The C1-C2 (1.364(4) Å) and C4-C5 (1.500(5) Å) distances represent double and single bonds, respectively. Those observations are in sharp contrast to the cases in previously reported silylene-NHC Ni complexes $[L^2Si:(CH_2)(NHC)NiBr_2]$ (L^2 = $CH(MeC=NAr)_2$). The Co1-H1 distance is 1.411 Å, which is in accordance with the literature reported Co-H bond distance.[108] The Si1-H1 distance of 1.966 Å is longer than those in the free ligand (1.338 Å) but in the range of non-classical Si-H interactions which suggest the oxidative addition of Si-H bond at the Co center and a non-classical interaction between Si and H atoms. The IR absorption at 1741 cm^{-1} and 1694 cm^{-1}of **3-18** also agree with those observations in terminal Co-H compounds and Si-H non-classical interactions, respectively.
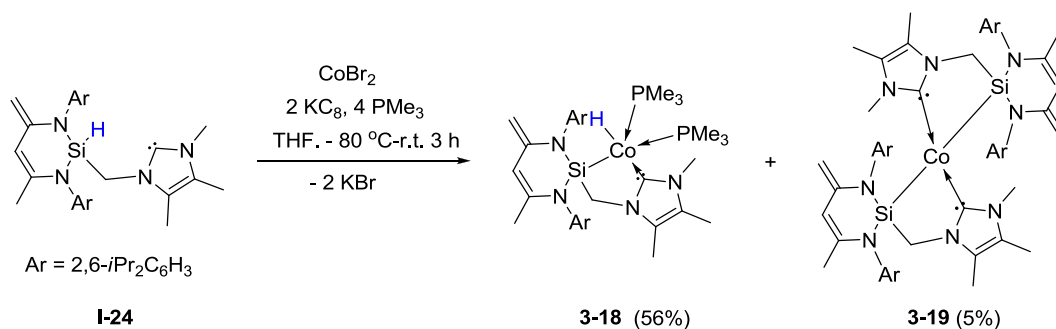
Scheme 3-21. Synthesis of NHC-silyl Co^{II} complex **3-18** and **3-19**.
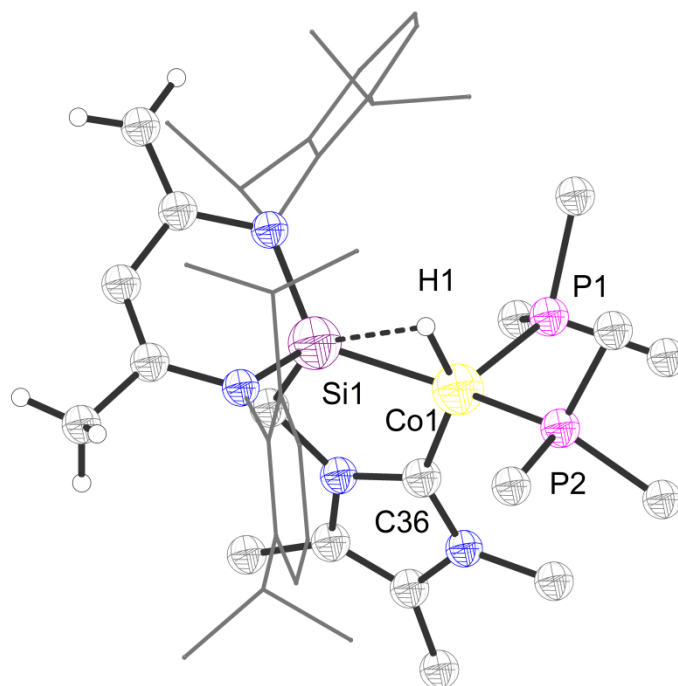
Figure 3-23 Molecular structure of compound **3-18** in solid state. Thermal ellipsoids are drawn at 50% probability level. The hydrogen atoms (except those on Co1, C1, and C5) and solvent molecules are omitted for clarity. Selected bond lengths (Å) and angles (deg): Co(1)-C(36) 1.950(3), Co(1)-Si(1) 2.2178(9), Co(1)-P(1) 2.2190(9), Co(1)-P(2) 2.2348(9), C(1)-C(2) 1.364(4), C(4)-C(5) 1.500(5), C(36)-Co(1)-Si(1) 84.92(9), C(36)-Co(1)-P(1) 92.93(9), Si(1)-Co(1)-P(1) 113.24(3), C(36)-Co(1)-P(2) 119.47(9), Si(1)-Co(1)-P(2) 138.73(4), P(1)-Co(1)-P(2) 99.11(3).
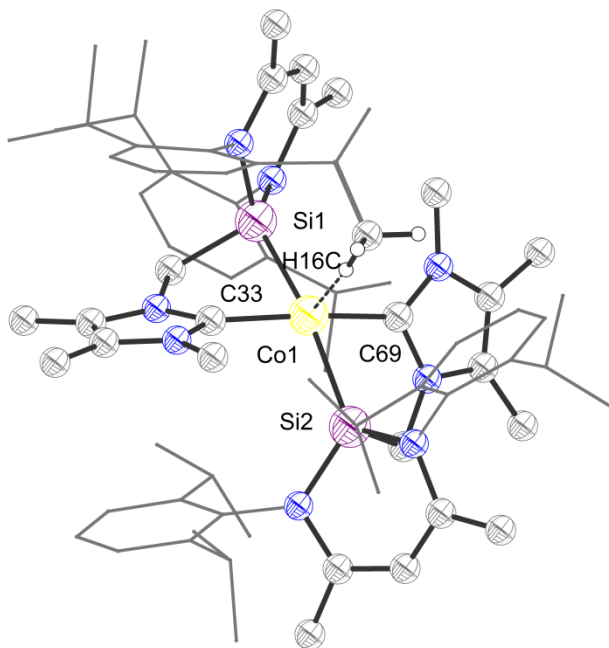
Figure 3-24 Molecular structure of compound **3-19** in solid state. Thermal ellipsoids are drawn at 50% probability level. The hydrogen atoms (except those on C16) and solvent molecules are omitted for clarity. Selected bond lengths (Å) and angles (deg): Co(1)-C(33) 1.975(7), Co(1)-Si(1) 2.187(2), Co(1)-P(2) 2.220(3), Co(1)-P(1) 2.234(3), C(1)-C(2) 1.536(10), C(4)-C(5) 1.512(9), C(33)-Co(1)-Si(1) 84.4(2), C(33)-Co(1)-P(2) 95.1(2), Si(1)-Co(1)-P(2) 118.38(10), C(33)-Co(1)-P(1) 115.9(3), Si(1)-Co(1)-P(1) 135.47(9), P(2)-Co(1)-P(1) 99.72(9).

The reaction of ligand **I-24** with $CoBr_2$, KC_8, and trimethylphosphine in THF also gave the bis-silyl cobalt(II) complex [{L^1Si (CH_2)(NHC)}$_2$Co] **3-19** as a side product (in 5 % yield, Scheme 3-21). The green crystal of **3-19** was obtained from the combined mother liquid of **3-18** at 0 °C after two days. The structure of **3-19** represents two silyl-NHC ligands coordinated to the Co^{II} center (Figure 3-24). The ligand backbone in **3-19** is quite similar to those in **3-18**. The C-H of dipp group forms a C-H to Co^{II} agostic interaction with the Co1-H16C bond distance of 2.137 Å.
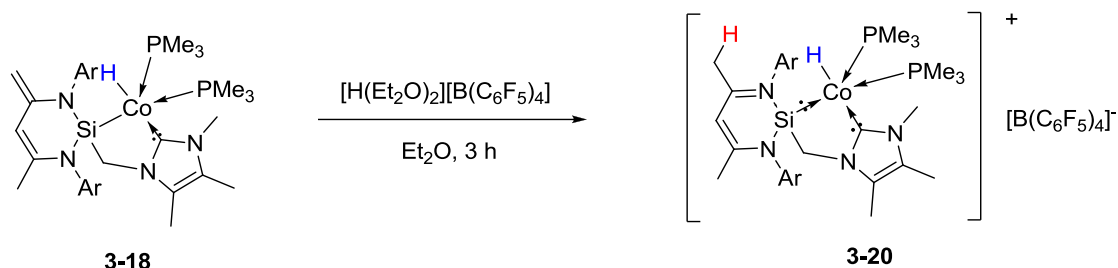
Scheme 3-22. Synthesis of silylene Co^{II} complex **3-20**.
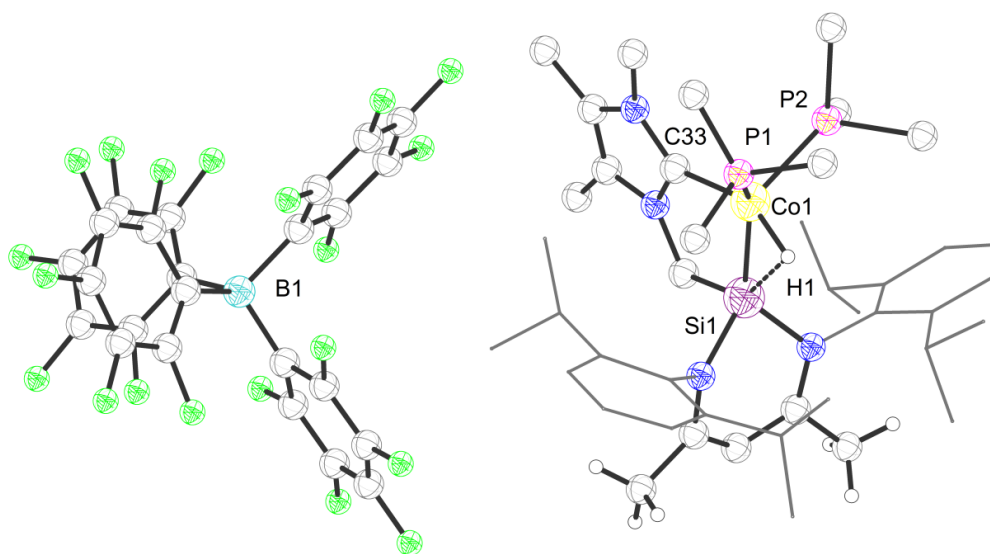
Figure 3-25. Molecular structure of compound **3-20** in solid state. Thermal ellipsoids are drawn at 50% probability level. The hydrogen atoms (except those on Co1, C1, and C5) and solvent molecules are omitted for clarity. Selected bond lengths (Å) and angles (deg): Co(1)-C(33) 1.975(7), Co(1)-Si(1) 2.187(2), Co(1)-P(2) 2.220(3), Co(1)-P(1) 2.234(3), C(1)-C(2) 1.536(10), C(4)-C(5) 1.512(9), C(33)-Co(1)-Si(1) 84.4(2), C(33)-Co(1)-P(2) 95.1(2), Si(1)-Co(1)-P(2) 118.38(10), C(33)-Co(1)-P(1) 115.9(3), Si(1)-Co(1)-P(1) 135.47(9), P(2)-Co(1)-P(1) 99.72(9).

Since the direct reaction of ligand **I-24** with cobalt precursor does not induce the H migration from Si or Co center to the β-diketiminato backbones which was observed in Ni complexes, we considered if an external proton source could be added to the β-diketiminato backbones. By the reaction of one molar equivalent of Jutzi acid [{H(Et$_2$O)$_2$}$^+${B(C$_6$F$_5$)$_4$}$^-$] with compound **3-18**, silylene-NHC Co complex **3-20** could be synthesized successfully and isolated as red crystals in 40 % yield (Scheme

3-22). The single crystal of **3-20** was crystallized from concentrated Et$_2$O solutions at 0 °C in the monoclinic space group $P2_1/c$ (Figure 3-25). **3-20** is ionic nature with a silylene-NHC coordinated Co^{II} hydride [L^{2}Si:(CH$_2$)(NHC)CoH(PMe$_3$)$_2$]$^+$ cation and a [B(C$_6$F$_5$)$_4$]$^-$ as counter-ion. The C1-C2 (1.536(10) Å) and C4-C5 (1.512(9) Å) bond distances are almost the same and agree with the bond distances in L^{2}Si:(CH$_2$)(NHC) (L^2 = CH(MeC=NAr)$_2$) backbone. The Co1-Si1 bond distance is 2.187(2) Å which is similar to those Co-Si bond distances in reported cobalt silylene complexes. The hydride H is still found on Co^{II} atom with a Co1-H1 distance of 1.486 Å which indicate the silylene-NHC cobalt(II) hydride nature. The IR absorption at 1768 cm^{-1} of **3-20** also reveals the terminal Co-H bond.

3-18   Ar = 2,6-iPr$_2$C$_6$H$_3$ **3-21**
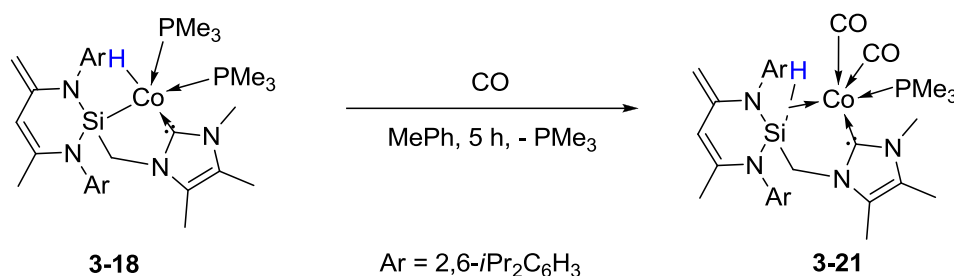
Scheme 3-23. Synthesis of η^2-(Si-H) cobalt complex **3-21**.
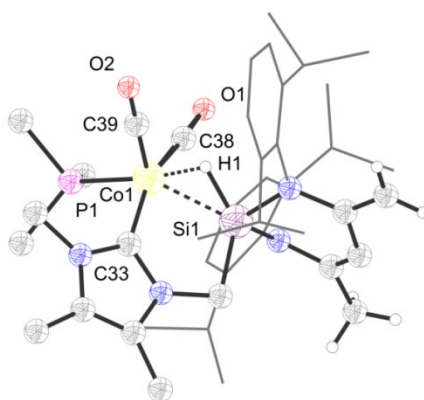
Figure 3-26. Molecular structure of compound **3-21** in solid state. Thermal ellipsoids are drawn at 50% probability level. The hydrogen atoms (except those on Si1, C1, and C5) and solvent molecules are omitted for clarity. Selected bond lengths (Å) and angles (deg): Co(1)-C(38) 1.712(4), Co(1)-C(39) 1.777(4), Co(1)-C(32) 1.943(4), Co(1)-P(1) 2.2099(13), Co(1)-Si(1) 2.2563(13), O(1)-C(38) 1.170(5), O(2)-C(39) 1.154(5), C(2)-C(1) 1.506(5), C(5)-C(4) 1.361(5), C(38)-Co(1)-C(39) 100.4(2),C(38)-Co(1)-C(32) 159.05(19), C(39)-Co(1)-C(32) 97.15(19), C(38)-Co(1)-P(1) 90.33(14),

C(39)-Co(1)-P(1)   106.76(15),   C(32)-Co(1)-P(1)   95.41(12),   C(38)-Co(1)-Si(1) 79.33(14), C(39)-Co(1)-Si(1) 117.42(15), C(32)-Co(1)-Si(1) 82.54(13), P(1)-Co(1)-Si(1) 135.72(5).

The reaction of compound **3-18** under CO atmosphere in toluene afforded yellow solutions (Scheme 3-23). Further crystallization in toluene gave the compound **3-21** as yellow crystals in 80 % yields. A single crystal diffraction analysis revealed that one PMe$_3$ ligand was replaced by two CO ligands (Figure 3-26). The C1-C2 distance (1.506(5) Å, double bond nature) is longer than that of C4-C5 (1.361(5) Å, single bond nature), which suggests a silyl backbone, L^{1}Si(CH$_2$)NHC (L^1 = CH(C=CH$_2$)-(CMe)(NAr)$_2$), in complex **3-21**. Unlike in compound **3-18**, the Si-H bond length (1.470 Å) in **3-21** is shorter than that of **3-18** and in the range of Si-H σ-complexes. This suggests the formation of a η^2-(Si-H) Co^0 σ-complex. The σ-complex nature of **3-21** was also supported by the typical Si-H σ-complex IR absorption appears at 1812 cm^{-1}.
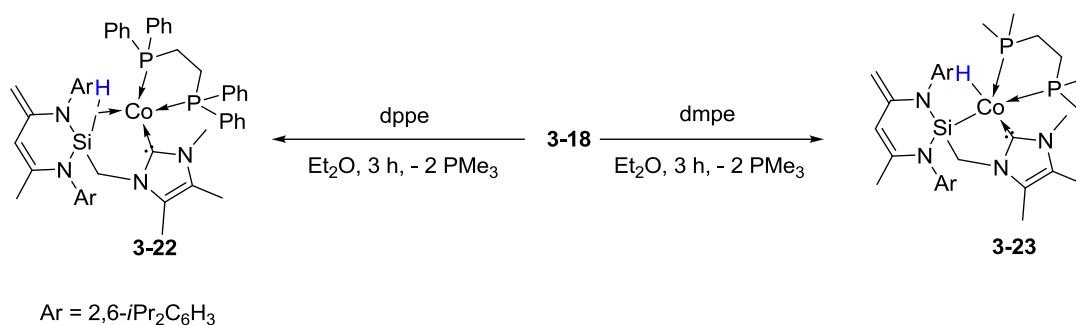
Scheme 3-24. Synthesis of silyl cobalt complex **3-22** and η^2-(Si-H) cobalt complex **3-23.**
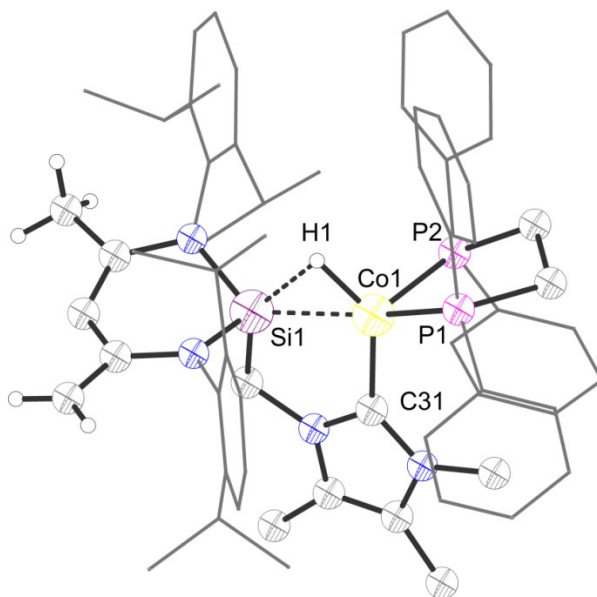
Figure 3-27. The molecular structure of compound **3-22** in the solid state. Thermal ellipsoids are drawn at 50% probability level. The hydrogen atoms (except those on Si1, C1, and C5) and solvent molecules are omitted for clarity. Selected bond lengths (Å) and angles (deg): Co(1)-C(31) 1.9680(17), Co(1)-P(1) 2.2233(5), Co(1)-P(2) 2.2267(5), Co(1)-Si(1) 2.2395(5), C(1)-C(2) 1.464(3), C(4)-C(5) 1.404(3), C(31)-Co(1)-P(1) 115.08(6), C(31)-Co(1)-P(2) 98.75(5), P(1)-Co(1)-P(2) 86.865(19), C(31)-Co(1)-Si(1) 83.81(5), P(1)-Co(1)-Si(1) 146.27(2), P(2)-Co(1)-Si(1) 119.12(2).

Similar to the ligand exchange reaction of **3-18** with CO, the ligand exchange experiments with chelating bis-phosphine ligands dppe, 1,2-bis(diphenylphosphino)ethane, and dmpe, 1,2-bis(dimethylphosphino)ethane, were also tested. The reactions of compound **3-18** with dppe and dmpe in Et_2O afforded the exchanged products **3-22** and **3-23** (Scheme 3-24, Figure 3-27, and Figure 3-28), respectively. The X-ray diffraction analysis suggested the $L^1Si(CH_2)NHC$ (L^1 = $CH(C=CH_2)$-$(CMe)(NAr)_2$) backbones (for **3-22**: C1-C2 bond distance 1.464(3) Å; C4-C5 bond distance 1.404(3). For **3-23**: C20-C23 bond distance 1.443(14) Å; C22-C24 bond distance 1.385(15)). However, the Si-H bond situations are quite different in two cases depending on the different σ-donating strength of chelating phosphine ligands. In compound **3-22**, the Si-H bond distance (1.794 Å) is similar to those in

compound **3-21** which indicate a η^2-(Si-H) Co^0 σ-complex. The infrared absorption of Si-H at 1718 cm^{-1} is in agreement with the Si-H frequency in literature known η^2-(Si-H) σ-complex and is red-shifted compared to those observations in **3-21**. In sharp contrast to those in **3-22**, by introducing the stronger σ donor phosphine dmpe yielded the Si-H oxidative addition product **3-23**. The IR spectrum of **3-23** shows absorption bands at 1752 cm^{-1}, which is in accordance with those observations in Co-H bonds.
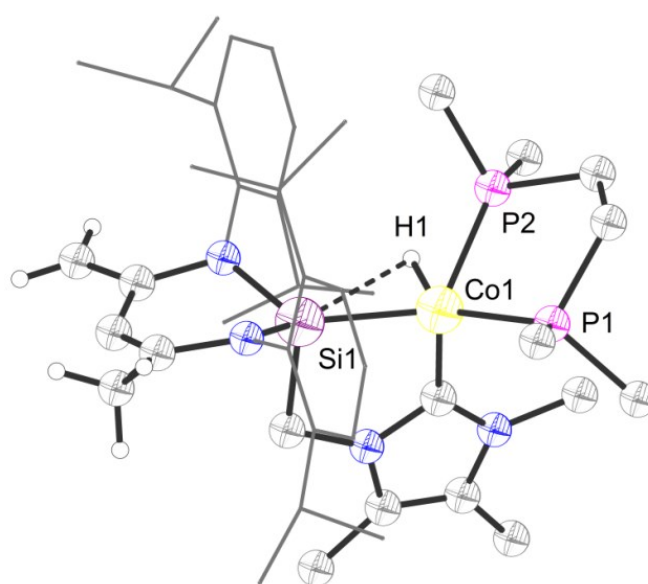
Figure 3-28. Molecular structure of compound **3-23** in solid state. Thermal ellipsoids are drawn at 50% probability level. The hydrogen atoms (except those on Si1, C1, and C5) and solvent molecules are omitted for clarity. Selected bond lengths (Å) and angles (deg): Co(1)-C(13) 1.928(11), Co(1)-P(1) 2.187(3), Co(1)-P(2) 2.212(4), Co(1)-Si(1) 2.217(3), Co(1)-H(1) 1.34(7), C(20)-C(23) 1.443(14), C(22)-C(24) 1.385(15), C(13)-Co(1)-P(1) 109.6(3), C(13)-Co(1)-P(2) 114.2(4), P(1)-Co(1)-P(2) 87.94(13), C(13)-Co(1)-Si(1) 86.0(3), P(1)-Co(1)-Si(1) 143.02(15), P(2)-Co(1)-Si(1) 116.80(13).

3.4.2 Olefin hydrosilylations catalyzed by Co complexes

Despite the great numbers of hydrosilylation catalysts reported, highly selective base metal-based (pre)catalysts are still rarely explored. Recently, Fout et al. reported the highly steric controlled selective 1,2-hydrosilylation of conjugated 1,3-dienes derivatives with cobalt NHC-based catalysts.[109a, 109c, 109h, 110] In this chapter, the cobalt complex **3-18** selectively hydrosilylates the mono-substituted olefins towards *gem*-disubstituted terminal olefins and enables the 1,2-hydrosilylation of nonconjugated dienes.

The initial optimization experiments indicate 0.1 mol% loading of **3-18** could catalyze the *anti*-Markovnikov hydrosilylation of 1-dodecene using phenylsilane as Si-H source with high conversion at room temperature in THF (62 %, Table 3-8, entry 1). In addition to the silyl Co hydride complex **3-18**, other cobalt complexes were also tested under the same condition. We found that only η^2-(Si-H) σ-complex **3-22** with dppe ligand was active but less efficient than that of **3-18** (28 %, Table 3-8, entry 5). The bis-silyl-NHC coordinated complex **3-19**, silylene cobalt hydride complex **3-20**, and η^2-(Si-H) cobalt carbonyl σ-complex **3-22** were not active (Table 3-8, entry 2-6). Interestingly, the silyl cobalt hydride complex **3-23** bearing chelating dmpe was also not active, which might be rationalized by the lower dissociation rate of the stronger binding chelating dmpe ligand which blocks the further active site for the reaction. I also tested different silanes. The corresponding optimization indicates that PhSiH$_3$ gave the highest conversion compared to the disubstituted silane Ph$_2$SiH$_2$. Probably because of the bulkiness of tri-substituted silanes, they are unsuitable for hydrosilylation reactions: (EtO)$_3$SiH, Et$_3$SiH, and PhMe$_2$SiH (Table 3-8, entry 7-9).

Table 3-8. The cobalt complexes catalyzed *anti*-Markovnikov hydrosilylation of alkenes using various reaction conditions[a]

$$n\text{-}C_{10}H_{21} \diagup \quad + \quad [Si]\text{-}H \quad \xrightarrow[\text{RT, THF, 2 h}]{\text{cat.}} \quad n\text{-}C_{10}H_{21} \diagdown [Si]$$

Ar = 2,6-*i*Pr$_2$C$_6$H$_3$

3-18   **3-19**   **3-20**

3-21   **3-22**   **3-23**

Entry	cat.	loading mol%	Silane	Conversion[b] %
1	**3-18**	0.1	PhSiH$_3$	62
2	**3-19**	0.1	PhSiH$_3$	ND
3	**3-20**	0.1	PhSiH$_3$	ND
4	**3-21**	0.1	PhSiH$_3$	ND
5	**3-22**	0.1	PhSiH$_3$	28
6	**3-23**	0.1	PhSiH$_3$	ND
7	**3-18**	0.1	(EtO)$_3$SiH	ND
8	**3-18**	0.1	Et$_3$SiH	ND
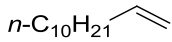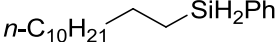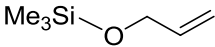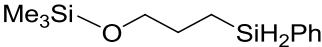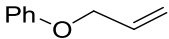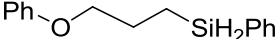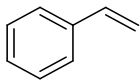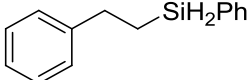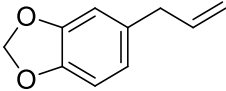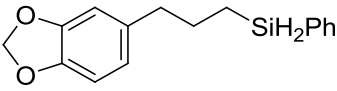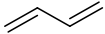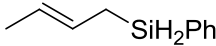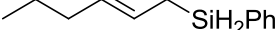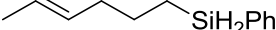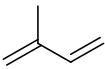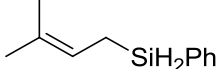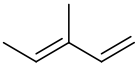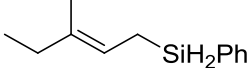
9	**3-18**	0.1	PhMe$_2$SiH	ND
10	**3-18**	0.1	Ph$_2$SiH$_2$	37
11	**3-18**	0.01	PhSiH$_3$	19
12	**3-18**	0.005	PhSiH$_3$	trace
13	**3-18**	0.5	PhSiH$_3$	70

[a] Reaction conditions: alkene (0.25 mmol), silane (0.275 mmol), T = room temperature, solvent = 1 mL, t = 2 h. [b] NMR Conversions.

Further, we investigated the catalytic performance of **3-18** with different olefins (Table 3-9 and 3-10). It was found that the catalyst was active for different kinds of terminal olefins and led to the formation of *anti*-Markovnikov hydrosilylation products. The hydrosilylations of the mono-substituted alkenes with alkyl, silyloxy, phenoxy, and benzyl substituents gave good yields (80 - 94 %, entry 1- 6, Table 3-9). However, the hydrosilylation of styrene gave a relatively lower yield only (58 %, entry 5, Table 3-9).

Table 3-9. The cobalt-catalyzed *anti*-Markovnikov hydrosilylation of different olefins [a]

Entry	Alkenes	Products	Yield[b] %
1	*n*-C$_6$H$_{13}$⁀⁀	*n*-C$_6$H$_{13}$⁀⁀SiH$_2$Ph	82

2	$n\text{-}C_{10}H_{21}$ ⟍⟍⟍	$n\text{-}C_{10}H_{21}$ ⟍⟍⟍SiH_2Ph	80
3	Me_3Si⟍O⟍⟍	Me_3Si⟍O⟍⟍SiH_2Ph	93
4	Ph⟍O⟍⟍	Ph⟍O⟍⟍SiH_2Ph	90
5	⟍⟍	⟍⟍SiH_2Ph	58
6	⟍⟍	⟍⟍SiH_2Ph	94
7	⟍⟍	⟍⟍SiH_2Ph	78
8	⟍⟍⟍	⟍⟍⟍SiH_2Ph	47
9	⟍⟍⟍	⟍⟍⟍SiH_2Ph	98
10	⟍⟍	⟍⟍SiH_2Ph	20
11	⟍⟍⟍	⟍⟍⟍SiH_2Ph	trace
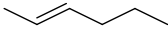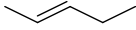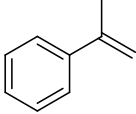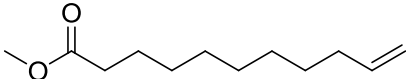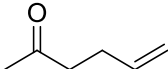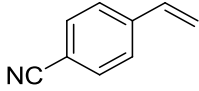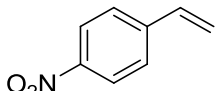
12		SiH_2Ph	71
13		SiH_2Ph	85
14		SiH_2Ph	75
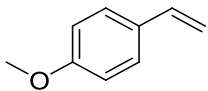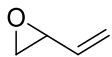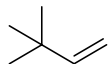
[a] Reaction conditions: alkene (0.25 mmol), $PhSiH_3$ (0.275 mmol), **3-18** (0.5 mol%), T = room temperature, solvent = 1 mL, t = 2 h. [b] NMR yield.

Subsequently, the hydrosilylations of dienes were examined. The hydrosilylation of conjugated linear and branched dienes (entry 7, 8, 10, and 11, Table 3-9) gave 1,4-addition products. The steric non-hindered 1,3-butadiene gave relatively high yield (78 %). The mono-substituted dienes (entry 8 and 10, Table 3-9) gave lower yield (47 % and 20 %, respectively). The disubstituted 3-methyl-1,3-pentadiene yielded only a trace amount of the product (entry 11, Table 3-9), which could be considered a result of the steric effects. The hydrosilylation of nonconjugated terminal/internal dienes gave the terminal hydrosilylation products, while the internal olefins remained inactive (entry 9 and 14, Table 3-9). Interestingly, the hydrosilylation of nonconjugated terminal dienes 2-methyl-1,4-pentadiene and 2-methyl-1,5-hexadiene indicate that the reaction happened selectively at a less hindered position and gave the highly selective 1,2-hydrosilylation products (entry 12 and 13, Table 3-9).

Control experiments with internal olefins gave no conversions (entry 1 and 2, Table 3-10). *gem*-disubstituted olefin α-methylstyrene and 2,3-dimethyl-1,3-butadiene (entry 3 and 10, Table 3-10) were also found to be inactive possibly due to their steric hinder effect. Because of the possible strong coordination of heteroatom with catalytically active sites, the reactions of the alkenes bearing carbonyl-, nitro-, nitrile-, and oxygen-containing groups gave no conversions (entry 4-9, Table 3-10).

Table 3-10. The cobalt-catalyzed hydrosilylation of different alkenes [a]
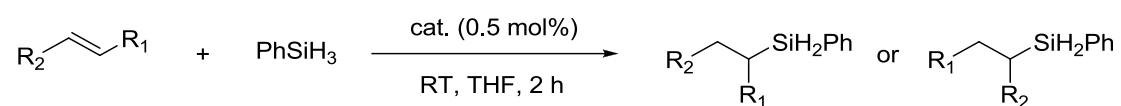
Entry	Alkenes	Conversion[b] %	Selectivity[b] %
1		ND	-
2		ND	-
3		ND	-
4		ND	-
5		ND	-
6		ND	-
7		ND	-

8		ND	-
9		ND	-
10		ND	-
11		ND	-

[a] Reaction conditions: alkene (0.25 mmol), PhSiH$_3$ (0.275 mmol), **3-18** (0.5 mol%), T = room temperature, solvent = 1 mL, t = 2 h. [b] NMR yield.

According to the Chalk-Harrod mechanism for olefin hydrosilylation which involves with a cobalt catalyst,[106a] the catalytic cycle starts with the formation of cobalt hydride active intermediate **A** from the ligands dissociation of complex **3-18** (Scheme 3-25). Due to the different coordination model of intermediate **A** in relation to terminal olefins and conjugated dienes, two different catalytic cycles were proposed (cycle 1 for terminal olefins and cycle 2 for dienes, Scheme 3-25). The intermediate **A** then coordinates with an olefin, producing alkene complex intermediate **B-1** or **B-2**, which then undergoes insertion of alkene into Co-H bond and generation of cobalt alkyl complex intermediate **C-1/C-2.** Further, the oxidative addition of PhSiH$_3$ into the cobalt center of intermediate **C-1/C-2** furnishes the corresponding intermediate **D-1/D-2**, which subsequently liberates the desired product through a reductive elimination step that regenerates the Co-H catalyst **A**.

Accordingly, the cobalt complex **3-21** (no conversion), **3-22** (28 % conversion), and **3-23** (no conversion) have also been tested as precatalysts but results in poor performances. This indicates that the stronger binding ligands (e.g., CO, dppe, and dmpe) decrease the activity of the catalysts due to high ligand dissociation energies. Moreover, the reduced catalytic activity of cationic cobalt silylene complex **3-20** can

be attributed to the higher ligand dissociation energy produced by a positively charged cobalt center.
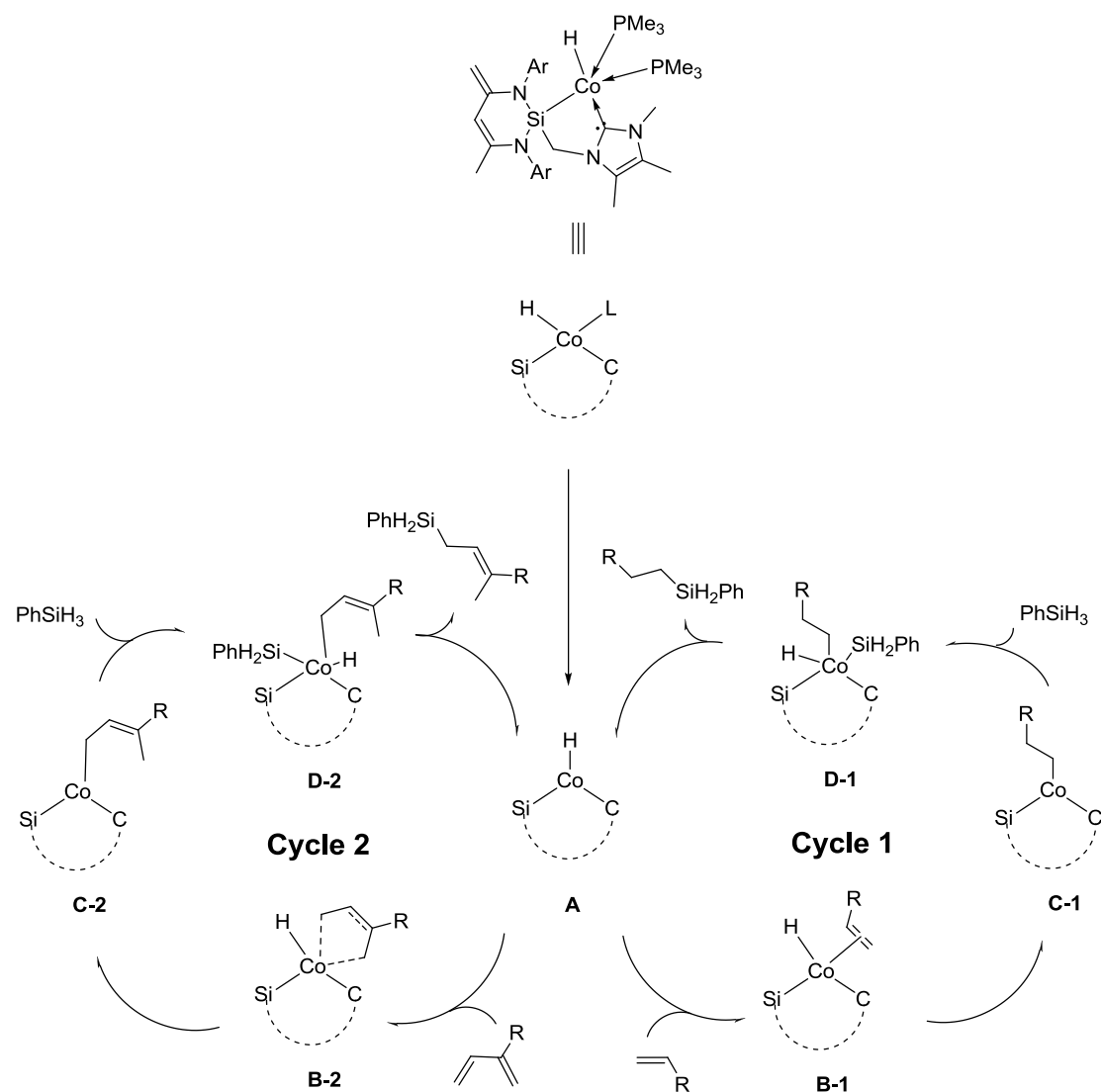
Scheme 3-25. Proposed mechanism for olefin hydrosilylation catalyzed by cobalt complexes.

4. SUMMARY

This work focused on the application of new multidentate *N*-heterocyclic silylenes (e.g., *N,N*-di(*tert*-butyl)amidinato NHSi derivatives and *β*-diketiminate NHSi derivatives) as supporting ligands for low-valent germanium compounds as well as in the coordination chemistry of transition-metals (e.g., nickel, manganese, and cobalt). The obtained transition-metal complexes were applied as (pre)catalysts for various organic transformations (e.g., amination, transfer semi-hydrogenation, and olefin hydrosilylation, Chart 4-1).
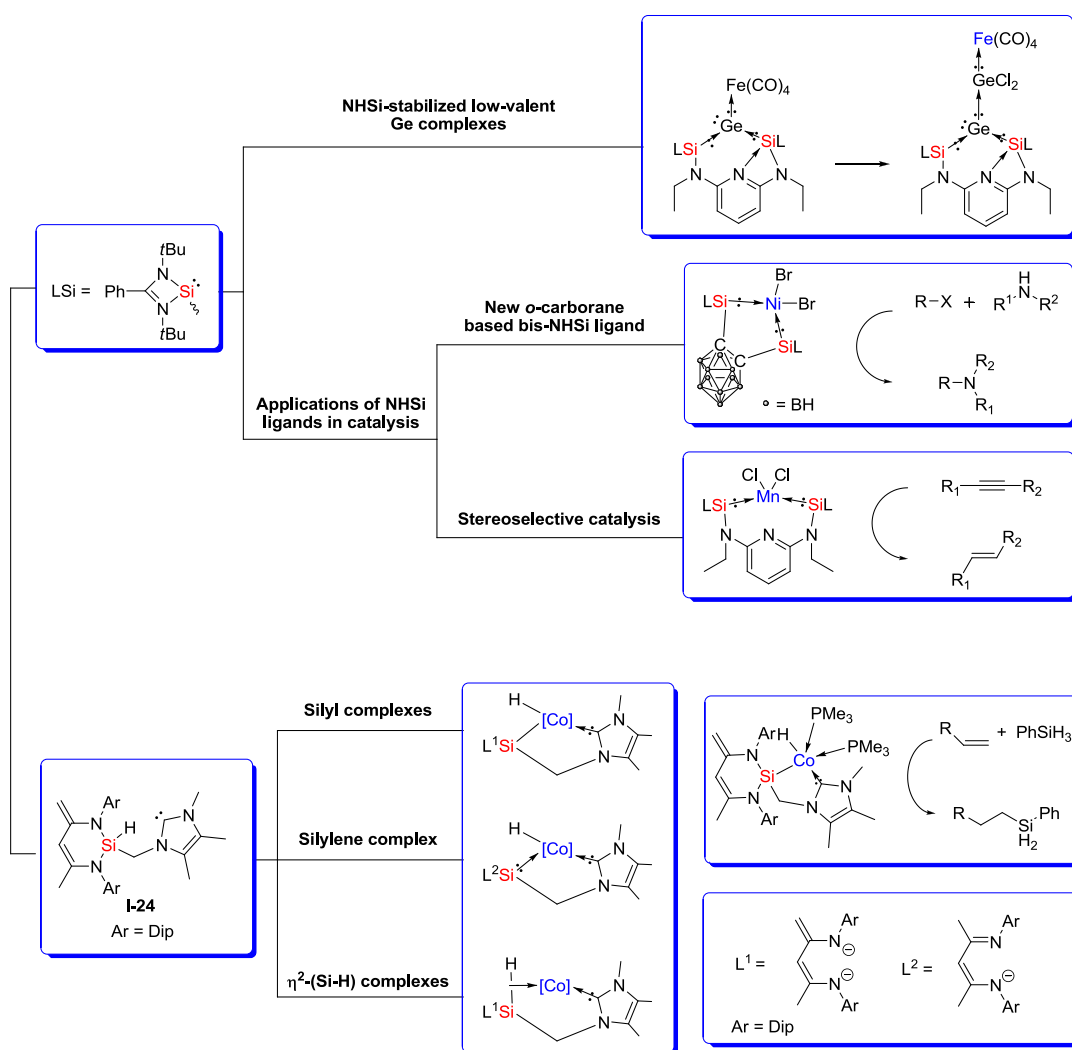
Chart 4-1. Summary of my PhD work.

In chapter 3.1, the synthesis and characterization of the first bis-NHSi stabilized germylone iron complex **3-3** is discussed. **3-3** was prepared by the reaction of NHSi stabilized chlorogermyliumylidene chloride **3-1** and Collman's reagent $K_2Fe(CO)_4$. A single-crystal X-ray diffraction analysis revealed that the Ge^0 center adopts a trigonal-pyramidal geometry with a Si-Ge-Si angle of $95.66(2)^\circ$. Remarkably, one of the Si^{II} donor atoms in the complex is five-coordinated because of additional (pyridine)N→Si coordination. Through the insertion of $GeCl_2$ into the Ge-Fe bond, the reaction of **3-3** with $GeCl_2$·dioxane afforded complex **3-4** which could be described as a new type of donor-acceptor stabilized isomeric form of heavier vinylidene (Scheme 4-1).
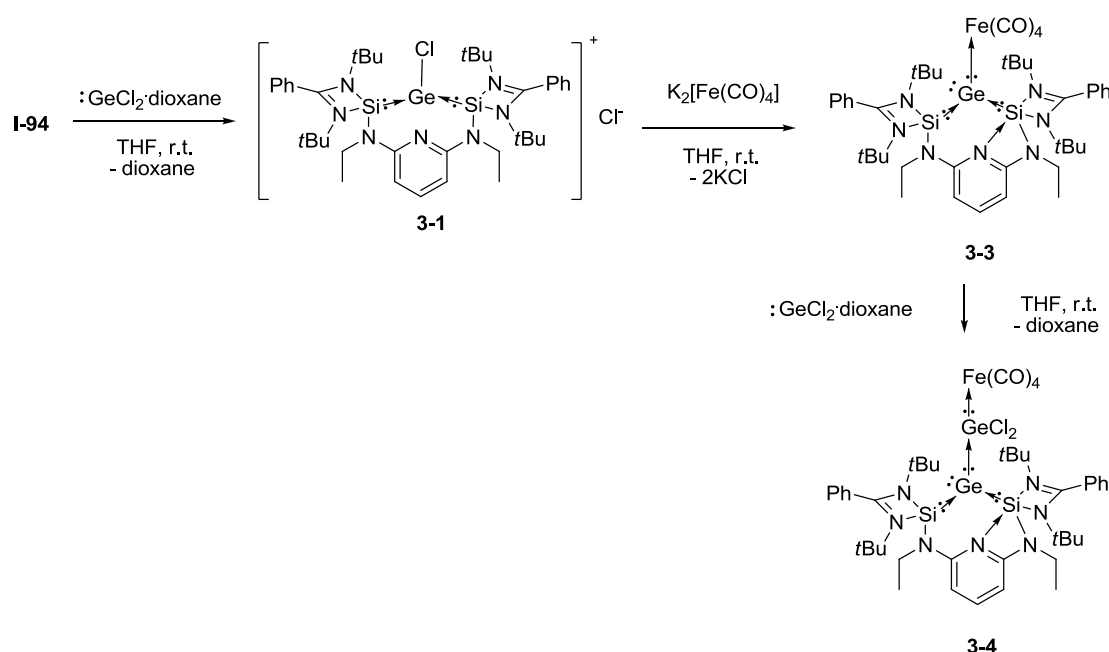
Scheme 4-1. Synthesis and reactivity of the germylone iron carbonyl complex **3-3** stabilized by the bis-NHSi pyridine pincer ligand **I-94**.

The first chelating bis(NHSi)-substituted *o*-carborane ligand **3-6** was synthesized by the reaction of *N,N*-di(*tert*-butyl)amidinato silylene chloride with a lithiated *o*-carborane backbone. Ligand **3-6** was fully characterized by single-crystal X-ray diffraction analysis, NMR, MS, etc. Coordination of the extraordinarily strong σ-donor ligand towards Ni^{II} yields the corresponding complex **3-7** which undergoes reduction with KC_8 in the presence of CO to afford the tetrahedral Ni^0 complex **3-8**. The CO stretching vibration modes of **3-8** indicate that the Si^{II} atoms in ligand **3-6** are even stronger σ-donors than the P^{III} atoms in phosphines and C^{II} atoms in *N*-heterocyclic carbene (NHC) ligands (Scheme 4-2).
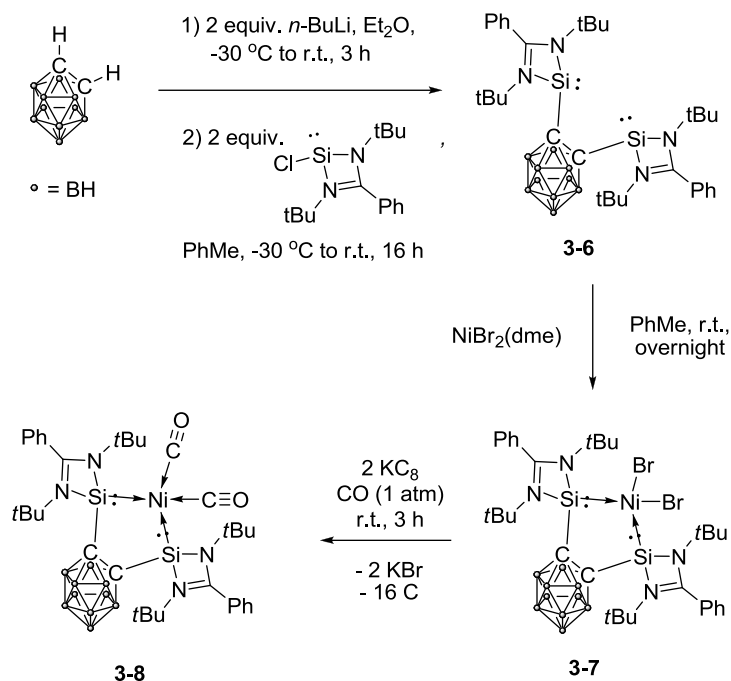
Scheme 4-2. Synthesis and coordination chemistry of bis(NHSi)-substituted *o*-carborane ligand **3-6**.

Compared with the ferrocendiyl-bridged bis(NHSi) analogue **3-9** and the related bis(phosphanyl)-substituted *o*-carborane containing complexes **3-11** and **3-13**, complex **3-7** shows a superior catalytic activity in Buchwald-Hartwig amination reactions of aryl halides with secondary amines. Screening and optimization experiments revealed that the catalytic amination of various aryl halides succeeds with 0.5 mol% of complex **3-7** in the presence of $AgBPh_4$ and KO*t*Bu. The utilizations of **3-9** or the phosphine analogous **3-11** and **3-13** give significantly lower yields of the desired product, indicating the superior steering role of the ligand **3-6** to facilitate metal-mediated C-N coupling reactions (Scheme 4-3).
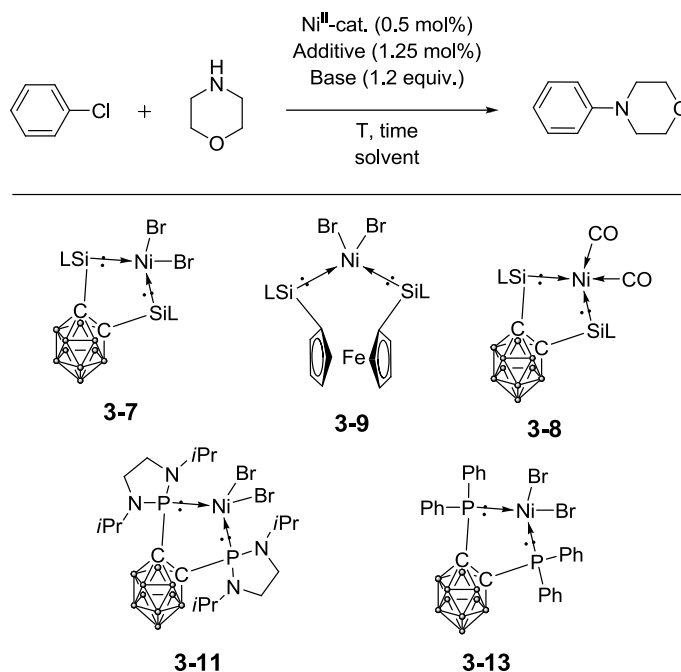
Scheme 4-3. The nickel-catalyzed Buchwald-Hartwig coupling using various NHSi and phosphine ligands.

The manganese complexes stabilized by pincer-type bis(NHSi)-pyridine ligand **I-94**, bidentate bis(NHSi)-ferrocene ligand **I-86**, and monodentate NHSi ligand **I-84** were also synthesized. The manganese complexes **3-14**, **3-15**, and **3-16** as well as ligand **3-6**, **I-93**, and **3-17** were applied successfully in transfer semi-hydrogenation of alkynes using ammonia-borane as a convenient hydrogen source under mild reaction conditions. They act as highly active and stereoselective Mn-based precatalysts (1 mol % loading) in transfer semi-hydrogenations of alkynes to give the corresponding (*E*)-olefins. The highest stereo-selectivity could be achieved by using the Mn complexes **3-14** supported by bis(NHSi) ligand **I-94** (Scheme 4-4).
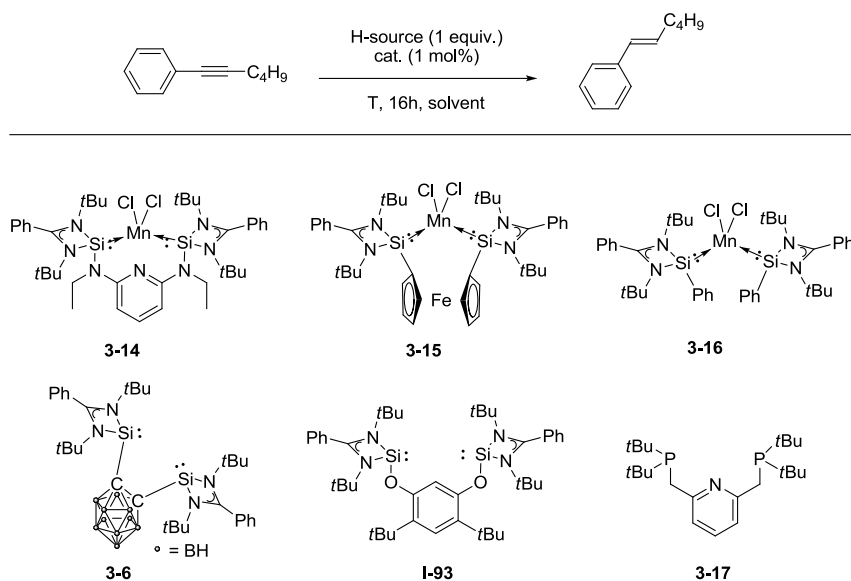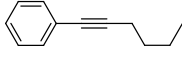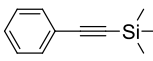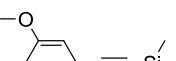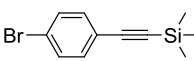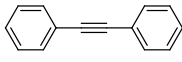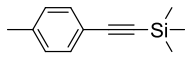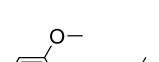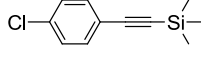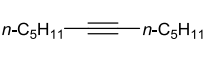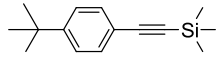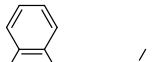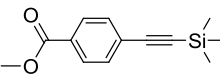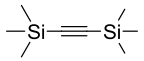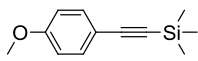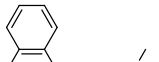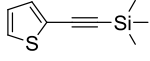
Scheme 4-4. The manganese-catalyzed transfer semi-hydrogenation of alkynes using various NHSi and phosphine ligands.

Furthermore, the catalytic performances of **3-14** with different alkynes were investigated. It turned out that the catalyst tolerates different functional groups and leads to the corresponding (*E*)-alkenes as main products. Complex **3-14** gives the best catalytic performance with quantitative conversion rates and excellent *E*-stereoselectivities (up to 98 %) for different alkyne substrates (Scheme 4-4). Different types of functional groups can be tolerated, except -CN, -NH$_2$, -NO$_2$, and -OH substituents at the phenyl rings (Table 4-1).

In chapter 3.4, the coordination chemistry of NHSi derivative **I-24** and subsequently catalytic investigations are described and discussed. The reaction of *N*-heterocyclicsilylcarbene **I-24** with CoBr$_2$ and KC$_8$ in the presence of PMe$_3$ generated the silyl-NHC cobalt hydride **3-18**. Further reactions of **3-18** with Jutzi acid, CO, and chelating bis-phosphine ligands gave the corresponding silylene-NHC cobalt hydride **3-20**, the η^2-(Si-H)-NHC cobalt σ-complexes **3-21** and **3-22**, as well as silyl-NHC cobalt hydride **3-23** (Scheme 4-5).

Table 4-1. The NHSi-Mn complex **3-14** catalyzed transfer semi-hydrogenation of different alkynes.

$$R_1 \equiv R_2 \xrightarrow[\text{55}^{\circ}\text{C, 16 h, THF}]{\substack{\text{BH}_3\text{NH}_3 \text{ (1 equiv.)} \\ \textbf{3-14} \text{ (1 mol\%)}}} \begin{array}{c} R_2 \\ R_1 \end{array}$$

(conversion, *E*-selectivity)

(> 99 %, 90 %)	(98 %, 92 %)	(97 %, 82 %)	(99 %, 94 %)
(97 %, 92 %)	(98 %, 93 %)	(99 %, 79 %)	(> 99 %, 96 %)
(67 %, 50 %)	(90 %, 91 %)	(96 %, 98 %)	(> 99 %, 60 %)
(-, -)[a]	(95 %, 92 %)		(81 %, 95 %)

[a] No products were detected.
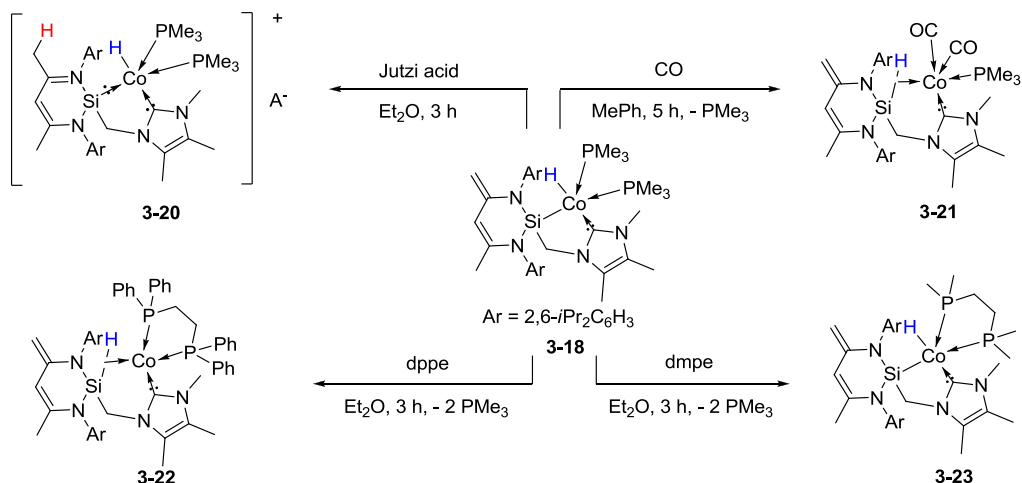
Scheme 4-5. Synthesis and reactivity of cobalt **3-18 – 3-23** based on *β*-diketiminate NHSi derivatives.

Subsequently, cobalt complexes were applied successfully in the *anti*-Markovnikov hydrosilylation of terminal alkenes. The optimization experiments indicate that a 0.1 mol% loading of **3-18** could effectively catalyze the *anti*-Markovnikov hydrosilylation of 1-dodecene. The η^2-(Si-H) σ-complex **3-22** with dppe ligand was also found to be active but less efficient than **3-18**. However, silylene-NHC cobalt complex **3-20**, η^2-(Si-H)-NHC cobalt complex **3-22,** as well as the silyl-NHC cobalt hydride complex **3-23** bearing chelating dmpe are inactive.

Table 4-2. The cobalt complex **3-18** catalyzed hydrosilylation of alkenes.
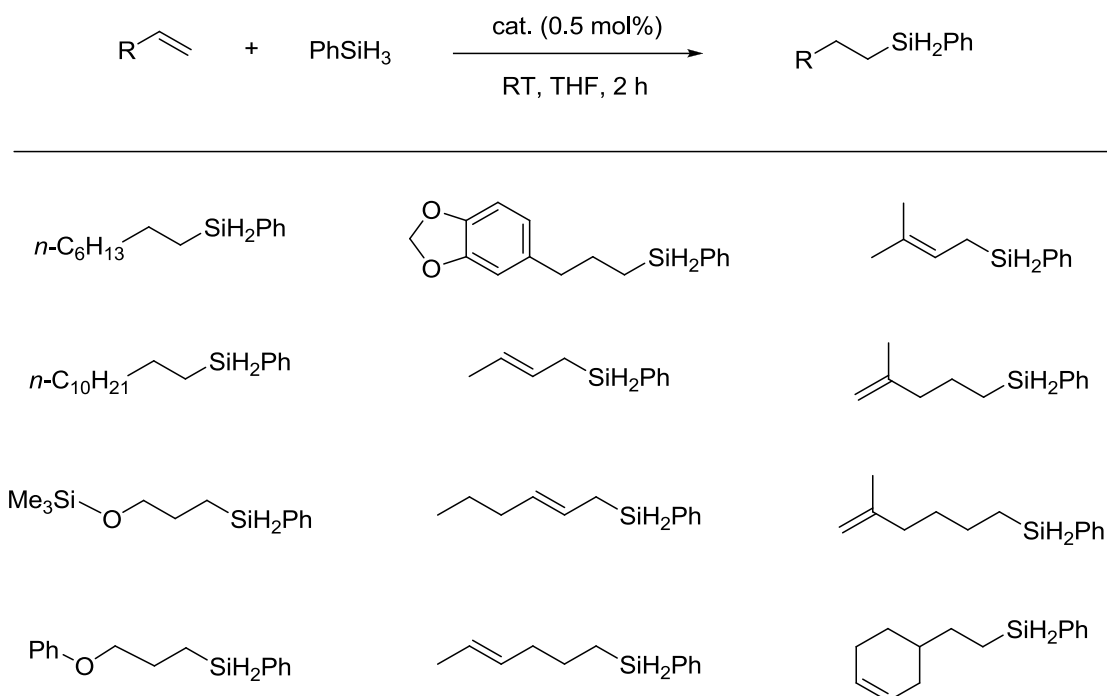
Further, the catalytic performance of **3-18** was investigated (Table 3-9 and 3-10). It emerged that **3-18** is active for different kinds of terminal olefins and led to the production of the corresponding *anti*-Markovnikov hydrosilylation products using the mono-substituted alkenes bearing alkyl, phenyl, silyloxy, phenoxy, benzyl, internal olefin, and *gem*-disubstituted terminal olefin substituents. The hydrosilylations of conjugated linear and branched dienes gave the 1,4-addition products. (Table 4-2).

In conclusion, my doctoral work extends the scope of low-valent group 14 chemistry, especially in using *N*-heterocyclic silylene ligands to stabilize low-valent germanium compounds and the utilization of *N*-heterocyclic silylene metal complexes for metal-mediated catalytic transformations of organic substrates.

5. EXPERIMENTAL SECTION

5.1 General consideration

All experiment and manipulations were carried out under dry oxygen-free nitrogen using standard Schlenk techniques or in a nitrogen-filled glovebox. The glassware used in all manipulations was dried at 150 °C prior to use, cooled to ambient temperature under high vacuum, and flushed with N_2. The handling of solid samples and the preparation of samples for spectroscopic measurements were carried out inside a glovebox, where the O_2 and H_2O levels were normally kept below 1 ppm.

All solvents were purified using conventional procedures and freshly distilled under N_2 atmosphere prior to use. They were stored in Schlenk flasks containing activated molecule-sieves. Benzene, toluene, *n*-hexane were purified by distillation from Na/benzophenone. Et_2O and THF were initially pre-dried over KOH and then distilled from Na/benzophenone. CH_2Cl_2 and chloroform were dried by stirring over CaH_2 at ambient temperature.

5.2 Analytical methods

NMR Measurements: NMR samples of air and/or moisture sensitive compounds were all prepared under an inert atmosphere and sealed off in an NMR tube *in vacuo* for measurement. The deuterated solvents were dried by stirring over Na mirror (benzene-d_6, toluene-d_8, and THF-d_8) or CaH_2 (CD_2Cl_2 and $CDCl_3$), distilled under N_2 atmosphere and stored in Schlenk flasks containing activated molecule-sieves. The ^1H- and ^{13}C-NMR spectra were recorded on ARX 200 (^1H, 200 MHz; ^{13}C, 50 MHz) and ARX 400 (^1H, 400 MHz; ^{13}C, 100.46 MHz) spectrometers from the *Bruker* Company. The ^{29}Si-NMR spectra were recorded only on ARX 400 (^{29}Si, 79.49 MHz) spectrometer. ^1H and $^{13}C\{^1H\}$ NMR spectra were referenced to residual solvent signals as internal standards (benzene-d_6, δ_H = 7.15 ppm and δ_C = 128.0 ppm; $CDCl_3$ δ_H = 7.27 ppm and δ_C = 77.0 ppm; THF-d_8, δ_H = 1.73 ppm and δ_C = 25.3 ppm; CD_2Cl_2, δ_H = 5.32 ppm and δ_C = 53.8 ppm; toluene-d_8, δ_H = 2.08 ppm and δ_C = 20.4 ppm. Heteronuclear spectra were calibrated as follows: $^{31}P\{^1H\}$: external 85% H_3PO_4. Whereby in each case a 1-mm glass capillary tube containing the standard substance

was placed in the appropriate solvent in a 5 mm NMR tube and the spectrum recorded. Unambiguous signal assignments were made by employing a combination of 2D NMR H,C-HMQC (Heteronuclear Multiple-Quantum Correlation) and DEPT (Distortionless Enhancement by Polarization Transfer) experiments. The abbreviations used to denote the multiplicity of the signals are as follows: s = singlet, d = doublet, t = triplet, q = quartet, sept = septet, m = multiplet, br = broad.

Infra-red spectroscopy IR spectra (4000 – 400 cm^{-1}) were recorded on a Perkin-Elmer Spectra 100 FT-IR spectrometer, bands were reported in wave-numbers (cm^{-1}). Samples of solids were measured as KBr pellets. Air or moisture sensitive samples were prepared in the glovebox and measured immediately. The spectra were processed using the program OMNIC and the abbreviations associated with the absorptions quoted are: vs = very strong; s = strong, m = medium; w = weak, br = broad, the intensities of which were assigned on the basis of visual inspection.

Mass Spectrometry Mass spectra were performed at the Chemistry Institute of Technical University Berlin. EI spectra were recorded on a 311A Arian MAT/AMD spectrometer. ESI mass spectra were recorded on a Thermo Scientific Orbitrap LTQ XL spectrometer. Solid samples were prepared in the glove box, and the solution of samples was prepared 15 min before the measurement under N_2 atmosphere. Mass spectra are presented in the standard form, m/z (percent intensity relative to the base peak).

Elemental analysis The C, H, N, and S analyses of all compounds were carried out on a Thermo Finnigan Flash EA 1112 Series instrument. Air or moisture sensitive samples were prepared in "tin-boats" in the glove box. Samples with halogen were filled in the "silver-boats" for better measuring accuracy.

Single crystal X-ray structure determinations: Crystals, suitable for the single crystal X-ray structure analysis, were put on a glass capillary with perfluorinated oil and measured in a cold nitrogen stream. The data of all measurements were collected with an Oxford Diffraction Xcalibur S Saphire diffractometer at 150 K (MoK$_\alpha$ radiation, λ = 0.71073 Å) or an Oxford Diffraction Supernova, a Single source at the offset, Atlas at 150 K (Cu-Kα-radiation, λ = 1.5418 Å). The structures were solved by direct methods. Refinements were carried out with the SHELXL-97 software package.[111] All thermal displacement parameters were refined anisotropically for non-H atoms

and isotropically for H atoms. All refinements were made by full matrix least-squares on F^2. In all cases, the graphical representation of the molecular structures was carried out using Diamond version 3.1. The details for the individual structure solutions included in this dissertation are available in the appendix.

DFT calculations: DFT calculations were performed at the B97-D/6-31G(d)[Fe, Ni, Si, Br: def2-TZVP] level of theory. Stationary points on the potential energy surface (PES) were characterized by harmonic vibrational frequency calculations. Electronic structure analysis was executed both at B97-D/6-31G(d)[Fe, Ni, Si, Br: def2-TZVP] and B3LYP/6-31G(d)[Fe, Ni, Si, Br: def2-TZVP]. Calculations were carried out using GAUSSIAN 09 program.[112]

5.3 Starting materials

Commercially available starting materials were used as received. The following important precursors were prepared according to literature procedures:

N,N'-di-*tert*-butyl(phenylamidinato)-chlorosilylene,[13] $K_2Fe(CO)_4$[113]   and bis(cyclodiaminophosphanyl)-*o*-carborane[78e] were synthesized according to reported procedures.

5.4 Synthesis and characterization of all the new compounds

5.4.1 Synthesis of the chlorogermyliumylidene chloride 3-1
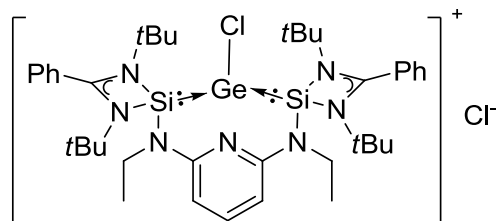
To a 50 mL Schleck flask containing **I-94** (136 mg, 0.2 mmol) and $GeCl_2 \cdot$dioxane (46 mg, 0.2 mmol), THF (30 mL) was added via cannula, forming an orange solution. After stirring at room temperature overnight, the precipitate of **3-1** was separated by filtration and dried under vacuum, affording the product as a yellow powder (105 mg, yield 62%). The single crystal of **3-1** was crystallized from the mixture solution of **I-94** (34 mg) and $GeCl_2 \cdot$dioxane (11 mg) in THF/toluene (1:1) at room temperature.

^{1}H NMR	δ(ppm) = 1.30 (s, 36 H, NC(CH_3)$_3$), 1.44 (t, $^3J_{\text{H-H}}$ = 7.0 Hz, 6 H, NCH$_2$CH_3), 3.48 (q, $^3J_{\text{H-H}}$ = 7.0 Hz, 4 H, NCH_2CH$_3$), 6.29 (d, $^3J_{\text{H-H}}$ = 8.1 Hz, 2 H, H-py), 7.56−7.67 (m, 11 H, H_{arom}).
^{13}C$\{^1$H$\}$ NMR	δ(ppm) = 14.98 (NCH$_2$CH_3), 31.48 (NC(CH$_3$)$_3$), 38.99 (NCH_2CH$_3$), 55.98 (NC(CH$_3$)$_3$), 99.64 (C-py), 128.95 (C_{arom}), 129.04 (C_{arom}),129.08 (C_{arom}), 129.16 (C_{arom}), 129.21 (C_{arom}), 132.21 (C_{arom}), 141.97 (C-py), 157.82 (C-py), 178.23 (NCN).
^{29}Si$\{^1$H$\}$ NMR	(79.49 MHz, CD$_2$Cl$_2$, 298 K): δ(ppm) = 3.60.
ESI-MS (m/z):	calcd for [C$_{39}$H$_{59}$N$_7$Si$_2$GeCl]$^+$ 790.3265; found 790.3264.

5.4.2 Synthesis of the germylone iron carbonyl complex 3-3
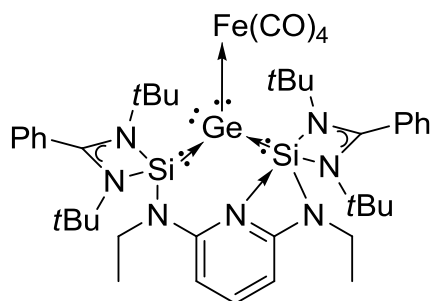
To a 50 mL Schleck flask containing **3-1** (165 mg, 0.2 mmol) and $K_2Fe(CO)_4$ (49 mg, 0.2 mmol), THF (30 mL) was added via cannula. After stirring at room temperature overnight, all volatiles were removed under vacuum. The residue was then washed with diethyl ether (30 mL) and extracted with THF (30 mL) affording the product as red solid (90 mg, yield 49%). The single crystal suitable for X-ray analysis was grown by diffusing diethyl ether into concentrated THF solution of **3-3**.

^{1}H NMR	(400.13 MHz, THF-d_8, 298 K): δ(ppm) = 1.26−1.40 (m, 42 H, NC(CH_3)$_3$ and NCH$_2$CH_3), 3.58 (overlap with THF, 4 H, NCH_2CH$_3$), 6.10 (m, 1 H, H-py), 7.22−7.90 (m, 12 H, H_{arom}).
^{13}C{^{1}H} NMR	(100.61 MHz, THF-d_8, 298 K): δ(ppm) = 15.74 (NCH$_2$CH_3), 29.40 (NCH_2CH$_3$), 31.95 (NC(CH_3)$_3$), 55.32 (NC(CH$_3$)$_3$), 114.61 (C-py), 128.38 (C_{arom}), 128.48 (C_{arom}), 129.19 (C_{arom}), 130.30 (C_{arom}), 131.39 (C_{arom}), 158.37 (C-py), 174.71 (NCN), 222.94 (CO).
^{29}Si{^{1}H} NMR	(79.49 MHz, THF-d_8, 298 K): δ(ppm) = −5.92.
APCI-MS (m/z):	calcd for [(C$_{43}$H$_{59}$N$_7$Si$_2$O$_4$GeFe + Cl)]$^+$ 958.2417; found 958.4046.

5.4.3 Synthesis of the germylone-germylene iron complex 3-4

To a 50 mL Schleck flask containing **3-3** (80 mg, 0.09 mmol) and GeCl$_2$·dioxane (20 mg, 0.09 mmol), THF (30 mL) was added via cannula. After stirring at room temperature overnight, all volatiles were removed under vacuum. The residue was then extracted with diethyl ether affording the product as yellow solid (60 mg, yield 65%). The single crystal suitable for X-ray analysis was grown from diethyl ether and THF mixed solution of **3-4** at room temperature.

^{1}H NMR	(400.13 MHz, THF-d_8, 298 K): δ(ppm) = 1.15−1.39 (m, 42 H, NC(CH_3)$_3$ and NCH$_2$CH_3), 3.58 (overlap with THF, 4 H, NCH_2CH$_3$), 5.62 (m, 1 H, H-py), 6.99−7.68 (m, 12 H, H_{arom}).
^{13}C{^{1}H} NMR	(100.61 MHz, THF-d_8, 298 K): δ(ppm) = 15.73 (NCH$_2$CH_3), 32.23 (NC(CH$_3$)$_3$), 37.00 (NCH_2CH$_3$), 56.34 (NC(CH$_3$)$_3$), 91.63 (C-py), 128.95 (C_{arom}), 129.12 (C_{arom}), 129.71 (C_{arom}), 131.77 (C_{arom}), 147.96 (C_{arom}), 159.29 (C-py), 182.83 (NCN), 227.59 (CO).
^{29}Si{^{1}H} NMR	(79.49 MHz, THF-d_8, 298 K): δ(ppm) = 2.14.
APCI-MS (m/z):	calcd for [(C$_{43}$H$_{59}$N$_7$Si$_2$O$_4$Ge$_2$Cl$_2$Fe - H]$^+$ 1065.1326; found 1065.2419.

5.4.4 Synthesis of bis-silylene 3-6

° = BH

0.8 mL of a solution of *n*-BuLi (2.5 M in hexane; 2.0 mmol), was added rapidly to a 20 mL ether solution of *o*-carborane (0.144 g, 1.0 mmol) at −30 °C, forming a colorless solution. After warming the reaction mixture to ambient temperature and stirring for 3 h, a white suspension was formed. The slurry was then cooled to −30 °C, and a solution of *N,N'*-di-*tert*-butyl(phenylamidinato)chlorosilylene (0.590 g, 2.0 mmol) in 20 mL of toluene was added dropwise *via* syringe. After stirring overnight with slowing warming up to room temperature, the white precipitate was separated by filtration. The yellow filtrate was concentrated to 10 mL and stored at −30 °C for one day to give light yellow crystals of the desired product (0.558 g, 84% yield).

^{1}H NMR	(200.13 MHz, benzene-d_6, 298 K): δ(ppm) = 1.25 (s, 36 H, NC(CH_3)$_3$), 6.87−7.30 (m, 10 H, H_{arom}).
^{13}C{^{1}H} NMR	(50.32 MHz, benzene-d_6, 298 K): δ(ppm) = 32.28 (NC(CH$_3$)$_3$), 54.21 (NC(CH$_3$)$_3$), 85.65 (cage C), 127.04 (C_{arom}), 128.31 (C_{arom}),128.56 (C_{arom}), 134.7 (C_{arom} quaternary Ph), 168.06 (NCN).
^{29}Si{^{1}H} NMR	(79.49 MHz, benzene-d_6, 298 K): δ(ppm) = 18.91.
HR-ESI-MS (*m/z*):	calcd for [($C_{32}H_{56}N_4Si_2B_{10}$, M]$^+$ 611.5005; found 611.5044.

5.4.5 Synthesis of silylene Ni^{II} complex 3-7
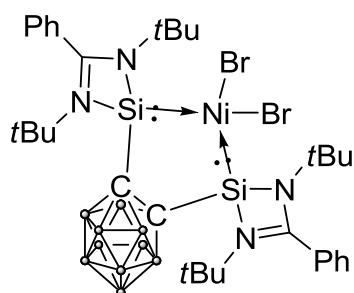
To a 50 mL Schlenk flask containing solid **3-6** (132 mg, 0.2 mmol) and NiBr$_2$(dme) (63 mg, 0.2 mmol), toluene (30 mL) was added via cannula, forming a clear brown solution. After stirring at room temperature overnight, a small amount of a black precipitate was formed which was separated by filtration. The clear filtrate was concentrated to 2 mL and left in a freezer at 0°C overnight affording yellow crystals of the desired complex (91 mg, 52% yield).

^{1}H NMR	(400.13 MHz, benzene-d$_6$, 298 K): δ(ppm) = 1.33 (s, 36 H, NC(CH_3)$_3$), 2.06 (s, 3 H, CH_3 from toluene), 6.83−7.55 (m, 15 H, H_{arom} and $H_{toluene}$).
^{13}C{^{1}H} NMR	(100.61 MHz, benzene-d$_6$, 298 K): δ(ppm) = 21.10 (CH_3 of toluene), 31.84 (NC(CH$_3$)$_3$), 56.34 (NC(CH$_3$)$_3$), 80.18 (cage C), 125.68 ($C_{toluene}$), 128.56 ($C_{toluene}$), 128.92 (C_{arom}), 129.33 ($C_{toluene}$), 129.88 (C_{arom}), 130.97 (C_{arom}), 137.90 (C_{arom} quaternary Ph), 179.30 (NCN).
^{11}B{^{1}H} NMR	(128.34 MHz, benzene-d$_6$, 298 K): δ(ppm) = 1.13−9.42 (m).
^{29}Si{^{1}H} NMR	(79.49 MHz, benzene-d$_6$, 298 K): δ(ppm) = 58.67 (s).
APCI-MS (*m/z*):	calcd for [(C$_{32}$H$_{56}$B$_{10}$N$_4$Si$_2$Br$_2$Ni + H), M + H]$^+$ 879.2819; found 879.2737.
Elemental analysis:	C$_{32}$H$_{56}$B$_{10}$N$_4$Si$_2$Br$_2$Ni·C$_7$H$_8$. Calc.: C 48.21, H 6.64, N 5.77. Found: C 47.66, H 6.94, N 5.39.

5.4.6 Synthesis of silylene Ni⁰ complex 3-8
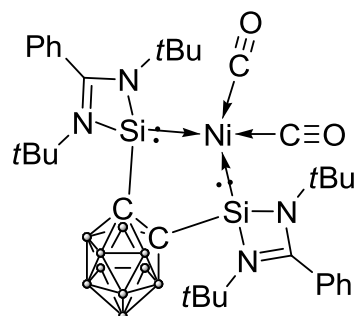
To a 50 mL Schleck flask containing **3-6** (88 mg, 0.1 mmol) and KC_8 (27 mg, 0.2 mmol), THF (30 mL) was added via cannula. Then the N_2-atmosphere was changed to CO through three freeze-pump-thaw cycles. After stirring the mixture under CO atmosphere at room temperature for 3 hours, the solid was separated by filtration. The filtrate was then concentrated to 1 mL and left in a freezer at 0°C overnight affording light yellow crystals of the desired complex (35 mg, 43% yield).

¹H NMR	(400.13 MHz, benzene-d_6, 298 K): δ(ppm) = 1.25 (s, 18 H, NC(CH_3)₃), 6.83−7.05 (m, 10 H, H_{arom}).
¹³C{¹H} NMR	(100.61 MHz, benzene-d_6, 298 K): δ(ppm) = 31.95 (NC(CH₃)₃), 55.35 (NC(CH₃)₃), 87.72 (cage C), 127.32 (C_{arom}), 130.19 (C_{arom}), 131.14 (C_{arom}), 132.25 (C_{arom} quaternary Ph), 173.13 (NCN), 207.56 (CO).
¹¹B{¹H} NMR	(128.34 MHz, benzene-d_6, 298 K): δ(ppm) = −10.07 to −0.52 (m).
²⁹Si{¹H} NMR	(79.49 MHz, benzene-d_6, 298 K): δ(ppm) = 86.00 (s)
IR (KBr pellet)	ν_{CO}(cm⁻¹) = 1982, 1934.
ESI-MS (*m/z*):	calcd for [($C_{34}H_{56}B_{10}N_4Si_2O_2Ni$ − CO + H), M − CO + H]⁺ 747.4422; found 747.4427.

5.4.7 Synthesis of silylene Ni^{II} complex 3-9
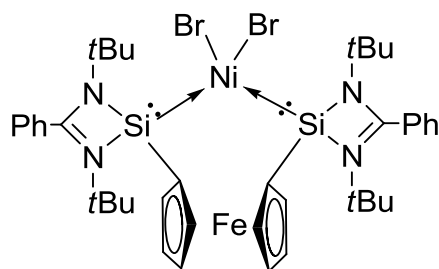
To a 50 mL Schleck flask containing **I-86** (140 mg, 0.2 mmol) and NiBr$_2$(dme) (63 mg, 0.2 mmol), toluene (30 mL) was added via cannula, forming an orange solution. After stirring at room temperature overnight, the small amount of a precipitate was separated by cannula filtration. The clear filtrate was concentrated to 2 mL and left in a freezer at 0°C overnight affording orange crystals of the desired complex (110 mg, 60% yield).

^{1}H NMR	(400.13 MHz, benzene-d$_6$, 298 K): δ(ppm) = 1.44 (s, 36 H, NC(CH_3)$_3$), 4.28 (t, 4 H, H_{Fc}), 4.50 (t, 4 H, H_{Fc}), 6.73−7.11 (m, 8 H, H_{arom}), 8.03−8.08 (m, 2 H, H_{arom}).
^{13}C{^{1}H} NMR	(100.61 MHz, benzene-d$_6$, 298 K): δ(ppm) = 31.88 (NC(CH$_3$)$_3$), 54.49 (NC(CH$_3$)$_3$), 71.65 (C_{Fc}), 73.53 (C_{Fc}), 77.29 ($C_{C\text{-}Si}$), 128.15 (C_{arom}), 130.27 (C_{arom}), 131.41 (C_{arom}), 132.01 (C_{arom} quaternary Ph), 170.71 (NCN).
^{29}Si{^{1}H} NMR	(79.49 MHz, benzene-d$_6$, 298 K): δ(ppm) = 49.31 (s).
ESI-MS (m/z):	calcd for [(C$_{40}$H$_{54}$N$_4$Si$_2$Br$_2$FeNi − Br), M − Br]$^+$ 841.1747; found 841.1738.

5.4.8 Synthesis of phosphine Ni[II] complex 3-11
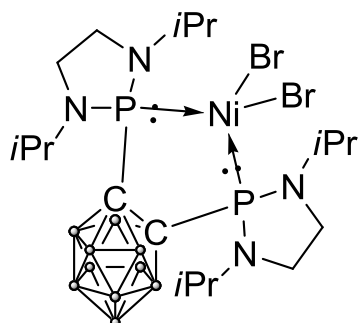
To a 50 mL Schleck flask containing the bis(diaminophosphino)-*o*-carborane ligand (97 mg, 0.2 mmol) and NiBr$_2$(dme) (63 mg, 0.2 mmol), toluene (30 mL) was added via cannula, forming an orange solution. After stirring at room temperature overnight, the solution was concentrated to 2 mL and left at room temperature overnight affording yellow crystals (65 mg, 46 % yield).

^{1}H NMR	(200.13 MHz, benzene-d$_6$, 298 K): δ(ppm) = 1.16 (d, 6 H, $^3J_{H-H}$ = 6.6 Hz, C*H*$_3$), 1.33 (d, 6 H, $^3J_{H-H}$ 6.4 = Hz, C*H*$_3$), 2.41−2.51 (m, 2 H, C*H*$_2$), 2.68−2.79 (m, 2 H, C*H*$_2$), 4.22−4.41 (m, 2 H, C*H*).
^{13}C{^{1}H} NMR	(50.32 MHz, benzene-d$_6$, 298 K): δ(ppm) = 20.81 (*C*H$_3$), 21.97 (t, *J* = 2.6 Hz, *C*H$_3$), 41.92 (*C*H), 49.72 (t, *J* = 6.5 Hz, *C*H$_2$),84.93 (m, cage *C*). ^{31}P{^{1}H} NMR (80.96 MHz, benzene-d$_6$, 298 K): δ(ppm) = 133.96 (s).
^{31}P{^{1}H} NMR	(80.96 MHz, benzene-d$_6$, 298 K): δ(ppm) = 133.96 (s).
^{11}B{^{1}H} NMR	(64.17 MHz, benzene-d$_6$, 298 K): δ(ppm) = −16.24 to −3.49 (m).
ESI-MS (*m/z*):	calcd for [(C$_{18}$H$_{46}$N$_4$B$_{10}$P$_2$Br$_2$Ni − Br), M − Br]$^+$ 627.2717; found 627.2730.

5.4.9 Synthesis of silylene Mn^{II} complex 3-14
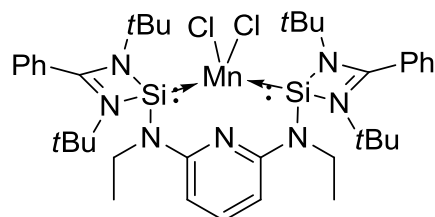
To a 50 mL Schlenk flask containing solid **I-94** (341 mg, 0.5 mmol) and MnCl$_2$ (63 mg, 0.5 mmol), THF (20 mL) and dioxane (10 mL) were added via cannula, forming a light yellow solution after stirring at room temperature overnight. All volatiles were removed under reduced pressure. The residue was then washed with *n*-hexane affording off-white solid of the desired product (326 mg, 74% yield). The single crystal of **3-14** was obtained from the toluene solution of **3-14** at 0°C overnight.

IR	(ATR-Diamond, cm^{-1}): 613(w), 632(m), 649(w), 683(w), 696(m), 708(s), 732(s), 761(s), 780(s), 796(w), 875(m), 929(m), 1023(m), 1072(m), 1086(m), 1108(m), 1156(m), 1208(m), 1249(s), 1277(w), 1314(m), 1329(w), 1367(m), 1377(w), 1393(s) 1441(s), 1517(w), 1573(s), 2870(w), 2905(w), 2930(w), 2967(m)
Elemental analysis	C$_{39}$H$_{59}$Cl$_2$MnN$_7$Si$_2$·C$_4$H$_8$O$_2$. Calc.: C 57.63, H 7.54, N 10.94. Found: C 58.01, H 7.51, N 10.81.
Evans	(THF-d_8, tetramethylsilylsilane capillary, 200 MHz for 1H): μ_{eff} = 6.15 μ_B.

5.4.10 Synthesis of silylene Mn^{II} complex 3-15
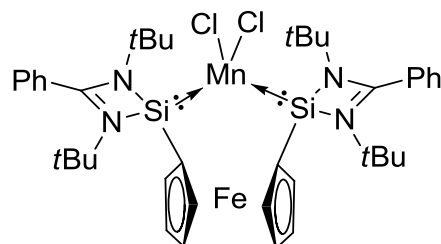
To a 50 mL Schlenk flask containing solid **I-86** (351 mg, 0.5 mmol) and MnCl$_2$ (63 mg, 0.5 mmol), THF (30 mL) was added via cannula. After stirring at room temperature overnight, all volatiles were removed under reduced pressure. The residue was washed with *n*-hexane and then dissolved in toluene. The yellow crystal of **3-15** was obtained from the concentrated toluene/THF/dioxane solution of **3-15** at 0°C overnight (280 mg, 56% yield).

IR	(ATR-Diamond, cm^{-1}): 631(m), 706 (s), 727(w), 761(s), 802(m), 838(w), 873(w), 899(w), 923(w), 1022(m), 1031(m), 1083(w), 1152(w), 1201(m), 1270(w), 1364(m), 1399(s), 1407(s), 1445(w), 1472(w), 1520(w), 1642(w), 2870(w), 2904(w), 2930(w), 2966(m).
Elemental analysis	C$_{40}$H$_{54}$Cl$_2$MnFeN$_4$Si$_2$·2C$_4$H$_8$O$_2$. Calc.: C 57.36, H 7.02, N 5.57. Found: C 57.39, H 7.40, N 5.34.
Evans	(THF-d_8, tetramethylsilylsilane capillary, 200 MHz for 1H): μ_{eff} = 5.94 μ_B.

5.4.11 Synthesis of silylene Mn^{II} complex 3-16
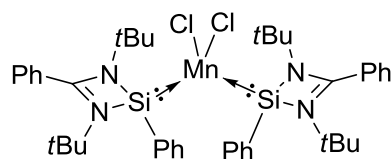
To a 50 mL Schlenk flask containing solid **I-84** (337 mg, 1.0 mmol) and MnCl$_2$ (63 mg, 0.5 mmol), THF (30 mL) was added via cannula, forming a clear yellow solution after stirring at room temperature overnight. Volatile was removed under reduced pressure. The residue was washed with *n*-hexane affording off-white solid of the desired product (212 mg, 50% yield). The single crystal of **3-16** was obtained from the toluene/dioxane solution of **3-16** at 0°C overnight.

IR	(ATR-Diamond, cm^{-1}): 614(w), 633(m), 699(s), 711(s), 724(m), 711(s), 766(s), 804(m), 853(w), 924(w), 997(w), 1022(w), 1032(w), 1093(m), 1126(w), 1032(s), 1284(m), 1363(s), 1403(s), 1444(w), 1472(m), 1521(w), 1577w), 1603(w), 1645(w), 2867(w), 2903(w), 2929(w), 2973(m), 3095(w).
Elemental analysis	C$_{42}$H$_{58}$Cl$_2$MnN$_4$Si$_2$·0.5C$_4$H$_8$O$_2$. Calc.: C 62.69, H 7.17, N 6.65. Found: C 62.39, H 7.73, N 6.77.
Evans	(THF-d_8, tetramethylsilylsilane capillary, 200 MHz for 1H): μ_{eff} = 6.07 μ_B.

5.4.12 Synthesis of NHC-silyl Co^{II} complex 3-18

Ar = 2,6-iPr$_2$C$_6$H$_3$
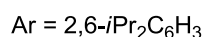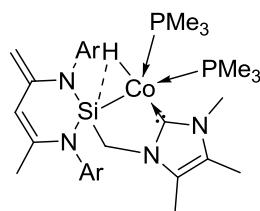
To a 50 mL Schlenk flask containing ligand **I-24** (285 mg, 0.5 mmol), CoBr$_2$ (109 mg, 0.5 mmol), and KC$_8$ (202 mg, 1.5 mmol), THF (30 mL) was added via cannula. The mixture was cooled at − 80 °C and then added 4 mL PMe$_3$ solution in hexane (1 mol/L) immediately, forming a black solution. After stirring for 3 h with slow warming up to room temperature, the precipitate was separated by filtration. All volatiles were then removed under vacuum. The product was extracted by Et$_2$O (30 mL) via cannula filtration. The product (220 mg, yield 56%) was crystallized from a concentrated Et$_2$O solution at 0 °C overnight as red crystals.

APCI-HR-MS	calcd. for [C$_{42}$H$_{70}$CoN$_4$P$_2$Si]$^+$: *m/z* 779.4177; found: *m/z* 779.4258.
Elemental analysis	calcd. for C$_{42}$H$_{70}$CoN$_4$P$_2$Si (%): C, 64.67; N, 7.18; H, 9.05; found: C, 64.30; N, 7.19; H, 9.15.
IR (KBr, cm^{-1}):	v = 584.92 (m), 590.21 (m), 640.76 (w), 656.29 (s), 666.27 (m), 699.04 (w), 708.11 (w), 732.72 (m), 757.49 (s), 787.11 (m), 769.85 (s), 841.35 (w), 934.20 (s), 971.70 (w), 1027.04 (s), 1041.84 (w), 1073.88 (w), 1089.98 (w), 1175.95 (m), 1202.15 (m), 1250.30 (m), 1273.11 (w), 1310.24 (m), 1353.70 (s), 1377.55 (m), 1433.01 (m), 1553.88 (w), 1694.45 (w), 1741.05 (w), 1836.56 (w), 2864.34 (m), 2898.49 (m), 2917.58 (m), 2963.05 (m).

5.4.13 Synthesis of NHC-silyl Co^{II} complex 3-19

Ar = 2,6-iPr$_2$C$_6$H$_3$
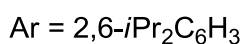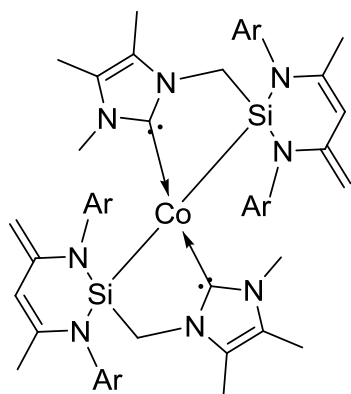
3-19 was crystallized from a concentrated mother liquid of **3-18** at 0 °C for 7 days as green crystals. (15 mg, yield 5%)

APCI-HR-MS	calcd for [C$_{72}$H$_{102}$CoN$_8$Si$_2$ + H]$^+$: *m/z* 1194.7176; found: *m/z* 1194.7181.
Elemental analysis	calcd for C$_{72}$H$_{102}$CoN$_8$Si$_2$·Et$_2$O (%): C, 71.94; H, 8.90; N, 8.83; found: C, 71.27; H, 8.98; N, 8.79.
IR (KBr, cm^{-1}):	*v* = 841.21 (w), 875.28 (w), 882.61 (m), 905.34 (m), 922.67 (s), 971.16 (w), 1008.17 (m), 1028.66 (m), 1109.31 (m), 1174.19 (m), 1191.14 (m), 1250.74 (w), 1304.23 (s), 1326.49 (w), 1347.58 (s), 1372.70 (s), 1431.93 (m), 1550.52 (w), 1627.71 (m), 2158.36 (w), 2884.96 (m), 2964.27 (m).

5.4.14 Synthesis of NHC-silylene Co^{II} complex 3-20

Ar = 2,6-iPr$_2$C$_6$H$_3$
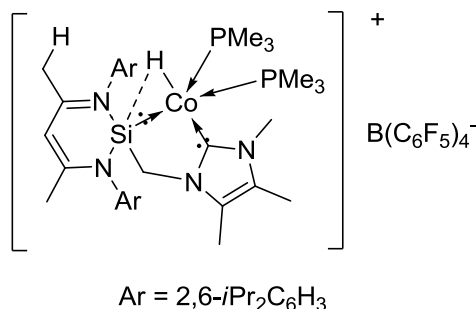
To a 50 mL Schlenk flask containing **3-18** (78 mg, 0.1 mmol) and Jutzi acid [H(Et$_2$O)$_2$]$^+$[B(C$_6$F$_5$)$_4$]$^-$ (83 mg, 0.1 mmol), Et$_2$O (30 mL) was added. The mixture was cooled at − 80 °C and stirring for 3 h with slow warming up to room temperature. The solution was concentrated, and the product (58 mg, yield 40%) was crystallized as dark red crystals at 0 °C overnight.

APCI-HR-MS calcd for [C$_{42}$H$_{70}$CoN$_4$P$_2$Si]$^+$ (cation): *m/z* 780.4255; found: *m/z* 780.4312.

IR (KBr, cm^{-1}): v = 601.68 (w), 610.05 (w), 660.70 (s), 683.74 (m), 710.10 (m), 726.00 (m), 755.33 (m), 773.69 (m), 802.18 (m), 874.72 (w), 888.71 (w), 938.57 (s), 951.61 (w), 977.98 (s), 1024.43 (w), 1083.69 (s), 1173.26 (w), 1274.31 (m), 1313.72 (m), 1372.04 (s), 1461.01 (s), 1512.77 (m), 1548.66 (w), 1642.75 (m), 1768.55 (w), 2086.16 (w), 2324.02 (w), 2870.58 (w), 2970.32 (m).

5.4.15 Synthesis of η^2-(Si-H) cobalt complex 3-21.

Ar = 2,6-iPr$_2$C$_6$H$_3$
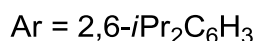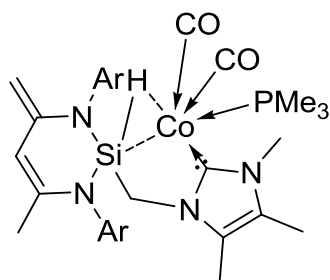
To a 50 mL Schlenk flask containing **3-18** (78 mg, 0.1 mmol), toluene (30 mL) was added. The mixture was stirring for 5 h under CO atmosphere at room temperature. The solution was concentrated, and the product (55 mg, yield 80%) was crystallized as yellow crystals at 0 °C overnight.

APCI-HR-MS:	calcd for $[C_{40}H_{62}CoN_4OPSi]^+$ $[M - CO]^+$: m/z 732.3763; found: m/z 732.3843.
Elemental analysis	calcd for $C_{41}H_{62}CoN_4O_2PSi$ (%): C, 64.71; H, 8.21; N, 7.36. Found: C, 65.12; H, 7.80; N, 7.18.
IR (KBr, cm^{-1}):	v = 579.07 (w), 586.79 (w), 593.33 (w), 613.54 (w), 643.04 (m), 667.75 (m), 682.02 (w), 718.17 (m), 734.34 (m), 758.33 (m), 787.92 (w), 798.31 (s), 845.66 (w), 896.67 (m), 982.71 (s), 1025.32 (m), 1056.92 (w), 1151.25 (s), 1201.28 (s), 1233.14 (s), 1303.52 (m), 1349.08 (m), 1374.15 (w), 1436.01 (m), 1619.85 (m), 1812.12 (w), 1916.60 (s), 1972.18 (s), 289.92 (m).

5.4.16 Synthesis of η^2-(Si-H) cobalt complex 3-22.
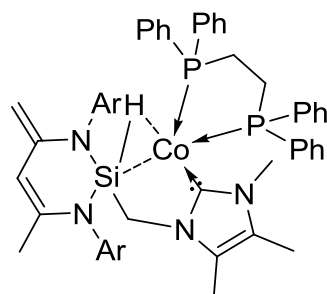
Ar = 2,6-iPr$_2$C$_6$H$_3$

To a 50 mL Schlenk flask containing **3-18** (78 mg, 0.1 mmol) and 1,2-bis(diphenylphosphino)ethane (dppe, 40 mg, 0.1 mmol), Et$_2$O (30 mL) was added. The mixture was stirring for 3 h at room temperature. The solution was then concentrated, and the product (60 mg, yield 54%) was crystallized as red crystals at 0 °C overnight.

ESI-HR-MS:	calcd for $[C_{36}H_{53}CoN_4Si]^+$ [M − dppe]$^+$: *m/z* 628.3371; found: *m/z* 628.3361.
Elemental analysis	calcd for $C_{62}H_{76}CoN_4P_2Si \cdot 0.5Et_2O$ (%): C, 72.29; H, 7.68; N, 5.27. Found: C, 71.86; H, 7.07; N, 5.00.
IR (KBr, cm^{-1}):	v = 577.64 (w), 586.36 (w), 593.21 (w), 619.55 (w), 644.26 (w), 671.24 (m), 692.51 (s), 726.07 (w), 734.96 (m), 746.59 (w), 784.24 (w), 801.39 (m), 843.95 (w), 872.13 (m), 900.86 (w), 932.86 (m), 998.76 (w), 1026.58 (m), 1067.67 (w), 1096.48 (m), 1173.83 (w), 1194.78 (w), 1251.81 (m), 1273.63 (m), 1308.68 (w), 1352.34 (m), 1374.06 (m), 1431.41 (s), 1403.00 (w), 1481.42 (w), 1549.50 (m), 1564.01 (w), 1628 (m), 1754.21 (w), 2864.44 (w), 2923.56 (w), 2961.49 (m).

5.4.17 Synthesis of NHC-silyl Co^{II} complex 3-23

Ar = 2,6-iPr$_2$C$_6$H$_3$
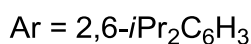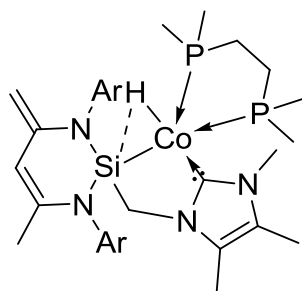
To a 50 mL Schlenk flask containing **2** (78 mg, 0.1 mmol), Et$_2$O (30 mL) and 0.1 mL 1,2-bis(dimethylphosphino)ethane (dmpe) hexane solution (1 mol/L) was added respectively. The mixture was stirring for 3 h at room temperature. The solution was concentrated, and the product (41 mg, yield 53%) was crystallized as red crystals at 0 °C overnight.

ESI-HR-MS: calcd for $[C_{36}H_{53}CoN_4Si]^+$ [M − dmpe]$^+$: *m/z* 628.3371; found: *m/z* 628.3362.

Elemental analysis calcd for $C_{42}H_{68}CoN_4P_2Si$(%): C, 64.84; H, 8.81; N, 7.20. Found: C, 64.25; H, 8.92; N, 6.82.

IR (KBr, cm^{-1}): ν = 568.28 (w), 575.63 (w), 580.55 (w), 587.74 (w), 602.42 (w), 610.21 (w), 667.34 (w), 687.33 (m), 700.82 (w), 720,42 (w), 737.19 (w), 783.08 (w), 798.17 (m), 828.75 (w), 893.84 (m), 933.23 (s), 969.36 (w), 1019.53 (m), 1053.70 (w), 1099.22 (w), 1121.37 (m), 1176.11 (w), 1202.73 (m), 1249.98 (m), 1274.89 (w), 1316.94 (m), 1353.09 (m), 1377.83 (m), 1414.73 (w), 1435.05 (w), 1459.82 (w), 1580.64 (w), 1610.75 (m), 1694.11 (w), 2864.42 (w), 2893.01 (m), 2958.68 (m).

5.5 Catalysis

5.5.1 General procedure of transfer semi-hydrogenation

To a 10 mL flask containing alkyne (0.5 mmol), ammonia-borane (15.3 mg, 0.5 mmol) and **3-14** (4 mg, 0.005 mmol), THF (5 mL) was added. The flask was then sealed and stirring at 55°C for 16 h. After passing through a pad of silica eluted with THF, all volatiles were removed under reduced pressure. *n*-Hexane was then added and pass through a pad of silica eluted with *n*-hexane. Volatiles were removed under reduced pressure and residue was analyzed by GC/MS and NMR to determine the conversion and E/Z ratio. The residue was then purified by column chromatography with *n*-hexane/THF affording the corresponding alkenes as products.

5.5.2 Characterization of products of transfer semi-hydrogenation
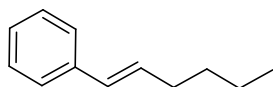
(*E*)-hex-1-enylbenzene

^{1}H NMR (200.13 MHz, CDCl$_3$, 298 K): δ(ppm) = 0.93 (t, *J* = 6.6 Hz, 3 H), 1.26−1.50 (m, 4 H), 2.21 (q, *J* = 6.2 Hz, 2 H), 6.22 (dt, *J* = 16.8, 6.4 Hz, 1 H), 6.39 (d, *J* = 16.0 Hz, 1 H), 7.14−7.37 (m, 5 H). ^{13}C{^{1}H} NMR (50.32 MHz, CDCl$_3$, 298 K): δ(ppm) = 14.10, 22.42, 31.68, 32.87, 126.05, 126.88, 128.61, 129.84, 131.37, 138.12.
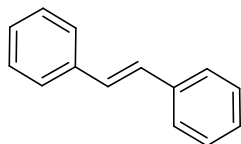
(*E*)-1,2-diphenylethene

^{1}H NMR (200.13 MHz, CDCl$_3$, 298 K): δ(ppm) = 7.19 (s, 2 H), 7.19−7.29 (m, 2 H), 7.32−7.40 (m, 4 H), 7.48−7.54 (m, 4 H). ^{13}C{^{1}H} NMR (50.32 MHz, CDCl$_3$, 298 K): δ(ppm) = 126.66, 127.77, 128.83, 128.86, 137.50.

1:1:1 mixture of

(*E*)-dodec-6-ene

(*Z*)-dodec-6-ene

dodec-6-yne
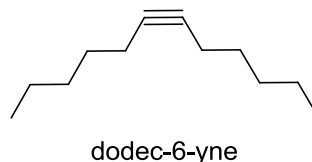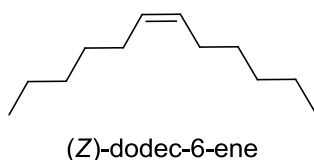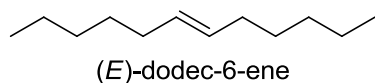
^{1}H NMR (200.13 MHz, CDCl$_3$, 298 K): δ(ppm) = 0.86−0.91 (m, 9 H), 1.29−1.50 (m, 18 H), 1.97−2.03 (m, 4 H) , 2.11−2.17 (m, 2 H) , 5.33−5.42 (m, 2 H). ^{13}C{^{1}H} NMR (50.32 MHz, CDCl$_3$, 298 K): δ(ppm) = 14.15, 14.22, 18.90, 22.33, 22.71, 27.33, 29.05, 29.50, 29.60, 31.24, 31.56, 31.69, 32.73, 80.39, 130.07, 130.53.
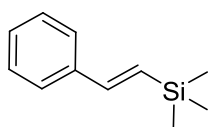
(*E*)-trimethyl(styryl)silane

^{1}H NMR (200.13 MHz, CDCl$_3$, 298 K): δ(ppm) = 0.16 (s, 9 H), 6.48 (d, *J* = 19.5 Hz, 1 H), 6.88 (d, *J* = 19.1 Hz, 1 H), 7.24−7.47 (m, 5 H). ^{13}C{^{1}H} NMR (50.32 MHz, CDCl$_3$, 298 K): δ(ppm) = 1.09, 126.50, 128.07, 128.65, 129.69, 138.52, 143.73.
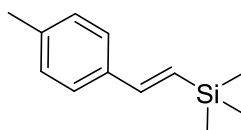
(*E*)-trimethyl(4-methylstyryl)silane

^{1}H NMR (200.13 MHz, CDCl$_3$, 298 K): δ(ppm) = 0.14 (s, 9 H), 2.34 (s, 3 H), 6.40 (d, *J* = 19.0 Hz, 1 H), 6.84 (d, *J* = 19.2 Hz, 1 H), 7.12 (d, *J* = 8.6 Hz, 2 H), 7.33 (d, *J* = 8.3 Hz, 2 H). ^{13}C{^{1}H} NMR (50.32 MHz, CDCl$_3$, 298 K): δ(ppm) = 1.05, 21.36, 126.41, 128.31, 129.35, 135.86, 137.93, 143.63.
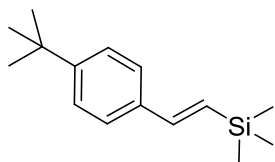
(*E*)-(4-*tert*-butylstyryl)trimethylsilane

^{1}H NMR (200.13 MHz, CDCl$_3$, 298 K): δ(ppm) = 0.15 (s, 9 H), 1.32 (s, 9 H), 6.42 (d, *J* = 19.1 Hz, 1 H), 6.86 (d, *J* = 19.1 Hz, 1 H), 7.32−7.41 (m, 4 H). ^{13}C{^{1}H} NMR (50.32 MHz, CDCl$_3$, 298 K): δ(ppm) = 1.05, 31.45, 34.74, 125.58, 126.20, 128.66, 135.85, 143.51, 151.23.
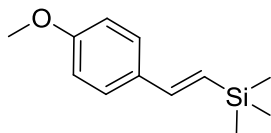
(*E*)-(4-methoxystyryl)trimethylsilane

^{1}H NMR (200.13 MHz, CDCl$_3$, 298 K): δ(ppm) = 0.14 (s, 9 H), 3.81 (s, 3 H), 6.30 (d, *J* = 19.1 Hz, 1 H), 6.77−6.88 (m, 3 H), 7.38 (d, *J* = 7.7 Hz, 2 H). ^{13}C{^{1}H} NMR (50.32 MHz, CDCl$_3$, 298 K): δ(ppm) = 1.01, 55.45, 114.05, 126.86, 127.53, 127.72, 131.55, 143.15.
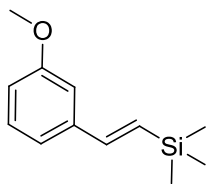
(*E*)-(3-methoxystyryl)trimethylsilane

^{1}H NMR (200.13 MHz, CDCl$_3$, 298 K): δ(ppm) = 0.16 (s, 9 H), 3.83 (s, 3 H), 6.47 (d, *J* = 19.1 Hz, 1 H), 6.78−6.90 (m, 3 H), 6.97−7.05 (m, 2 H), 7.24 (t, *J* = 7.8 Hz, 1 H). ^{13}C{^{1}H} NMR (50.32 MHz, CDCl$_3$, 298 K): δ(ppm) = 0.46, 56.02, 112.11, 114.66, 119.92, 130.25, 130.69, 140.58, 144.24, 160.67.
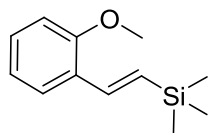
(*E*)-(2-methoxystyryl)trimethylsilane

^{1}H NMR (200.13 MHz, CDCl$_3$, 298 K): δ(ppm) = 0.16 (s, 9 H), 3.85 (s, 3 H), 6.45 (d, *J* = 19.3 Hz, 1 H), 6.84−6.98 (m, 2 H), 7.18−7.33 (m, 2 H), 7.65 (dd, *J* = 7.7, 1.7 Hz, 1 H). ^{13}C{^{1}H} NMR (50.32 MHz, CDCl$_3$, 298 K): δ(ppm) = 1.14, 55.49, 110.93, 120.60, 126.21, 127.53, 128.93, 129.93, 137.81, 156.52.
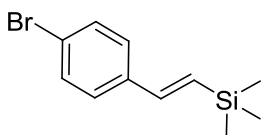
(*E*)-(4-bromostyryl)trimethylsilane

^{1}H NMR (200.13 MHz, CDCl$_3$, 298 K): δ(ppm) = 0.15 (s, 9 H), 6.46 (d, *J* = 19.1 Hz, 1 H), 6.80 (d, *J* = 19.1 Hz, 1 H), 7.29 (d, *J* = 8.4 Hz, 2 H), 7.45 (d, *J* = 8.4 Hz, 2 H). ^{13}C{^{1}H} NMR (50.32 MHz, CDCl$_3$, 298 K): δ(ppm) = 1.17, 121.88, 128.03, 130.84, 131.75, 137.46, 142.41.
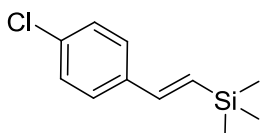
(*E*)-(4-chlorostyryl)trimethylsilane

^{1}H NMR (200.13 MHz, CDCl$_3$, 298 K): δ(ppm) = 0.15 (s, 9 H), 6.45 (d, *J* = 19.1 Hz, 1 H), 6.82 (d, *J* = 19.2 Hz, 1 H), 7.28−7.38 (m, 4 H). ^{13}C{^{1}H} NMR (50.32 MHz, CDCl$_3$, 298 K): δ(ppm) = 0.00, 123.05, 129.19, 132.01, 132.92, 138.62, 143.58.
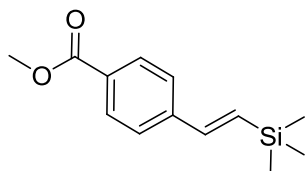
(*E*)-methyl 4-(2-(trimethylsilyl)vinyl)benzoate

^{1}H NMR (200.13 MHz, CDCl$_3$, 298 K): δ(ppm) = 0.18 (s, 9 H), 3.92 (s, 3 H), 6.63 (d, *J* = 19.2 Hz, 1 H), 6.92 (d, *J* = 19.1 Hz, 1 H), 7.49 (d, *J* = 8.2 Hz, 2 H), 8.01 (d, *J* = 8.6 Hz, 2 H). ^{13}C{^{1}H} NMR (50.32 MHz, CDCl$_3$, 298 K): δ(ppm) = 1.21, 52.19, 126.39, 129.84, 130.05, 133.36, 142.66, 142.75, 167.08.
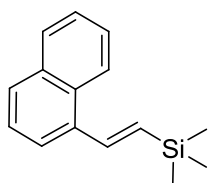
(*E*)-trimethyl(2-(naphthalen-1-yl)vinyl)silane

^{1}H NMR (200.13 MHz, CDCl$_3$, 298 K): δ(ppm) = 0.36 (s, 9 H), 6.69 (d, *J* = 18.9 Hz, 1 H), 7.55−7.68 (m, 3 H), 7.76−8.00 (m, 4 H), 8.21−8.33 (m, 1 H). ^{13}C{^{1}H} NMR (50.32 MHz, CDCl$_3$, 298 K): δ(ppm) = 0.00, 124.69, 126.66, 126.75, 126.80, 127.11, 129.22, 129.66, 134.79, 135.00, 141.84.
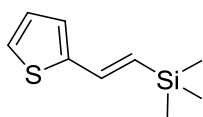
(*E*)-trimethyl(2-(thiophen-2-yl)vinyl)silane

^{1}H NMR (200.13 MHz, CDCl$_3$, 298 K): δ(ppm) = 0.13 (s, 9 H), 6.24 (d, *J* = 18.8 Hz, 1 H), 6.87 (d, *J* = 19.1 Hz, 1 H), 7.17−7.27 (m, 3 H). ^{13}C{^{1}H} NMR (50.32 MHz, CDCl$_3$, 298 K): δ(ppm) = 1.10, 122.62, 125.04, 126.03, 129.39, 137.57.

5.5.2 General procedure of olefin hydrosilylation

To a 5 mL flask containing alkene (0.25 mmol), silane (34 μL, 0.275 mmol) and **3-18** (1 mL, 1 mg/mL in THF) was added. The flask was then sealed and stirring at room temperature in the glovebox for 2 h. After passing through a pad of silica eluted with THF, all volatiles were removed under reduced pressure. *n*-Hexane was then added and purified by column chromatography eluted with *n*-hexane affording corresponding products. Volatiles were then removed under reduced pressure and residue was analyzed by NMR.

5.5.2 Characterization of products olefin hydrosilylation
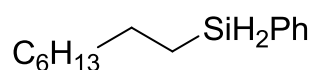
octyl(phenyl)silane

^{1}H NMR (200.13 MHz, CDCl$_3$, 298 K): δ(ppm) = 0.86−1.01 (m, 5 H), 1.28−1.53 (m, 12 H), 4.30 (t, J = 3.7 Hz, 2 H), 7.33−7.40 (m, 3 H), 7.56−7.61 (m, 2 H). ^{13}C{^{1}H} NMR (50.32 MHz, CDCl$_3$, 298 K): δ(ppm) = 10.02, 14.11, 22.68, 25.09, 29.21, 31.90, 32.85, 127.95, 129.46, 132.86, 135.22.
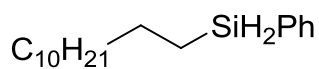
dodecyl(phenyl)silane

^{1}H NMR (200.13 MHz, CDCl$_3$, 298 K): δ(ppm) = 0.91−1.04 (m, 5 H), 1.30−1.37 (m, 20 H), 4.33 (t, J = 3.7 Hz, 2 H), 7.31−7.45 (m, 3 H), 7.60−7.64 (m, 2 H). ^{13}C{^{1}H} NMR (50.32 MHz, CDCl$_3$, 298 K): δ(ppm) = 10.04, 14.13, 22.72, 25.10, 28.99, 29.20, 29.29, 29.39, 29.56, 29.69, 31.95, 32.87, 127.95, 129.46, 132.85, 135.21.
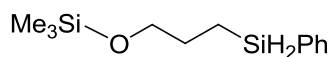
trimethyl(3-(phenylsilyl)propoxy)silane

^{1}H NMR (200.13 MHz, CDCl$_3$, 298 K): δ(ppm) = 0.12 (s, 9 H), 0.90−1.02 (m, 2 H), 1.63−1.78 (m, 2 H), 3.59 (t, J = 6.6 Hz, 2 H), 4.33 (t, J = 3.7 Hz, 2 H), 7.36−7.40 (m, 3 H), 7.56−7.61 (m, 2 H). ^{13}C{^{1}H} NMR (50.32 MHz, CDCl$_3$, 298 K): δ(ppm) = 0.36, 6.29, 28.29, 64.71, 128.10, 129.66, 132.72, 135.32.

Ph∖O∕∖∕SiH$_2$Ph
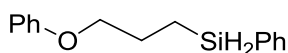
(3-phenoxypropyl)(phenyl)silane

^{1}H NMR (200.13 MHz, CDCl$_3$, 298 K): δ(ppm) = 1.03−1.21 (m, 2 H), 1.90−2.05 (m, 2 H), 3.98 (t, J = 6.5 Hz, 2 H), 4.39 (d, J = 3.7 Hz, 2 H), 6.89−7.00 (m, 3 H), 7.30−7.44 (m, 5 H), 7.60−7.64 (m, 2 H). ^{13}C{^{1}H} NMR (50.32 MHz, CDCl$_3$, 298 K): δ(ppm) = 6.68, 25.07, 69.68, 114.65, 120.70, 128.18, 129.54, 129.79, 132.36, 135.34, 159.08.
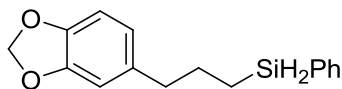
(3-(benzo[*d*][1,3]dioxol-5-yl)propyl)(phenyl)silane

^{1}H NMR (200.13 MHz, CDCl$_3$, 298 K): δ(ppm) = 0.87−1.03 (m, 2 H), 1.67−1.82 (m, 2 H), 2.60 (t, J = 7.5 Hz, 2 H), 4.31 (t, J = 3.7 Hz, 2 H), 5.02 (s, 2 H), 6.58−6.75 (m, 3 H), 7.33−7.42 (m, 3 H), 7.54−7.59 (m, 2 H). ^{13}C{^{1}H} NMR (50.32 MHz, CDCl$_3$, 298 K): δ(ppm) = 9.74, 27.36, 38.79, 77.16, 100.85, 108.20, 109.07, 121.37, 128.15, 129.72, 133.75, 135.36, 136.13, 145.71, 147.65.

∖∕∖SiH$_2$Ph
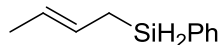
but-2-enyl(phenyl)silane

^{1}H NMR (200.13 MHz, CDCl$_3$, 298 K): δ(ppm) = 1.53−1.57 (m, 3 H), 1.85−1.92 (m, 2 H), 4.31 (t, J = 3.7 Hz, 2 H), 5.35−5.58 (m, 2 H), 7.36−7.42 (m, 3 H), 7.56−7.62 (m, 2 H). ^{13}C{^{1}H} NMR (50.32 MHz, CDCl$_3$, 298 K): δ(ppm) = 11.37, 12.48, 123.28, 125.02, 127.95, 129.67, 132.25, 135.23.
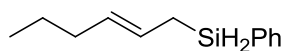
hex-2-enyl(phenyl)silane

^{1}H NMR (200.13 MHz, CDCl$_3$, 298 K): δ(ppm) = 0.91 (t, J = 7.3 Hz, 3 H), 1.30−1.49 (m, 2 H), 1.89−2.25 (m, 3 H), 4.33 (t, J = 3.7 Hz, 2 H), 5.32−5.57 (m, 2 H), 7.35−7.41 (m, 3 H), 7.55−7.64 (m, 2 H). ^{13}C{^{1}H} NMR (50.32 MHz, CDCl$_3$, 298 K): δ(ppm) = 11.73, 13.84, 22.74, 29.11, 124.04, 127.95, 129.44, 129.67, 132.23, 135.24.
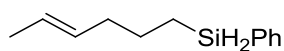
hex-4-enyl(phenyl)silane

^{1}H NMR (200.13 MHz, CDCl$_3$, 298 K): δ(ppm) = 0.90−1.01 (m, 2 H), 1.45−1.61 (m, 2 H), 1.65−1.67 (m, 2 H), 2.01−2.67 (m, 2 H), 4.31 (t, J = 3.7 Hz, 2 H), 5.40−5.46 (m, 2 H), 7.36−7.41 (m, 3 H), 7.56−7.61 (m, 2 H). ^{13}C{^{1}H} NMR (50.32 MHz, CDCl$_3$, 298 K): δ(ppm) = 9.58, 17.93, 25.11, 35.63, 125.37, 127.97, 129.50, 130.91, 132.71, 135.23.
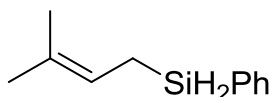
(3-methylbut-2-enyl)(phenyl)silane

^{1}H NMR (200.13 MHz, CDCl$_3$, 298 K): δ(ppm) = 1.45−1.48 (m, 3 H), 1.69−1.71 (m, 3 H), 1.86−1.89 (m, 2 H), 4.32(t, J = 4.0 Hz, 2 H), 5.11−5.21 (m, 1 H), 7.32−7.41 (m, 3 H), 7.55−7.61 (m, 2 H). ^{13}C{^{1}H} NMR (50.32 MHz, CDCl$_3$, 298 K): δ(ppm) = 13.56, 16.38, 25.19, 117.58, 127.93, 129.65, 132.28, 135.20.
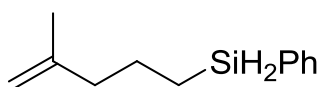
(4-methylpent-4-enyl)(phenyl)silane

^{1}H NMR (200.13 MHz, CDCl$_3$, 298 K): δ(ppm) = 0.83−0.99 (m, 3 H), 1.53−1.64 (m, 2 H), 1.68 (s, 3 H), 2.08 (t, J = 7.5 Hz, 2 H), 4.30 (t, J = 3.7 Hz, 2 H), 4.66−4.71 (m, 2 H), 7.31−7.41 (m, 3 H) , 7.51−7.60 (m, 2 H). ^{13}C{^{1}H} NMR (50.32 MHz, CDCl$_3$, 298 K): δ(ppm) = 9.53, 22.22, 23.06, 40.79, 110.28, 127.98, 129.52, 132.61, 135.20, 145.45.
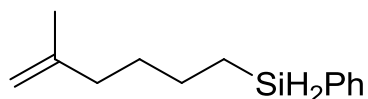
(5-methylhex-5-enyl)(phenyl)silane

^{1}H NMR (200.13 MHz, CDCl$_3$, 298 K): δ(ppm) = 0.88−1.02 (m, 3 H), 1.47−1.53 (m, 4 H), 1.70 (s, 3 H), 2.02 (t, J = 7.1 Hz, 2 H), 4.30 (t, J = 3.7 Hz, 2 H), 4.66−4.69 (m, 2 H), 7.36−7.39 (m, 3 H) , 7.56−7.60 (m, 2 H). ^{13}C{^{1}H} NMR (50.32 MHz, CDCl$_3$, 298 K): δ(ppm) = 9.93, 22.36, 24.77, 30.76, 37.44, 109.73, 127.97, 129.51, 132.71, 135.21, 145.95.
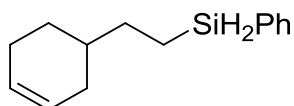
(2-(cyclohex-3-enyl)ethyl)(phenyl)silane

^{1}H NMR (200.13 MHz, CDCl$_3$, 298 K): δ(ppm) = 0.83−1.02 (m, 3 H), 1.26−1.81 (m, 6 H), 2.00−2.09 (m, 6 H), 4.29 (t, J = 3.7 Hz, 2 H), 5.65−5.68 (m, 2 H), 7.35−7.39 (m, 3 H), 7.51−7.60 (m, 2 H). ^{13}C{^{1}H} NMR (50.32 MHz, CDCl$_3$, 298 K): δ(ppm) = 7.17, 25.19, 28.43, 31.52, 31.80, 36.11, 126.53, 127.07, 127.97, 129.51, 132.68, 135.20.

6. REFERENCES

[1] a) T. Iwamoto, S. Ishida, in *Organosilicon Compounds*, Academic Press, **2017**, pp. 361-532; b) S. S. Sen, S. Khan, S. Nagendran, H. W. Roesky, *Acc. Chem. Res.* **2012**, *45*, 578-587; c) S. Yao, Y. Xiong, M. Driess, *Organometallics* **2011**, *30*, 1748-1767; d) M. Asay, C. Jones, M. Driess, *Chem. Rev.* **2011**, *111*, 354-396; e) Y. Mizuhata, T. Sasamori, N. Tokitoh, *Chem. Rev.* **2009**, *109*, 3479-3511.

[2] P. Jutzi, D. Kanne, C. Krüger, *Angew. Chem. Int. Ed. in English* **1986**, *25*, 164-164.

[3] M. Denk, R. Lennon, R. Hayashi, R. West, A. V. Belyakov, H. P. Verne, A. Haaland, M. Wagner, N. Metzler, *J. Am. Chem. Soc.* **1994**, *116*, 2691-2692.

[4] a) P. Zark, A. Schäfer, A. Mitra, D. Haase, W. Saak, R. West, T. Müller, *J. Organomet. Chem.* **2010**, *695*, 398-408; b) A. Mitra, J.-C. Brodovitch, C. Krempner, P. W. Percival, P. Vyas, R. West, *Angew. Chem. Int. Ed.* **2010**, *49*, 2893-2895; c) H. Cui, Y. Shao, X. Li, L. Kong, C. Cui, *Organometallics* **2009**, *28*, 5191-5195.

[5] a) A. C. Tomasik, A. Mitra, R. West, *Organometallics* **2009**, *28*, 378-381; b) W. Li, N. J. Hill, A. C. Tomasik, G. Bikzhanova, R. West, *Organometallics* **2006**, *25*, 3802-3805.

[6] a) B. Gehrhus, P. B. Hitchcock, M. F. Lappert, J. Heinicke, R. Boese, D. Bläser, *J. Organomet. Chem.* **1996**, *521*, 211-220; b) B. Gehrhus, M. F. Lappert, J. Heinicke, R. Boese, D. Blaser, *J. Chem. Soc., Chem. Commun.* **1995**, 1931-1932; c) M. Denk, J. C. Green, N. Metzler, M. Wagner, *J. Chem. Soc., Dalton Trans.* **1994**, 2405-2410.

[7] B. Gehrhus, P. B. Hitchcock, M. F. Lappert, *Z. Anorg. Allg. Chem.* **2005**, *631*, 1383-1386.

[8] M. Driess, S. Yao, M. Brym, C. van Wüllen, D. Lentz, *J. Am. Chem. Soc.* **2006**, *128*, 9628-9629.

[9] a) A. Meltzer, S. Inoue, C. Präsang, M. Driess, *J. Am. Chem. Soc.* **2010**, *132*, 3038-3046; b) A. Meltzer, C. Präsang, M. Driess, *J. Am. Chem. Soc.* **2009**, *131*, 7232-7233.

[10] Y. Xiong, S. Yao, M. Driess, *Chem. Asian J.* **2010**, *5*, 322-327.

[11] G. Tan, S. Enthaler, S. Inoue, B. Blom, M. Driess, *Angew. Chem. Int. Ed.* **2015**, *54*, 2214-2218.

[12] C.-W. So, H. W. Roesky, J. Magull, R. B. Oswald, *Angew. Chem. Int. Ed.* **2006**, *45*, 3948-3950.

[13] S. S. Sen, H. W. Roesky, D. Stern, J. Henn, D. Stalke, *J. Am. Chem. Soc.* **2010**, *132*, 1123-1126.

[14] S. S. Sen, A. Jana, H. W. Roesky, C. Schulzke, *Angew. Chem. Int. Ed.* **2009**, *48*, 8536-8538.

[15] a) K. Junold, M. Nutz, J. A. Baus, C. Burschka, C. Fonseca Guerra, F. M. Bickelhaupt, R. Tacke, *Chem. Eur. J.* **2014**, *20*, 9319-9329; b) F. M. Mück, K. Junold, J. A. Baus, C. Burschka, R. Tacke, *Eur. J. Inorg. Chem.* **2013**, *2013*, 5821-5825; c) K. Junold, J. A. Baus, C. Burschka, R. Tacke, *Angew. Chem. Int. Ed.* **2012**, *51*, 7020-7023.

[16] M. Kira, S. Ishida, T. Iwamoto, C. Kabuto, *J. Am. Chem. Soc.* **1999**, *121*, 9722-9723.

[17] T. Abe, R. Tanaka, S. Ishida, M. Kira, T. Iwamoto, *J. Am. Chem. Soc.* **2012**, *134*, 20029-20032.

[18] S. Ishida, T. Abe, F. Hirakawa, T. Kosai, K. Sato, M. Kira, T. Iwamoto, *Chem. Eur. J.* **2015**, *21*, 15100-15103.

[19] M. Asay, S. Inoue, M. Driess, *Angew. Chem. Int. Ed.* **2011**, *50*, 9589-9592.

[20] D. Gau, T. Kato, N. Saffon-Merceron, F. P. Cossío, A. Baceiredo, *J. Am. Chem. Soc.* **2009**, *131*, 8762-8763.

[21] a) R. Rodriguez, D. Gau, Y. Contie, T. Kato, N. Saffon-Merceron, A. Baceiredo, *Angew. Chem. Int. Ed.* **2011**, *50*, 11492-11495; b) D. Gau, T. Kato, N. Saffon-Merceron, A. De Cózar, F. P. Cossío, A. Baceiredo, *Angew. Chem. Int. Ed.* **2010**, *49*, 6585-6588.

[22] D. Gau, R. Rodriguez, T. Kato, N. Saffon-Merceron, A. de Cózar, F. P. Cossío, A. Baceiredo, *Angew. Chem. Int. Ed.* **2011**, *50*, 1092-1096.

[23] I. Alvarado-Beltran, A. Baceiredo, N. Saffon-Merceron, V. Branchadell, T. Kato, *Angew. Chem. Int. Ed.* **2016**, *55*, 16141-16144.

[24] T. Kosai, S. Ishida, T. Iwamoto, *Angew. Chem. Int. Ed.* **2016**, *55*, 15554-15558.

[25] H. Wang, T. L. Chan, Z. Xie, *Chem. Commun.* **2018**, *54*, 385-388.

[26] G.-H. Lee, R. West, T. Müller, *J. Am. Chem. Soc.* **2003**, *125*, 8114-8115.

[27] a) T. J. Hadlington, J. A. B. Abdalla, R. Tirfoin, S. Aldridge, C. Jones, *Chem. Commun.* **2016**, *52*, 1717-1720; b) A. V. Protchenko, A. D. Schwarz, M. P. Blake, C.

Jones, N. Kaltsoyannis, P. Mountford, S. Aldridge, *Angew. Chem. Int. Ed.* **2013**, *52*, 568-571; c) A. V. Protchenko, K. H. Birjkumar, D. Dange, A. D. Schwarz, D. Vidovic, C. Jones, N. Kaltsoyannis, P. Mountford, S. Aldridge, *J. Am. Chem. Soc.* **2012**, *134*, 6500-6503.

[28] B. D. Rekken, T. M. Brown, J. C. Fettinger, H. M. Tuononen, P. P. Power, *J. Am. Chem. Soc.* **2012**, *134*, 6504-6507.

[29] S. Inoue, M. Ichinohe, A. Sekiguchi, *J. Am. Chem. Soc.* **2007**, *129*, 6096-6097.

[30] A. C. Filippou, O. Chernov, G. Schnakenburg, *Chem. Eu. J.* **2011**, *17*, 13574-13583.

[31] a) S. Inoue, K. Leszczyńska, *Angew. Chem. Int. Ed.* **2012**, *51*, 8589-8593; b) P. Jutzi, K. Leszczyńska, B. Neumann, W. W. Schoeller, H.-G. Stammler, *Angew. Chem. Int. Ed.* **2009**, *48*, 2596-2599; c) P. Jutzi, A. Mix, B. Rummel, W. W. Schoeller, B. Neumann, H.-G. Stammler, *Science* **2004**, *305*, 849-851.

[32] a) T. Iwamoto, T. Abe, C. Kabuto, M. Kira, *Chem. Commun.* **2005**, 5190-5192; b) S. Ishida, T. Iwamoto, C. Kabuto, M. Kira, *Nature* **2003**, *421*, 725-727.

[33] a) C. A. Dyker, V. Lavallo, B. Donnadieu, G. Bertrand, *Angew. Chem. Int. Ed.* **2008**, *47*, 3206-3209; b) R. Tonner, G. Frenking, *Angew. Chem. Int. Ed.* **2007**, *46*, 8695-8698.

[34] a) G. Frenking, M. Hermann, D. M. Andrada, N. Holzmann, *Chem. Soc. Rev.* **2016**; b) G. Frenking, R. Tonner, S. Klein, N. Takagi, T. Shimizu, A. Krapp, K. K. Pandey, P. Parameswaran, *Chem. Soc. Rev.* **2014**, *43*, 5106-5139; c) G. Frenking, *Angew. Chem. Int. Ed.* **2014**, *53*, 6040-6046; d) N. Takagi, T. Shimizu, G. Frenking, *Chem. Eur. J.* **2009**, *15*, 3448-3456; e) N. Takagi, T. Shimizu, G. Frenking, *Chem. Eur. J.* **2009**, *15*, 8593-8604; f) R. Tonner, G. Frenking, *Chem. Eur. J.* **2008**, *14*, 3260-3272; g) R. Tonner, G. Frenking, *Chem. Euro. J.* **2008**, *14*, 3273-3289; h) M. Kosa, M. Karni, Y. Apeloig, *J. Chem. Theo. and Comp.* **2006**, *2*, 956-964.

[35] T. Troadec, T. Wasano, R. Lenk, A. Baceiredo, N. Saffon-Merceron, D. Hashizume, Y. Saito, N. Nakata, V. Branchadell, T. Kato, *Angew. Chem. Int. Ed.* **2017**, *56*, 6891-6895.

[36] a) Y.-L. Shan, B.-X. Leong, H.-W. Xi, R. Ganguly, Y. Li, K. H. Lim, C.-W. So, *Dalton Trans.* **2017**, *46*, 3642-3648; b) Y.-L. Shan, W.-L. Yim, C.-W. So, *Angew. Chem. Int. Ed.* **2014**, *53*, 13155-13158.

[37] H. Wang, L. Wu, Z. Lin, Z. Xie, *J. Am. Chem. Soc.* **2017**, *139*, 13680-13683.

[38] a) S. Raoufmoghaddam, Y.-P. Zhou, Y. Wang, M. Driess, *J. Organomet. Chem.* **2017**, *829*, 2-10; b) D. Gallego, B. Blom, G. Tan, M. Driess, in *Reference Module in Chemistry, Molecular Sciences and Chemical Engineering*, Elsevier, **2015**; c) B. Blom, D. Gallego, M. Driess, *Inorg. Chem. Front.* **2014**, *1*, 134-148; d) Z. Benedeka, T. Szilvási, *RSC Adv.*, **2015**, *5*, 5077-5086.

[39] A. Furstner, H. Krause, C. W. Lehmann, *Chem. Commun.* **2001**, 2372-2373.

[40] M. Stoelzel, C. Präsang, B. Blom, M. Driess, *Aust. J. Chem.* **2013**, *66*, 1163-1170.

[41] B. Blom, S. Enthaler, S. Inoue, E. Irran, M. Driess, *J. Am. Chem. Soc.* **2013**, *135*, 6703-6713.

[42] T. Troadec, A. Prades, R. Rodriguez, R. Mirgalet, A. Baceiredo, N. Saffon-Merceron, V. Branchadell, T. Kato, *Inorg. Chem.* **2016**, *55*, 8234-8240.

[43] T. Iimura, N. Akasaka, T. Iwamoto, *Organometallics* **2016**, *35*, 4071-4076.

[44] T. Iimura, N. Akasaka, T. Kosai, T. Iwamoto, *Dalton Trans.* **2017**, *46*, 8868-8874.

[45] Y. Wang, A. Kostenko, S. Yao, M. Driess, *J. Am. Chem. Soc.* **2017**, *139*, 13499-13506.

[46] R. Rodriguez, T. Troadec, T. Kato, N. Saffon-Merceron, J.-M. Sotiropoulos, A. Baceiredo, *Angew. Chem. Int. Ed.* **2012**, *51*, 7158-7161.

[47] M. Zhang, X. Liu, C. Shi, C. Ren, Y. Ding, H. W. Roesky, *Z. Anorg. Allg. Chem.* **2008**, *634*, 1755-1758.

[48] W. Wang, S. Inoue, S. Yao, M. Driess, *J. Am. Chem. Soc.* **2010**, *132*, 15890-15892.

[49] S. C. I., H. Michael, W. Wenyuan, E. Stephan, I. Shigeyoshi, *Chem. Lett.* **2013**, *42*, 286-288.

[50] D. Gallego, A. Brück, E. Irran, F. Meier, M. Kaupp, M. Driess, J. F. Hartwig, *J. Am. Chem. Soc.* **2013**, *135*, 15617-15626.

[51] W. Wang, S. Inoue, S. Enthaler, M. Driess, *Angew. Chem. Int. Ed.* **2012**, *51*, 6167-6171.

[52] M. Schmidt, B. Blom, T. Szilvási, R. Schomäcker, M. Driess, *Eur. J. Inorg. Chem.* **2017**, *2017*, 1284-1291.

[53] A. Brück, D. Gallego, W. Wang, E. Irran, M. Driess, J. F. Hartwig, *Angew. Chem. Int. Ed.* **2012**, *51*, 11478-11482.

[54] J. A. Cabeza, P. Garcia-Alvarez, L. Gonzalez-Alvarez, *Chem. Commun.* **2017**, *53*, 10275-10278.

[55] H. Ren, Y.-P. Zhou, Y. Bai, C. Cui, M. Driess, *Chem. Eur. J.* **2017**, *23*, 5663-5667.

[56] D. Gallego, S. Inoue, B. Blom, M. Driess, *Organometallics* **2014**, *33*, 6885-6897.

[57] T. T. Metsanen, D. Gallego, T. Szilvasi, M. Driess, M. Oestreich, *Chem. Sci.* **2015**, *6*, 7143-7149.

[58] M.-P. Luecke, D. Porwal, A. Kostenko, Y.-P. Zhou, S. Yao, M. Keck, C. Limberg, M. Oestreich, M. Driess, *Dalton Trans.* **2017**, *46*, 16412-16418.

[59] a) K. C. Mondal, H. W. Roesky, M. C. Schwarzer, G. Frenking, B. Niepötter, H. Wolf, R. Herbst-Irmer, D. Stalke, *Angew. Chem. Int. Ed.* **2013**, *52*, 2963-2967; b) Y. Xiong, S. Yao, G. Tan, S. Inoue, M. Driess, *J. Am. Chem. Soc.* **2013**, *135*, 5004-5007; c) Y. Xiong, S. Yao, S. Inoue, J. D. Epping, M. Driess, *Angew. Chem. Int. Ed.* **2013**, *52*, 7147-7150; d) Y. Li, K. C. Mondal, H. W. Roesky, H. Zhu, P. Stollberg, R. Herbst-Irmer, D. Stalke, D. M. Andrada, *J. Am. Chem. Soc.* **2013**, *135*, 12422-12428.

[60] a) T. Chu, L. Belding, A. van der Est, T. Dudding, I. Korobkov, G. I. Nikonov, *Angew. Chem. Int. Ed.* **2014**, *53*, 2711-2715; b) B. Su, R. Ganguly, Y. Li, R. Kinjo, *Angew. Chem. Int. Ed.* **2014**, *53*, 13106-13109.

[61] a) M. Kira, *Chem. Commun.* **2010**, *46*, 2893-2903; b) M. Kira, T. Iwamoto, S. Ishida, H. Masuda, T. Abe, C. Kabuto, *J. Am. Chem. Soc.* **2009**, *131*, 17135-17144; c) T. Iwamoto, H. Masuda, C. Kabuto, M. Kira, *Organometallics* **2005**, *24*, 197-199.

[62] N. Wiberg, H.-W. Lerner, S.-K. Vasisht, S. Wagner, K. Karaghiosoff, H. Nöth, W. Ponikwar, *Eur. J. Inorg. Chem.* **1999**, *1999*, 1211-1218.

[63] C.-W. So, H. W. Roesky, J. Magull, R. B. Oswald, *Angew. Chem.* **2006**, *118*, 4052-4054.

[64] a) B. Blom, M. Stoelzel, M. Driess, *Chem. Eur. J.* **2013**, *19*, 40-62; b) S. Raoufmoghaddam, Y.-P. Zhou, Y. Wang, M. Driess, *J. Organomet. Chem.* **2017**, *829*, 2-10.

[65] Y. Xiong, S. Yao, S. Inoue, A. Berkefeld, M. Driess, *Chem. Commun.* **2012**, *48*, 12198-12200.

[66] A. P. Singh, H. W. Roesky, E. Carl, D. Stalke, J.-P. Demers, A. Lange, *J. Am. Chem. Soc.* **2012**, *134*, 4998-5003.

[67] a) K. Junold, J. A. Baus, C. Burschka, T. Vent-Schmidt, S. Riedel, R. Tacke, *Inorg. Chem.* **2013**, *52*, 11593-11599; b) K. Junold, J. A. Baus, C. Burschka, R. Tacke, *Angew. Chem.* **2012**, *124*, 7126-7129.

[68] Y. Xiong, S. Yao, R. Müller, M. Kaupp, M. Driess, *J. Am. Chem. Soc.* **2010**, *132*, 6912-6913.

[69] Y. Xiong, S. Yao, M. Karni, A. Kostenko, A. Burchert, Y. Apeloig, M. Driess, *Chem. Sci.* **2016**, *7*, 5462-5469.

[70] B. Su, R. Ganguly, Y. Li, R. Kinjo, *Chem. Commun.* **2016**, *52*, 613-616.

[71] T. Ochiai, D. Franz, X.-N. Wu, S. Inoue, *Dalton Trans.* **2015**, *44*, 10952-10956.

[72] A. Jana, M. Majumdar, V. Huch, M. Zimmer, D. Scheschkewitz, *Dalton Trans.* **2014**, *43*, 5175-5181.

[73] A. Rit, J. Campos, H. Niu, S. Aldridge, *Nat. Chem.*, DOI: 10.1038/NCHEM.2597.

[74] a) G. Prabusankar, A. Sathyanarayana, P. Suresh, C. Naga Babu, K. Srinivas, B. P. R. Metla, *Coord. Chem. Rev.* **2014**, *269*, 96-133; b) S. M. I. Al-Rafia, M. R. Momeni, R. McDonald, M. J. Ferguson, A. Brown, E. Rivard, *Angew. Chem. Int. Ed.* **2013**, *52*, 6390-6395.

[75] a) P. Ghana, M. I. Arz, U. Das, G. Schnakenburg, A. C. Filippou, *Angew. Chem. Int. Ed.* **2015**, *54*, 9980-9985; b) A. Jana, V. Huch, D. Scheschkewitz, *Angew. Chem. Int. Ed.* **2013**, *52*, 12179-12182.

[76] Z. Benedek, T. Szilvasi, *RSC Advances* **2015**, *5*, 5077-5086.

[77] W. Wang, S. Inoue, E. Irran, M. Driess, *Angew. Chem. Int. Ed.* **2012**, *51*, 3691-3694.

[78] a) V. I. Bregadze, *Chem. Rev.* **1992**, *92*, 209-223; b) J. F. Valliant, K. J. Guenther, A. S. King, P. Morel, P. Schaffer, O. O. Sogbein, K. A. Stephenson, *Coord. Chem. Rev.* **2002**, *232*, 173-230; c) M. E. El-Zaria, H. Arii, H. Nakamura, *Inorg. Chem.* **2011**, *50*, 4149-4161; d) Z. Xie, G.-X. Jin, *Dalton Trans.* **2014**, *43*, 4924-4924; e) M. Joost, A. Zeineddine, L. Estévez, S. Mallet−Ladeira, K. Miqueu, A. Amgoune, D. Bourissou, *J. Am. Chem. Soc.* **2014**, *136*, 14654-14657; f) M. Joost, A. Amgoune, D. Bourissou, *Angew. Chem. Int. Ed.* **2015**, *54*, 15022-15045; g) M. Joost, L. Estévez, K. Miqueu, A. Amgoune, D. Bourissou, *Angew. Chem. Int. Ed.* **2015**, *54*, 5236-5240.

[79] N. M. Scott, H. Clavier, P. Mahjoor, E. D. Stevens, S. P. Nolan, *Organometallics* **2008**, *27*, 3181-3186.

[80] a) D. S. Surry, S. L. Buchwald, *Angew. Chem. Int. Ed.* **2008**, *47*, 6338-6361; b) J. F. Hartwig, *Acc. Chem. Res.* **2008**, *41*, 1534-1544; c) J. P. Wolfe, S. Wagaw, J.-F. Marcoux, S. L. Buchwald, *Acc. Chem. Res.* **1998**, *31*, 805-818; d) J. F. Hartwig, *Angew. Chem. Int. Ed.* **1998**, *37*, 2046-2067.

[81] a) R. M. Bullock, *Science* **2013**, *342*, 1054-1055; b) S. Chakraborty, P. Bhattacharya, H. Dai, H. Guan, *Acc. Chem. Res.* **2015**, *48*, 1995-2003; c) P. J. Chirik, *Acc. Chem. Res.* **2015**, *48*, 1687-1695; d) P. L. Holland, *Acc. Chem. Res.* **2015**, *48*, 1696-1702; e) E. McNeill, T. Ritter, *Acc. Chem. Res.* **2015**, *48*, 2330-2343; f) J. Miao, H. Ge, *Eur. J. Org. Chem.* **2015**, *2015*, 7859-7868; g) R. H. Morris, *Acc. Chem. Res.* **2015**, *48*, 1494-1502; h) B. Su, Z.-C. Cao, Z.-J. Shi, *Acc. Chem. Res.* **2015**, *48*, 886-896; i) S. Z. Tasker, E. A. Standley, T. F. Jamison, *Nature* **2014**, *509*, 299-309; j) S. A. Johnson, *Dalton. Trans.* **2015**, *44*, 10905-10913; k) T. Kurahashi, S. Matsubara, *Acc. Chem. Res.* **2015**, *48*, 1703-1716; l) E. A. Standley, S. Z. Tasker, K. L. Jensen, T. F. Jamison, *Acc. Chem. Res.* **2015**, *48*, 1503-1514; m) A. Thakur, J. Louie, *Acc. Chem. Res.* **2015**, *48*, 2354-2365; n) M. Tobisu, N. Chatani, *Acc. Chem. Res.* **2015**, *48*, 1717-1726.

[82] V. Ritleng, M. Henrion, M. J. Chetcuti, *ACS Cata.* **2016**, *6*, 890-906.

[83] a) A. R. Martin, Y. Makida, S. Meiries, A. M. Z. Slawin, S. P. Nolan, *Organometallics* **2013**, *32*, 6265-6270; b) S. Kuhl, Y. Fort, R. Schneider, *J. Organomet. Chem.* **2005**, *690,* 6169-6177; c) R. Omar-Amrani, A. Thomas, E. Brenner, R. Schneider, Y. Fort, *Org. Lett.* **2003**, *5*, 2311-2314; d) B. t. Gradel, E. Brenner, R. Schneider, Y. Fort, *Tetrahedron Lett.* **2001**, *42*, 5689-5692; e) R. A. Green, J. F. Hartwig, *Angew. Chem. Int. Ed.* **2015**, *54*, 3768-3772; f) A. Borzenko, N. L. Rotta-Loria, P. M. MacQueen, C. M. Lavoie, R. McDonald, M. Stradiotto, *Angew. Chem. Int. Ed.* **2015**, *54*, 3773-3777; g) N. H. Park, G. Teverovskiy, S. L. Buchwald, *Org. Lett.* **2014**, *16*, 220-223; h) S. S. Kampmann, A. N. Sobolev, G. A. Koutsantonis, S. G. Stewart, *Adv. Synth. Catal.* **2014**, *356*, 1967-1973; i) S. Ge, R. A. Green, J. F. Hartwig, *J. Am. Chem. Soc.* **2014**, *136*, 1617-1627; j) L. Hie, S. D. Ramgren, T. Mesganaw, N. K. Garg, *Org. Lett.* **2012**, *14*, 4182-4185; k) S. D. Ramgren, A. L. Silberstein, Y. Yang, N. K. Garg, *Angew. Chem. Int. Ed.* **2011**, *50*, 2171-2173; l) T. Shimasaki, M. Tobisu, N. Chatani, *Angew. Chem. Int. Ed.* **2010**, *49*, 2929-2932; m) G. Manolikakes, A. Gavryushin, P. Knochel, *J. Org. Chem.* **2008**, *73*, 1429-1434; n) Chen, L.-M. Yang, *J. Org. Chem.* **2007**, *72*, 6324-6327; o) C. Desmarets, R.

Schneider, Y. Fort, *Tetrahedron* **2001**, *57*, 7657-7664; p) E. Brenner, R. Schneider, Y. Fort, *Tetrahedron* **1999**, *55*, 12829-12842.

[84] K. Matsubara, K. Ueno, Y. Koga, K. Hara, *J. Org. Chem.,* **2007**, *72*, 5069-5076.

[85] a) Y.-P. Zhou, S. Raoufmoghaddam, T. Szilvási, M. Driess, *Angew. Chem. Int. Ed.* **2016**, *55*, 12868-12872; b) M.-P. Luecke, D. Porwal, A. Kostenko, Y.-P. Zhou, S. Yao, M. Keck, C. Limberg, M. Oestreich, M. Driess, *Dalton Trans.,* **2017**.

[86] J. Prunet, *Angew. Chem. Int. Ed.* **2003**, *42*, 2826-2830.

[87] H. D. Lindlar, R. , *Org. Synth.* **1966**, *46*, 89.

[88] a) J. Lei, L. Su, K. Zeng, T. Chen, R. Qiu, Y. Zhou, C.-T. Au, S.-F. Yin, *Chem. Eng. Sci.* **2017**, *171*, 404-425; b) M. K. Karunananda, N. P. Mankad, *Organometallics* **2017**, *36*, 220-227; c) K. Tokmic, A. R. Fout, *J. Am. Chem. Soc.* **2016**, *138*, 13700-13705; d) K. T. Neumann, S. Klimczyk, M. N. Burhardt, B. Bang-Andersen, T. Skrydstrup, A. T. Lindhardt, *ACS Cata.,* **2016**, *6*, 4710-4714; e) R. Kusy, K. Grela, *Org. Lett.* **2016**, *18*, 6196-6199; f) S. Furukawa, T. Komatsu, *ACS Cata.,* **2016**, *6*, 2121-2125; g) S. Fu, N.-Y. Chen, X. Liu, Z. Shao, S.-P. Luo, Q. Liu, *J. Am. Chem. Soc.* **2016**, *138*, 8588-8594; h) E. Richmond, J. Moran, *J. Org. Chem.,* **2015**, *80*, 6922-6929; i) M. Leutzsch, L. M. Wolf, P. Gupta, M. Fuchs, W. Thiel, C. Farès, A. Fürstner, *Angew. Chem. Int. Ed.* **2015**, *54*, 12431-12436; j) Z. Chen, M. Luo, Y. Wen, G. Luo, L. Liu, *Org. Lett.* **2014**, *16*, 3020-3023; k) A. M. Whittaker, G. Lalic, *Org. Lett.* **2013**, *15*, 1112-1115; l) D. Srimani, Y. Diskin-Posner, Y. Ben-David, D. Milstein, *Angew. Chem. Int. Ed.* **2013**, *52*, 14131-14134; m) K. Radkowski, B. Sundararaju, A. Fürstner, *Angew. Chem. Int. Ed.* **2013**, *52*, 355-360.

[89] a) M. M. Najafpour, G. Renger, M. Hołyńska, A. N. Moghaddam, E.-M. Aro, R. Carpentier, H. Nishihara, J. J. Eaton-Rye, J.-R. Shen, S. I. Allakhverdiev, *Chem. Rev.* **2016**, *116*, 2886-2936; b) K. Jin, H. Seo, H. Ha, Y. Kim, K. H. Cho, J. S. Hong, K. T. Nam, *Catal. Today* **2016**; c) A. Indra, P. W. Menezes, M. Driess, *ChemSusChem* **2015**, *8*, 776-785; d) H. Dau, C. Limberg, T. Reier, M. Risch, S. Roggan, P. Strasser, *ChemCatChem* **2010**, *2*, 724-761.

[90] a) D. A. Valyaev, G. Lavigne, N. Lugan, *Coord. Chem. Rev.* **2016**, *308, Part 2*, 191-235; b) M. Garbe, K. Junge, M. Beller, *Eur. J. Org. Chem.*, 724-761.

[91] a) M. B. Widegren, G. J. Harkness, A. M. Z. Slawin, D. B. Cordes, M. L. Clarke, *Angew. Chem. Int. Ed.* **2017**, 724-761; b) N. A. Espinosa-Jalapa, A. Nerush, L. J. W. Shimon, G. Leitus, L. Avram, Y. Ben-David, D. Milstein, *Chem. Eur. J.* **2017**, *23*,

5934-5938; c) A. Bruneau-Voisine, D. Wang, T. Roisnel, C. Darcel, J.-B. Sortais, *Catal. Commun.* **2017**, *92*, 1-4; d) S. Elangovan, C. Topf, S. Fischer, H. Jiao, A. Spannenberg, W. Baumann, R. Ludwig, K. Junge, M. Beller, *J. Am. Chem. Soc.* **2016**, *138*, 8809-8814; e) S. Elangovan, M. Garbe, H. Jiao, A. Spannenberg, K. Junge, M. Beller, *Angew. Chem.* **2016**, *128*, 15590-15594; f) F. Kallmeier, T. Irrgang, T. Dietel, R. Kempe, *Angew. Chem. Int. Ed.* **2016**, *55*, 11806-11809; g) M. Garbe, K. Junge, S. Walker, Z. Wei, H. Jiao, A. Spannenberg, S. Bachmann, M. Scalone, M. Beller, *Angew. Chem. Int. Ed.* **2017**, *56*, 11237-11241; h) A. Dubey, L. Nencini, R. R. Fayzullin, C. Nervi, J. R. Khusnutdinova, *ACS Cata.,* **2017**, *7*, 3864-3868.

[92] a) A. Zirakzadeh, S. R. M. M. de Aguiar, B. Stöger, M. Widhalm, K. Kirchner, *ChemCatChem* **2017**, n/a-n/a; b) M. Perez, S. Elangovan, A. Spannenberg, K. Junge, M. Beller, *ChemSusChem* **2017**, *10*, 83-86.

[93] a) T. K. Mukhopadhyay, C. L. Rock, M. Hong, D. C. Ashley, T. L. Groy, M.-H. Baik, R. J. Trovitch, *J. Am. Chem. Soc.* **2017**, *139*, 4901-4915; b) J. Zheng, S. Elangovan, D. A. Valyaev, R. Brousses, V. César, J.-B. Sortais, C. Darcel, N. Lugan, G. Lavigne, *Adv. Synth. Catal.* **2014**, *356*, 1093-1097; c) T. K. Mukhopadhyay, M. Flores, T. L. Groy, R. J. Trovitch, *J. Am. Chem. Soc.* **2014**, *136*, 882-885; d) V. Vasilenko, C. K. Blasius, H. Wadepohl, L. H. Gade, *Angew. Chem. Int. Ed.* **2017**, *56*, 8393-8397; e) G. Zhang, H. Zeng, J. Wu, Z. Yin, S. Zheng, J. C. Fettinger, *Angew. Chem. Int. Ed.* **2016**, *55*, 14369-14372; f) V. K. Chidara, G. Du, *Organometallics* **2013**, *32*, 5034-5037.

[94] J. Chai, H. Zhu, Y. Peng, Herbert W. Roesky, S. Singh, H.-G. Schmidt, M. Noltemeyer, *Eur. J. Inorg. Chem.* **2004**, *2004*, 2673-2677.

[95] M. H. Al-Afyouni, V. M. Krishnan, H. D. Arman, Z. J. Tonzetich, *Organometallics* **2015**, *34*, 5088-5094.

[96] Y.-P. Zhou, M. Karni, S. Yao, Y. Apeloig, M. Driess, *Angew. Chem. Int. Ed.* **2016**, *55*, 15096-15099.

[97] M. C. Couldwell, J. Simpson, *J. Chem. Soc., Dalton Trans.* **1976**, 714-719.

[98] D. Wang, D. Astruc, *Chem. Rev.* **2015**, *115*, 6621-6686.

[99] a) A. Rossin, M. Peruzzini, *Chem. Rev.* **2016**, *116*, 8848-8872; b) J. Yang, A. Sudik, C. Wolverton, D. J. Siegel, *Chem. Soc. Rev.* **2010**, *39*, 656-675; c) A. Staubitz, A. P. M. Robertson, I. Manners, *Chem. Rev.* **2010**, *110*, 4079-4124.

[100] a) S. Li, W. Meng, H. Du, *Org. Lett.* **2017**, *19*, 2604-2606; b) E. Korytiakova, N. O. Thiel, F. Pape, J. F. Teichert, *Chem. Commun.* **2017**, *53*, 732-735; c) Q. Zhou, L. Zhang, W. Meng, X. Feng, J. Yang, H. Du, *Org. Lett.* **2016**, *18*, 5189-5191; d) Z. Shao, S. Fu, M. Wei, S. Zhou, Q. Liu, *Angew. Chem. Int. Ed.* **2016**, *55*, 14653-14657; e) S. Li, G. Li, W. Meng, H. Du, *J. Am. Chem. Soc.* **2016**, *138*, 12956-12962; f) T.-P. Lin, J. C. Peters, *J. Am. Chem. Soc.* **2013**, *135*, 15310-15313; g) X. Yang, L. Zhao, T. Fox, Z.-X. Wang, H. Berke, *Angew. Chem. Int. Ed.* **2010**, *49*, 2058-2062; h) R. Barrios-Francisco, J. J. García, *Applied Catalysis A: General* **2010**, *385*, 108-113; i) Y. Jiang, O. Blacque, T. Fox, C. M. Frech, H. Berke, *Organometallics* **2009**, *28*, 5493-5504; j) E. Vasilikogiannaki, I. Titilas, G. Vassilikogiannakis, M. Stratakis, *Chem. Commun.* **2015**, *51*, 2384-2387.

[101] M. Gediga, C. M. Feil, S. H. Schlindwein, J. Bender, M. Nieger, D. Gudat, *Chem. Eur. J.*, **2017**, *46*, 7976-7997.

[102] a) F. J. Fernández-Alvarez, R. Lalrempuia, L. A. Oro, *Coord. Chem. Rev.* **2017**, *350*, 49-60; b) M. Simon, F. Breher, *Dalton Trans.,* **2017**, *46*, 7976-7997.

[103] J. Y. Corey, *Chem. Rev.* **2016**, *116*, 11291-11435.

[104] a) Y. Nakajima, S. Shimada, *RSC Advances* **2015**, *5*, 20603-20616; b) A. K. Roy, in *Adv. Organomet. Chem., Vol. 55* (Eds.: R. West, A. F. Hill, M. J. Fink), Academic Press, **2007**, pp. 1-59.

[105] a) X. Du, Z. Huang, *ACS Cata.,* **2017**, *7*, 1227-1243; b) J. Sun, L. Deng, *ACS Cata.,* **2016**, *6*, 290-300; c) I. Buslov, F. Song, X. Hu, *Angew. Chem. Int. Ed.* **2016**, *55*, 12295-12299.

[106] a) A. J. Chalk, J. F. Harrod, *J. Am. Chem. Soc.* **1967**, *89*, 1640-1647; b) J. F. Harrod, A. J. Chalk, *J. Am. Chem. Soc.* **1965**, *87*, 1133-1133.

[107] M. Brookhart, B. E. Grant, *J. Am. Chem. Soc.* **1993**, *115*, 2151-2156.

[108] Z. Mo, Y. Liu, L. Deng, *Angew. Chem. Int. Ed.* **2013**, *52*, 10845-10849.

[109] a) H. L. Sang, S. Yu, S. Ge, *Chemical Science* **2018**, *9*, 973-978; b) C. Wang, W. J. Teo, S. Ge, *ACS Cata.,* **2017**, *7*, 855-863; c) B. Raya, S. Jing, V. Balasanthiran, T. V. RajanBabu, *ACS Cata.,* **2017**, *7*, 2275-2283; d) Y. Liu, L. Deng, *J. Am. Chem. Soc.* **2017**, *139*, 1798-1801; e) B. Cheng, P. Lu, H. Zhang, X. Cheng, Z. Lu, *J. Am. Chem. Soc.* **2017**, *139*, 9439-9442; f) C. H. Schuster, T. Diao, I. Pappas, P. J. Chirik, *ACS Cata.,* **2016**, *6*, 2632-2636; g) B. Raya, S. Biswas, T. V. RajanBabu, *ACS Cata.,* **2016**, *6*, 6318-6323; h) A. D. Ibrahim, S. W. Entsminger, L. Zhu, A. R. Fout, *ACS Cata.,*

2016, *6*, 3589-3593; i) X. Du, Y. Zhang, D. Peng, Z. Huang, *Angew. Chem. Int. Ed.* **2016**, *55*, 6671-6675; j) C. Chen, M. B. Hecht, A. Kavara, W. W. Brennessel, B. Q. Mercado, D. J. Weix, P. L. Holland, *J. Am. Chem. Soc.* **2015**, *137*, 13244-13247; k) C. C. H. Atienza, T. Diao, K. J. Weller, S. A. Nye, K. M. Lewis, J. G. P. Delis, J. L. Boyer, A. K. Roy, P. J. Chirik, *J. Am. Chem. Soc.* **2014**, *136*, 12108-12118.

[110] S. E. Parker, J. Börgel, T. Ritter, *J. Am. Chem. Soc.* **2014**, *136*, 4857-4860.

[111] G. M. Sheldrick, SHELX-97 Program for Crystal Structure Determination, Universität Göttingen (Germany) 1997.

[112] Gaussian 09, Revision D.01, Frisch, M. J.; Trucks, G. W.; Schlegel, H. B.; Scuseria, G. E.; Robb, M. A.; Cheeseman, J. R.; Scalmani, G.; Barone, V.; Mennucci, B.; Petersson, G. A.; Nakatsuji, H.; Caricato, M.; Li, X.; Hratchian, H. P.; Izmaylov, A. F.; Bloino, J.; Zheng, G.; Sonnenberg, J. L.; Hada, M.; Ehara, M.; Toyota, K.; Fukuda, R.; Hasegawa, J.; Ishida, M.; Nakajima, T.; Honda, Y.; Kitao, O.; Nakai, H.; Vreven, T.; Montgomery, J. A., Jr.; Peralta, J. E.; Ogliaro, F.; Bearpark, M.; Heyd, J. J.; Brothers, E.; Kudin, K. N.; Staroverov, V. N.; Kobayashi, R.; Normand, J.; Raghavachari, K.; Rendell, A.; Burant, J. C.; Iyengar, S. S.; Tomasi, J.; Cossi, M.; Rega, N.; Millam, M. J.; Klene, M.; Knox, J. E.; Cross, J. B.; Bakken, V.; Adamo, C.; Jaramillo, J.; Gomperts, R.; Stratmann, R. E.; Yazyev, O.; Austin, A. J.; Cammi, R.; Pomelli, C.; Ochterski, J. W.; Martin, R. L.; Morokuma, K.; Zakrzewski, V. G.; Voth, G. A.; Salvador, P.; Dannenberg, J. J.; Dapprich, S.; Daniels, A. D.; Farkas, Ö.; Foresman, J. B.; Ortiz, J. V.; Cioslowski, J.; Fox, D. J. Gaussian, Inc., Wallingford CT, 2009.

[113] M. Yamashita, M. Uchida, H. Tashika, R. Suemitsu, *Bull. Chem. Soc. Jpn.* **1989**, *62*, 2728-2729.

7. APPENDIX

7.1 Crystal data and structure refinement

Table 7.1.1 Crystal data and structure refinement for complexes 3-1, 3-3, and 3-4

Complex	**3-1**	**3-3**	**3-4**
formula	C42.5H63Cl2GeN7Si2	C43H59FeGeN7O4Si2	C45H64Cl2FeGe2N7O4.5Si2
M_r	871.67	922.59	1103.14
space group	$P2_1/c$	$P2_1/c$	$P2_1/c$
crystal system	monoclinic	monoclinic	monoclinic
a [Å]	12.8747(2)	22.5376(2)	23.1730(4)
b [Å]	12.8747(2)	11.67740(10)	17.3288(2)
c [Å]	18.3160(3)	17.80130(10)	26.0810(4)
α [°]	90	90	90
β [°]	105.995(2)°	101.4130(10)	94.301(2)
γ [°]	90	90	90
V [Å^3]	4557.68(12)	4592.32(6)	10443.6(3)
Z	4	4	8
ρ_{calcd} [mg m^{-3}]	1.270	1.334	1.403
wavelength [Å]	1.54184	1.54184	1.54184
size [mm^3]	0.23 x 0.14 x 0.12	0.30×0.19×0.09	0.62 x 0.05 x 0.05
Θ limits [°]	3.57 to 67.49	4.00 to 67.49	3.06 to 67.50
completeness to Θ = 67.49°[%]	99.8	100.0	99.9
reflns measured[a]	17788	31486	40082
independent reflns	8202 [R(int) = 0.0344]	8256 [R(int) = 0.0299]	18804 [R(int) = 0.0624]
parameters	538	574	1174
R_1 (R_1 all data)	0.0389 (0.0472)	0.0341 (0.0405)	0.0529 (0.0816)
wR_2 (wR_2 all data)	0.1012 (0.1094)	0.0843 (0.0888)	0.1294 (0.1547)
GOF	1.015	1.021	0.954
max., min. peaks [eÅ^{-3}]	1.237 and -0.319	0.571 and -0.738	1.196 and -0.983

[a] Observation criterion: $I>2\sigma(I)$. [b] $R_1 = \Sigma\,|\,|F_o|$ - $|F_c|\,|\,/\,\Sigma\,|F_o|$. [c] $wR_2 = \{\Sigma[w\text{-}(F_o{}^2 - {}_c{}^2)^2]/\Sigma[w(F_o{}^2)^2]\}^{1/2}$

Table 7.1.2 Crystal data and structure refinement for complexes 3-6, 3-7, and 3-9

Complex	3-6	3-7	3-9
Formula	C64H112B20N8Si4	C46H72B10Br2N4NiSi2	C47H62Br2FeN4NiSi2
M_r	1322.18	1063.89	1013.57
space group	$P2_1/c$	$P2_1/c$	$P2_1/c$
crystal system	monoclinic	monoclinic	monoclinic
a [Å]	27.1017(3)	16.33440(10)	29.2617(4)
b [Å]	15.6600(2)	13.62690(10)	8.97920(10)
c [Å]	26.8284(3)	24.08500(10)	17.6242(2)
α [°]	90	90	90
β [°]	115.784(2)	91.3140(10)	92.0990(10)
γ [°]	90	90	90
V [Å^3]	10252.7(2)	5359.60(6)	4627.59(10)
Z	4	4	4
ρ_{calcd} [mg m^{-3}]	0.857	1.318	1.455
wavelength [Å]	1.54184	1.54184	1.54184
crystal size [mm^3]	0.20 x 0.12 x 0.11	0.15×0.13×0.10	0.26 x 0.06 x 0.02
Θ limits [°]	3.30 to 67.50	2.71 to 67.50	3.02 to 67.50
completeness to Θ = 67.5° [%]	100.0	99.9	100.0
reflns measured[a]	69652	36389	30160
independent reflns	18464 [R(int) = 0.0484]	9656 [R(int) = 0.0239]	8339 [R(int) = 0.0487]
parameters	889	600	537
R_1 (R_1 all data)[b]	0.0530 (0.0704)	0.0304 (0.0317)	0.0392 (0.0497)
wR_2 (wR_2 all data)[c]	0.1411 (0.1514)	0.0819 (0.0830)	0.0956 (0.1023)
GOF	0.972	1.050	1.035
max., min. peaks [eÅ^{-3}]	0.509 and -0.289	0.772 and -0.769	1.281 and -0.654

[a] Observation criterion: $I>2\sigma(I)$.

[b] $R_1 = \Sigma\,|\,|F_o|$ - $|F_c|\,|\,/\,\Sigma\,|F_o|$.

[c] $wR_2 = \{\Sigma[w\text{-}(F_o{}^2 - {}_c{}^2)^2]/\Sigma[w(F_o{}^2)^2]\}^{1/2}$

Table 7.1.3 Crystal data and structure refinement for complexes 3-11, 3-14, and 3-15

Complex	3-11	3-14	3-15
Formula	C25H54B10Br2N4NiP2	C39H59Cl2MnN7Si2	C54H70Cl2FeMnN4Si2
M_r	799.29	807.95	1013.01
space group	$P2_1/c$	$P2_1/n$	P-1
crystal system	monoclinic	monoclinic	Triclinic
a [Å]	10.1791(2)	17.1789(2)	10.4353(3)
b [Å]	32.1548(8)	17.2684(2)	11.7715(2)
c [Å]	11.3590(2)	17.3905(2)	22.0042(5)
α [°]	90	90	98.387(2)
β [°]	92.685(2)	105.7040(10)	99.342(2)
γ [°]	90	90	93.018(2)
V [Å^3]	3713.80(13)	4966.36(10)	2630.52(11)
Z	4	4	2
ρ_{calcd} [mg m^{-3}]	1.430	1.081	1.279
wavelength [Å]	1.54184	1.54184	1.54184
crystal size [mm^3]	0.24×0.13×0.09	0.11 x 0.08 x 0.05	0.28 x 0.13 x 0.11
Θ limits [°]	2.75 to 67.50	3.21 to 67.50	1.75 to 26.25
completeness to Θ = 67.50° [%]	100.0	99.9	96.6
reflns measured[a]	14220	20000	18597
independent reflns	6697 [R(int) = 0.0632]	8950 [R(int) = 0.0269]	10239 [R(int) = 0.0248]
parameters	406	474	591
GOF	0.987	1.043	1.102
R_1 (wR_2)	R_1 = 0.0454	R_1 = 0.0355	R_1 = 0.0437
	wR_2 = 0.0920	wR_2 = 0.0904	wR_2 = 0.1131
R_1 (wR_2 all data)	R_1 = 0.0750	R_1 = 0.0430	R_1 = 0.0502
	wR_2 = 0.1067	wR_2 = 0.0952	wR_2 = 0.1168
max., min. peaks [eÅ^{-3}]	0.531 and -0.615	0.374 and -0.298	0.483 and -0.693

[a] Observation criterion: $I > 2\sigma(I)$.

[b] $R_1 = \Sigma \mid |F_o| - |F_c| \mid / \Sigma |F_o|$.

[c] $wR_2 = \{\Sigma[w\text{-}(F_o^2 - {}_c^2)^2]/\Sigma[w(F_o^2)^2]\}^{1/2}$

Table 7.1.4 Crystal data and structure refinement for complexes 3-16, 3-18, and 3-19

	3-16	3-18	3-19
formula	C45.5H60Cl2MnN4Si2	C42H70CoN4P2Si	C76H112CoN8Si2
formula weight	844.99	779.98	1268.84
crystal system	Triclinic	Triclinic	monoclinic
space group	$P\text{-}1$	$P\text{-}1$	$P2_1/c$
a/Å	14.1492(4)	11.7543(6)	12.3276(2)
b/Å	17.2552(6)	11.8043(6)	32.1844(5)
c/Å	20.8774(8)	18.7249(7)	17.9780(4)
α/deg	105.926(3)	76.814(4)	90
β/deg	106.906(3)	75.448(4)	97.478(2)
γ/deg	90.002(3)	60.963(5)	90
V/Å^3	4672.0(3)	2181.30(18)	7072.2(2)
Z	4	2	4
ρ_{calcd}/g·cm^{-3}	1.201	1.188	1.192
crystal size/mm^3	0.2 x 0.16 x 0.08	0.33 x 0.06 x 0.05	0.23 x 0.10 x 0.09
θ range/deg	5.346 to 136.486	3.75 to 67.49	3.07 to 67.50
collected data	16982	14539	42160
unique data	16982 [R(int) = 0.0454]	7856	12576
completeness to θ	100.0	99.8	98.4
data/restraints/parameters	16982/0/1008	474	439
final R indices [$I>2\sigma(I)$]	$R_1 =$ 0.1079 $wR_2 = 0.3054$	$R_1 = 0.0604$ $wR_2 = 0.1566$	$R_1 = 0.0732$ $wR_2 = 0.0953$
R indices (all data)	$R_1 = 0.1221$ $wR_2 = 0.3140$	$R_1 = 0.0687$ $wR_2 = 0.1716$	$R_1 = 0.1881$ $wR_2 = 0.2075$
GOF on F^2	1.109	1.004	1.020
Largest diff peak/hole (e·Å^{-3})	1.34 and -1.45	0.255 to -0.331	0.538 to -0.622

[a] Observation criterion: $I>2\sigma(I)$. [b] $R_1 = \Sigma \mid |F_o| - |F_c| \mid / \Sigma |F_o|$. [c] $wR_2 = \{\Sigma[w\text{-}(F_o^2 - {}_c^2)^2]/\Sigma[w(F_o^2)^2]\}^{1/2}$

Table 7.1.5 Crystal data and structure refinement for complexes 3-20 and 3-21.

Complex	3-20	3-21
Formula	C66H71BCoF20N4P2Si	C41H61CoN4O2PSi
M_r	1460.04	759.93
space group	$P2_1/c$	$P2_1/n$
crystal system	monoclinic	monoclinic
a [Å]	11.5334(5)	11.7994(4)
b [Å]	24.4725(13)	17.2934(5)
c [Å]	24.2950(14)	19.8730(8)
α [°]	90	90
β [°]	94.926(4)	94.042(3)
γ [°]	90	90
V [Å^3]	6832.0(6)	4045.0(2)
Z	4	4
ρ_{calcd} [mg m^{-3}]	1.419	1.248
wavelength [Å]	1.54178	1.54178
crystal size [mm^3]	0.24 x 0.09 x 0.08	0.10 x 0.08 x 0.06
Θ limits [°]	2.43 to 67.50	3.05 to 67.50
completeness to $\Theta = 65.00°$ [%]	100.0	99.9
reflns measured[a]	43401	15592
independent reflns	11651	7276
parameters	935	480
R_1 (wR_2 all data)	$R_1 = 0.0961$	$R_1 = 0.0600$
	$wR_2 = 0.2252$	$wR_2 = 0.1289$
R_1 (wR_2 all data)	$R_1 = 0.1610$	$R_1 = 0.1067$
	$wR_2 = 0.2909$	$wR_2 = 0.1528$
GOF	1.207	1.002
max., min. peaks [eÅ^{-3}]	0.698 to -0.445	2.148 (-0.731)

[a] Observation criterion: $I>2\sigma(I)$. [b] $R_1 = \Sigma \mid |F_o| - |F_c| \mid / \Sigma |F_o|$. [c] $wR_2 = \{\Sigma[w \cdot (F_o^2 - {}_c^2)^2]/\Sigma[w(F_o^2)^2]\}^{1/2}$

Table 7.1.6 Crystal data and structure refinement for complexes 3-22 and 3-23.

	3-22	3-23
formula	C66H86CoN4OP2Si	C42H67CoN4P2Si
formula weight	1100.35	776.95
crystal system	Triclinic	Monoclinic
space group	*P-1*	*C c*
a/Å	11.8673(4)	11.9731(5)
b/Å	12.7852(5)	19.9825(9)
c/Å	20.9132(6)	36.4424(17)
α/deg	85.315(3)	90
β/deg	77.328(3)	96.534(4)
γ/deg	77.149(3)	90
V/Å^3	3016.44(18)	8662.3(7)
Z	2	8
ρ_{calcd}/g·cm^{-3}	1.211	1.192
θ range/deg	3.41-67.50	3.42-67.50
collected data	20705	8963
unique data	10862	8963
completeness to θ	99.9	97.9
GOF on F^2	1.029	1.037
final R indices [$I>2\sigma(I)$]	$R_1 = 0.0361$	$R_1 = 0.0690$
	$wR_2 = 0.0865$	$wR_2 = 0.1600$
R indices (all data)	$R_1 = 0.0426$	$R_1 = 0.1041$
	$wR_2 = 0.0905$	$wR_2 = 0.1838$
Largest diff peak/hole (e·Å^{-3})	0.469 to -0.405	0.619/-0.316

[a] Observation criterion: $I>2\sigma(I)$. [b] $R_1 = \Sigma \mid \mid F_o \mid - \mid F_c \mid \mid / \Sigma \mid F_o \mid$. [c] $wR_2 = \{\Sigma[w\text{-}(F_o^2 - {}_c{}^2)^2]/\Sigma[w(F_o^2)^2]\}^{1/2}$

7.2 Optimized (B3LYP‾D3(BJ)/6-311G(d,p)) molecular xyz coordinates; energies in Hartrees, free energies at 298.15K

[SiNSi]Ge

E= -4011.227645

Free energy= -4010.770535

6	-0.125608000	4.023329000	-1.821009000
6	-0.007670000	2.767648000	-1.193625000
6	-2.218758000	2.997200000	-0.340074000
6	-2.389753000	4.256888000	-0.913269000
6	-1.318619000	4.730733000	-1.675522000
1	0.701767000	4.448499000	-2.368315000
1	-3.292529000	4.832264000	-0.766507000
1	-1.404573000	5.702034000	-2.150880000
7	-1.081588000	2.281324000	-0.554086000
7	-2.952893000	2.206910000	0.478360000
7	1.112091000	1.983354000	-1.133124000
6	-4.252042000	2.541656000	1.002102000
1	-4.978517000	2.718238000	0.198795000
1	-4.607880000	1.702781000	1.599686000
1	-4.222530000	3.433749000	1.640175000
6	2.249388000	2.363349000	-1.966295000
1	2.747768000	3.269747000	-1.602594000
1	2.976116000	1.553554000	-1.969711000

1	1.926896000	2.533661000	-2.997452000
14	-1.722349000	0.849570000	0.682142000
14	1.347208000	0.885022000	0.302329000
7	-2.126654000	-0.323997000	-0.695285000
7	-3.049899000	-0.506928000	1.237362000
7	2.213344000	-0.533750000	-0.642777000
7	3.197496000	0.866365000	0.637242000
6	-2.933137000	-1.092686000	0.051656000
6	3.370721000	-0.281279000	-0.046828000
6	-3.470892000	-2.402641000	-0.344328000
6	-4.794197000	-2.747973000	-0.045751000
6	-2.654970000	-3.322245000	-1.015619000
6	-5.295414000	-3.988949000	-0.421166000
1	-5.425386000	-2.033432000	0.468372000
6	-3.157767000	-4.565246000	-1.382534000
1	-1.623870000	-3.061714000	-1.220886000
6	-4.478993000	-4.899737000	-1.090055000
1	-6.322792000	-4.246867000	-0.192541000
1	-2.518325000	-5.276497000	-1.892228000
1	-4.870443000	-5.867791000	-1.379819000
6	4.583059000	-1.101916000	-0.070122000
6	4.500262000	-2.495979000	0.057557000
6	5.840594000	-0.498201000	-0.213725000
6	5.656078000	-3.267896000	0.040404000
1	3.533685000	-2.962794000	0.198314000
6	6.990151000	-1.276589000	-0.244742000
1	5.905667000	0.578350000	-0.312901000

6	6.901879000	-2.663022000	-0.116221000
1	5.585191000	-4.343296000	0.153195000
1	7.957301000	-0.803199000	-0.366011000
1	7.800640000	-3.267905000	-0.134373000
6	1.883050000	-1.536790000	-1.622485000
1	1.301141000	-1.076031000	-2.426043000
1	2.779708000	-1.986485000	-2.054190000
1	1.270875000	-2.327003000	-1.176291000
6	3.971402000	1.320254000	1.776621000
1	4.655265000	2.129968000	1.502420000
1	3.274760000	1.701432000	2.527760000
1	4.551740000	0.507158000	2.218959000
6	-3.363747000	-1.181245000	2.482324000
1	-2.569243000	-0.969896000	3.202979000
1	-4.309594000	-0.816239000	2.896407000
1	-3.433679000	-2.264479000	2.357784000
6	-2.046248000	-0.245704000	-2.135639000
1	-2.407508000	-1.162513000	-2.604947000
1	-2.635291000	0.596399000	-2.515808000
1	-1.007146000	-0.085258000	-2.430911000
32	0.065527000	0.504643000	2.187850000

m-[SiNSi]GeFe

E= -5728.5378802

Free Energy = -5728.051786

32	-0.067076000	0.459160000	-1.769421000
14	1.924987000	0.955653000	-0.532623000
26	-0.540585000	-2.001297000	-1.672780000
14	-1.256014000	1.299605000	0.118701000
7	3.057732000	2.303524000	-1.005751000
7	2.378419000	0.461710000	1.176964000
8	1.316763000	-2.081896000	-3.936063000
6	0.090841000	-1.952105000	-0.040226000
6	-0.852648000	-3.737566000	-1.612630000
6	-2.186568000	-1.540758000	-2.091750000
6	0.575416000	-2.050297000	-3.046397000
7	-0.927518000	2.923332000	0.798993000
7	-2.171912000	0.432378000	1.509040000
7	-3.080798000	1.291671000	-0.225581000
6	2.353028000	3.370765000	-0.558198000
6	4.349129000	2.388573000	-1.645010000
6	3.165928000	-0.539302000	0.760837000
6	2.051992000	0.851398000	2.526537000
8	0.506123000	-1.987261000	1.053742000
8	-1.052575000	-4.870689000	-1.565615000
8	-3.277603000	-1.255236000	-2.386053000
6	0.215457000	3.601296000	0.437275000
6	-1.971541000	3.670812000	1.496940000
6	-3.319843000	0.503480000	0.821344000
6	-1.872056000	-0.463646000	2.610042000
6	-3.974143000	1.696903000	-1.289933000
7	1.238594000	2.849225000	0.011985000

6	2.569040000	4.750389000	-0.594022000
1	4.304413000	2.967577000	-2.574511000
1	4.683961000	1.380782000	-1.885802000
7	3.215873000	-0.459110000	-0.565190000
6	3.859613000	-1.523539000	1.606517000
6	0.377388000	4.999136000	0.462553000
1	-2.713212000	2.971510000	1.877406000
1	-2.476858000	4.385741000	0.837928000
6	-4.583093000	-0.169443000	1.158650000
1	3.460917000	5.175642000	-1.030814000
6	1.557927000	5.538451000	-0.048233000
6	3.692498000	-1.490845000	-1.467648000
6	5.222256000	-1.762299000	1.392085000
6	3.185737000	-2.214012000	2.619567000
1	-0.407459000	5.643615000	0.827008000
6	-5.245837000	-0.949214000	0.204491000
6	-5.117511000	-0.029502000	2.444885000
1	1.677220000	6.616491000	-0.045896000
1	5.742284000	-1.221915000	0.610927000
6	5.905842000	-2.673975000	2.187899000
6	3.872508000	-3.134455000	3.403639000
1	2.124199000	-2.063489000	2.747626000
1	-4.810552000	-1.082342000	-0.777427000
6	-6.436301000	-1.583618000	0.544809000
6	-6.315889000	-0.653650000	2.770273000
1	-4.600446000	0.576226000	3.179337000
1	6.961896000	-2.849742000	2.021430000

6	5.230846000	-3.362685000	3.193726000
1	3.343415000	-3.681490000	4.174878000
6	-6.974532000	-1.433111000	1.820852000
1	-6.940597000	-2.200213000	-0.189300000
1	-6.733407000	-0.535841000	3.763036000
1	5.761382000	-4.080151000	3.808717000
1	-7.904706000	-1.926060000	2.078009000
1	5.096007000	2.847671000	-0.985828000
1	-5.013797000	1.597683000	-0.973499000
1	-3.778464000	2.741493000	-1.539228000
1	-3.813435000	1.085353000	-2.179339000
1	-2.617141000	-1.258044000	2.678298000
1	-0.902391000	-0.926316000	2.437217000
1	-1.849466000	0.080096000	3.560084000
1	3.102448000	-1.461756000	-2.381057000
1	4.744078000	-1.335795000	-1.732993000
1	3.584962000	-2.485027000	-1.028784000
1	1.138136000	0.359663000	2.874976000
1	2.862982000	0.598388000	3.212819000
1	1.893500000	1.930209000	2.551953000
1	-1.551137000	4.215484000	2.346909000

m-[SiNSi]GeGeFe

E= -8726.1652703

Free Energy = -8725.681157

1	4.830098000	3.879998000	1.282977000
6	4.068208000	3.376992000	1.889662000
7	2.863292000	3.136142000	1.129809000
1	4.473137000	2.418663000	2.211795000
17	0.143827000	-1.793830000	3.613453000
14	1.919011000	1.680554000	0.586942000
6	2.153020000	4.091765000	0.479889000
32	-0.498949000	-1.252775000	1.500574000
32	-0.143292000	1.215796000	1.702411000
7	2.666202000	1.152100000	-0.985135000
7	3.166136000	0.283311000	0.902585000
7	1.174528000	3.415705000	-0.175965000
6	2.250502000	5.481446000	0.383356000
26	0.098931000	-2.920190000	-0.102178000
17	-2.779378000	-1.120385000	1.823444000
14	-1.320392000	1.749072000	-0.305010000
6	3.354306000	0.150195000	-0.407784000
6	2.501719000	1.466808000	-2.385185000
6	3.575764000	-0.608879000	1.969941000
6	0.164960000	4.013824000	-0.819668000
1	3.031406000	6.034693000	0.884400000
6	1.270470000	6.106044000	-0.384521000
6	0.495618000	-1.585780000	-1.159072000
6	0.638310000	-4.099876000	-1.311263000
6	1.245031000	-3.558176000	1.098135000
6	-1.583454000	-3.504289000	-0.079927000

1	-3.791751000	-1.771003000	-0.925715000
7	-0.865878000	3.195110000	-1.248176000
7	-3.136174000	1.898226000	0.059288000
7	-2.258563000	0.661784000	-1.458627000
6	4.109950000	-0.895052000	-1.110370000
6	0.220183000	5.407940000	-0.984238000
1	1.302729000	7.184146000	-0.497007000
8	0.744915000	-0.741373000	-1.917368000
8	1.019719000	-4.848142000	-2.094953000
8	2.063495000	-3.980749000	1.791297000
8	-2.668274000	-3.884035000	-0.156394000
6	-4.701252000	-1.199155000	-1.034589000
6	-1.844532000	3.777287000	-2.171065000
6	-3.398146000	0.900067000	-0.794625000
6	-3.885793000	2.209504000	1.267916000
6	-2.097852000	-0.190663000	-2.624749000
6	4.977860000	-0.555149000	-2.155451000
6	3.944532000	-2.238705000	-0.757132000
1	-0.550492000	5.936436000	-1.523126000
6	-4.671134000	0.198443000	-0.965620000
6	-5.918648000	-1.853467000	-1.172356000
1	-2.494977000	2.985606000	-2.537880000
1	-2.466335000	4.537619000	-1.686994000
1	5.123561000	0.484558000	-2.419952000
6	5.666350000	-1.550129000	-2.839519000
6	4.616690000	-3.230678000	-1.461155000
1	3.268980000	-2.511270000	0.037227000

6	-5.861270000	0.931900000	-1.039784000
1	-5.938615000	-2.935834000	-1.196864000
6	-7.101836000	-1.122148000	-1.259382000
1	6.343592000	-1.281819000	-3.641494000
6	5.478893000	-2.889095000	-2.500131000
1	4.457700000	-4.269020000	-1.197724000
6	-7.073084000	0.270272000	-1.196701000
1	-5.829728000	2.013375000	-0.986455000
1	-8.048860000	-1.637540000	-1.368409000
1	6.003907000	-3.664229000	-3.045731000
1	-7.993403000	0.837798000	-1.263217000
1	-1.336489000	4.225887000	-3.028104000
1	2.825100000	-1.375675000	2.173317000
1	4.522079000	-1.096583000	1.727876000
1	3.705160000	-0.026396000	2.883174000
1	1.493678000	1.851828000	-2.537553000
1	3.215864000	2.232894000	-2.706155000
1	2.620702000	0.576940000	-3.001556000
1	-4.662694000	1.466779000	1.444426000
1	-3.203436000	2.194819000	2.119833000
1	-4.337507000	3.201959000	1.192683000
1	-3.008780000	-0.172186000	-3.225849000
1	-1.263151000	0.176504000	-3.217817000
1	-1.878410000	-1.219615000	-2.336856000
1	3.872304000	3.986114000	2.778786000

Cartesian geometry of [**SiCCSi]NiBr₂** in Angstrom [Å].

C	-0.835092	-1.87824	-0.103795
B	0.18193	-2.338607	-1.421658
B	0.18483	-4.114161	-1.443855
B	0.889626	-4.675166	0.112671
B	-0.889132	-4.675268	-0.113058
B	-0.184394	-4.114236	1.443504
B	1.323506	-3.225658	1.063881
B	1.55141	-3.226358	-0.699185
C	0.83525	-1.878153	0.103547
B	-0.181691	-2.338722	1.4214
B	-1.551101	-3.226573	0.698878
B	-1.323164	-3.225751	-1.064204
Si	-1.493925	-0.037435	-0.110043
C	-3.765274	-0.131966	0.016662
C	-5.2441	-0.200768	0.104266
Ni	-0.000082	1.478091	0.000045
Si	1.493881	-0.037289	0.110033
C	3.765233	-0.131809	-0.016619
C	5.244055	-0.200696	-0.104207
Br	1.843006	3.018991	0.27446
Br	-1.843136	3.01896	-0.274463
N	-2.906819	-0.072863	1.054177
C	-3.146645	0.243158	2.491525
C	-1.851892	0.883064	3.037529

N	-3.026967	-0.172337	-1.109269
C	-3.432458	-0.162393	-2.541583
C	-2.145996	-0.399671	-3.355777
N	3.026905	-0.172248	1.109302
C	3.43237	-0.162398	2.541621
C	2.145947	-0.399952	3.355804
N	2.906798	-0.07255	-1.054138
C	3.146665	0.243491	-2.49147
C	1.851939	0.88342	-3.037516
C	-4.290872	1.265417	2.670949
C	-3.46139	-1.062874	3.250566
C	-4.455698	-1.278635	-2.842348
C	-4.016397	1.216301	-2.926678
C	4.45581	-1.278479	2.842314
C	4.016057	1.216364	2.92683
C	3.461453	-1.062517	-3.25054
C	4.290888	1.265772	-2.670781
C	5.837658	-1.427847	-0.454897
C	7.234331	-1.52519	-0.536952
C	8.034133	-0.39908	-0.281224
C	7.436814	0.827521	0.05597
C	6.041839	0.930936	0.146973
H	5.205648	-2.297087	-0.643441
H	7.695881	-2.478866	-0.799826
H	9.121127	-0.476002	-0.34765
H	8.056668	1.706291	0.243389

H	5.565144	1.882777	0.380568
C	-6.041852	0.930882	-0.146923
C	-7.436827	0.827525	-0.055845
C	-8.034181	-0.399035	0.281431
C	-7.234411	-1.525166	0.537171
C	-5.837739	-1.427879	0.45505
H	-5.565142	1.882699	-0.380578
H	-8.056651	1.706316	-0.243266
H	-9.121175	-0.475911	0.347912
H	-7.695985	-2.478813	0.800109
H	-5.205758	-2.297132	0.643624
H	-4.290912	1.601293	3.719541
H	-4.120422	2.137183	2.021308
H	-5.274743	0.830134	2.453887
H	-1.992026	1.10807	4.10613
H	-0.995869	0.202631	2.940013
H	-1.623222	1.812964	2.497447
H	-3.603871	-0.839811	4.32017
H	-4.385037	-1.519193	2.862885
H	-2.637623	-1.783017	3.144174
H	-4.637685	-1.304031	-3.928409
H	-4.070205	-2.259362	-2.528331
H	-5.413244	-1.092007	-2.337854
H	-4.165791	1.24503	-4.018298
H	-4.990847	1.37997	-2.447585
H	-3.329702	2.022433	-2.632047

H	-2.375383	-0.30773	-4.427885
H	-1.385921	0.355838	-3.098212
H	-1.741446	-1.401999	-3.168363
H	1.991979	1.108006	-4.10622
H	0.995793	0.203193	-2.939641
H	1.623505	1.81355	-2.497733
H	3.604278	-0.839379	-4.320083
H	4.384924	-1.518993	-2.862631
H	2.637563	-1.782564	-3.144453
H	4.290873	1.601868	-3.719305
H	4.120468	2.137405	-2.020956
H	5.274766	0.830429	-2.453856
H	2.375295	-0.30785	4.427907
H	1.385692	0.355356	3.098172
H	1.741632	-1.402387	3.168462
H	4.63757	-1.304102	3.928407
H	4.070616	-2.259217	2.527969
H	5.413419	-1.091496	2.338071
H	4.16584	1.244888	4.018403
H	4.990279	1.380432	2.44741
H	3.329035	2.022375	2.632628
H	0.305497	-1.593988	-2.334902
H	-2.253088	-3.092837	-1.793439
H	-2.635415	-3.084047	1.171458
H	-0.30532	-1.594156	2.33468
H	2.253419	-3.092666	1.793103

H	2.6357	-3.08367	-1.171763
H	0.315137	-4.698524	-2.478355
H	-1.532534	-5.679324	-0.196051
H	-0.314633	-4.698665	2.477977
H	1.533152	-5.679147	0.195608

Cartesian geometry of [**SiCCSi**]**Ni(CO)₂** in Angstrom [Å].

C	0.744081	-0.289506	1.445237
B	-0.228739	0.986773	2.087234
B	-0.31473	0.70081	3.843298
B	-1.137216	-0.881155	4.093031
B	0.647386	-0.777059	4.200089
B	-0.122904	-2.159211	3.337957
B	-1.559793	-1.526193	2.48092
B	-1.676027	0.213014	2.789657
C	-0.955653	-0.375818	1.340418
B	-0.042864	-1.814944	1.591554
B	1.325013	-1.364979	2.656463
B	1.210008	0.385355	2.958033
Si	1.589022	-0.037092	-0.315075
C	3.875146	0.099141	0.015543
C	5.358154	0.207985	0.069702
Ni	0.10765	-0.024254	-1.929021
Si	-1.566422	-0.05959	-0.5099
C	-3.865372	0.134502	-0.253146
C	-5.334964	0.244903	-0.051412

C	0.21602	1.507088	-2.854981
C	0.170494	-1.575258	-2.819125
N	3.157183	-1.032926	-0.114842
C	3.626304	-2.398409	-0.474482
C	2.432585	-3.355764	-0.304688
N	2.994178	1.116898	0.092196
C	3.244111	2.579187	0.013488
C	1.901131	3.274055	0.299462
N	-3.169906	-1.005265	-0.422975
C	-3.639338	-2.372867	-0.758958
C	-2.432176	-3.319963	-0.607136
N	-2.97128	1.141491	-0.209777
C	-3.201184	2.610677	-0.158054
C	-1.931307	3.288535	-0.708822
C	4.073139	-2.411346	-1.954609
C	4.772433	-2.87302	0.446638
C	4.277822	3.040782	1.063839
C	3.708604	2.950683	-1.413543
C	-4.771475	-2.845038	0.180294
C	-4.107535	-2.395801	-2.232779
C	-3.441867	3.067314	1.297358
C	-4.394721	3.041458	-1.043956
C	-5.807455	0.312531	1.273368
C	-7.185856	0.3892	1.520073
C	-8.09336	0.402059	0.448075
C	-7.620165	0.340834	-0.873688

C	-6.243147	0.261735	-1.125593
H	-5.093062	0.287975	2.097921
H	-7.549433	0.435784	2.548376
H	-9.16634	0.46122	0.64108
H	-8.322933	0.358169	-1.709021
H	-5.87009	0.235796	-2.149822
C	6.123704	0.370508	-1.099125
C	7.52135	0.462776	-1.013603
C	8.156027	0.393475	0.236975
C	7.391057	0.231898	1.404878
C	5.995245	0.139199	1.323984
H	5.625711	0.423488	-2.067857
H	8.111724	0.587955	-1.923335
H	9.243533	0.46465	0.30203
H	7.881432	0.177139	2.378678
H	5.392693	0.011244	2.224537
H	4.350012	-3.43716	-2.247175
H	3.250158	-2.069795	-2.600402
H	4.947299	-1.761608	-2.104362
H	2.733403	-4.360624	-0.638448
H	2.121953	-3.407786	0.746574
H	1.580239	-3.029691	-0.915939
H	4.945681	-3.945024	0.261689
H	5.710906	-2.337867	0.253605
H	4.493233	-2.741586	1.50323
H	4.291157	4.142289	1.081424

H	3.994371	2.67813	2.063816
H	5.290781	2.690058	0.828522
H	3.825965	4.043888	-1.490403
H	4.676779	2.483731	-1.64345
H	2.960503	2.625461	-2.151996
H	2.018382	4.359816	0.162485
H	1.129384	2.917457	-0.398198
H	1.576439	3.0777	1.3297
H	-2.041514	4.380104	-0.616789
H	-1.043595	2.981584	-0.141801
H	-1.775669	3.035894	-1.765949
H	-3.621109	4.154728	1.309727
H	-4.322754	2.563437	1.721338
H	-2.568805	2.844966	1.925059
H	-4.377462	4.138648	-1.139234
H	-4.305965	2.60317	-2.05043
H	-5.360357	2.752771	-0.61021
H	-2.72668	-4.327696	-0.937732
H	-1.592115	-2.984112	-1.231296
H	-2.103571	-3.372303	0.43776
H	-4.95527	-3.915012	-0.006364
H	-4.474544	-2.718537	1.231852
H	-5.708827	-2.300874	0.005208
H	-4.378754	-3.42479	-2.519254
H	-4.989853	-1.754831	-2.372057
H	-3.298066	-2.046911	-2.892492

H	-0.275953	2.023913	1.516482
H	2.189259	1.067185	2.98777
H	2.384548	-1.882233	2.479451
H	0.0408	-2.582007	0.693682
H	-2.529338	-2.155146	2.193582
H	-2.72615	0.767532	2.70637
H	-0.413018	1.622452	4.599376
H	1.243193	-0.917863	5.227762
H	-0.082536	-3.28787	3.731662
H	-1.834819	-1.092515	5.041696
O	0.210071	-2.631324	-3.32722
O	0.318125	2.54486	-3.3902

The cartesian geometry of [**SiFcSi**]**NiBr₂** in Angstrom [Å].

C	0.93974	2.990981	-1.70878
C	1.475193	2.252475	-0.5804
C	1.988725	3.244436	0.342116
C	1.764335	4.553418	-0.201746
C	1.121811	4.396614	-1.47539
Fe	-0.000069	3.520108	-0.000115
C	-0.939811	2.991359	1.708537
C	-1.122008	4.396907	1.474675
C	-1.764431	4.55326	0.20091
C	-1.988612	3.244072	-0.34258
C	-1.475132	2.252425	0.580359
Si	-1.513003	0.398382	0.285969

C	-3.697126	-0.182034	-0.141765
C	-5.053227	-0.723597	-0.409415
Si	1.512959	0.398463	-0.286116
C	3.697084	-0.182011	0.141795
C	5.053189	-0.723525	0.409556
Ni	0.000115	-1.114824	-0.00024
Br	-1.394949	-2.772198	1.126846
N	-2.7618	0.161969	-1.062181
C	-2.671471	-0.22699	-2.494663
C	-1.426552	0.489474	-3.05416
N	-3.145025	-0.011733	1.062259
C	-3.752816	0.079005	2.409165
C	-2.577275	0.13008	3.406632
N	2.761729	0.162022	1.062175
C	2.671498	-0.226455	2.494762
C	1.426777	0.490471	3.054122
N	3.145069	-0.011591	-1.062232
C	3.752924	0.078459	-2.409146
C	2.577434	0.129545	-3.406675
Br	1.394831	-2.772678	-1.126426
C	-3.918555	0.249138	-3.271363
C	-2.48859	-1.753184	-2.635319
C	-4.577424	1.383813	2.489677
C	-4.631665	-1.14802	2.733582
C	3.918774	0.249715	3.271161
C	2.488363	-1.752551	2.636058

C	4.631416	-1.148958	-2.733052
C	4.577906	1.382996	-2.490106
C	6.138253	0.133467	0.665747
C	7.411857	-0.407605	0.896505
C	7.597743	-1.800041	0.878471
C	6.510542	-2.653242	0.622857
C	5.236664	-2.119713	0.381788
H	5.979904	1.213094	0.687443
H	8.25626	0.256482	1.091957
H	8.589312	-2.219518	1.060676
H	6.655229	-3.735183	0.60317
H	4.384416	-2.763322	0.155723
C	-6.138246	0.133277	-0.666182
C	-7.411845	-0.407868	-0.896814
C	-7.597757	-1.800289	-0.878187
C	-6.51058	-2.653391	-0.622129
C	-5.23673	-2.11978	-0.381114
H	-5.979873	1.21289	-0.688387
H	-8.256198	0.256165	-1.092661
H	-8.58931	-2.219838	-1.060311
H	-6.65526	-3.735327	-0.602062
H	-4.384488	-2.763318	-0.15483
H	-4.979579	1.508978	3.508285
H	-3.944566	2.250742	2.244633
H	-5.422251	1.345155	1.784366
H	-4.924278	-1.095954	3.794789

H	-5.546069	-1.167439	2.126392
H	-4.059606	-2.071515	2.563504
H	-2.970951	0.179345	4.433453
H	-1.954645	-0.770175	3.297637
H	-1.962738	1.026005	3.231779
H	-3.750612	0.083863	-4.347442
H	-4.81835	-0.304877	-2.974533
H	-4.091962	1.324822	-3.10443
H	-1.306666	0.242248	-4.119897
H	-1.527251	1.581477	-2.950009
H	-0.525976	0.154015	-2.516096
H	-2.356328	-2.009255	-3.699389
H	-1.6036	-2.090781	-2.075382
H	-3.371604	-2.286673	-2.255969
H	1.306009	0.24239	4.119563
H	1.528247	1.582506	2.950993
H	0.526278	0.156073	2.515268
H	3.750689	0.085438	4.347372
H	4.818322	-0.304989	2.974844
H	4.092712	1.325164	3.103299
H	2.357184	-2.008184	3.700375
H	1.602721	-2.090134	2.077171
H	3.370834	-2.286404	2.255996
H	4.924612	-1.097006	-3.794101
H	5.545484	-1.168772	-2.125361
H	4.058844	-2.072188	-2.563248

H	2.971165	0.178183	-4.433506
H	1.954475	-0.770438	-3.297329
H	1.963216	1.025784	-3.232246
H	4.980122	1.507631	-3.508755
H	3.945276	2.250195	-2.245434
H	5.422704	1.344383	-1.784761
H	2.425966	3.019136	1.31156
H	1.995578	5.497938	0.286585
H	0.784359	5.200742	-2.126134
H	0.446612	2.553982	-2.572786
H	-2.425811	3.018429	-1.311962
H	-1.995655	5.497589	-0.287803
H	-0.784948	5.201387	2.125191
H	-0.446741	2.554693	2.57275